Silver Nanowire Networks in Electrochromic Devices

by

Jonathan Cole Atkinson

A thesis

presented to the University of Waterloo

in fulfillment of the

thesis requirement for the degree of

Doctor of Philosophy

in

Electrical and Computer Engineering - Nanotechnology

Waterloo, Ontario, Canada, 2023

Examining Committee Membership

The following served on the Examining Committee for this thesis. The decision of the Examining Committee is by majority vote.

External Examiner

NAME: Donling Ma
Title: Professor at Institut National de la Recerche Scientifique

Supervisor(s)

NAME: Irene A. Goldthorpe
Title: Professor of Electrical & Computer Engineering at University of Waterloo

Internal Member

NAME: Na Young Kim
Title: Professor of Electrical & Computer Engineering at University of Waterloo

Internal Member

NAME: Bo Cui
Title: Professor of Electrical & Computer Engineering at University of Waterloo

Internal-external Member

NAME: Michael Collins
Title: Professor Mechanical and Mechatronics Engineering at University of Waterloo

Author's Declaration

I hereby declare that I am the sole author of this thesis. This is a true copy of the thesis, including any required final revisions, as accepted by my examiners.

I understand that my thesis may be made electronically available to the public.

Abstract

Transparent electrodes are a necessary component of electrochromic devices. These electrodes are most commonly made from indium tin oxide (ITO), but this material is far from ideal. ITO is expensive, brittle and thus unsuitable for flexible applications, and has low transparency in the near infrared (NIR) region which limits the solar heat gain of smart windows in the winter. Random networks of silver nanowires are a promising alternative material to replace ITO since they are cheaper, simpler to deposit, have deposition temperatures compatible with plastic substrates and are much more mechanically flexible. This thesis is an examination of if and how silver nanowires can improve the performance of electrochromic devices.

Two unresolved problems with silver nanowire electrodes that hinder their widespread use is tackled. First, their low lifetime due to silver corrosion and their surface roughness. In chapter 2 a passivation strategy that meets the requirements for electrochromic devices is explored. Unlike many nanowire electrode passivation materials used in the literature, the use of a non-conductive passivation layer is researched here which allows the use of transparent polymers. Of the candidates tested, polyurethane (PU) was found to perform the best with electrode resistance only increasing 1.8X after six months. PU is cheap and easy to deposit, 96% transparent across the visible and NIR regions, increases the mechanical flexibility of nanowire electrodes, and improves nanowire adhesion and surface roughness. It is shown through simulation and electrostatic force microscopy measurements that despite the non-conductive nature of the passivation material, the magnitude of the electric field above the electrode is quite uniform, decreasing by at most a factor of 0.5 above nanowire gaps compared to directly above a nanowire. Electrochromic displays made with PU-passivated nanowire electrodes have a uniform colour switch across the device area.

In Chapter 3, the PU-passivated nanowire electrodes are integrated into mechanically flexible PEDOT:PSS based electrochromic displays. Compared to the same devices that used ITO electrodes, these devices have improved colour changing properties and a longer lifetime. Most noteworthy is their far superior mechanical properties. After 50 bending cycles, the devices with nanowire electrodes had little change in performance whereas devices with ITO no longer worked. Also, the capability of making these displays not only flexible, but recyclable as well is demonstrated by successfully printing working nanowire/PEDOT:PSS electrochromic devices on biodegradable paper in place of plastic substrates.

One issue with PEDOT:PSS as an electrochromic material is its low conductivity, causing PEDOT:PSS based electrochromic devices to have slow switching speeds and elevated operating voltages. In Chapter 4,

it is shown that sheet resistance can be lowered from 280 Ω/sq to 34 Ω/sq by mixing silver nanowires into the PEDOT:PSS electrochromic layer. The longest, thinnest nanowires at a concentration of 3.0 mg/ml led to the best performance. The addition of nanowires into the electrochromic layer more than halved switching times and lowered the turn-on voltage from 1.5 to 1.1 V. Furthermore, the increased conductivity allows the device to operate well without transparent electrodes thereby reducing cost and complexity. Passivation of the silver nanowires in solution before mixing with PEDOT:PSS was attempted using two small molecules, MuA and MBI. However, the performance of electochromic devices using these passivated nanowires was poor due to nanowire clumping. Alternative suggestions for passivating silver nanowire surfaces in solution are given.

One advantage of silver nanowire electrodes that has received little attention in the literature is their high transparency in the NIR region, which is highly desirable for some applications including smart windows. In Chapter 5 it is shown that for electrodes that are 96% transparent in the visible, ones made from ITO are only 35% transparent at a wavelength of 2500 nm, while those made from silver nanowires maintain a transparency as a high as 94%. Experiments and modelling show that to minimize the transparency drop from the visible to the NIR, the nanowires should be sparse and larger in diameter. This is found to be attributed to both the larger average spacing between nanowires in such networks and the lower absorption losses of larger diameter nanowires in the NIR.

In Chapter 6, silver nanowire electrodes are integrated into tungsten oxide/nickel oxide based electrochromic smart windows and compared to the same windows with ITO electrodes through both experiments and modelling. Windows using passivated nanowire electrodes are shown to have higher NIR transparency, leading to a lower U-factor and higher solar heat gain in the winter with similar U-factor and solar heat gain in the summer compared to ITO window devices. This would allow more heat to enter a building in the winter, thereby improving energy efficiencies in cold climates.

Acknowledgements

I would like to thank Prof. Irene Goldthorpe for guidance and thought-provoking conversation through the entire length of my Doctoral Degree. She kept me motivated to keep going when I needed it when the results and experiments were not as expected. I would also like to thank Dr. Marwa Abd-Ellah for her guidance and existence with experimental work over two separate periods during my Doctoral Degree.

Additionally, I would like to thank my friends and lab colleagues: Hadi, Nupur, Jianjin, Geoff, Alexandra, Mina, Muhammed, Tianqi, and Hubert for all their help, support, and discussions that helped immensely in the completion of this work.

Furthermore, I would like to acknowledge Prof. Aline Rougier and Dr. Issam Mjerji at the University of Bordeaux in Bordeaux, France for the amazing experience I had living and performing research related to this project for four months. The knowledge and experiences they shared were a great help in finishing this work.

I would also like to thank Prof. Michael Collins and Prof. Michael Pope at the University of Waterloo for the use of their labs to perform countless measurements that added great value to completing this work.

Finally, I would like to acknowledge and thank my partner, Chloe. Without her by my side encouraging me to keep going when I did not want to and being someone to lean on when I needed it, I would not be where I am today.

Dedication

I hereby dedicate this thesis to my Mom, Dad, and Grandfather for their unending support over the years to help me get to this point.

Table of Contents

List of Figures

List of Tables

Chapter 1
Introduction

1.1 Electrochromic Devices

1.1.1 Device Basics

An electrochromic device alters its optical properties when a difference in electric potential is applied across it. The four most common application areas of electrochromic devices are: (1) information displays, which are patterned to display and change messages in real time to broadcast information; (2) variable reflectance mirrors, which change their reflectance based upon required conditions, eg. rear view mirrors in motor vehicles; (3) smart windows, which can improve the energy efficiency of vehicles or buildings by controlling the amount of light and heat that is transmitted through the window, and lastly, (4) variable emittance surfaces, which can be used on space vehicles for temperature control [1]. In this work, information displays and smart windows were fabricated and characterized, though much of the lessons learned are applicable to electrochromic devices of all types.

In general, the active layer of an electrochromic device has three main components: (i) a primary electrochromic film, (ii) an ion conductor or electrolyte, and (iii) an ion storage layer or secondary electrochromic film [1]. These layers are sandwiched between two electrodes, at least one of which is optically transparent to allow light to pass through [1]. Figure 1.1(a) shows a schematic of a typical electrochromic device. The electrochromic film undergoes a colour change when an ion (commonly hydrogen or lithium) from the electrolyte moves to bond with the atoms in the electrochromic film [1]. For charge balance, an electron is either added or ejected to or from the outer shell of each atom in the material [1]. Upon the loss or gain of these electrons, the atomic structure of the material changes, altering its optical properties and hence the wavelengths at which it absorbs light [1]. The movement of the electrons or ions is done by the application of an electric field through an applied voltage potential. The ions and electrons move back and forth through the ion conductor material between the primary electrochromic film and ion storage or secondary electrochromic film [1]. When the voltage is turned off, the electrochromic films will return to their original colour and atomic configuration [1].

Electrochromic materials are mostly either transition metal oxides or polymers as these materials are capable of showing a reversible colour change from a redox reaction [1]. Both transition metal oxides and polymers that are electrochromic have a bandgap that changes with the insertion or extraction of ions or electrons that is not seen in conductors or very high band gap dielectrics. Transition metal oxides are either cathodic or anodic depending on their atomic configuration as shown in Figure 1.1(b) [1]. The most commonly used primary electrochromic material is tungsten oxide (WO_3), which has been widely used as a material in electrochromic devices such as displays and smart windows [1]. WO_3 along with nickel oxide (NiO), the most commonly used ion storage or secondary electrochromic material, have a good response time and exhibit the biggest elementary change in transparency from the on to the off state which is advantageous for display and smart window applications[1].

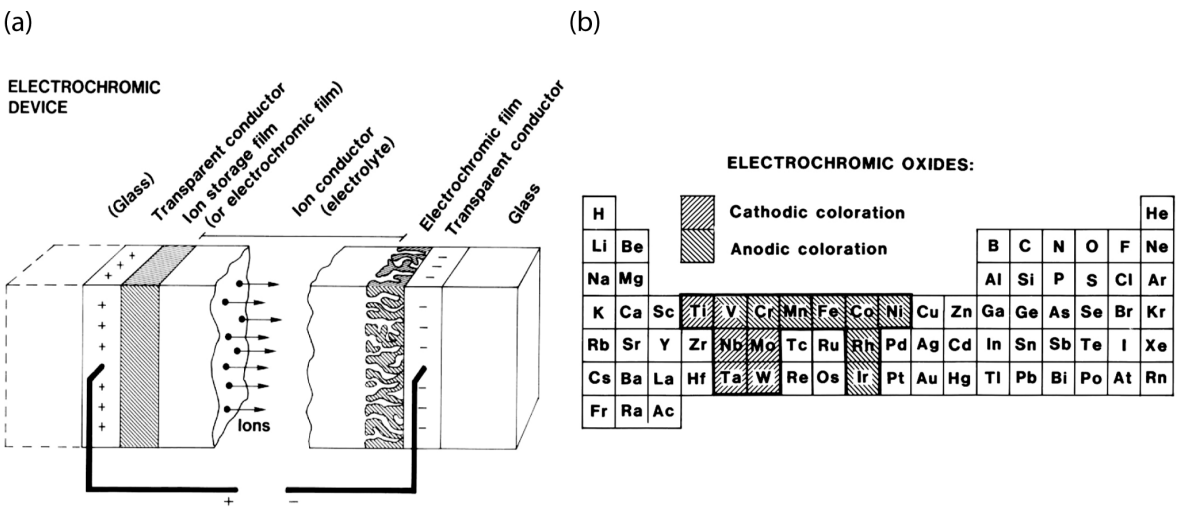

Figure 1.1: (a) Schematic of a five-layer electrochromic device. (b) Cathodic and anodic electrochromic metal oxides in the periodic table. This figure was published in Thin Solid Films, Vol. 564, C.G. Granqvist, Electrochromics for Smart Windows: Oxide-based thin films and devices page 5-7, Copyright Elsevier (2014). [2]

Regarding electrochromic polymers, there are two main classes: viologens and conducting polymers [3], [4]. Viologens are compounds with the chemical formula $(C_5H_4NR)_2^{n+}$ as the monomer unit and their subsequent derivatives [3], [4]. The best made viologen devices are displays that have very short switching times and exceptionally long device lifetimes [3], [4]. The most commonly used conducting polymer in electrochromic devices is PEDOT:PSS (poly(3,4-ethylenedioxythiophene) polystyrene sulfonate) [3], [4]. PEDOT:PSS and other conducting polymers are known for their good efficiency and colour tunability [3],

[4]. However, after many switches these devices are known to degrade in performance [3], [4]. Devices made with metal oxides, on the other hand, have shown to be stable over a wide temperature range along with good electrical and chemical stability over a long lifetime [1]. Both PEDOT: PSS and metal oxides, specifically WO_3 and NiO, are used to make devices in this research.

1.2 Polymeric Electrochromic Displays

Electrochromic displays have many applications including image and data displays and flexible/disposable displays [1], [5]. The latter application in particular calls for cheap fabrication over large areas as well as mechanical flexibility [1], [5]. The most common electrochromic materials are metal oxides. However, in general these are not mechanically flexible and are costly and more difficult to fabricate at a high throughput over large areas [3], [4]. Organic materials are cheaper and easier to fabricate in solution in large batches [3], [4]. They also have a high degree of tunability in terms of the exact colour change that the electrochromic material can undergo compared to transition metal oxides [3], [4]. PEDOT:PSS is the most extensively studied of the conductive polymers as mentioned in Section 1.1. It has a high colouration efficiency and optical modulation and is easy to fabricate in large batches [3], [4]. It is also mechanically flexible. However, its electrical conductivity is low which can lead to long switching times and high turn-on voltages [3], [4]. Long switching times decrease the rate at which information can be displayed and high turn on voltages increase the amount of energy that these devices use. Adding indium tin oxide (ITO) transparent electrodes can help with the switching time and turn-on voltage of the device. A schematic of this PEDOT:PSS flexible device is shown in Figure 1.2. The primary and secondary electrochrome are the same material in this case. In this way, the display can be reversible and both sides can be used. However, ITO is not ideal for flexible, inexpensive devices because it is costly and brittle, the former causing it to lose conductivity with repeated bending [6]. More flexible materials that can be used as transparent electrodes must be researched and studied for these devices.

Adding conductive dopants or nanoparticles to the PEDOT:PSS in order to improve the conductivity could also improve switching times and, voltages and may also make the PEDOT: PSS conductive enough to not need a transparent electrode at all [3], [4]. However, this requires extensive study as the dopant should not significantly compromise other performance metrics of the displays as well as affect the lifetime or stability

of the device. This research will study both replacing ITO with a flexible electrode and mixing conductive nanoparticles into the PEDOT:PSS in order to improve flexible electrochromic devices on plastic and paper.

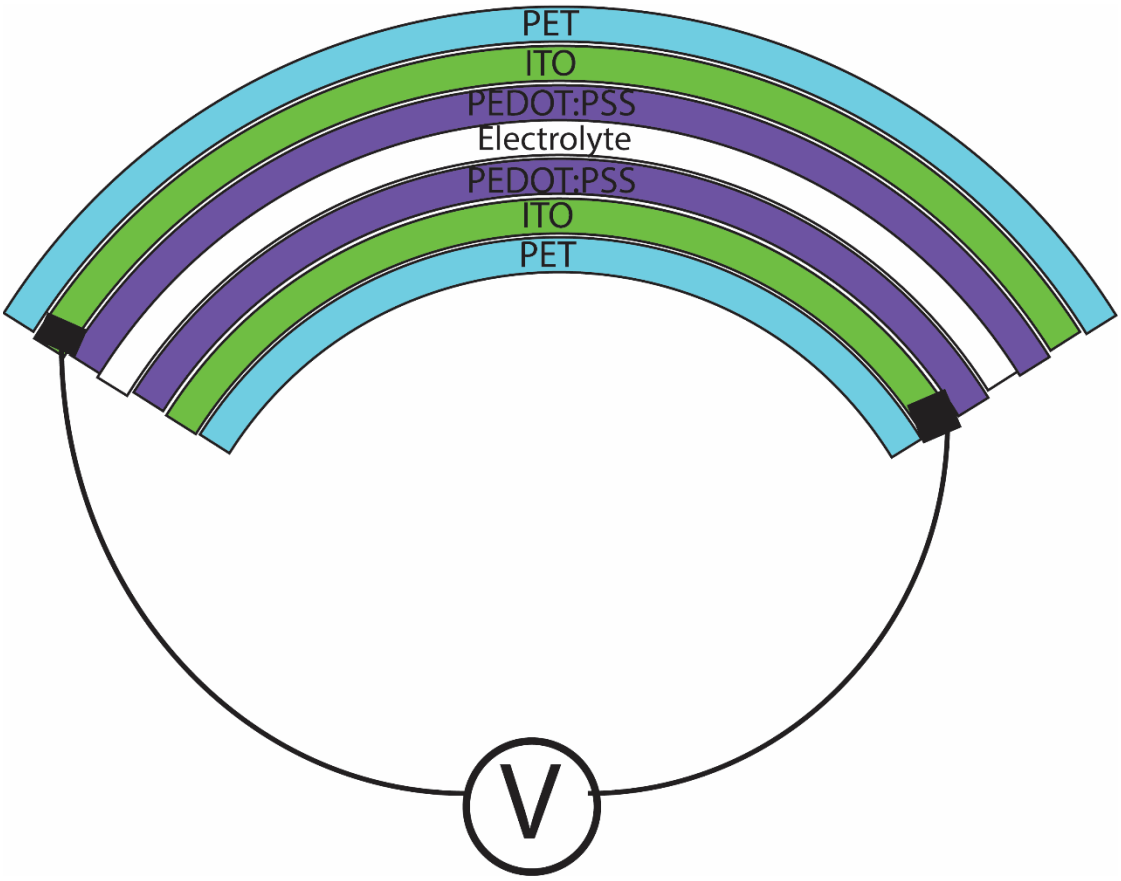

Figure 1.2: (a) Schematic of a flexible PEDOT:PSS electrochromic display.

1.3 Electrochromic Smart Windows

Windows can transfer ten times more heat than that of the same area of an insulated wall [7], [8]. This heat gain from windows in buildings results in one billion dollars' worth of energy to be wasted across the province of Ontario every year [9]. This wasted energy also creates unnecessary greenhouse gas emissions [9].

A smart window, or smart glass, can be used to manage the light and heat transfer across a window by altering its transmission properties, usually through the application of a voltage, as shown in the photo in Figure 1.3(a), where 2/3 of the panels are turned on and 1/3 of the windows are left off. The market for smart windows has been consistently increasing with the market set to reach $5 billion in 2030 [10] (Figure 1.3(b)). As such, it is highly desirable to use materials that are cheaper and outperform current technology in window coatings [11]. There are several technologies to implement smart windows, the most common of which are liquid crystal, suspended particle and electrochromic [12]. Liquid crystal-based windows switch from a transparent state to a cloudy, opaque state [12]. This technology is best suited to privacy windows as it cannot be in a semi-transparent state like a suspended particle or electrochromic device. Of these latter two technologies, electrochromic is the more promising. It has the lowest haze, lowest operating voltage required to switch the window, and the best on/off transmittance ratio of any smart window device [12].

The ideal spectral profile of a window is dependent on the outdoor conditions. Figure 1.4(a) shows the wavelengths that are given off by the sun and transmitted through the atmosphere to the earth's surface (blue curve). The visible region for wavelengths visible to the eye is in the range from 400 nm to 700 nm. Solar heat is considered to be at the wavelengths beyond this, the majority of which occurs in the near infrared region (NIR) which spans from 780 nm to 2500 nm [13]. Room temperature heat occurs further into the infrared region from 5000 nm to about 30,000 nm (red curve) and peaks around 10,000 nm [13]. In all seasons, the window should be transparent to visible light from the sun and block these longer IR wavelengths from room temperature sources. In summer, NIR wavelengths from the sun should be blocked from entering the window as well, to prevent the NIR radiation from heating the building. However, in winter, this solar heat is beneficial and thus the window should be transparent to NIR wavelengths. Therefore, in variable climates like Canada where it is very cold in the winter and hot in the summer, a window coating that can alter its NIR transparency depending on the outdoor temperature is highly advantageous. Low-E coatings only block longer infrared regions from leaving buildings. Switchable window coatings that can alter their transmittance in the NIR can reduce building energy costs by up to 25% [14][15].

(a)

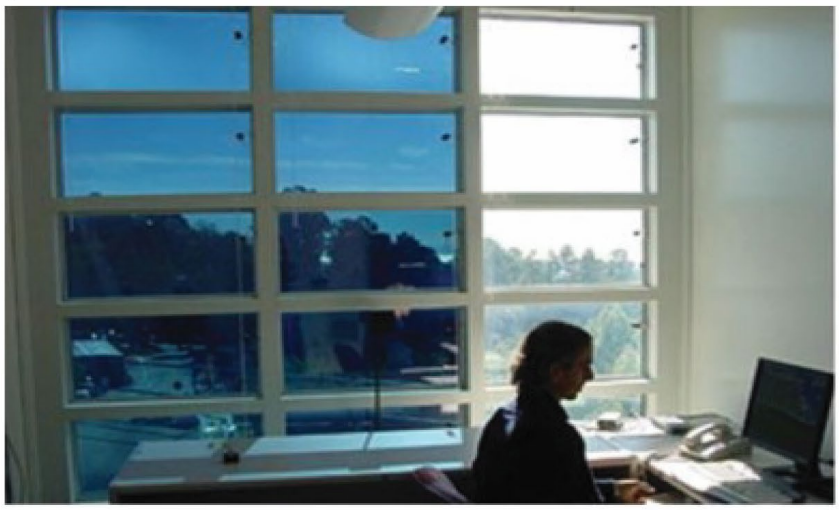

(b)

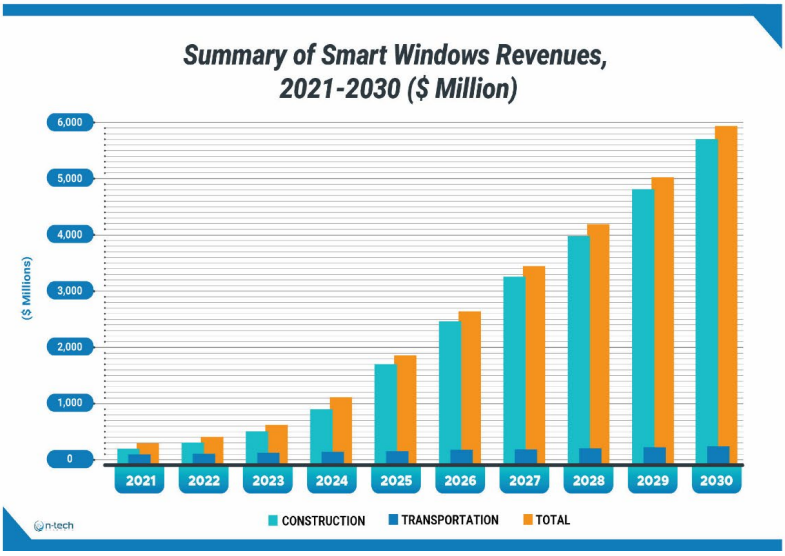

Figure 1.3: (a) A smart window installed in a building with 2/3 of the panels in the on state and the other 1/3 in the off state [2] **(b) future market projection of smart windows** [10]**.**

The vast majority of electrochromic smart windows use metal oxide layers such as ITO and fluorine-doped tin oxide (FTO) as the transparent electrode [2]. Although they have good transparency in the visible region, these layers have much lower transparency in the NIR range, which blocks much of the solar heat that could otherwise enter a building in the winter. As will be shown in Chapter 5, an ITO layer that is 96% transparent in the visible is only 35% transparent at a wavelength of 2500 nm. Because two ITO electrodes are used in a smart window, the electrodes alone can block most of the radiation in the NIR region. FTO has even lower transparency than ITO in the NIR [16]. Therefore, solar heat gain in the winter is limited. Replacing the metal oxide layers with alternative transparent conductive materials that are more transparent in the NIR would lead to higher energy efficiency. The high cost of ITO is also an issue. A schematic of the transparency of the smart window in the on and off state, in hot and cold climates, is shown in Figure 1.4(b).

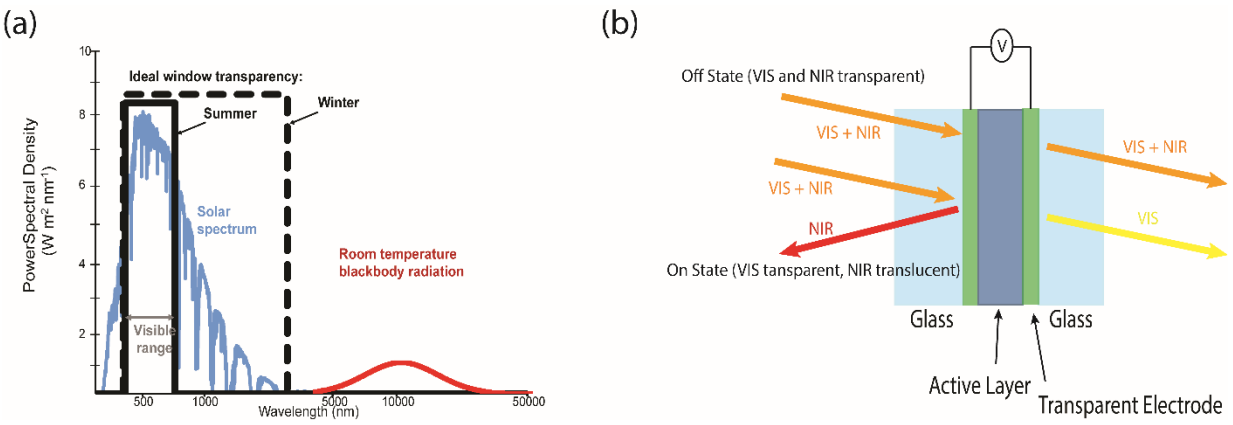

Figure 1.4: (a) The solar spectrum (blue curve) that is transmitted through earth's atmosphere and the ideal spectral selectivity in both hot and cold weather. (b) Schematic of a smart window showing an active layer between two transparent electrodes. Ideally the window should transmit NIR wavelengths in the winter, when the window will be in the off-state, and block NIR wavelengths in the summer (on-state). Transmission of larger longer IR wavelengths are blocked in either state.

1.4 Transparent Electrodes

Transparent electrodes are a required component of electrochromic devices to create an electric field across the active layer, while at the same time being transparent to the desired electromagnetic radiation wavelengths that will transfer through or reflect from the device. Most electrochromic devices use doped metal oxides as the transparent conductor, most commonly indium ITO, but FTO and aluminum zinc oxide (AZO) are used as well [17]. ITO can have a relatively low resistivity (e.g. sheet resistance of ~30 Ohm/sq) while being transparent in the visible (> 85%) [17]. These metal oxides are far from ideal, however. They are deposited using either a pyrolytic process or high vacuum process at high temperatures using specialized equipment. This, combined with the high cost of indium, makes ITO expensive. Furthermore, deposition on plastic substrates, like the commonly used polyethylene terephthalate (PET), is limited to temperatures < 150 °C [18]. As this is far lower than the ideal deposition temperature (~ 300 °C), metal oxide resistivities on plastic substrates are worse than on glass [19]. Metal oxides are also brittle, and thus not ideal for up-and-coming flexible electronic applications; the films crack upon repeated bending, causing resistance to increase [20]. A less discussed disadvantage of metal oxides is their low transparency in the near infrared (NIR) region, which as briefly discussed above, limits the amount of solar heat that can pass through an electrochromic window in the winter.

Transparent electrodes are also widely used in many other optoelectronic applications including touch panels [21], liquid crystal displays[22], light emitting diodes [23] and solar cells [24]. Metal oxides are predominantly used in these applications as well, but due to their drawbacks and the advancement of nanomaterials and processes, several materials have been studied as possible alternative transparent conductors. These include carbon nanotube networks, graphene, conductive polymers, and metal nanostructured grids and meshes. Many of these options are cheaper, printable and mechanically flexible. Each of these materials will be briefly reviewed in Section 1.4.2. But first we define the important metrics used to evaluate transparent electrodes: transmittance, haze, and sheet resistance.

1.4.1 Transparent Electrode Figures of Merit & Characterization Techniques

Transmittance

When light from a light source encounters an object or sample, the incident light can be transmitted, absorbed or reflected. The ratio of transmitted light to incident light is defined as the total transmittance of the object, T_t, typically stated as a percentage. It is measured with a light detector that consists of a material

sensitive to the wavelength of light from the light source. The transmittance of an object can vary in response to the wavelength of the incident light. Hence, when reporting the value of transmittance for an object, the wavelength must be mentioned. Typically, when the transmittances of devices or films in this work are discussed, the wavelength will be at 550 nm, in the middle of the visible spectrum, unless otherwise stated. The wavelength of 550 nm is used as this is the wavelength that the human eye is most sensitive to [25]. Additionally, the transmittance given is that of the film-only, not the film plus the glass or plastic substrate, unless otherwise stated. In this, the total transmittance T_t is measured with an integrating sphere. The sphere is represented by the black semicircle in Figure 1.5. The total transmittance is defined as $T_t = T_d + T_s$ where T_d is the diffuse transmittance (light detected that is transmitted through the sample but scattered away from normal incidence) and T_s is the specular transmittance, taken at normal incidence.

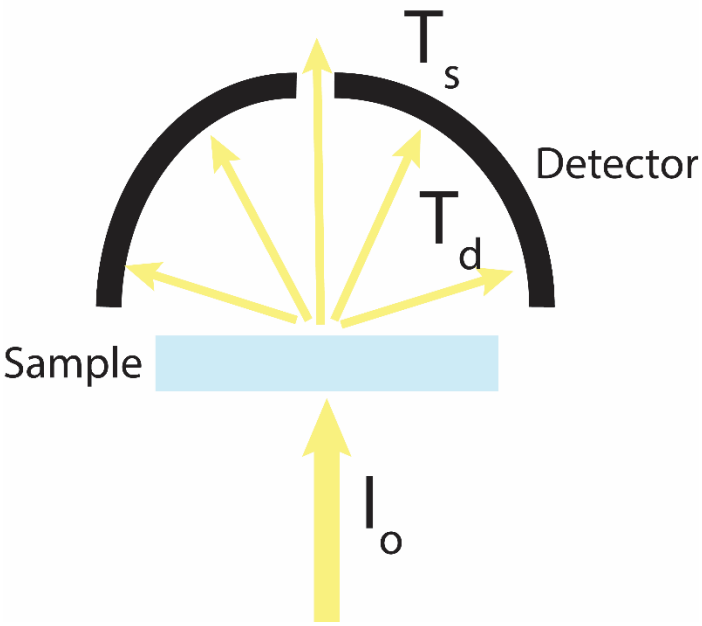

Figure 1.5: Schematic of the experimental setup used to measure the transmittance and haze of a sample.

Haze

For applications such as electrochromic displays and smart windows, the electrode's haze is important as it affects the quality of the image or the amount of distortion we see when we look through the device. Haze is defined as

$$Haze = \frac{T_t - T_s}{T_t} = \frac{T_d}{T_t} \quad (1.1)$$

An acceptable value for the haze measurement of a window or display is typically < 10% [39-41].

Sheet Resistance

Sheet resistance is a common measure to determine how electrically conductive a film is and is the predominant way to characterize the resistance of transparent electrodes. It is related to resistivity through Equation 1.2:

$$R = \frac{\rho L}{Wt} = \frac{R_S L}{W} \tag{1.2}$$

where W is the width of the film, L is the length of the film along which current flows, t is the film thickness, ρ is the material resistivity, and R_s is the sheet resistance of the film. Thicknesses of films can be difficult to measure or even impossible to define in some cases, thus sheet resistance where film thickness are not needed is the industry standard. Defining a thickness is particularly difficult for electrodes made up of nanowires, nanotubes or grids because the "film" is not uniformly thick. Sheet resistance has the units of Ω/sq. It is most commonly measured with a 4-point probe system. The system consists of 4 probes all in the same plane with the same spacing between each probe. The two outer probes are used to apply a current and the induced voltage is measured between the two inner probes. This avoids the contact resistance issues incurred in a 2-probe measurement.

Due to the randomness of the nanowire films in this work, five measurements using different orientations of the substrate over 4 different samples were averaged to calculate the sheet resistance of each sample.

1.4.2 Alternative Transparent Electrode Materials

There are currently a few noteworthy materials that have been proposed for substitution of ITO in devices. They include carbon nanotubes, graphene, transparent conductive polymers, metal grids, and random meshes of metallic nanowires. These are discussed below.

Carbon Nanotubes

Transparent electrodes can be formed when carbon nanotubes are deposited as a random mesh. The electron mobility of a single nanotube has been shown to reach more than 100 000 cm^2/Vs [26]. Even though the current must flow from one nanotube to the next, the junction resistances of overlapping nanotubes has been shown to be very high [27]. This results in quite poor sheet resistance (eg. >1000 Ω/sq at 90% transparency [28]). Additionally, when carbon nanotubes are synthesized, both metallic and semiconductor

tubes are formed, and it is not easy to separate these different tubes. The semiconducting tubes have a high resistance and hence do not contribute much to overall film conductivity, while at the same time lower transparency [17].

Graphene

Graphene is made up of a film of hexagonally bonded carbon atoms that are only one atom thick. Because of the very low thickness of the graphene, the transparency in the visible and NIR is high. Graphene has the capability of adding external dopants in order to increase film conductivity [29]. However, fabricating a single sheet of graphene over large areas is expensive and requires chemical vapour deposition [30]. Furthermore, because of the high deposition temperature it cannot be directly fabricated on most flexible substrates. Transferring from a growth substrate over to a flexible substrate is an option, but this is complex and would be difficult to scale. On flexible substrates it is more common for an electrode to consist of overlapping graphene flakes. These films are much thicker and the resistance at the junctions between flakes is on the order of several kΩ [6] Hence, the sheet resistance is not good enough to be used in most applications.

Conductive Polymers

Transparent conductive polymers are highly flexible, low cost, and light weight. They have been integrated into industrial devices. The most common transparent conductive polymer is PEDOT:PSS which has been used and studied extensively in organic electronics. However, it is not as conductive as ITO at a given transparency (eg. 400 Ω/sq at 85% transparency [31]) and does not have long lifetimes. Additionally, it has poor transparency in the NIR region. For example, a PEDOT:PSS transparent electrode that is 85% in the visible is only 27% transparent at a wavelength of 2500 nm [32].

Metal Nanostructures

Metal nanostructured grids are a good alternative material to metal oxides as a transparent conductive film. The dimensions of the grids can be easily controlled in order to change the sheet resistance of the film. They can have as high a transparency in the visible as ITO, at an even lower sheet resistance [33]. However, they are fabricated using lithography which is expensive and not easily scalable to large areas, making metal grids inappropriate for flexible electrochromic devices.

1.5 Silver Nanowire Electrodes

A major focus of this work is to research an alternative transparent electrode to metal oxides for electrochromic devices that is cheaper, simpler to deposit, has a deposition temperature compatible with plastic substrates, can tolerate mechanical strain, and is more transparent in the NIR. For reasons to be outlined in Section 1.5.2, silver nanowire networks are identified as the most promising technology. These networks are composed of wires that are 30 ~ 120 nm in diameter and 3 to over one hundred micrometers in length [34]. They are synthesized and stored in a solution until they are printed in a random network on a substrate as shown in Figure 1.6. The nanowires overlap each other and form junctions in order to create an electrical pathway for electrons to flow from one side of the network to the other.

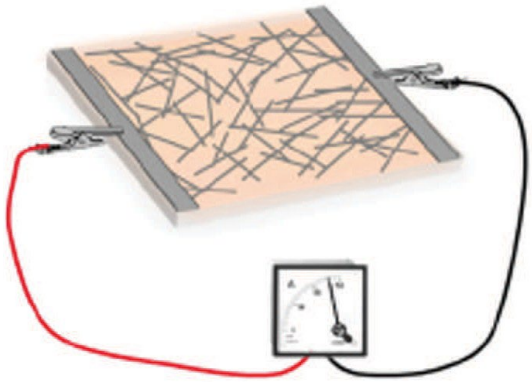

Figure 1.6: If the density of nanowires on a substrate is high enough, a conductive path can exist from one side to another. And because only a fraction of the surface is covered, the film is visibly transparent [schematic courtesy of former groupmate Alexandra Madeira].

1.5.1 Synthesis of Silver Nanowires

There are several methods to synthesize silver nanowires, but in recent years the polyol method has become the most popular and is widely used in industry due to its simplicity, low cost and high yield [35], [36]. There are variations in the method, but a typical one involves a solution of ethylene glycol (EG), poly (vinyl pyrrolidone) (PVP), and NaCl (salt) heated to an elevated temperature (~170°C) [35], [36]. A mixture of silver nitrate ($AgNO_3$) and EG is slowly added to this first solution [35], [36]. This creates Ag^+ ions which in turn forms Ag nanoparticles. The PVP has a stronger interaction with the Ag {100} planes and passivates them [35], [36]. This results in a slowing down of the addition of

silver onto these surfaces. This means the {100} facets grow much quicker than {111}, leading to the growth of a one-dimensional wire structure as shown in Figure 1.7 [35], [36]. The end result is crystalline silver nanowires with a pentagonal cross section, with five twin planes extending along the length [35], [36]. The nanowires have an orientation along the <110> direction, the sidewalls are {100} planes, and the two ends of the nanowire are bounded by {111} facets [35], [36]. Some control over diameter and length is achievable, with diameters being as small as 20 nm and lengths being up to 150 μm or more [35], [36].

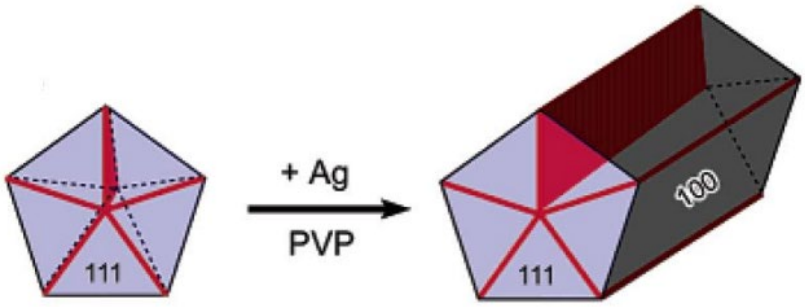

Figure 1.7: Crystallographic facets of silver nanowires grown via the polyol method [35]**.**

1.5.2 Properties of Silver Nanowire Electrodes

Silver nanowire electrodes have been identified as the most promising alternative to metal oxide electrodes [34] and have many advantages. Silver nanowires can be synthesized in solution in large batches, then easily printed as electrodes in atmosphere using high-throughput roll-to-roll methods, at room temperature if desired. Random meshes of nanowires are printed using standard solution deposition techniques such as rod coating or spray coating [34]. As is always the case for transparent conductive materials, there is a trade-off between conductivity and transparency – at higher nanowire densities, the conductivity improves but the film is less transparent.

Unlike carbon nanotubes, all the nanowires are metallic, and the overlapping nanowire junctions can be sintered or welded to achieve relatively low junction resistances. As will be shown in Chapter 2, the resulting sheet resistance and transparency values of silver nanowire networks are similar to ITO on glass, and better than ITO on plastic. Figure 1.8 compares the sheet resistance and transparency of silver nanowire electrodes to other alternative materials. Silver nanowire electrodes have better sheet resistance and transparency compared to copper nanowire networks, graphene, CNT networks and

conductive polymers liked PEDOT:PSS [32]. Lithographically-defined metal grids can have a better sheet resistance but, as mentioned above, are not appropriate for flexible electrochromic applications due to its high cost and limited scalability.

Silver is costly and the estimated material cost to synthesize silver nanowires is $32.50/g [37], much higher than the cost per weight of ITO of $2.40/g [38]. However, only very little silver nanowire mass is required to fabricate an electrode, especially for the high transparency electrodes used in electrochromic devices. Khaligh et al estimated that a 50 Ω/sq silver nanowire electrode had a material cost of $0.70/m^2, versus $1.60 for ITO of the same sheet resistance [22]. Furthermore, the fabrication cost of nanowire electrodes is cheaper and more convenient than ITO as they can be deposited using scalable, high-throughput solution deposition techniques in atmosphere and room temperature.

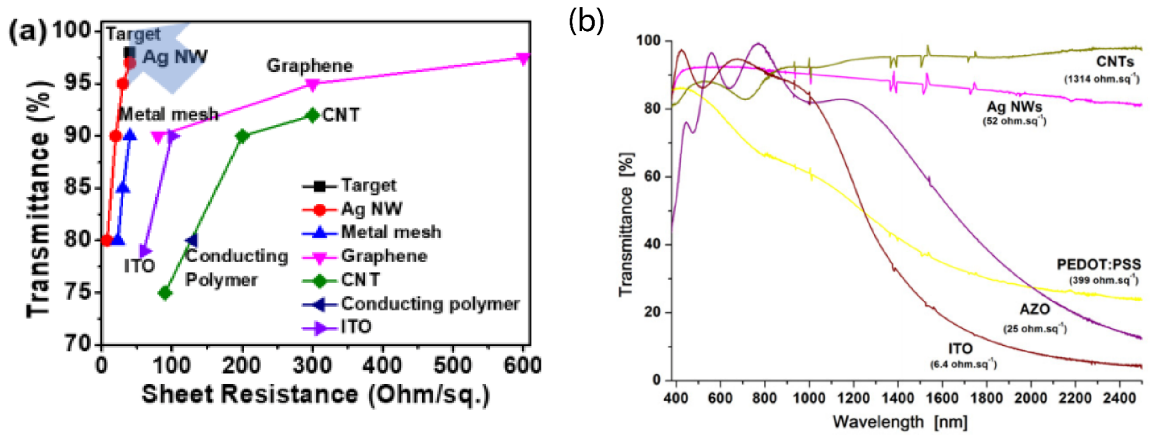

Figure 1.8: (a) Sheet resistance vs transmittance in the visible for alternative transparent conductive materials. These alternative materials do not have as high of a transmittance and low of a sheet resistance as silver nanowire networks [39]**. (b) Many transparent conductive materials are fabricated to have high transparency in the visible region, however, the transmittance of many transparent conductive materials in the near infrared is low** [40]**.**

Since the fabrication of silver nanowire networks can be completed at low or even room temperature, it is fully compatible with plastic substrates. The nanowire networks are highly flexible, and it has been shown by several groups that they incur very minimal resistance increase after being put under repeated strain [41]. For example, after 500,000 cycles of being put under 4% strain, the sheet resistance of a silver nanowire electrode increased by < 20%, compared to > 100,000 % for ITO [42].

Another advantage of silver nanowires which has so far received minimal attention is their high transparency in the near infrared region. This is not only highly desirable for smart window applications

but for other applications as well such as multi-junction solar cells, photodetectors for biosensing [43] and switchable electrochromic devices for optical communications [44]. The transmittance of ITO and other metal oxides decreases exponentially at wavelengths above 1000 nm, due to the surface plasmon resonance (the collective oscillation of free electrons in the conductive band) (Figure 1.8(b)) [45]. Silver nanowires have a plasmon resonance as well, but it is in the UV region of the electromagnetic spectrum, causing silver nanowires to be much more transparent in the NIR region than ITO. Additionally, as shown in Figure 1.8(b), the transparency of silver nanowires is far superior in the NIR than alternative materials at a given sheet resistance. Carbon nanotubes and graphene have a slightly higher transparency at NIR wavelengths, but their sheet resistance is poor. It will be shown in Chapter 5 that silver nanowire networks that are 96% transparent in the visible, for example, can have transparency as high as 94% at a wavelength of 2500 nm (compared to 35% for ITO).

In summary, silver nanowire electrodes address the many issues of ITO for electrochromic devices: they are less expensive, have a simple low temperature roll-to-roll compatible fabrication process, have similar sheet resistances on plastic compared to glass, are mechanically flexible and have high transparency in the NIR region in addition to in the visible.

1.6 Silver Nanowire Electrodes in Electrochromic Devices

Silver nanowire transparent electrodes have received much attention in the past decade and have been demonstrated for use in many devices such as solar cells [24], organic light emitting diodes [23], liquid crystal displays [46] and transparent heaters [47]. Several companies including Lenovo and LG have used silver nanowire networks as the transparent electrode for commercial devices, namely touch sensors in PCs and tablets [48]. Research on the use of nanowire electrodes in electrochromic devices, however, is limited and more study is needed on appropriate passivation materials, how the electrodes affect electrochromic device performance, and how to design the electrodes to improve this performance. Below we review the literature of silver nanowires in devices relevant to this work: PEDOT:PSS electrochromic displays and in electrochromic smart windows.

1.6.1 Silver Nanowires in PEDOT: PSS Electrochromic Displays

To date, there have been a few studies that have made PEDOT:PSS based electrochromic displays/devices using silver nanowire networks as the electrodes. Lin et al. made such a device that operated in transmission mode (changes its transmittance instead of reflectance upon the application of a voltage) [49]. However, the PEDOT: PSS was separated from the AgNWs by an electrolyte layer which could lead to longer switching times and higher switching voltages due to the PEDOT:PSS not having direct contact with the much more conductive AgNW electrode. Also, they only showed characterization results for the first 10 cycles of operation. Lee et al. also successfully used AgNW electrodes to make a PEDOT:PSS based electrochromic device, in this case one operating in the reflectance mode. It had an excellent reflectance difference between the on and off states, but this dropped by 20 percentage points after 500 cycles. It is now well known from this and other application areas that silver nanowires corrode [50], causing device performance to degrade over time. Passivation of the nanowire electrodes is critical for their real-world use.

A few subsequent PEDOT:PSS-based electrochromic studies did passivate the AgNW electrodes, resulting in far more stable devices. Both Kim et al. and Deng et al. used graphene encapsulated AgNW electrodes in PEDOT:PSS electrochromic devices [20], [51]. Kim's device has a transmittance modulation (ΔT) of 15% and showed that the electrochromic properties stayed consistent throughout 500 cycles. Deng's device had a ΔT of 20% for up to 10,000 cycles whereas the ΔT of a device using unpassivated nanowire electrodes reduced to 5% after only 10 cycles. Yu et al. used PMMA as a AgNW network passivation [52]. A layer of PEDOT:PSS and a gel electrolyte were used to fabricate an electrochromic device with these passivated electrodes in transmittance mode. The transmittance modulation was found to be 18% with switching on and off times of 8.5 and 6 seconds, respectively. The device also showed a high degree of stability over 200 off/on cycles with the transmittance change undergoing next to no difference between the 1st and 200th cycle. However, improvement can be made on the optical modulation or change in transmittance of the device as it only changed by 18% where other studies have shown better. Additionally, the surface roughness of the PMMA on AgNW films were not measured. If this is large, it can result in device performance issues.

The above works show the promise of using AgNW networks in PEDOT:PSS based electrochromic devices, but more study is needed before AgNWs can be used in industrial applications. Most papers, especially the ones where a passivation is used, focus on the fabrication, properties of the nanowire electrode and only use the device as a demonstration, with little discussion of the device performance and

how the nanowire electrode effects it. No direct comparison of silver nanowire networks versus ITO in PEDOT:PSS devices in terms of all electrochromic figures of merit including stability, lifetime, turn-on voltage, switching time, colour change, and change in reflectance has been reported, and will be completed in this thesis. Secondly, a recent review paper by Huang et al. on nanowire electrodes in electrochromic devices identified long-term stability, surface roughness and performance reproducibility as key issues [53]. As mentioned in the paragraph above, graphene has been shown to be an effective passivation material, but in both cases, it was deposited by chemical vapour deposition which is costly, difficult to scale to larger substrates, and is highly inconvenient given that all other components of the device can be deposited by solution processible techniques in atmosphere. Also, graphene lowers the transmittance of AgNW electrodes without improving their conductivity, since the conductivity of graphene is so much lower than that of AgNW networks. For the PMMA passivated AgNWs, there was no long-term study of the change in sheet resistance. This needs to be done in order to show the long-term viability of the AgNWs since AgNWs can oxidize over time. Additionally, as mentioned above, the surface roughness of the PMMA on AgNWs could be high. This can lead to short circuiting in a device. In this work, an inexpensive, solution-processible, scalable, polymeric passivation layer is coated over our AgNW networks to solve all three of the problems of stability, surface roughness and reproducibility. Thirdly, the mechanical properties of PEDOT:PSS based electrochromic devices with AgNW electrodes have not been directly compared to devices with ITO electrodes; the ITO electrode devices have just been stated to be insufficient. In this thesis, PEDOT:PSS devices made with ITO and passivated AgNW electrodes will have their mechanical properties compared and contrasted directly.

A limitation of PEDOT:PSS as an electrochromic material is its low conductivity. To improve the conductivity of PEDOT:PSS itself and thus improve switching time, operating voltage, and current density, Gomes et al. mixed several conductive different conductive additives with PEDOT:PSS [54]. Out of the conductive fillers tested (graphite, graphene, silver nanowires and antimony doped zinc oxide), AgNWs were the most promising because they improved the sheet resistance of the PEDOT:PSS film the most with very little transparency drop. It was shown that mixing in AgNWs improved the conductivity, current density, and transition time of the device, though the change in absorbance was lower compared to pure PEDOT:PSS. The purpose of this paper was to compare conductive additives and did not focus on AgNWs. Thus films and devices made from mixed PEDOT:AgNWs were not fully characterized nor explored. Neither the effect of AgNW concentration nor the effect of NW diameter or length on the properties of the films and device performance was studied. Oxidation of the AgNWs was brought up as a concern but strategies to minimize it were not studied. The promise of mixing PEDOT:PSS with AgNWs in the electrochromic layer warrants further study and will be done so in Chapter 4.

1.6.2 Silver Nanowire Electrodes in Smart Windows

Silver nanowires have been reported as the transparent electrode in several smart windows technologies. When integrated into a smart window based on polymer dispersed liquid crystals, the window was desirably more transparent in the on-state and less transparent in the off-state compared to the same device using ITO electrodes [22]. The turn-on voltage was also less. Regarding electrochromic windows, there have been a few studies that have examined integrating silver nanowire electrodes into tungsten oxide devices [55]–[57]. The nanowire electrodes had improved sheet resistance at the same transparency as ITO, resulting in a significant improvement in the switching time and the optical modulation in the visible region. For example, Mallikarjuna et al. used graphene oxide coated AgNW electrodes in WO_3 smart windows and found that the switching time improved from 15 seconds to 9 seconds, compared to the same devices with ITO [20]. Zhou et al. successfully used unpassivated silver nanowire electrodes for a non-ion storage containing electrochromic smart window and reported that the electrodes increased the transmittance modulation between the on and off states to 57% compared to 43% when ITO was used [56]. These studies provide evidence that silver nanowire networks are a viable alternative to ITO in smart windows. Not only can NW networks be cheaper and easier to deposit than ITO, but the smart windows built on them can have better performance.

One performance aspect that has not been investigated in detail with regards to window performance metrics is the higher NIR transparency of AgNW networks compared to ITO. As was mentioned in Section 1.3, using a transparent electrode that is more transparent than ITO in the NIR can improve energy efficiency in varying climate locations like Canada where the outside temperature can vary between -40C and +40C. Figure 1.9 shows the ideal electrochromic smart widow operation in the summer and winter. The window should block some visible radiation and this solar heat in the summer and allow high visible and solar heat (NIR wavelengths) transmission in the winter to reduce building heating costs. However, if the transparent electrode is not very transparent in the NIR region, like ITO, much of the solar heat is blocked by the two electrodes. An electrode material that is very transparent in the NIR, like AgNW networks, will permit more solar heat to enter a building. The AgNW electrodes will not sacrifice cooling efficiency in the summer as NIR wavelengths will be blocked from the active layer of the electrochromic device when in the on-state.

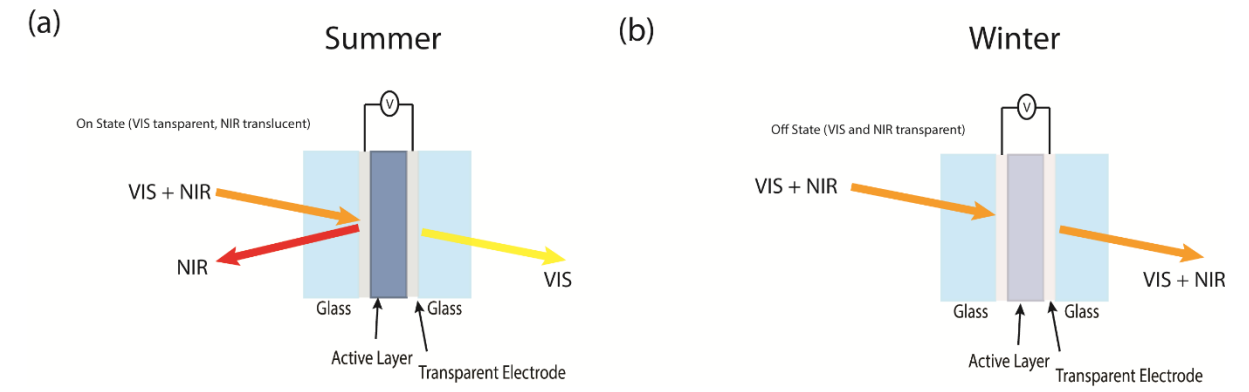

Figure 1.9: In both summer and winter, the electrochromic window should be semi-transparent to the visible. However, in the summer (a) the electrochromic window will be in the on state to reflect some visible and NIR wavelengths, while in the winter (b) the electrochromic window will be in the off state, allowing visible and NIR transmission to assist in the heating of the building.

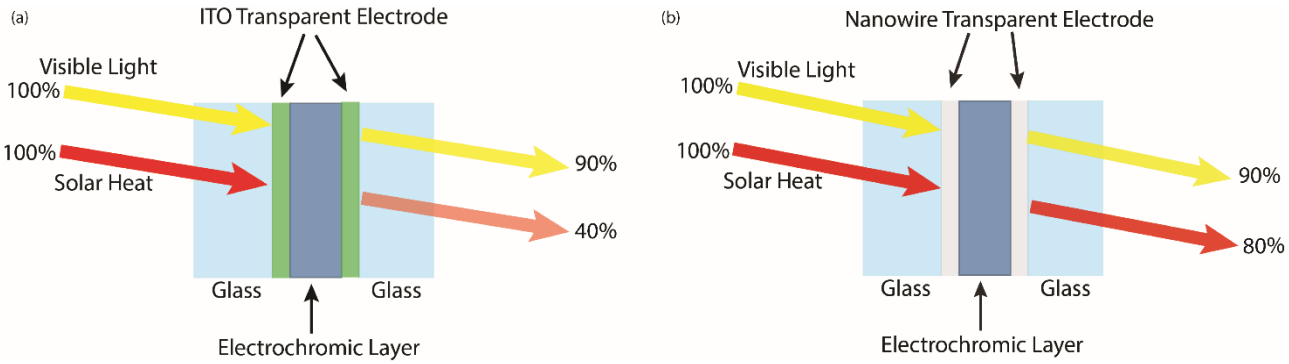

Figure 1.10: An electrochromic window in the winter/off-state using (a) ITO and (b) AgNWs as the transparent electrodes.

The increase in the NIR transparency could be as high as 40 percentage points, just by replacing the ITO with silver nanowire networks while the transparency in the visible remains the same. This is illustrated in Figure 1.10 for a device with ITO electrodes (a) and silver nanowire network electrodes (b). Additionally, using AgNW electrodes could allow for devices to be fabricated on flexible substrates and then in turn retrofitted to existing windows, lowering the cost significantly instead of installing a new window.

The transparency of silver nanowire networks in the visible region has been extensively studied, and there exists a few papers on their transparency to infrared wavelengths > 5 μm [58], [59]. However, there are no studies focusing on the properties of silver nanowire networks in the NIR region. Therefore, in Chapter 5 a study will be completed showing how nanowire networks can be designed to maximize their NIR transparency, and in Chapter 6, how the NIR transparency can improve the performance of electrochromic

smart windows will be investigated. Additionally, the lifetime and stability at high and low temperatures of smart window devices with passivated AgNW electrodes has yet to be studied and will also be looked into in Chapter 6.

1.7 Electrochromic Device Characterization Techniques & Figures of Merit

The performance of electrochromic devices using AgNWs will be assessed through the typical figures of merit used for electrochromic devices. These are: colouration efficiency, colour change, response time, transmittance on/off ratio and cycle life. Cyclic voltammetry, cyclic amperometry, ellipsometry, and spectrophotometry are characterization techniques used to acquire the figures of merit. Each of these will be described briefly below.

1.7.1 Characterization Techniques – Electrochromic Films & Devices

In order to test the optical and electrical properties of electrochromic films and devices, cyclic voltammetry (CV) is required. It is noted that in electrical engineering, C-V plots often refer to capacitance-voltage measurements and J is used for current density. However, in electrochemistry and this work, the CV abbreviation strictly refers to cyclic voltammetry. Cyclic voltammetry is a widely known electrochemical technique that is used for various optoelectronic devices. Cyclic voltammetry analysis mainly measures the current that builds up in an electrochemical cell. An electrochromic cell consists of three electrodes: the working electrode (WE), counter electrode (CE), and reference electrode (RE) [60]. The working electrode is the sample electrochromic film being measured, the counter electrode forms a closed circuit, and the reference electrode allows the voltage to be accurately applied to the device to measure the current. When taking the CV curve of an electrochromic film-only (i.e. one transparent electrode with an electrochromic film on top), the samples are placed in an electrolyte to conduct electrons or ions and measure a current. This is illustrated below in Figure 1.11(a). For device measurements, where the entire five-layer device is fabricated with two transparent electrodes, a primary electrochrome, ion storage layer, and solid or gel electrolyte, it is slightly different. The counter electrode and reference electrode are connected together and hooked up to one side of the device while the working electrode is connected to the opposite side of the device. This is illustrated in Figure 1.11(b).

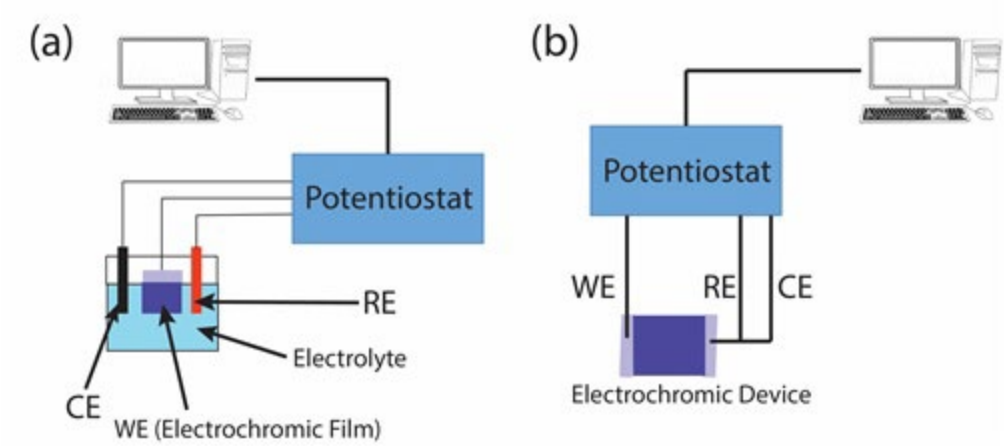

Figure 1.11: Schematic showing the experimental setup for a cyclic voltammetry (CV) measurement of an electrochromic film (a) and an electrochromic device (b).

During characterization, the current is measured while the voltage of the sample is ramped up to a certain value. The voltage is then reversed, and the current is measured as the redox reaction reverses and returns to its original state. A typical CV curve is shown in Figure 1.12(a), where the cycle direction is shown and the peaks where oxidation and reduction occur are indicated. The curve in a cyclic voltammetry experiment should be a closed loop. The purpose of this experiment is to determine the stoichiometry and the stability of the redox reaction as well as to observe the presence of any intermediate molecules that may form.

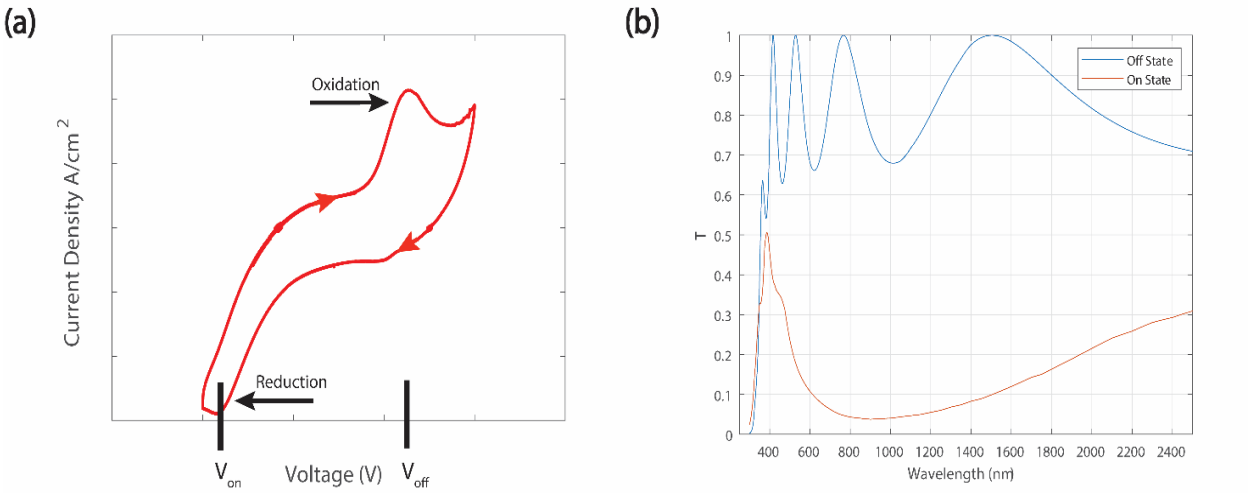

Figure 1.12: (a) The cyclic voltammogram plots voltage applied vs measured current at the working electrode (WE). (b) The transmittance, T, of a WO_3 film measured in the on and off state.

The kinetics of an electrochromic film or device is also very important. To do this, the chromoamperometry (CA) curve must be measured. This involves applying a constant potential (at the magnitude of the switching voltage, as determined from the CV) on the working electrode film and then measuring the current at the working electrode versus time. This information is important for measuring switching time and colouration efficiency of the electrochromic film or device.

Spectrophotometry measures the reflectance and transmittance over a range of wavelengths in the ultraviolet, visible, and near infrared regions of the electromagnetic spectrum. An example transmittance spectrum is shown in Figure 1.12(b). This provides information about the change in reflectance or transmittance of films or devices in the on or off state.

Ellipsometry measures the reflectance at a variety of angles in the visible region of the electromagnetic spectrum. This information is then used to measure the refractive index and extinction coefficient of thin films.

1.7.2 Figures of Merit

Colouration efficiency

The colouration efficiency (ξ) is an important figure of merit in electrochromic materials which measures the amount of colour change that occurs per amount of charge consumed by the electrochomic device. It is mathematically defined as

$$\xi = \frac{\Delta OD}{Q * A} \tag{1.5}$$

ΔOD is the change in the log of the transmission percentage when the device is turned on and off, Q is the charge density passed through the active electrochromic layer, and A is the area of the device. The charge, Q, can be found from the total area under the CV curve [1]. Mathematically this is represented by

$$Q = \int I \, dt \tag{1.6}$$

where I is the current, and t is the time. ΔOD is calculated as follows

$$\Delta OD = -\log_{10}(T_b - T_c) \tag{1.7}$$

where T_b and T_c are the transmittance of the film in the bleached and coloured state, respectively. The values of the transmittances are taken at the wavelength where the difference between T_b and T_c is the greatest. Higher colouration efficiencies are better. The colouration efficiency of WO_3 for example is reported to be as high as 70 ξ/cm^2C^{-1} [1].

Colour change

The colour change between the on and off states, ΔE, can be used to evaluate colour contrast and help to determine the optimal thickness of the system. A colorimeter can measure the chromaticity parameters L^*, a^*, and b^*which are directly related to the colour of a film. It does this by sending specific wavelengths of light that are assigned to different colours to the sample and then it is reflected back to the detector. Using the Beer-Lambert Law, the absorbance is detected for each colour and compared to known values in a microprocessor and then assigned the parameters L^*, a^*, and b^*. The measurement is done in the oxidation and reduction state 5 times for 3 different samples, and the average was taken for each parameter value.

L^* is the intensity of the light or colour ranging from 0 – 100 as shown in Figure 1.13. a^* is how red or green a colour is: +a is redder while -a is greener. Finally, b^* represents how yellow or blue the colour is where +b is more yellow and -b is bluer. The values of a* and b* range from -128 to +127.

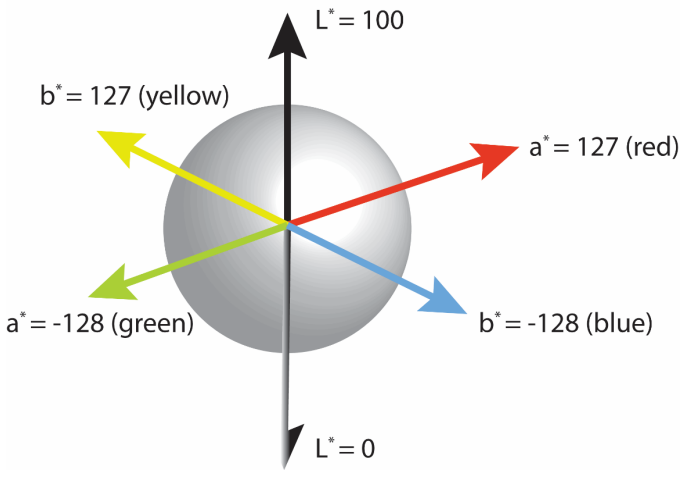

Figure 1.13: The chromaticity parameters to represent colour in electrochromic films.

When calculating the colour contrast between the on and off states, the equation for ΔE is

$$\Delta E = [(L^*_{red} - L^*_{ox})^2 + (a^*_{red} - a^*_{ox})^2 + (b^*_{red} - b^*_{ox})^2]^{1/2} \quad (1.8)$$

where the subscripts "red" and "ox" represent the electrochromic device in the reduced and oxidized state respectively [61].

Reflectance Difference

The difference in reflectance is another well-used way to define the contrast between the on and the off state of an electrochromic film. It is defined mathematically as

$$\Delta R = R_o - R_x \quad (1.9)$$

where R_o is the reflectance of the film/device in the off state and R_x is the reflectance of the film or device in the on state. The values for the reflectance are taken at the wavelength where the difference in reflectance between the on and the off state is the largest. It is usually defined as a percentage, such as 7%. The higher the value, the better the device performance. Values as high as 60% have been reported for polymer based electrochromic devices [61].

Switching Time

The switching time of an electrochromic device determines how quick the smart window can change from its bleached state to its coloured state. The typical response values reported for electrochromic devices are on the order of five to ten seconds, depending on the materials used in the active layers and transparent electrodes [61], [62]. The response time can be calculated accurately from the current applied to the electrode vs time curve when the device is switched on and off. It is defined as the time it takes for the measured current to reach 95% of its final value when the device is switched on or off [61]. This can be improved by having high conductivity in the transparent electrode and ion conducting layers.

Turn-On/Off Voltage

The ideal voltage window for an electrochromic material to work in is highly dependent on the materials being used. Ideally, the on-voltage should be as low as possible to conserve the energy needed to operate the device. The turn-on/off voltage is taken from the CV curve for the film or device. The on (off) voltage occurs at the voltage where the current reaches its valley (peak) value as shown in Figure 1.12(a).

Transmittance on/off Differential

The transmittance on/off values are more relevant for smart windows, unlike colour change and reflectance which are more relevant for displays. The difference in transmittance in the on and off state determines the maximum change in transparency the window can reach. The higher this value is, the better the performance of the window. However, it is still important to be able to see out of the window so the transmittance in the off state must be translucent enough in the visible for the human eye to see through the window. Figure 1.12(b) shows the simulated transmittance of an electrochromic WO_3 film in the on and off state.

1.8 Outline of this thesis

This research investigates if and how silver nanowires can improve the performance of electrochromic devices. In Chapter 2, after outlining how silver nanowire electrodes are fabricated and processed for this work, non-conductive passivation materials are investigated for use in electrochromic devices. Several non-conductive polymers are compared. The best performing one, polyurethane, is optimized as a nanowire electrode passivation layer and tested in an electrochromic device. Its impact on parameters including electric field uniformity, device performance and lifetime is evaluated through models and experiments. Next, these passivated silver nanowire electrodes will be integrated and evaluated in flexible electrochromic PEDOT:PSS displays on plastic and compared to the same devices on ITO (Chapter 3). In Chapter 4, silver nanowires will be mixed directly with PEDOT:PSS and shown that it improves device switching time and turn-on voltage. Additionally, passivation of the individual nanowires that are mixed with PEDOT:PSS will be discussed and implemented. After that, Chapter 5 presents the first in-depth study on the dependence of the NIR transparency of silver nanowire networks on nanowire diameter, length, and concentration. In Chapter 6, silver nanowire networks are used as transparent electrodes in electrochromic smart windows and their performance, particularly their ability to improve window efficiencies by better modulating solar heat, will be evaluated, and compared to the same devices with ITO electrodes. Finally, in Chapter 7 the results of this work will be summarized, and future work will be discussed.

Chapter 2

Nanowire Electrode Fabrication and Passivation

In this chapter the fabrication process of the silver nanowire electrodes is first presented and then the electrodes main figures of merit: sheet resistance and transmittance, are characterized. Their need for passivation is then discussed and four polymers are considered for this purpose. The impact of the winning passivation material, polyurethane, on the electric field above the nanowire electrode is studied both experimentally and with modelling. Finally, the passivated nanowire electrodes are integrated into an electrochromic display and its performance is compared to displays with unpassivated nanowire networks.

2.1 Nanowire Electrode Fabrication

Nanowire electrodes were fabricated on 2.5 cm x 2.5 cm BK7 glass (Ted Pella, # 26005, 1 mm thick) and 2.5 cm x 2.5 cm polyethylene terephthalate (PET) films (Dupont Inc., Tianjin, China, 127 μm thick). Silver nanowires dispersed in ethanol with nominal diameters of 30 nm, 70 nm, and 100 nm were purchased from Novarials Corporation (A30UL, A70UL, and A100UL, Woburn, MA). Silver nanowires dispersed in ethanol with a nominal diameter of 120 nm were purchased from ACS Materials (Pasadena, CA). The actual measured average diameters and lengths with distributions for all these nanowire diameter and lengths will be discussed in detail in Section 2.2. The longest, thinnest nanowires available were chosen for this and the next chapter. It will be shown in Chapter 5 that networks made from longer nanowires have lower sheet resistance, and networks made from thinner nanowires have smaller gaps between nanowires which should result in the most uniform switching when integrated into electrochromic devices.

The nanowire solution was diluted in ethanol depending on the desired film density. The silver nanowires were deposited on the substrates using the commonly used Mayer Rod technique (Figure 2.1): 40 μL of nanowire solution was pipetted at one end of the substrate, which was then drawn across the substrate with a Mayer rod (RDS #10). 4 coats were applied, with the substrate being rotated 90° between each coat to increase nanowire spatial uniformity across the substrate.

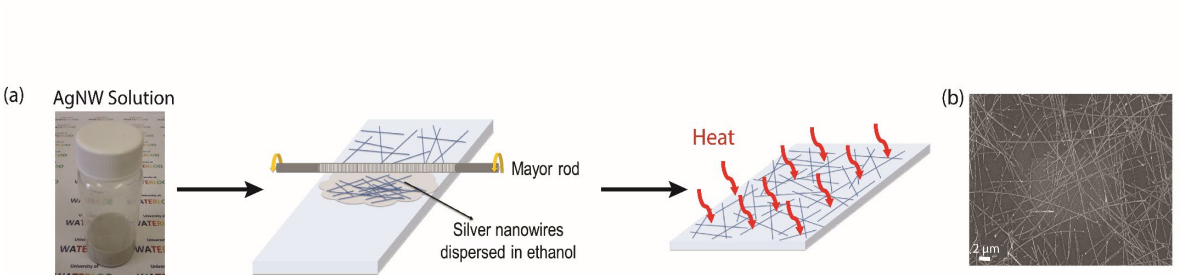

Figure 2.1: (a) Mayer rod coating nanowires on a glass substrate, followed by annealing in a vacuum oven. (b) SEM image of a silver nanowire network.

After coating on glass, the nanowire network was annealed for 30 minutes at 150 °C in a low vacuum oven in N_2 atmosphere. This welds the nanowire junctions and thereby reduces sheet resistance. For nanowires on PET, because the plastic substrate cannot tolerate temperatures around 150°C, an alternative method in place of thermal annealing was used to weld the nanowire junctions: mechanical pressure [63]. The electrodes were first passed once through a rolling press (MSK-HRP-01, MTI Coporation) at room temperature (Figure 2.2(a)). The rolling speed was 5 mm/s and the spacing between the rollers was 60 um. Then, the rollers were heated to 80°C where the PET can be softened, and the roller spacing was adjusted to 70 µm (Figure 2.2(b)). A second clean, PET substrate which was the same size as the electrode was placed on top of the electrode. This allows for a more even pressure to be applied across the sample. The covered electrode was then passed through the hot rollers two more times. The rolling press applies both heat and pressure which presses and welds the AgNWs together and into the PET, resulting in a reduction in sheet resistance and surface roughness (Figure 2.2(c)), and improves adhesion as well [63].

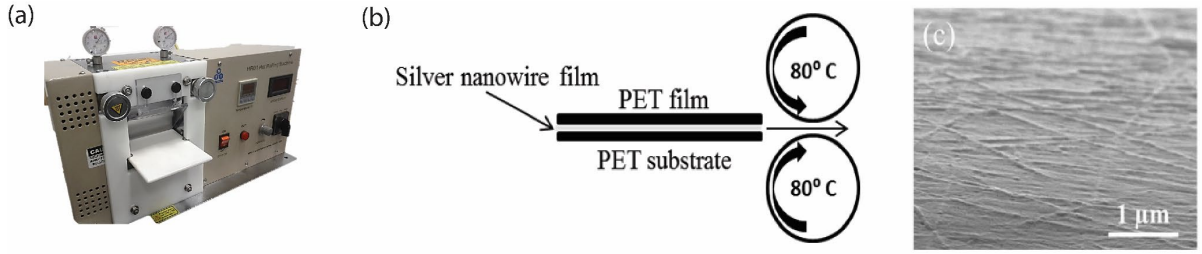

Figure 2.2: (a) The hot-rolling machine to roll the nanowires. (b) The silver nanowire film on the PET substrate is fed through the two rollers at 80°C in order to weld the nanowire junctions and push the silver nanowires into the PET to lower the surface roughness. (c) An 85° tilted SEM image of the pressed silver nanowire network on the PET film (image courtesy of former groupmate Hadi Hosseinzadeh Khaligh).

2.2 Nanowire Electrode Characterization

To determine the diameter and lengths of the nanowires, they were drop-cast and Mayer rod coated onto a silicon substrate at a relatively sparse concentration of 0.5 mg/ml. Then, SEM areal images were taken at different locations and magnifications. Using ImageJ software along with the ImageJ plugins DiameterJ and RidgeDetectionJ, the average length and diameter were calculated. DiameterJ adjusted the image to become a binary image (either black or white pixels) and then calculated the average diameter of all the NWs. RidgeDetectionJ measured the total length of all the NWs and then divided by the number of NWs in the image to get the average NW length. The distribution of the nanowire diameter and length are shown below in Figures 2.3 and 2.4, respectively. The average diameter and length along with the distribution are additionally shown in Table 2.1.

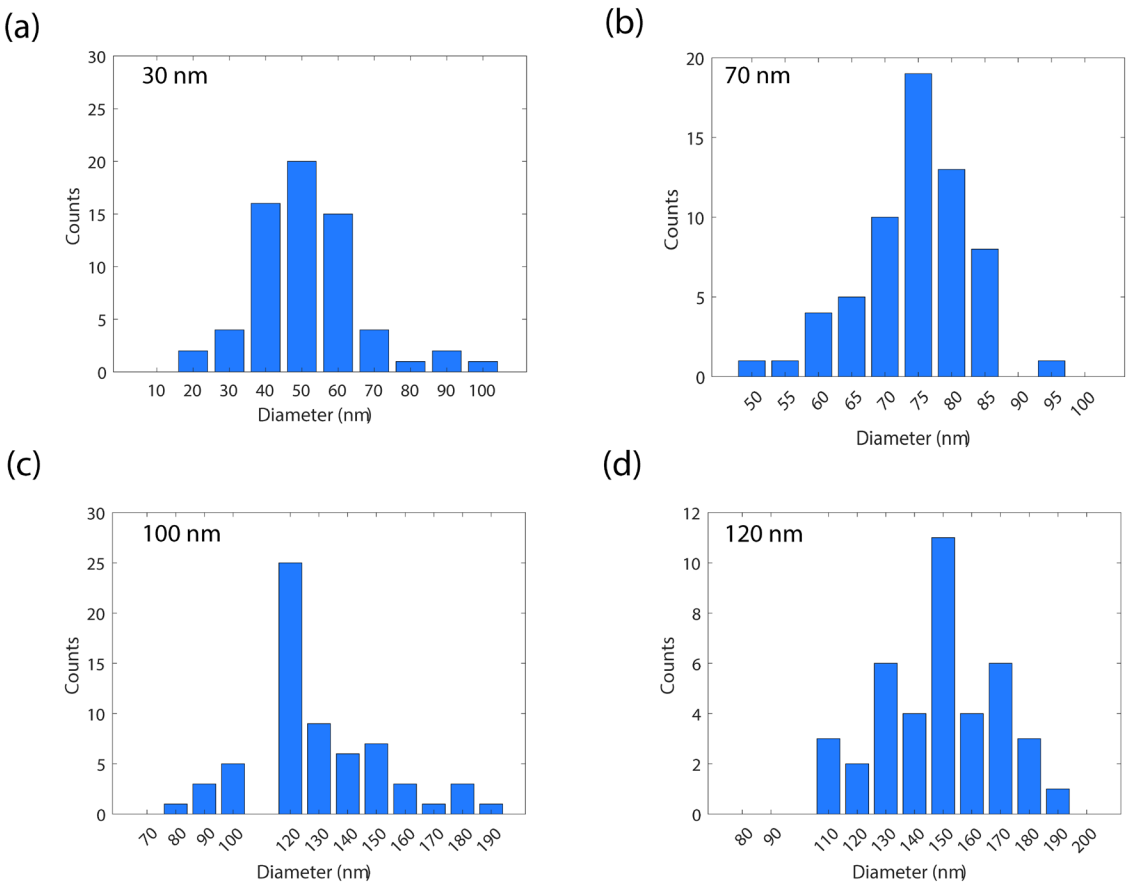

Figure 2.3: The nanowire diameter distribution calculated from ImageJ for nominal nanowire diameters of 30 nm (a), 70 nm (b), 100 nm (c), and 120 nm (d).

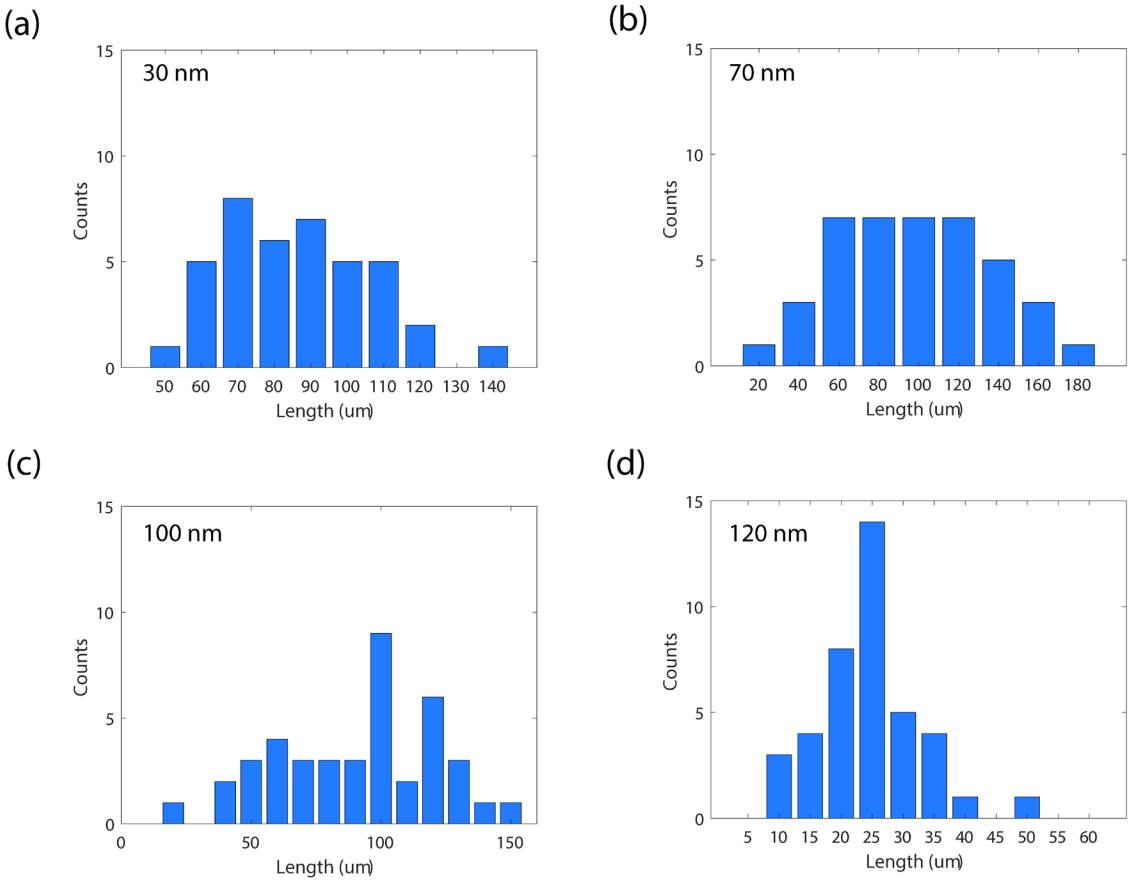

Figure 2.4: The nanowire length distribution calculated from ImageJ for nominal nanowire diameters of 30 nm (a), 70 nm (b), 100 nm (c), and 120 nm (d).

Table 2.1: The nanowire diameter and length distributions calculated from ImageJ for nominal nanowire diameters of 30 nm, 70 nm, 100 nm, and 120 nm.

	Diameter (nm)	**Length (μm)**
30 nm	49 ± 15	88 ± 19
70 nm	72 ± 8	88 ± 36
100 nm	123 ± 24	86 ± 31
120 nm	144 ± 20	22 ± 7.5

In order to determine how transparent the silver nanowire electrodes are, the transmittance was measured using a Perkin-Elmer 1050 Spectrophotometer. The measurements were performed at normal incidence with an integrating sphere at wavelengths of 400 – 800 nm. The transmittance of the substrate was subtracted from the total transmittance in order to determine the transparency of the nanowires alone. The resulting spectra are shown in Figure 2.5(a). Electrodes made with a higher nanowire concentration have a higher nanowire density and are thus less transparent. The dip in transmittance at lower wavelengths occurs from the collective oscillation of electrons from the surface plasmon resonance in silver, that occurs at a wavelength of 375 nm for 30 nm diameter silver nanowires [64]. Otherwise, the transparency across the visible range is quite flat. The properties of the transmittance in the near infrared (NIR) region will be discussed in Chapter 5.

The sheet resistance of the AgNW electrodes was measured using a four-point probe (Osilla, Sheffield, UK) as explained in Section 1.4.1. The resulting sheet resistance and transparency values at a wavelength of 550 nm are shown in Figure 2.5(b). The numbers above each point in the plot represent the concentration of silver nanowires in solution used to make the nanowire electrode. The sheet resistances were measured 5 times per sample and 5 samples were measured with a four point probe. The averages over all 25 of those measurements are show in the plot. As with any transparent electrode, there is a trade-off between conductivity and transparency. Denser networks of nanowires have higher conductivity (lower sheet resistance) but lower transparency.

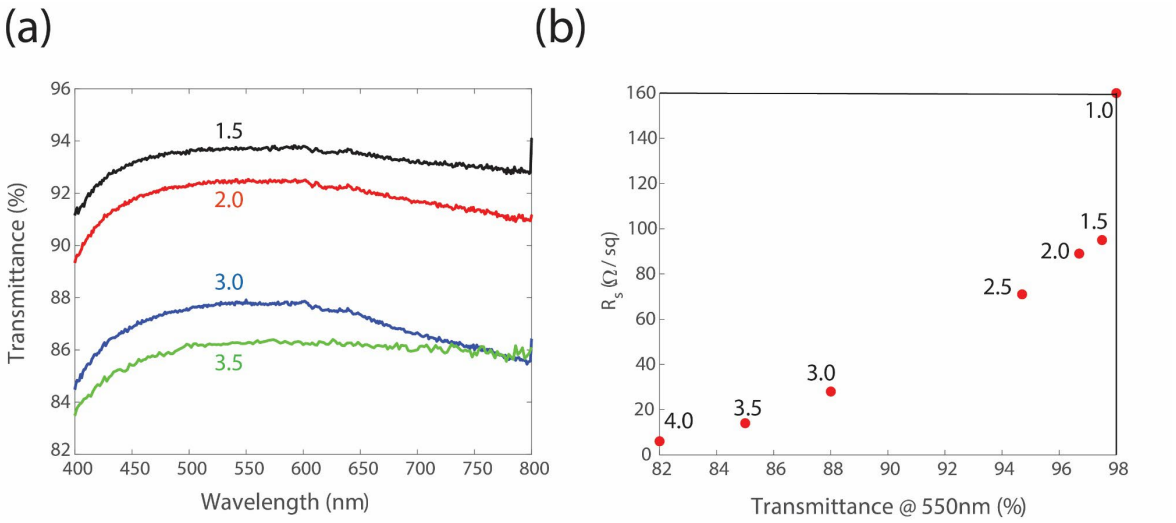

Figure 2.5: (a) The transmittance vs wavelength of nanowire transparent electrodes on PET made using solution concentrations ranging from 1.5 - 3.5 mg/ml. (b) The sheet resistance vs transmittance in the visible (550 nm) for nanowire electrodes on PET made using concentrations ranging from 1.0 – 4.0 mg/ml.

The performance of nanowire electrodes will be compared to ITO in Chapter 3. The transparency of the ITO (on PET) used was 88%, with an average sheet resistance of 45 Ω/sq. As such, a concentration of 3.0 mg/ml on PET was selected for this and the next chapter as it also has a transparency of 88%, with an average sheet resistance of 27 Ω/sq.

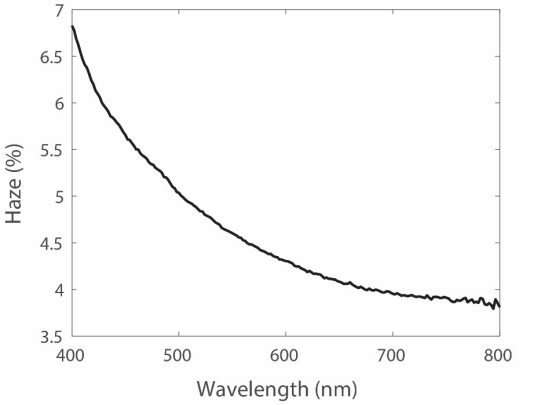

Figure 2.6: The haze for 30 nm diameter silver nanowire networks in the visible region at a concentration of 3.0 mg/ml.

Another important parameter of transparent electrodes is haze (defined and discussed in Chapter 1.6). The value of haze of a material is considered good enough to see through if it is less than 10%. Our chosen concentration meets the requirement of having a haze value of < 10% across all visible wavelengths (Figure 2.6) in order for objects on the other side of the electrode to not appear blurry.

2.3 Nanowire Electrode Passivation

2.3.1 The need for Passivation

Bulk silver is well known to oxidize over time. Deignan et al. showed that AgNWs also corrode due to reactions with hydrogen sulfide and carbonyl sulfide in the atmosphere [50]. In as little as two weeks, spherical particles appear on the surface of the nanowires (Figure 2.7(a)), and after longer time the nanowires can become discontinuous (Figure 2.7(b)). This of course has negative effects on the performance of AgNW electrodes. The conductivity of AgNW electrodes left in atmosphere decreases over

time and can become non-conductive after periods as short as 6 months [50]. It is important to increase the longevity of AgNWs because of the recent increasing interest in using AgNW networks as a replacement for ITO.

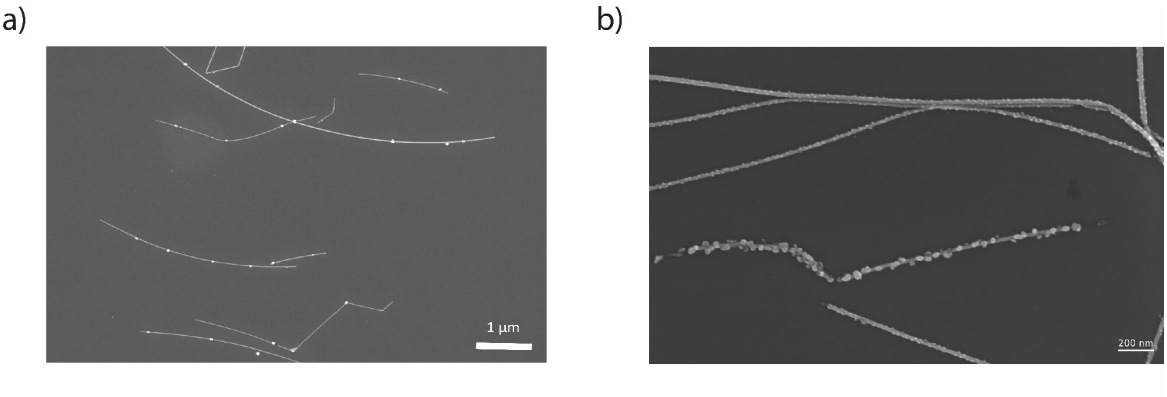

Figure 2.7: (a) Silver nanowire degradation after just two weeks in ambient conditions. (b) More significant silver nanowire degradation after 60 days in ambient conditions (both images courtesy of groupmate Geoffrey Diegnan).

Once the AgNW electrodes are integrated into devices, there are additional issues that can affect their stability and lifetime. One potential issue is Joule heating. Kaligh et al. showed that when a constant current density of 17 mA/cm^2 was applied across a AgNW electrode, the electrode would fail to be conductive after a time as short as two days [65]. However, in our smart window and electrochromic display devices, unlike other devices like solar cells, this should not be as prominent of an issue as the measured current densities from the CV curves, as will be seen later in the chapter and in chapter 3, are in the range of 0.1 – 0.5 mA/cm^2. However, even with the low current densities, the repeated cycling of an electrochromic device will still accelerate the oxidation/sulfidation of AgNWs. During cycling the voltage applied on the electrode is switched between positive to negative, causing electrons to be continually taken to and away from the silver in the nanowires. When Ag^+ ions are formed, they are much more susceptible to form silver oxide or silver chloride, both of which are non-conductive and significantly reduce the conductivity of the silver nanowire network.

Another problem associated with the electrochromic devices fabricated in this and the next two chapters, is the use of the conductive polymer, PEDOT:PSS specifically. Mayousse et al. show that the sheet resistance of AgNWs covered in a layer of PEDOT:PSS will have its sheet resistance increase by a factor of 480% after a period of 2 years [66]. This was attributed to the low pH of PEDOT:PSS (pH = 2.5) and the tendency of PEDOT:PSS to absorb water, which is known to accelerate the oxidization of silver.

Our goal is to provide protection for the silver nanowire electrodes from sources of oxygen and sulfur as well as PEDOT:PSS in order to increase their lifetime when used in devices.

2.3.2 Silver Nanowire Passivation Methods

There exist many studies on different types of passivation of AgNWs in order to improve their lifetime. The vast majority coat the AgNW network with an electrically conductive material. For example, for electrochromic displays and smart windows using AgNW electrodes, passivation materials that have been used include reduced graphene oxide, conductive polymers and molybdenum disulfide [20], [67], [68]. In one paper where nanowire electrodes were used in an electrochromic device, the authors stated that the nanowire passivation layer should be conductive in order for the electrode to be conductive between the gaps in the nanowire network (since the nanowire network is not a continuous film like ITO), to avoid the so-called "blooming effect" [68], [69]. The blooming effect is when there is non-uniform switching. Of specific concern would be a lower degree of colour switching at the locations above the nanowire gaps. However, in this chapter, it will be shown that even with a non-conductive passivation layer, electrochromic switching is uniform to the eye.

Using a non-conductive material as the passivation layer opens up a far wider choice of passivation materials, and as such, materials that are cheaper and easier to deposit do not reduce the transparency of the electrode and are mechanically flexible can be chosen. Transparent polymers are the perfect choice as they meet the just-mentioned criteria. There exists one study in the literature where an electrochromic device used a non-conductive polymer overtop the silver nanowires in the electrode [70], but the polymer (polyimide in this case) was mixed with the nanowires rather than coated on top. This mixing approach lowers conductivity of the nanowire network since the non-conductive polymer inhibits electrical contact between nanowires. And because the purpose of the polyimide in this study was to increase adhesion and AgNW dispersion, rather than reduce AgNW degradation, lifetime tests (i.e. resistance vs time) were not conducted. Other studies using AgNW electrodes for other types of devices have coated non-conductive polymers over nanowire networks, but in many cases the polymer layer was thick (> 500 nm) [71], [72]. A thick polymer is okay for some applications, like transparent heaters [47], but inappropriate for electrochromic devices as it would increase the voltage required to obtain a given electric field. In other cases, a polymer was coated over a nanowire network on glass or PET, cured, then the resulting

nanowire/polymer composite was peeled off the glass with the polymer as the new substrate [72]–[74]. The top surface of the AgNW network remains exposed so it can make electrical contact with the device layer. However, the peeling process is finicky and not amenable to scaling. Lastly, all works study only one passivation material, and it is difficult to compare between studies since they use different thicknesses and ageing conditions. Since different device applications require different properties (eg. material compatibility with the active material, flexibility, transparency in the NIR), having a selection of passivation materials is useful.

2.3.3 Passivation Requirements

In order to be a viable passivation layer for smart window and electrochromic display applications, there are several requirements that should be met:

(1) The passivation layer should not reduce, or only minimally reduce, the in-plane conductivity of the electrode.

(2) The electric field generated between the electrodes must also not be significantly reduced so that the ions in the active layer can still move from one side of the device to the other. Therefore, it is necessary for the passivation layer to remain thin enough for the electric field not to fall off significantly while still acting as a barrier layer to the PEDOT:PSS, oxygen and other ambient elements (Figure 2.8(a)).

(3) The passivation layer should be very transparent in the visible, and for smart window applications transparent in the NIR range as well to allow the passage of solar heat in the winter (Figure 2.8(b)).

(4) The passivation material should be inexpensive to synthesize and deposit. Ideally the deposition method should be scalable and solution-processible to align with the advantages of nanowire electrode fabrication.

(5) Since the nanowire electrode is mechanically flexible and, in the case of electrochromic displays, the PEDOT:PSS is also flexible, the passivation layer should also be flexible to enable a flexible device.

(6) The passivation layer should lower the surface roughness of the AgNW network. If the AgNW network is too rough, the device could short circuit and cause other problems such as the layers being deposited on top of the electrodes being non-uniform in thickness. The passivation layer should fill the holes between the nanowires in order to reduce the average surface roughness R_a (Figure 2.8(c)).

(7) The passivation material should not react and should otherwise be compatible with the active layer on top.

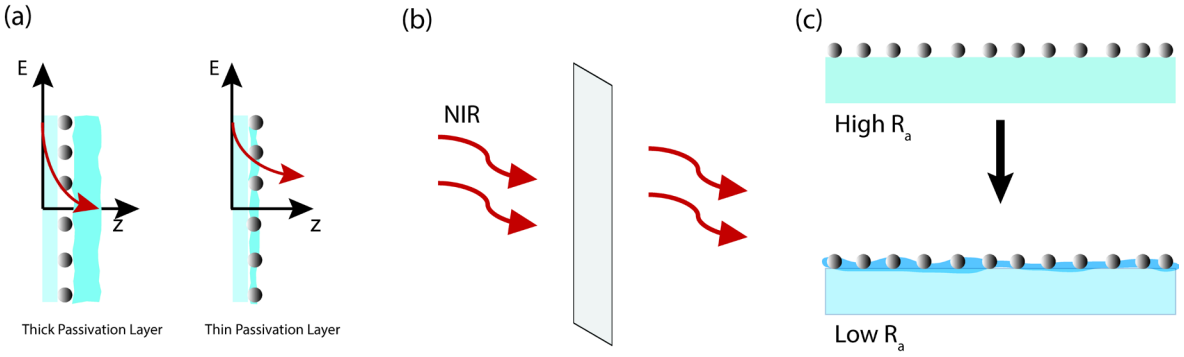

Figure 2.8: Some requirements of the passivation layer for the silver nanowire network are for it to (a) be thin so as not to significantly reduce the electric field generated between it and the other electrode, (b) have a high transparency (>90%) in the NIR and, (c) decrease the surface roughness of the network.

Four transparent polymers that meet the above requirements were identified. Poly(methyl methacrylate) (PMMA), cyclotene, polyurethane (PU), and an optical adhesive (OA) will be studied for their passivation effectiveness.

2.4 Fabrication of Passivated Electrodes

2.4.1 Synthesis of Passivation Solutions

To synthesize PMMA solution, 0.5 g of poly(methyl methacrylate) (Aldrich, 200336) was mixed with 9.5 g of anisole (Aldrich, 123226) in a 20 ml glass vial to form a 5 wt% solution of PMMA. The solution was

then stirred at 75 °C for 1 hour while covered with aluminum foil. The molecular weight of PMMA used was chosen to be 15,000 kg/kmol. This was to ensure the PMMA molecules would fit between the NW spacings.

To synthesize PU, 1.0 g of polyurethane (BASF, Raygloss) was mixed with 9.0 g of chloroform (Aldrich, C2432) in a 20 ml glass vial and stirred for 2 hours to ensure uniform distribution of the PU in the chloroform.

To synthesize cyclotene, 2.0 g of cyclotene (Dow Chemicals, 3022-35) was mixed with 8.0 g of mesitylene (Sigma Aldrich, M7200) in a 20 ml glass vial to form a 20 wt% solution of cyclotene. The solution was covered and stirred at room temperature for 2 hours.

To synthesize the OA, 1.0 g of an optical adhesive (Norland, NOA 83H) was mixed with 9.0 g of acetone in a 20 ml glass vial to form a 10 wt% solution of OA. The solution was covered and stirred at room temperature for 2 hours.

2.4.2 Fabrication of Passivated Electrodes

Passivation layers were deposited on top of the AgNW electrodes using spin coating. This method allows the polymer to fill the spaces between the nanowires resulting in a smoother electrode surface. A deposition method that would instead be more conformal to the nanowire network would result in an undesirably rougher surface. For electrochromic devices, it is preferable for current to be able to flow between the active layer and the electrode, so a passivation layer thickness of ~150 nm was used as it resulted in the top surfaces of some of the nanowires to remain exposed or only minimally covered. Furthermore, as mentioned above, a thin polymer layer is desired to achieve a larger electric field in the device.

To achieve a layer thickness of ~150 nm, the spin coating parameters and polymer solution viscosities were chosen accordingly. The coating speed was 3000 RPM, and the spin time was 60 seconds. After spinning, PMMA passivated electrodes were annealed at 180 °C for 90 seconds on a hot plate and cyclotene films were annealed at 150 °C for 3 minutes on a hot plate. Short annealing times were used as 30 nm diameter silver nanowires become morphologically unstable during extended anneals above 150 °C. PU and OA

passivated electrodes were cured using a UV oven (Norland, Traydex-18 UV/Visible Oven) for 180 seconds. A Bruker Dektak XT stylus profilometer was used to determine the thickness of each passivation layer. For these thickness measurements, each passivation layer was spin coated on a 2.5 cm x 2.5 cm x 0.5 mm thick silicon wafer piece and cured using the same conditions as above. The thicknesses were measured to be 140 nm, 135 nm, 158 nm, and 142 nm for PU, OA, cyclotene, and PMMA, respectively. The thickness measurements were not done directly on the AgNW electrodes on PET as the surface roughness of the PET is high. Additionally, adding the AgNWs make the surface roughness even higher so this would make the thickness measurements inaccurate. Silicon wafers are atomically smooth so it was considered to be more accurate.

2.5 Characterization of Passivated Electrodes

2.5.1 Imaging and Passivation Effectiveness

Figure 2.9(a) shows a cross-sectional SEM image of a PU layer deposited on silicon, without nanowires. The thickness matches what was measured with the profilometer. Figure 2.9(b) shows an 85° tilted SEM image of the AgNW network passivated with a 140 nm thick layer of PU (the image quality is poor due to electron charging of the PU). It is seen that some AgNWs remain exposed on their top surfaces to allow electrical current to flow into and out of the nanowires, as required in some optoelectronic devices including electrochromic displays. The PU still covers most of the NW surfaces to achieve a passivation effect.

Figure 2.9(c) shows an SEM image of unpassivated AgNWs after 3 months left in air under room light. As with Figure 2.7(a) and Figure 2.7(b), there is clear formation of spherical particles and breaking up of the nanowires. Top-down imaging of the passivated electrodes in the SEM is not easy due to electron charging in the non-conductive layer, so optical images of these samples were taken instead. Figure 2.9(d) shows an optical microscope image of the PU-passivated AgNWs left under room light and in ambient air for two weeks. We can see that the PU did not affect the distribution of the NWs. Although the ageing time is quite short, there is little evidence of AgNW breakdown. The passivation effectiveness is assessed more concretely with lifetime resistance measurements.

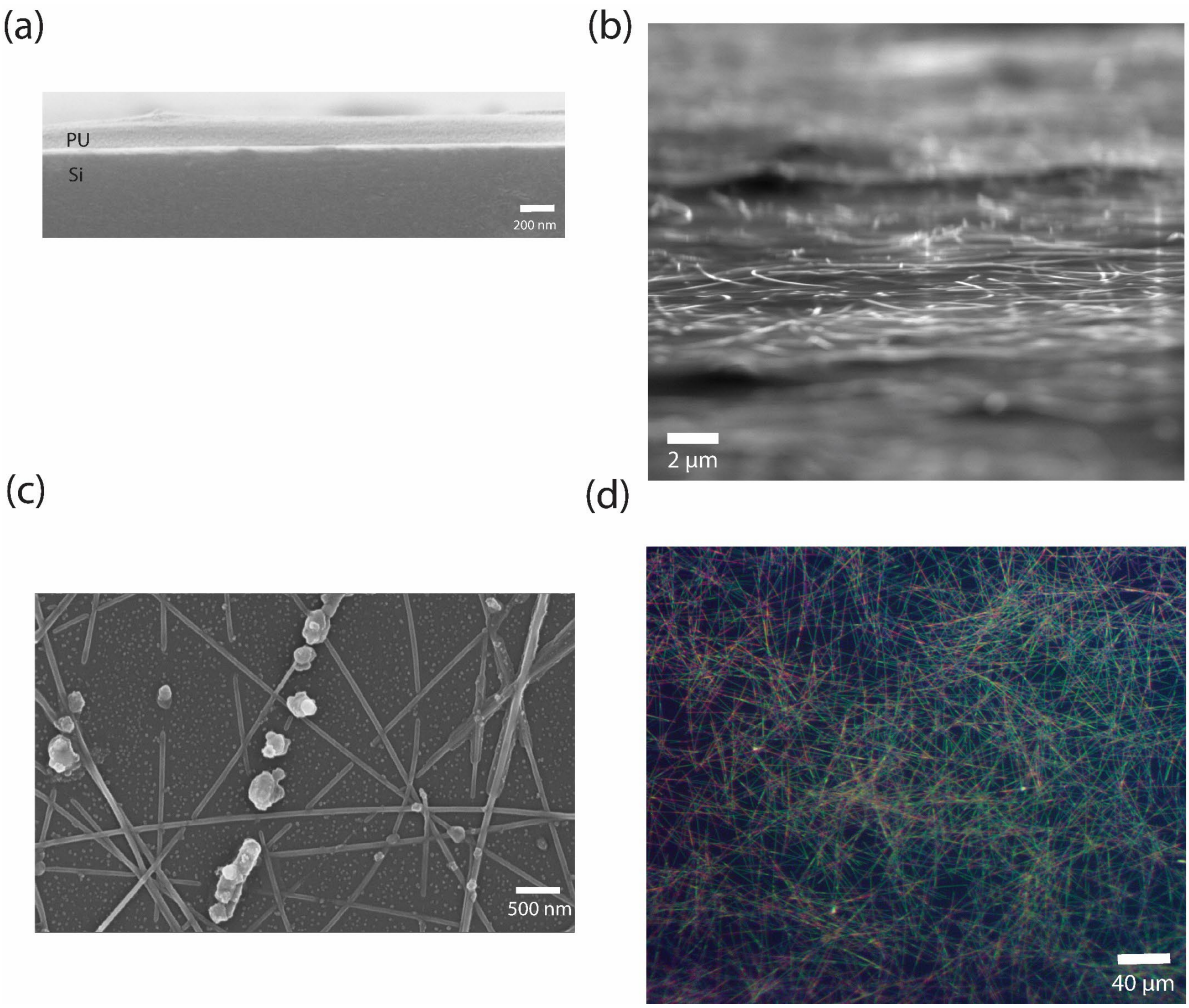

Figure 2.9: (a) SEM image of a polyurethane film on a silicon substrate. (b) SEM image of a PU-covered 30 nm AgNW network showing that the PU does not cover the entire network, allowing current to flow into and out of the nanowires. (c) SEM image of an aged silver nanowire electrode without passivation (d) An optical microscope image of a silver nanowire electrode passivated with polyurethane.

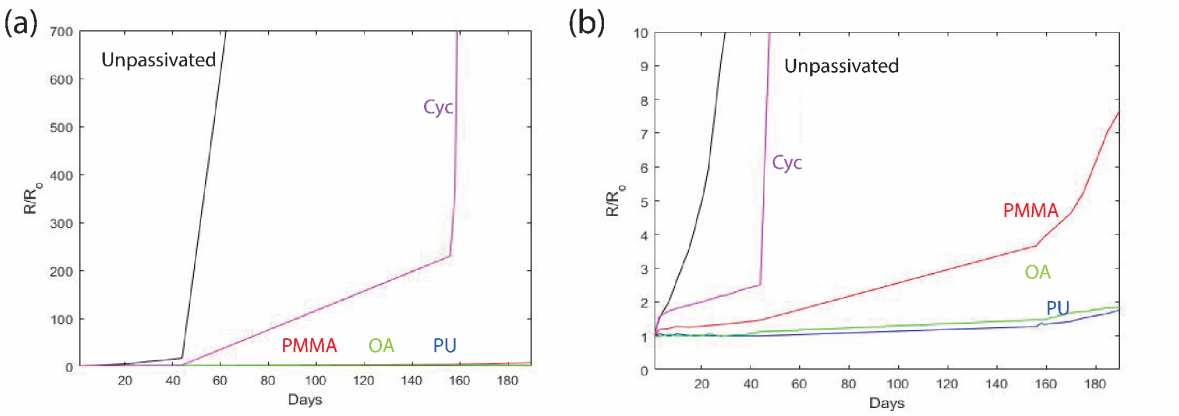

Figure 2.10: Change in sheet resistance of nanowire electrodes with various passivation layers and no passivation layer. (b) is of the same plot as (a) but with a zoomed-in y-axis.

The sheet resistance of bare nanowire electrodes on PET versus electrodes passivated with the four different polymers was tracked for 190 days (Figure 2.10). 4-point probe measurements were avoided since repeated measurements can cause damage [75]. Therefore, a strip of silver conductive paste (Ted Pella Inc.) was painted along two opposing edges of each square electrode (before deposition of the polymer for passivated samples), and the resistance was measured throughout the time period with a multimeter and converted to sheet resistance. The samples were then left under laboratory lighting and in open air.

The unpassivated electrode became completely non-conductive after a period of just 45 days. The cyclotene performed the worst of the passivated electrodes by becoming non-conductive after a period of 160 days. However, the electrodes passivated with PMMA, OA, and PU, remained conductive after the full 190 days. The sheet resistance increased by 657%, 86%, and 81% for PMMA, OA, and PU, respectively. The starting sheet resistances for these samples was 14, 7, and 8 Ω/sq, respectively. The final sheet resistance of the PMMA was measured to be 106 Ω/sq. This is a little bit too high for most device applications. However, the OA and PU final sheet resistances were only 13 and 14.5 Ω/sq. Both of these values are very acceptable to maintain a high quality of device operation.

2.5.2 Transmittance, Haze, Roughness and Adhesion

In order to make sure the transparency of the passivation layers is high throughout both the visible and NIR, the transmittance of the four passivation layer candidates was measured using a Perkin-Elmer 1050 spectrophotometer. The measurements were performed at normal incidence from 250 – 2500 nm and with

the passivation layers deposited on glass. The transmittance of bare BK7 glass was subtracted from the total transmittance in order to determine the transparency of the passivation layers alone. The results are shown in Figure 2.11(a). The transmittance is nearly identical for all four passivation candidates and remains high (> 94%) and constant across the visible and NIR. The transmittance of the PU and OA are 97% and 95.5% at 550 nm, and 96% and 96% at 2500 nm.

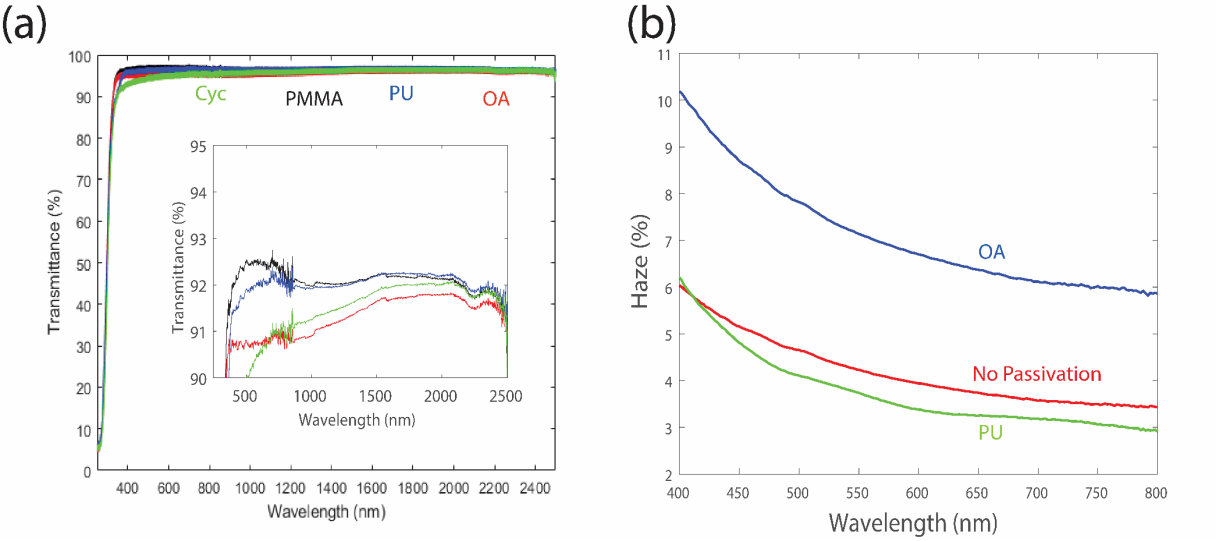

Figure 2.11: (a) The visible and near-infrared transmittance of the four candidate passivation materials. All materials have transmittance >94% across the visible and near infrared regions. Inset: the same plot zoomed-in on the y-axis. (b) Haze of the nanowire electrodes with and without passivation.

Since PU and OA are the most effective passivation materials, according to the lifetime resistance results, most of the subsequent characterization was performed on only these two materials. Figure 2.11(b) shows the haze of PU and OA-passivated and unpassivated AgNW electrodes in the visible region. Haze is mainly relevant in the visible as it is associated with how blurry the transmission is to the human eye. The unpassivated nanowire network has a haze value below 6% across the entire visible region. This is considered acceptable as a haze of < 10% is the standard for a translucent film to be considered a good product in industry. When the OA passivation layer is added, the haze increases to 7 – 10%, still within the acceptable limit. However, when PU is deposited as the passivation layer, the haze actually decreases, potentially due to the electrode surface being less rough than the bare nanowires. And compared to OA, PU has slightly higher crystallinity and is a smaller molecule than OA which may cause less scattering.

The adhesion of the AgNWs to the surface of the substrate is also of importance as AgNWs can peel off with disturbance to the material. AgNW electrodes were deposited on PET substrates at a concentration of 5.0 mg/ml and two samples were subsequently passivated with either PU or OA. A standard way of testing the adhesion of a film to a substrate is the Scotch tape test. Here, a piece of Scotch tape is pressed with finger pressure onto the film and then removed. For electrical measurements, a strip of silver conductive paste was placed on each side of the 2.5 cm x 2.5 cm PET substrate after nanowire coating and before polymer deposition.

The resistance of each sample before and after the tape test is shown below in Table 2.2. First to note is the initial sheet resistances; the deposition of PU only increased the initial resistance (i.e. compared to the unpassivated electrode) slightly to 12 Ω/sq, and the resistance remained unchanged for the OA passivated sample. This shows that the passivation layer has minimal to no effect on the conductivity of the electrodes. After the tape test, the resistance of the unpassivated sample increased greatly, by 640%, whereas that of the PU-coated sample increased by only 17% and that of the OA-coated sample remained unchanged. This demonstrates that the passivation materials are effective in improving adhesion.

Table 2.2: The change in sheet resistance using the Scotch tape test of silver nanowire electrodes on PET before and after passivation.

	Unpassivated	**PU**	**OA**
Initial R_s (Ω/sq)	10	12	10
R_s after tape test (Ω/sq)	640	14	10

Another important metric of the electrodes is surface roughness. Nanowire electrodes have much higher surface roughness than ITO which, if unaddressed, will cause device performance issues. It can cause active layers deposited on top to have non-uniform thicknesses, it can create non-uniform electric fields, and in more extreme cases create an electrical short between the two electrodes causing the device not to work at all. A 150 nm layer of PU can fill in the spaces between the AgNWs in order to reduce the surface roughness.

A Bruker Dimension Fast Scan atomic force microscope using a FastScan head at a sample frequency of 0.497 Hz using a sampling rate of 256 lines/sample was used to measure the surface roughness of passivated

and unpassivated AgNW electrodes. The scan area was 20 µm x 20 µm. The raw data was flattened and the root mean square (RMS) surface roughness R_q, which is the weighted root mean square average of the distance between peaks and valleys, was calculated directly using the Nanoscope Analysis 1.8 Software. R_{max} was also collected, which is the distance from the largest peak to the largest valley in the scan area.

The first sample measured was glass only, to be used as a reference point. R_q was found to be 0.901 nm (Figure 2.12(a)). When a 30 nm AgNW film was coated on top at a concentration of 1.0 mg/ml, R_q increases to 26 nm with a R_{max} of 346 nm (Figure 2.12(b)). Figures 2.12(c) and (d) show the AFM height images when layers of OA, and polyurethane, respectively are placed on top of the 30 nm AgNW electrodes. The R_q and R_{max} values on glass are shown in Table 2.3, OA only minimally reduced roughness, whereas PU reduces it more.

Table 2.3: The average surface roughness (R_q) and max peak to valley height (R_{max}) for unpassivated and passivated AgNWs on glass at a concentration of 1.0 mg/ml.

	Glass Only	**Glass w/ NWs**	**Glass w/ NWs +PU**	**Glass w/ NWs + OA**
R_q	0.901 nm	26 nm	16 nm	25 nm
R_{max}	32 nm	346 nm	241 nm	268 nm

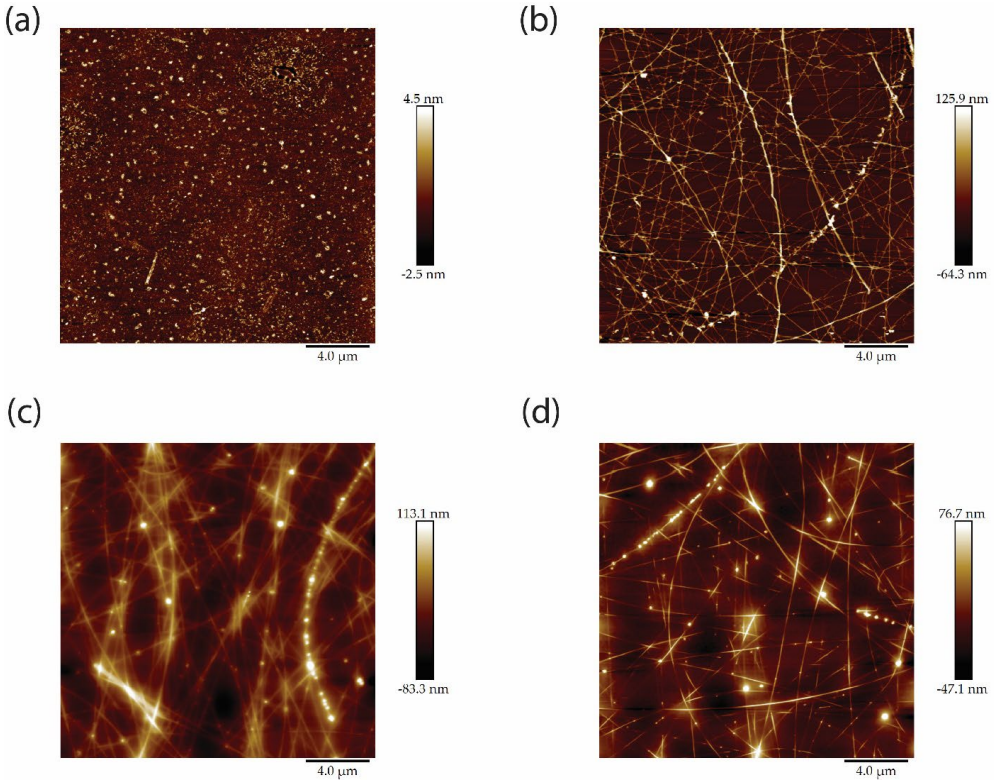

Figure 2.12: AFM images for silver nanowire samples on glass for (a) glass only, (b) silver nanowires, (c) silver nanowires with an optical adhesive passivation layer, and (d) silver nanowires with a polyurethane passivation layer.

If we make similar samples, but this time on PET, R_q and R_{max} increase. This is explained by the fact that R_q and R_{max} for bare PET are 16 nm and 230 nm (Figure 2.13(a)). When a AgNW film was coated on top at a concentration of 1.0 mg/ml, R_q increases to 28 nm with a R_{max} of 276 nm (Figure 2.13(b)). Figures 2.13(c) and (d) show the AFM height images when layers of OA and polyurethane, respectively, are placed on top of the AgNW electrodes. The R_q values are found to be 33 nm and 13 nm for OA and PU, respectively. Additionally, the R_{max} values are calculated to be 304 nm and 192 nm. These are all summarized in Table 2.4. OA actually resulted in a roughness increase, whereas PU reduced both R_q and R_{max}.

Table 2.4: The average surface roughness (R_q) and max peak to valley height (R_{max}) for unpassivated and passivated AgNWs on PET at a concentration of 1.0 mg/ml.

	PET Only	PET w/ NWs	PET w/ NWs +PU	PET w/ NWs + OA
R_q	16 nm	28 nm	13 nm	33 nm
R_{max}	230 nm	276 nm	192 nm	304 nm

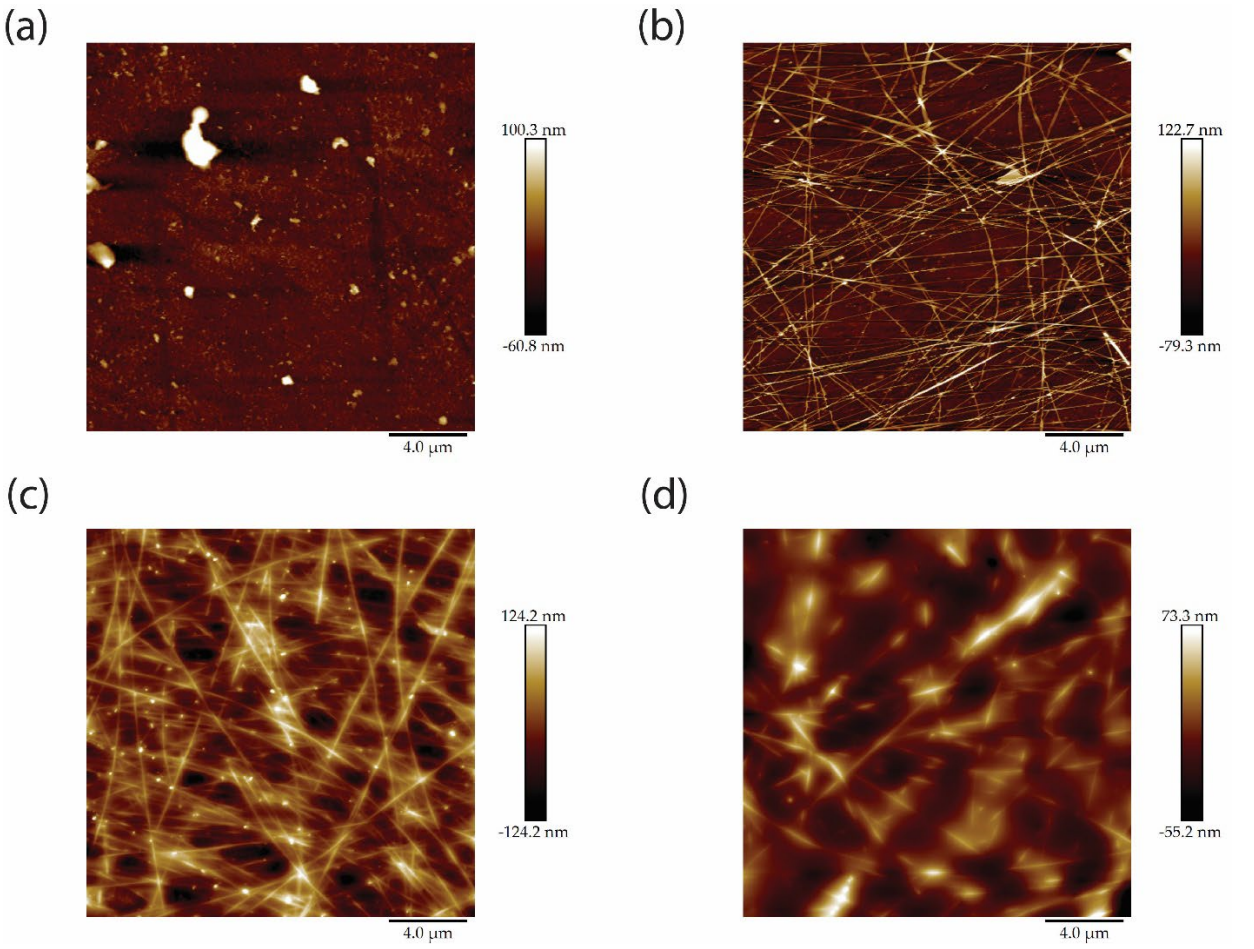

Figure 2.13: AFM for silver nanowire samples on PET for (a) PET only, (b) silver nanowires, (c) silver nanowires with an optical adhesive passivation layer, and (d) silver nanowires with a polyurethane passivation layer.

In an attempt to reduce the surface roughness further, the passivated electrodes were attempted to be fabricated in an alternative way. They were first spin coated the polymer first on bare PET, then deposited the AgNW network on top of the polymer. Hot rolling was then used to press the AgNWs into the polymer.

Figures 2.14(a) and (b) show the AFM height images when layers of OA and polyurethane, respectively are placed underneath the AgNW networks. The resulting surface roughness parameters are shown in Table 2.5. There was no improvement in the surface roughness compared to when the passivation layers were deposited on top of the nanowires, and thus this strategy was not used going forward. When comparing the roughness of PU vs OA passivated nanowires, PU is the superior choice with lower R_q and R_{max} than OA on both glass and PET.

Table 2.5: The average surface roughness (R_q) and max peak to valley height (R_{max}) for unpassivated and passivated AgNWs on PET at a concentration of 1.0 mg/ml with the passivation layer on the bottom.

	PET w/ NWs +PU	**PET w/ NWs + OA**
R_q	18 nm	33 nm
R_{max}	210 nm	428 nm

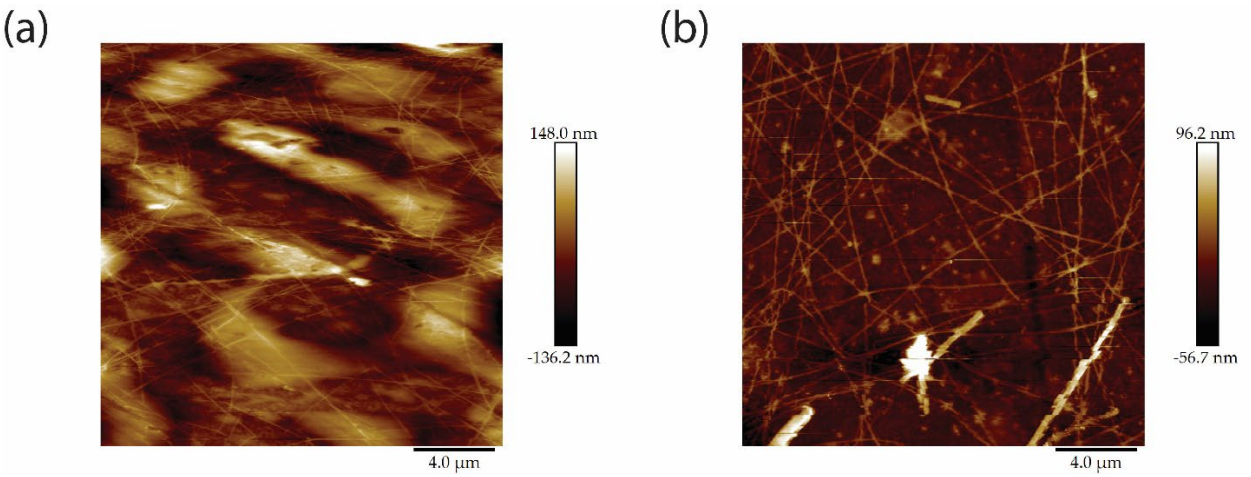

Figure 2.14: AFM images of silver nanowire networks on PET pressed into a layer of (a) optical adhesive and (b) polyurethane passivation layer. This approach did not improve the roughness compared to spin-coating the polymers overtop the nanowire networks.

2.5.3 Strain and Bending

Mechanical flexibility is becoming more desired in electronic devices such as bendable and rollable displays and wearables. As briefly mentioned above, one advantage of nanowire electrodes versus ITO is that they are bendable and even stretchable [72], [76]. Therefore, passivated nanowire electrodes should be as well. Both stretching and bending tests were performed. For the strain cycling tests, AgNWs at a concentration of 5 mg/ml were deposited on TPU (thermoplastic polyurethane, Bemis, ST-604). TPU was used as the substrate as it is stretchable, unlike PET which is not elastic. The AgNWs were then annealed in a vacuum oven at a temperature of 80 °C for 30 minutes. The lower temperature was required as the TPU thermal budget is not high enough to anneal at the optimal temperature of 150 °C for 30 nm diameter AgNWs. PU and OA solutions were spin coated on top of two of the AgNW networks after a strip of silver conductive paste (Ted Pella Inc) was placed on two opposite edges of the 2.5 cm x 2.5 cm substrate. The samples were mounted in a linear stage (Zaber Technologies, X-LHM150A) which stretched the three samples to 20% strain and then reduced the strain back to unstrained for 300 cycles. During the test, a multimeter (Siglent Technologies, SDM3045X) was connected to each side of the linear stage where an electrical contact between the linear stage and sample was made. Figure 2.15(a) shows the change in sheet resistance over time for the unpassivated and passivated samples, represented as R/R_o. The unpassivated electrode had a sharp increase in sheet resistance to $2R_o$ after the first few cycles. After the full 300 cycles, the sheet resistance was $3.5R_o$. For the OA passivated sample, the sheet resistance stays at $1.5R_o$ for the first 125 cycles. However, it then undergoes a sharp increase and finishes off close to $3.5R_o$ which is very similar to the unpassivated AgNWs. The PU passivated AgNWs have the best performance of the three samples. The sheet resistance undergoes almost no increase in sheet resistance and stays at $R = R_o$ over the entire 300 strain cycles undergone by the sample. A similar test was done using 5 mg/ml of 120 nm diameter nanowire networks, but all the samples broke and the sheet resistance became very large for both passivated and unpassivated samples. This implies that 120 nm AgNWs are more brittle when it comes to strain. This is because smaller nanowire diameters show a better hardening with less grain boundaries [77]. Along a grain boundary, nanowires are more likely to fracture when undergoing strain [77]. Hence, the Young's modulus is higher for the 30 nm nanowires compared to the 120 nm nanowires. It is therefore more favourable to use thinner AgNWs.

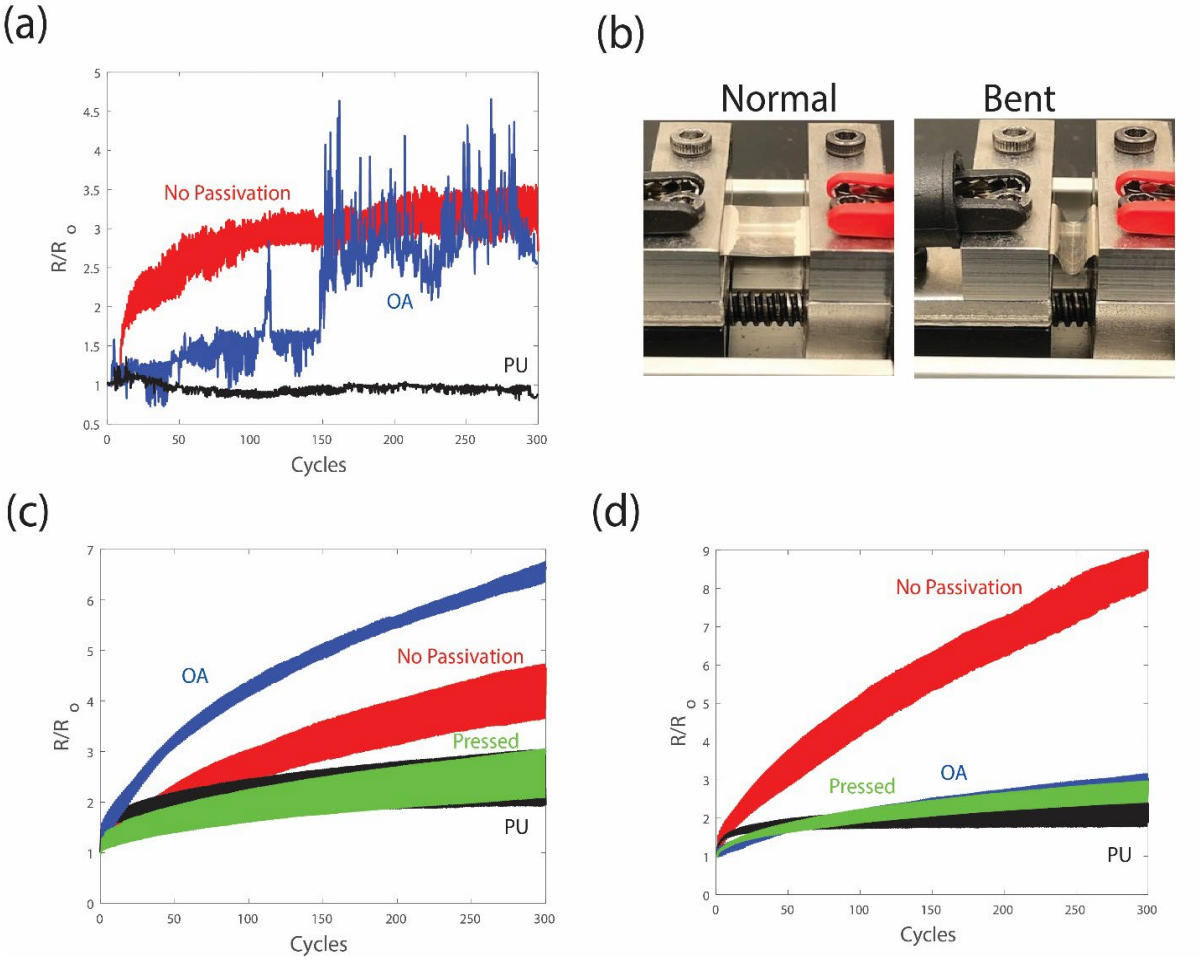

Figure 2.15: (a) Stretching tests: the change in sheet resistance of nanowire electrodes with PU, OA, and no passivation layer during strain cycling to 20% strain. Bending tests: (b) photos of the nanowire electrode in the normal and bent position on the linear stage. The change in sheet resistance of 30 nm (c) and 120 nm (d) nanowire electrodes with PU, OA, and no passivation layer (the "No Passivation" sample was annealed, and the "Pressed" sample was hot-rolled) during bend cycling to an angle of 80°.

Bending tests were performed where both 30 nm and 120 nm diameter AgNWs were deposited on PET. One unpassivated sample was annealed at 150 °C with no hot rolling. A second unpassivated sample, called the "pressed" sample, was rolled once at room temperature and then hot rolled twice at 80 °C. For the passivated samples, the AgNW electrodes were also pressed in this same manner, and then a layer of PU or OA was spin coated on top of the AgNWs. The samples were then mounted in the linear stage and attached to the multimeter as described above. For the bending test, instead of increasing the distance of the two contacts and creating a strain, the distance between the two contacts of the linear stage were reduced from a separation distance of 2 cm to 1.5 cm.

This created a bending angle of 80°. Images of the films in the bent and unbent stage are shown in Figure 2.15(b).

It can be seen in Figure 2.15(c) that for all samples, the sheet resistance increases steadily over a period of 300 cycles. As expected, the unpassivated/unpressed AgNWs increased a significant amount to $5R_o$. Pressed AgNWs performed much better as the hot rolling helped with the adhesion of the AgNWs to the substrate. Surprisingly, the OA passivated sample faired the worst, with a final value of almost $7R_o$. The best performing sample proved to be the combination of hot rolled AgNWs that were passivated with PU.

The 120 nm diameter unpassivated AgNWs in Figure 2.15(d) perform worse than the 30 nm AgNWs as the sheet resistance increases to $R = 9R_o$ after the 300 bending cycles compared to $R = 7R_o$ for the 30 nm AgNWs. Thinner AgNWs are known to have more flexibility so this explains the smaller increase in sheet resistance. The pressed and pressed + PU AgNWs perform the best again as the sheet resistance only increases to $1.5R_o$ after the bending cycles. The OA performs better for the 120 nm wires compared to the 30 nm wires by only increasing to $3R_o$ after the 300 cycles. However, still overwhelmingly the consensus is that the pressed + PU passivation technique works the best for both 30 nm and 120 nm AgNWs.

A tensile tester (Instron 5548 Micro-tester) was used to collect stress/strain curves of PU and OA films (with nanowires) on TPU. The PU had a higher Young's modulus (10 100 N/m^2) compared to OA (6400 N/m^2) and hence can tolerate a higher amount of stress. This helps explain why the PU has better mechanical properties than the OA.

2.5.4 The Preferred Passivation Solution

The preferred passivation solution used going forward will be PU. In nearly all tests it performed the best of all polymers investigated. It had the lowest increase in resistance after more than 6 months by only increasing by 81%. It is 96% transparent across both the visible and NIR, and reduced the haze compared to an unpassivated electrode. The in-plane conductivity of the electrode only minimally increased after passivation. The PU reduced the surface roughness, the adhesion of the nanowires to the substrate, and improved the mechanically properties of the electrode. It is an inexpensive polymer and can easily be deposited using various scalable solution-deposition techniques, then quickly UV cured for quick and easy integration into a fabrication process.

2.6 Electric Field Simulations

In addition to the properties discussed above, it is important that the passivated nanowire electrodes do not interfere with or degrade the performance of the device they are integrated into. For the displays and smart windows this passivation is designed for, as well as other devices such as touch panels and e-paper, the electric field needs to remain high to assist in switching. Also of concern is uniform switching. Unlike ITO which is a continuous film, the AgNW electrode is not, with gaps on the order of 1 μm between nanowires. Because PU is non-conductive it does not increase the conductivity between nanowires. Thus, the uniformity of the electric field and in turn the uniformity of switching above the nanowire electrode needs to be assessed. These issues are investigated in this subchapter both through modelling and experiment.

The electric field profile of electrochromic devices with passivated and unpassivated nanowire electrodes are modelled in Lumerical (Ansys Ltd). The devices modelled match the experimental devices used in Section 2.7 and Chapter 3 and will be discussed in more detail there. The device layers with and without a PU electrode passivation are shown in Figure 2.16(a) and (d), respectively. PEDOT:PSS is the electrochromic material and a gel type electrolyte called LITFSI: Emim TFSI (Lithium bis(trifluoromethanesulfonyl)imide I-ethyl-3-methyl imidazolium bis(trifuloromethanesulfonylimide)), mixed with 40 wt% PMMA and 5 wt% of TiO_2 nanoparticles, was the electrolyte in the middle.

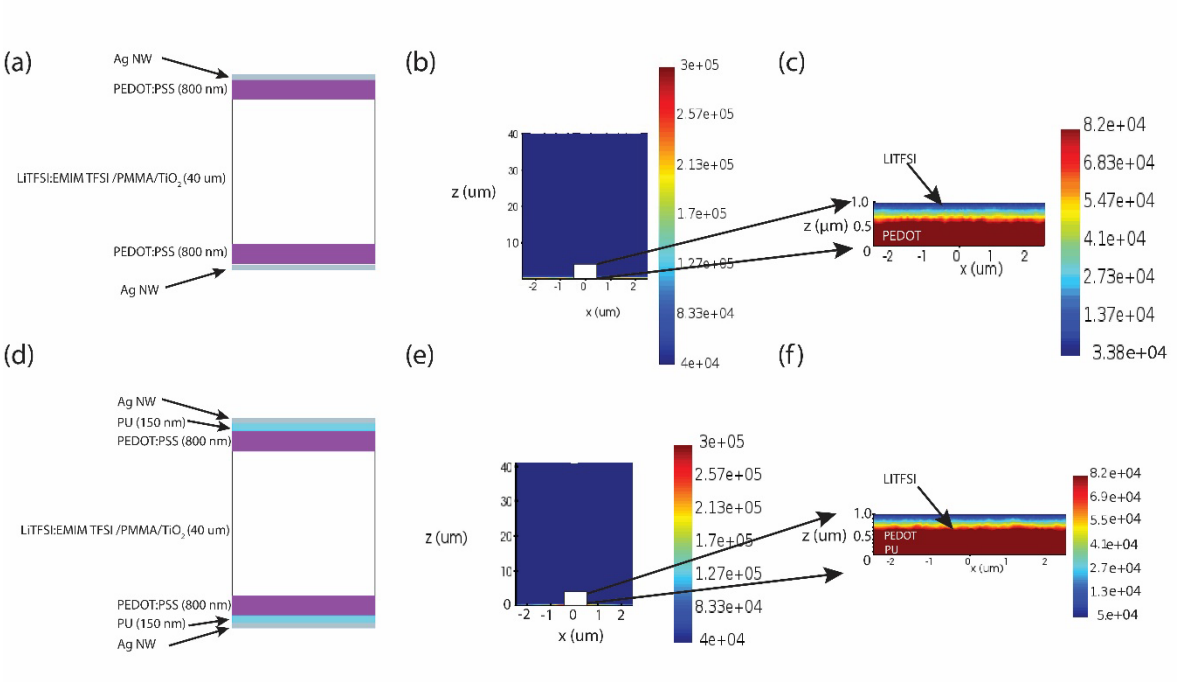

Figure 2.16: Schematic of an electrochromic device (not to scale) with an (a) unpassivated and (d) passivated nanowire electrode. The E-field throughout the (b) unpassivated device and (e) passivated device. Magnification of the bottom electrode in an unpassivated device (c) and passivated device (f).

The Lumerical CHARGE software as part of the Lumerical (Ansys Ltd) Suite was used to simulate the electric properties of the electrochromic device. To build the AgNW electrodes, a grid was built with a nanowire diameter of 30 nm and periodicity of 500 nm. This grid spanned a total area of 5 μm x 5 μm. The electrical conductivity of the silver was set at 6.3×10^7 S/m. A voltage of 1.0 V was applied to one of the grids, with the grid on the other side of the device set to ground. PEDOT:PSS is a semiconductor and the parameters used were: dielectric permittivity $\varepsilon = 13.7$, electronic bandgap $E_g = 1.11452$ eV, intrinsic carrier concentration $n_i = 1.05 \times 10^{10}$ cm^{-3}, effective mass of electrons and holes $m_n = 0.8098$ and $m_h = 1.18$, electron and hole carrier mobility $\mu_n = \mu_h = 1$ cm^2/Vs [78], carrier lifetime $\tau_n = 3.3$ μs and $\tau_h = 4.0$ μs, and electron doping concentration $N_D = 8 \times 10^{22}$ cm^{-3} [78] [79]. The thickness of the PEDOT:PSS layer was 800 nm.

The LITFSI:Emim TFSI electrolyte layer was simulated as a gel dielectric layer. The layer thickness was 40 μm. The dielectric permittivity was set as $\varepsilon = 8$, density $\rho = 1.52$ kg/cm^3, and viscosity $\upsilon = 0.035$ Pa*s [80].

For the passivated AgNWs, the PU layer was simulated as a very wide bandgap semiconductor since to see E-field profiles in CHARGE, the material must be simulated as a semiconductor. The parameters were set as: dielectric permittivity $\varepsilon = 3$, electronic bandgap $E_g = 10$ eV, effective carrier mass of electrons and holes $m_n = m_h = 1$, electron and hole carrier mobility $\mu_n = \mu_h = 0.001$ cm^2/Vs, and a complex refractive index $n = 1.3 + 0.01i$ [81].

An electric field monitor was setup to inspect the static electric field across the device. The voltage on the electrode is chosen to be 1.0 V because this was found to be the operating voltage for our electrochromic device experimentally (to be discussed in Section 2.7). The distance between electrodes for the unpassivated device is 41.6 μm and for the passivated device 41.9 μm, and as such the E-field profile along the z-axis is nearly identical in the two devices. The E-field in the middle of the PEDOT:PSS layer is 8.2×10^4 V/m in the passivated devices, with the E-field in this layer being only 18% less than the unpassivated device, at 1.0×10^5 V/m. In the middle of the electrolyte layer, the E-field is 4.0×10^4 V/m in both the unpassivated and passivated devices. Therefore, according to the modelling, the use of a non-conductive polymer should have little effect on the E-field throughout the device and should have no discernable difference in device switching to the eye.

Secondly, in Figures 2.16(c) and (f), and when the plot is zoomed-in on as much as possible in the simulation software, there is no variation in the E-field along the x-axis. There was concern that the gaps between nanowires could cause an uneven E-field in the x-y plane above the electrode, but this does not appear to be the case. For both the passivated and unpassivated cases, the E-field is uniform along the x-axis. These results indicate that switching should be uniform across the device area and there is no need for the passivation layer to be conductive.

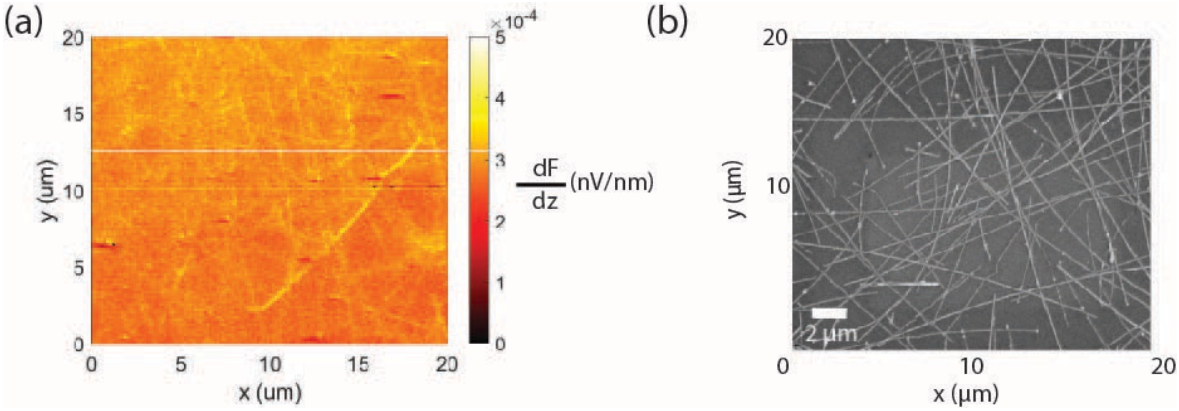

Figure 2.17: (a) The change in electrostatic force 150 nm above a PU-passivated 30 nm AgNW network. (b) SEM image of a 30 nm AgNW network at the same concentration over a 20 x 20 µm area.

Electrostatic force microscopy (EFM) was used to experimentally assess the uniformity of the electric force above a passivated electrode. EFM is based on AFM. An AC voltage is applied to the tip, and the change in the phase difference of this voltage is measured as the tip moves across the surface of the sample. In order to convert the phase difference into a more useable form, the phase difference can be related to the electrostatic force gradient through Equation 2.1:

$$\frac{\partial F}{\partial z} = -\frac{k}{Q}\tan(\Delta\delta) \tag{2.1}$$

where k is the spring constant of the tip, Q is the tip quality factor, and $\Delta\delta$ is the phase difference undergone by the applied voltage on the tip as a result of the electrostatic force applied by the sample on the EFM tip [82].

A 30 nm AgNW network with a concentration of 1.0 mg/ml was fabricated on a glass substrate and then two strips of silver conductive paste (Ted Pella) were placed parallel to each other on opposite sides of the AgNW network. Electrical wire was soldered to each strip of silver conductive paste to create an electrical contact. Then the AgNW network in between the two strips of silver conductive paste was passivated with a 150 nm thick layer of PU. The wires were connected to a DC voltage supply and a potential difference of 1.0 V was applied across the passivated AgNW network. A Bruker Dimension Fast Scan Atomic Force Microscope using a FastScan head at a sample frequency of 0.497 Hz and a sampling rate of 256 lines/sample over a 20 µm x 20 µm area of the sample was used to perform the EFM. A nitride tip coated with silicon (Bruker, SCANASYST-AIR), 115 µm in length x 25 µm in width with a spring constant of k = 0.4 N/m and a centre frequency of f_o = 70 kHz, was used. The quality factor of the tip was calculated

directly from the Nanoscope Analysis 1.8 software and found to be 219. No potential bias was applied to the EFM tip. The tip was held at a constant distance of 150 nm above the passivated electrode surface. The phase difference data was collected when 0 V and 1V were applied across the sample. The electrostatic force gradient using Equation 2.1 was calculated for both scenarios. The gradient at 0 V was then subtracted from the gradient at 1 V and the resulting electrostatic force gradient is plotted in Figure 2.17(a). The main point to note from this plot is that the electrostatic force gradient at most drops to 0.5 of the peak value, and in most cases less, when measured above a AgNW gap compared to directly above an AgNW, where the electrostatic force is expected to be much stronger. Therefore, the electric force gradient or electric field gradient is quite uniform above the electrode, and uniform switching of the electrochromic device should be expected across the entire device area.

2.7 Performance of Passivated Electrode in Electrochromic Devices

The next step in measuring the performance of our passivated AgNWs is to integrate them into electrochromic devices. Here, they are integrated into a commonly used PEDOT:PSS based device which can be used as a display. Two different voltage windows were used to characterize the devices: [-1.0, +1.0] V and [-1.5, +1.5] V. The devices are more stable at the lower voltage, but the use of a higher voltage window can lead to a stronger colour change (ΔE) and reflectance values.

2.7.1 Device Performance Before Cycling

Electrochromic devices using PEDOT:PSS as the electrochromic layers and a LITFSI-based electrolyte in the middle were prepared using 2.5 cm x 2.5 cm nanowire electrodes on PET substrates, with and without PU passivation. The device fabrication will be described in detail in Section 3.2.

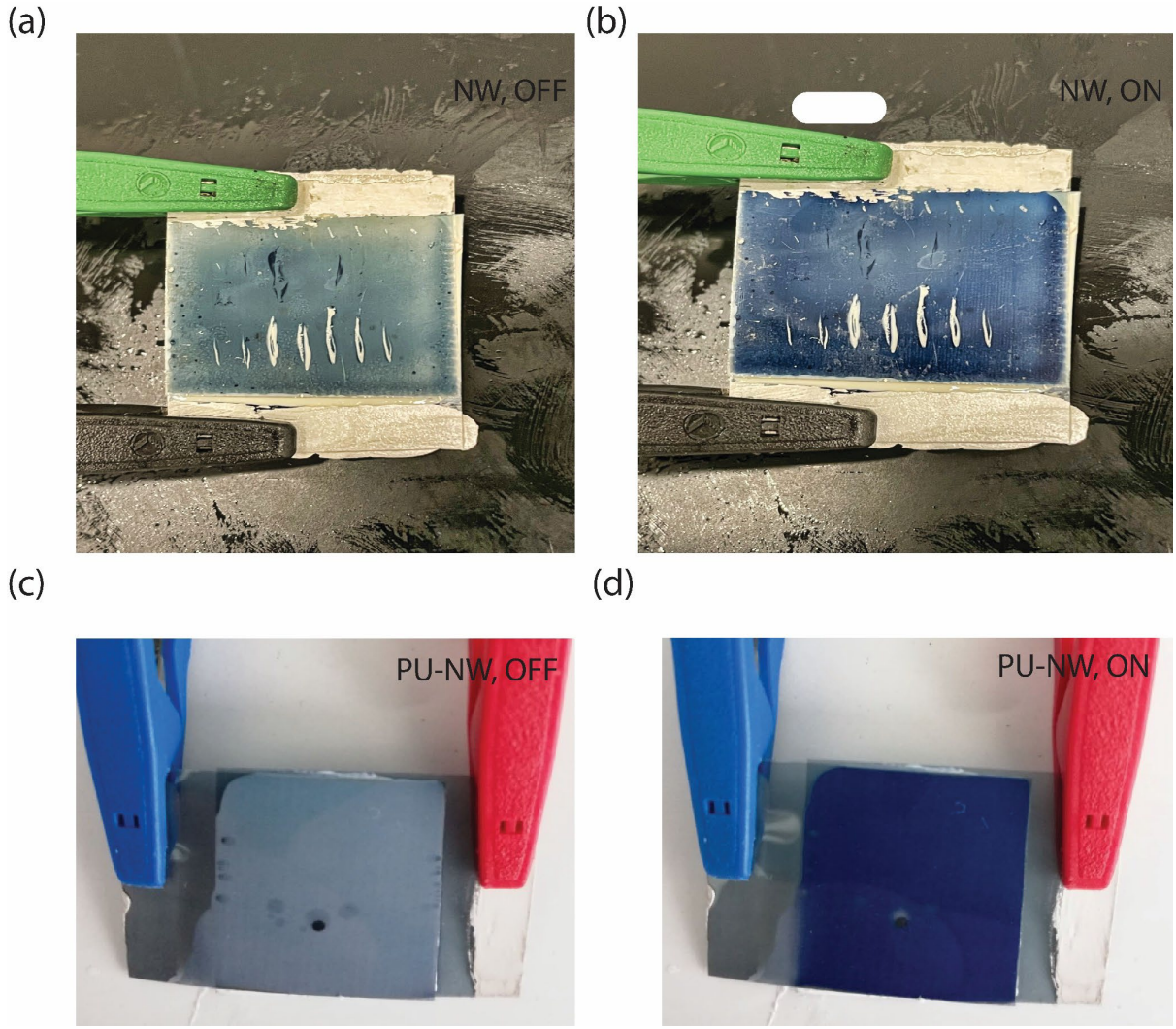

Figure 2.18: An unpassivated nanowire PEDOT:PSS device in the off state (a) and on state (b). A passivated nanowire PEDOT:PSS device in the off state (c) and on state (d).

Photos of the unpassivated and passivated nanowire devices are shown in the off and on states in Figure 2.18. Here, a voltage of 1.5V was used. To the eye, the passivated devices switch at least as well and as uniformly as the unpassivated device. The colour change between the on and off states, ΔE, was measured and tabulated in Table 2.6. The values of the two devices are nearly identical at a voltage of +/-1.0 V, and at +/-1.5 V, ΔE is higher in the passivated device. A possible reasoning for this is the PU protecting the oxidization and sulfidization of AgNWs from the air, which is more significant at the higher operating voltage, a higher conductivity and thus higher current, which in turn results in more charged transferred between the electrode and electrochromic layer. Sulfur exits in air in the form of sulfur oxides which can come from the burning of fossil fuels [83]. More charge transfer creates a higher ΔE. Additionally, it is

well known from Fresnel's theory of reflection that the reflection can be reduced (increase in transmittance) from a film when a coating is placed between two mediums with a refractive index between the incident medium (PET, n = 1.64) and the silver nanowires/air (n = 1 or n = 0.13). The refractive index of PU is 1.62. A reduced reflection increases ΔE as it results in increased absorption. In turn, an increase in absorption creates a larger colour change.

Table 2.6: The colour change (ΔE) for devices with unpassivated and passivated AgNW electrodes at operating voltages of +/-1.0 V and +/-1.5 V, before 1000 on/off cycles.

	Ag NW Electrodes (ΔE)	**Ag NW Electrodes w/ PU (ΔE)**
[- 1.0 +1.0] V	14.70	14.79
[- 1.5 +1.5] V	17.7	21.24

The reflectance of the electrochromic display is also an important figure of merit. The same passivated device as described above had its reflectance measured vs time at a wavelength of 550 nm, as this is the wavelength of light the human eye is most sensitive to, in a Perkin Elmer Lambda 35 in reflectance mode. The Emstat 3+ potentiostat was hooked up in the two electrode device setup as shown in Figure 1.11(b). Since the lid would not fully close with the potentiostat leads, a black fleece blanket was placed over the spectrophotometer to prevent room light from affecting the reflectance. The reflectance change remained constant over several cycles at a value of ΔR = 13% as shown in Figure 2.19(a). Additionally, the time it took for the reflectance to change was quick as the off time was 0.2 seconds and the on time was 0.5 seconds as calculated from Figure 2.19(b). The inset shows the device in the on state (R = 8.5%) and off state (R = 21%). The operating voltage was +/-1.5 V.

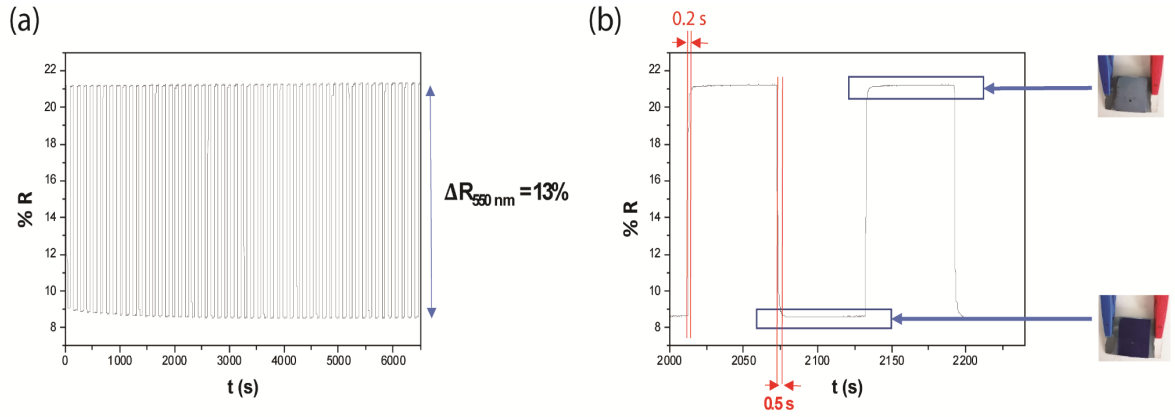

Figure 2.19: (a) Reflectance vs time of a device with passivated AgNW electrodes on PET at a operating voltage of +/-1.5 V.

Figure 2.20 compares the reflectance of the unpassivated and passivated devices in the on and off states at a voltage of +/-1.5 V. Compared to the unpassivated device, the passivated device desirably has a higher reflectance in the off state and a lower reflectance in the on state, resulting in a better ΔR. This is due to the law of Fresnel reflection mentioned above and aligns with the earlier result where the colour change for the passivated device was larger than the unpassivated device at +/- 1.5 V.

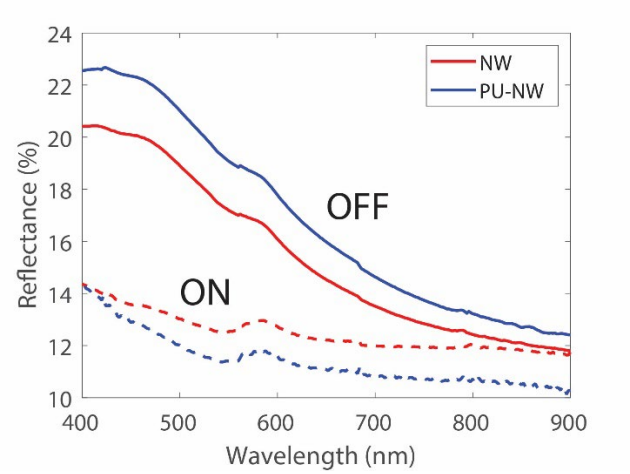

Figure 2.20: Reflectance of the PEDOT:PSS device with passivated and unpassivated AgNW electrodes in the off and on states at +/-1.5 V.

The last figure of merit examined here is the colouration efficiency of the devices at the two different voltages for the passivated and unpassivated devices. The description of the colouration efficiency calculation is described in detail in Section 1.6. Table 2.7 shows the calculated colouration efficiencies. Due to the better ΔR for the passivated samples, the colouration efficiency is higher. This means it takes

less charge transferred from the electrode to the PEDOT:PSS layer in order to create the same change in reflectance of the device.

Table 2.7: The colouration efficiencies of the unpassivated and passivated devices at operating voltages of +/-1.0 V and +/-1.5 V.

	Unpassivated (cm^2/C)	**Passivated (cm^2/C)**
+/-1.0 V	56.62	94.95
+/-1.5 V	28.87	37.81

In this section it has been found that the initial devices (i.e. devices before significant cycling) with passivated electrodes outperform the unpassivated electrodes on all figures of merit tested, particularly at the higher operation voltage.

2.7.1 Device Performance After Cycling

To compare the stability of the devices with passivated and unpassivated electrodes, the devices were switched for 1000 on/off cycles and various measurements were taken before and after cycling. Figure 2.21 shows the unpassivated and passivated devices after cycling in the on and off states. It can be seen that the unpassivated device has "browning" caused by oxidation/corrosion of the AgNWs (Figure 2.21(a) and (b)). The passivated device has much less browning colour (Figure 2.21(c) and (d)) as the PU protects the nanowires from oxidating components and the PEDOT:PSS. In Figure 2.21, the colour difference between the off and on states of the unpassivated device is also visibly less than that of the passivated devices. Table 2.8 shows the colour change, ΔE, at the two different switching voltages, after the 1000 cycles (Table 2.6 shows ΔE before 1000 cycles), in the passivated and unpassivated devices. ΔE of the unpassivated devices drop after cycling. This drop-off in ΔE is not seen in the passivated devices and even increases after cycling. However, with the error and repeatability of the colorimeter, the change in ΔE can be considered to be none.

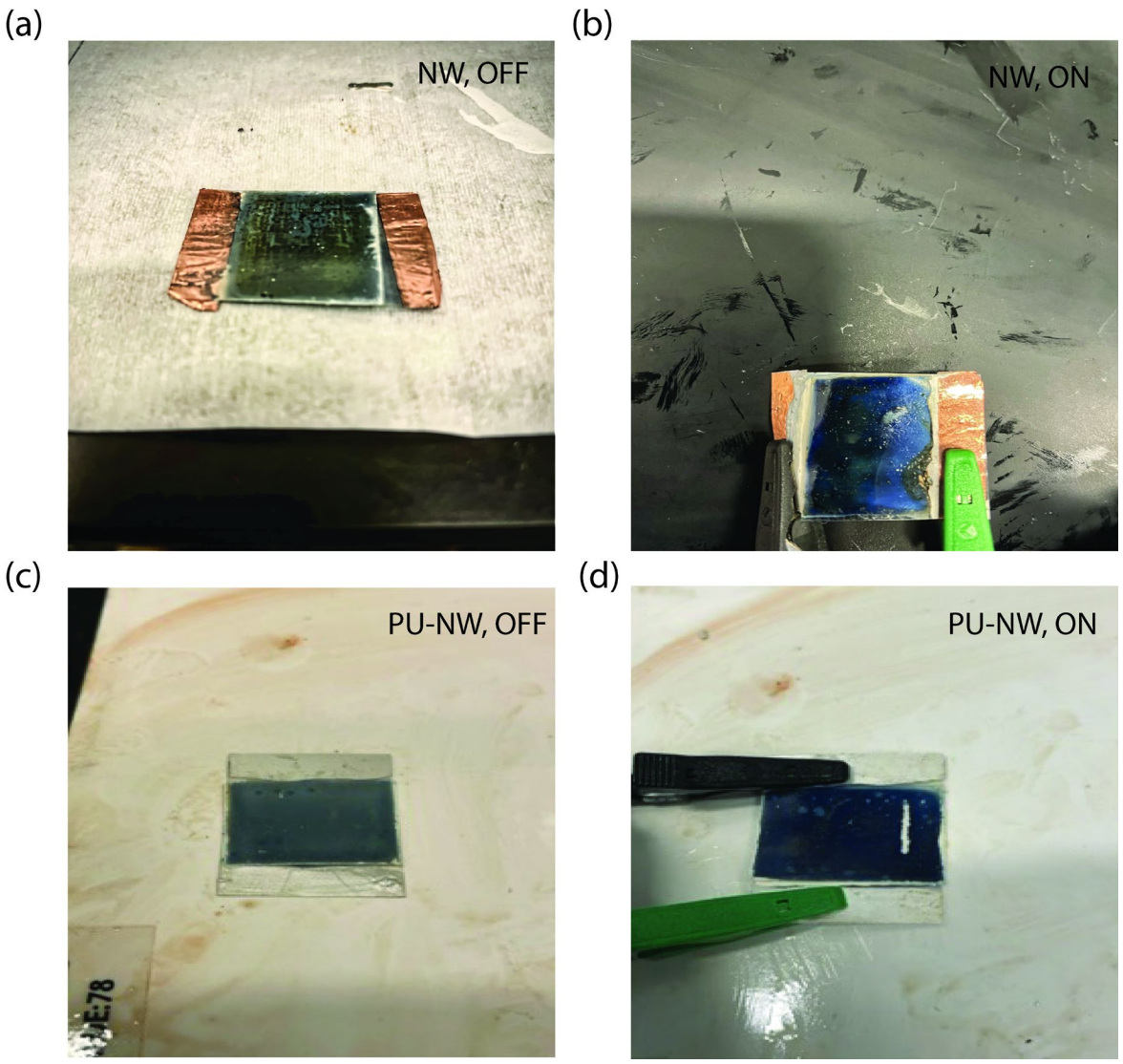

Figure 2.21: Photos of symmetrical PEDOT:PSS devices after 1000 cycles of on/off switching at +/- 1.5 V with unpassivated ((a) and (b)) and passivated Ag NW electrodes ((c) and (d)) in the off state ((a) and (c)) and the on state ((b) and (d)).

Table 2.8: The colour change (ΔE) for devices with unpassivated and passivated AgNW electrodes at operating voltages of +/-1.0 V and +/-1.5 V after 1000 on/off cycles.

	Ag NW Electrodes (ΔE)	**Ag NW Electrodes w/ PU (ΔE)**
[- 1.0 +1.0] V After 1000 Cycles	9.36	16.61
[- 1.5 +1.5] V After 1000 Cycles	15	22.42

CV and CA measurements were done to investigate the stability of the devices in more detail. The CV curves of the first 5 and the last 5 of 1000 cycles of the two devices at both voltage ranges are shown in Figure 2.22. The starting current is slightly lower in the passivated devices as expected, since the PU is insulating and lowers the out-of-plane conductivity of the electrode by covering many NW surfaces. Thus less current flows between the PEDOT:PSS and the electrode. However, as seen before and will see, the important specifications of an electrochromic display, ΔE, ΔR, colouration efficiency and lifetime, are still better with the existence of the PU. At the smaller voltage window (Figure 2.22(a) and (b)), it is clear that the passivated devices are more stable, with the curves matching those before cycling except at the end voltage values. The current of the unpassivated drops at all voltages after cycling and becomes lower than the current from the passivated devices.

At the larger voltage range, the stability in both devices is worse. Before cycling, the curves have extraneous small peaks, though the passivated curves have less. It has been noted by Gomes et al. that at -0.5 V and +0.5 V there is a redox reaction taking place with the AgNWs [54]. After cycling, the current drops in both devices, but in the unpassivated device there remain small peaks at +/-0.5 V from the redox reactions of the silver nanowires. In the passivated samples, these peaks are less pronounced. The peak current levels at +/-1.5 V after cycling are similar for the passivated and unpassivated samples.

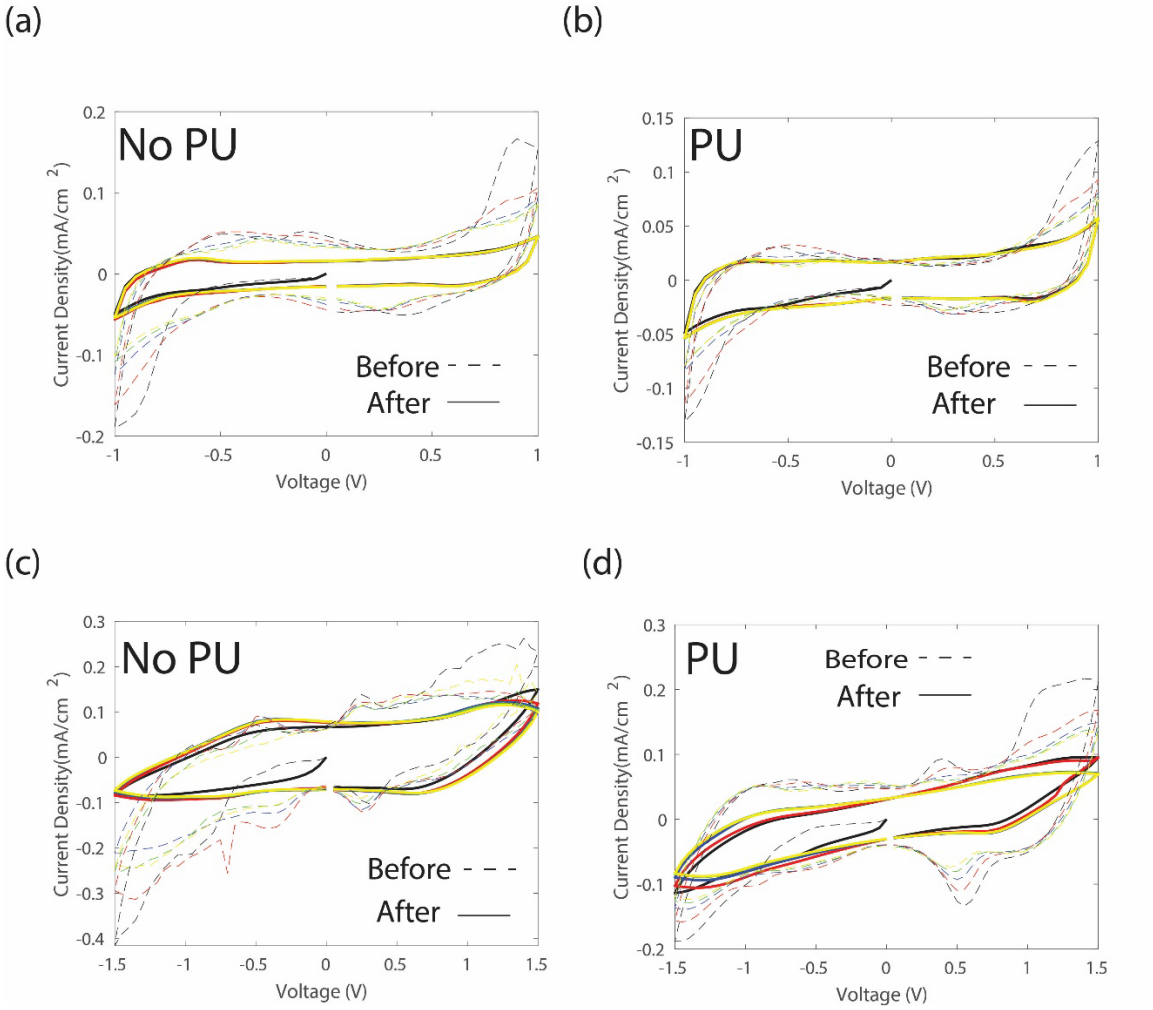

Figure 2.22: CV curves of PEDOT:PSS devices before and after 1000 cycles with unpassivated ((a) and (c)) and passivated AgNW electrodes ((b) and (d)) at an operating voltage of +/- 1.0 V ((a) and (b)) and +/- 1.5 V ((c) and (d)).

The CA plots show the current density vs time of the devices when an electric potential to turn the device on is applied across the two electrodes, and then 30 seconds later, a positive potential is applied to turn the device off. The CA plots of the unpassivated and passivated devices throughout the 1000 cycles are shown in Figure 2.23. The main thing to note here is the stability of the CA plots. At +/- 1.0 V it can be seen that there is fluctuation in the current level in the unpassivated electrode device (Figure 2.23(a)) which creates device instability. The device with the passivated electrode is more stable (Figure 2.23(b)). At +/- 1.5 V, the current density of the unpassivated device continuously decreases over all cycles to finish at a value below 1 mA/cm^2 (Figure 2.23(c)). The current density of the passivated device does not level off nearly as severely (Figure 2.231(d)). Repeatability and stability are very important for device longevity. The unpassivated devices are less stable due to the oxidation and degradation of the AgNWs.

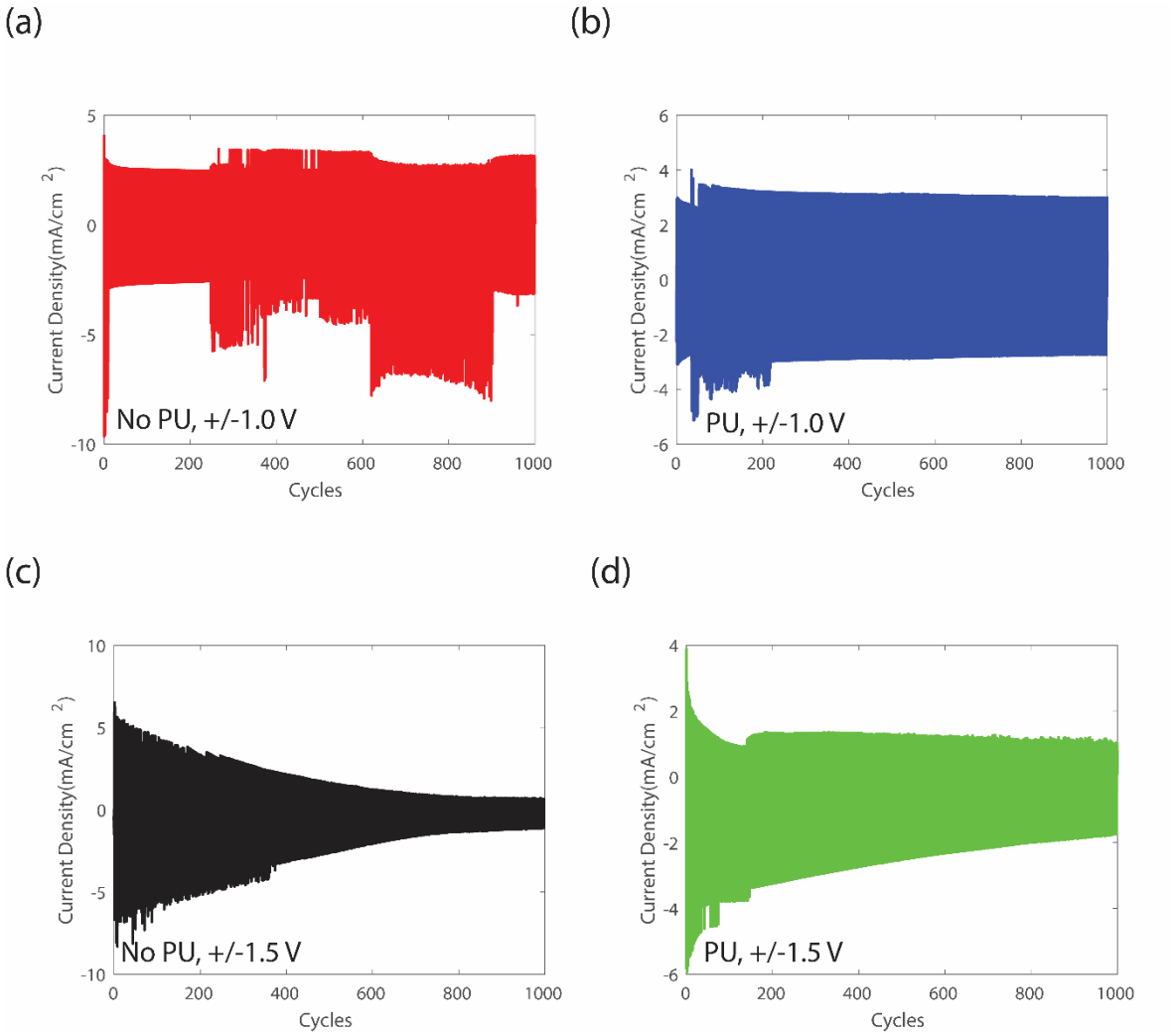

Figure 2.23: CA curves of PEDOT:PSS devices over 1000 cycles with unpassivated ((a) and (c)) and passivated AgNW electrodes ((b) and (d)) at an operating voltage of +/- 1.0 V ((a) and (b)) and +/- 1.5 V ((c) and (d)).

Another important parameter in electrochromic displays is switching time. The quickness of the switching time as well as repeatability over long periods are both important. The switching times for passivated and unpassivated devices, before and after 1000 cycles, at +/-1.0 V and +/-1.5 V are tabulated in Table 2.9. At +/- 1.0 V, the initial switching times of the unpassivated devices are faster than those of the unpassivated device, due to the higher currents in the unpassivated devices. However, after cycling the switching time of the passivated electrodes are faster. At +/-1.5 V, the switching time deteriorates much more in the unpassivated devices with cycling. Overall, at both higher and lower operating voltages, the passivated devices have more stable switching times, and after cycling switch faster than unpassivated devices.

Table 2.9: The on and off switching times measured from the CA when the current falls off to 95% of its peak value, before and after 1000 on/off cycles.

	Ag NW Electrodes, t_{on}(sec)	Ag NW Electrodes, t_{off} (sec)	Ag NW Electrodes w/ PU, t_{on} (sec)	Ag NW Electrodes w/ PU, t_{off} (sec)
[- 1.0 +1.0] V Before 1000 Cycles	1.0	3.0	3.6	3.8
[- 1.0 +1.0] V After 1000 Cycles	3.5	2.0	1.4	1.2
[- 1.5 +1.5] V Before 1000 Cycles	2.8	3.4	1.7	4.5
[- 1.5 +1.5] V After 1000 Cycles	9.9	10.7	4	6.2

2.8 Conclusion

AgNW transparent electrodes were coated using simple, low temperature deposition techniques. The transparency and sheet resistance values outperform ITO on PET. Four nanowire passivation candidates were investigated and compared on several specifications, and PU emerged as the clear #1 candidate. Unlike many nanowire electrode passivation materials used in the literature, which are typically restricted to conductive materials, PU is cheap, can be deposited using simple and scalable techniques, is 96% transparent across the entire visible and NIR regions, and is mechanically flexible. PU not only reduced NW degradation and thus helped maintain electrode sheet resistance over time, it also improved haze, adhesion, surface roughness and the mechanical properties of the electrode compared to unpassivated electrodes. It was shown through modelling and experiment that neither the gaps between nanowires nor the PU interferes with the ability of an electrochromic device to uniformly switch. When implemented into a device, the passivation increased stability, and had higher ΔE, ΔR and colour efficiency than devices without passivation. For the remainder of the thesis, only passivated electrodes will be used in devices. Although this passivation was developed in the context of electrochromic devices, passivating silver nanowire electrodes with polyurethane could be used for other types of devices where nanowire electrodes are used, such as e-paper, smart windows, and displays based on other switching technologies.

Chapter 3
Silver Nanowire Electrodes for Improved Flexible Electrochromic Displays

In this chapter, commonly used indium tin oxide (ITO) is replaced with silver nanowire electrodes in electrochromic displays on flexible substrates. The performance of passivated silver nanowire electrodes against ITO electrodes is compared in terms of change in reflectance, lifetime, switching time, colour change, and turn-on voltage. Additionally, the effect of integrating a silver nanowire network in an electrochromic display is examined and how it affects the performance metrics of the displays. Finally, the stability and lifetime of nanowire electrode-based electrochromic displays on disposable and flexible paper substrates is discussed.

3.1 Introduction

The global market for flexible displays is expected to reach $39 billion USD [84] by the year 2025. It is important for materials used in such displays to not only have great electrical and optical properties, but mechanical properties as well. Electrochromic materials have been extensively studied for their use in displays, with organic materials becoming more and more common. More specifically, PEDOT:PSS has become widely studied. It is inexpensive, easy to synthesize, mechanically flexible, and easily scaled up in order to make films over large areas [85]. All these positive points are critical to make long lasting flexible electronic displays. The redox reaction that PEDOT:PSS undergoes when ions and electrons move in and out of the PEDOT:PSS is:

$$PEDOT^{+}{:}PSS^{-}(transparent/light\ blue) + Li^{+} + e^{-} \rightarrow PEDOT^{0} + Li^{+}{:}PSS^{-}(dark\ blue) \quad (3.1)$$

where e^- is an electron, Li^+ is a lithium ion from the electrolyte, and PEDOT and PSS are the components of the PEDOT:PSS conductive polymer [86]. A schematic showing PEDOT:PSS implemented in a device in shown in Figure 1.2. The displays are designed to be in reflective mode and are two sided, meaning either side can display the information. It is important for all the components in flexible electronics to be easily scalable, inexpensive, and flexible, while maintaining their optical and electrical properties over long periods of time. PEDOT:PSS and electrolytes, in general are good at this. However, the transparent

electrode predominantly used, ITO, is not due to the lack of better transparent electrode materials. ITO is costly, and unlike PEDOT:PSS and the electrolyte which can be deposited using cheap, scalable solution-deposition processes, ITO requires expensive, high-vacuum deposition equipment. ITO has worse resistance on flexible substrates compared to glass because lower-than-ideal deposition temperatures must be used. Most importantly, ITO is brittle and its conductivity reduces with repeated bending [87], [88]. Because of the brittleness of the ITO, device performance will decrease drastically after undergoing strain. As a result, the display will no longer undergo a colour change or change in transmittance/reflectance after just a few strain cycles. The lifetime of these devices are hence poor and impractical for flexible applications.

As discussed in Chapter 1, silver nanowires can address the above challenges with ITO. They can be deposited using inexpensive methods such as rod coating and drop casting, and as such, along with PEDOT:PSS and the electrolyte, the entire device can be deposited using solution deposition methods over large areas using high-throughput roll-to-roll setups. Their material costs are lower than ITO [22] and use low annealing temperatures (<150°C) that are compatible with plastic substrates. Most importantly, NW electrodes retain their electrical and optical properties upon undergoing repeated strain. As reviewed in Section 1.6.1, there exist a few studies of using silver nanowire electrodes in flexible PEDOT:PSS devices, but not all electrochromic figures of merit including stability, lifetime, turn-on voltage, switching time, colour change, and change in reflectance have been reported and compared directly to the same device on ITO. Directly comparing the mechanical properties (bending/stretching) of the two types of devices has also not been done. Lastly, most of the fabrication processes of the passivation materials used are expensive, instead of using inexpensive, easy to deposit polymers.

3.2 Experimental

For the AgNW electrodes, 2.5 cm x 2.5 cm PET substrates (Dupont Inc., Tianjin, China, 127 μm thick) were cleaned in subsequent ultrasonication baths with acetone, IPA, and DI water for 60 seconds each, then dried with a nitrogen gun. AgNWs with average measured diameter and length of 49 nm and 88 μm, respectively (A30UL form Novarials Corporation, Woburn, MA), with a concentration of 3.0 mg/ml were rod-coated and hot rolled using the same method outlined in Section 2.1. As determined in Section 2.1, these electrodes have a sheet resistance of 30 Ω/sq at a transparency of 88%. A strip of silver conductive

paste was put along one side of the AgNW network. Then a 150 nm PU layer was spin coated on top and UV annealed using the same process as outlined in Section 2.3. ITO coated PET with an average sheet resistance of 60 Ω/sq was purchased from Sigma Aldrich. These ITO samples were chosen as they have the same transparency as my fabricated AgNW electrodes. The ITO samples were cut into 2.5 x 2.5 cm square pieces, cleaned in subsequent ultrasonication baths with acetone, IPA, and DI water for 60 seconds each, then dried with a nitrogen gun.

PEDOT:PSS (EL-P3165, AGFA) was mixed overnight with ethanol at a stirring rate of 1500 RPM at a proportion of 70 wt% (PEDOT:PSS) : 30 wt% (ethanol). The solution was then ultrasonicated with a probe sonicator continuously for 60 min at a frequency 1 kHz. Then 0.5 ml of solution was pipetted across the top of the AgNW and ITO electrodes, making sure not to cover the silver conductive paste, and an RDS #95 Mayer Rod was used to coat a 1200 nm thick coating of PEDOT:PSS. The film was then placed in a petri dish on a hot plate at 130 °C and annealed for 10 minutes. To measure the thickness of the PEDOT:PSS layer, PEDOT:PSS was coated in the same manner but on a plain silicon substrate, due to its atomic smoothness. A Bruker Dektak mechanical profilometer was used to measure its thickness.

The electrochromic properties of the PEDOT:PSS on the electrodes (which are called "electrochromic films") were characterized by placing them in an LITFSI: Emim TFSI electrolyte solution (Solvionic, E047500) and attaching them to the working electrode of a PALMSENS Emstat 3 Potentiostat. The counter electrode was platinum (Pt) (PALMSENS, IS-2MM.PT-WE.3) and the reference electrode was Ag/AgCl (PALMSENS, IS-AG/AGCL.AQ.RE.1). A schematic of this was shown in Figure 1.11(a).

To fabricate the complete devices, an electrolyte that can bind two electrochromic films together is required. LITFSI: EmimTFSI with 40 wt% PMMA in butanone (Solvionic, EM023500) was mixed with 18 nm diameter anatase titanium dioxide nanoparticles (US Research NanoMaterials Inc, Anatase, TiO_2 nanoparticles) at a ratio of 95 wt% to 5 wt%. The purpose of the TiO_2 was to increase the contrast and show a change in colour between the on and off state in a symmetrical electrochromic device. The electrolyte without the TiO_2 is clear and no colour difference would be seen between on and off. It is noted that TiO_2 is a photocatalyst but with the PU layer covering the AgNWs, there was no noted or observed degradation directly related to the TiO_2. The mixture was stirred overnight using a magnetic stirrer at a rate of 1500 RPM. Next, the solution was sonicated using a probe sonicator to evenly distribute the nanoparticles for 60 minutes at a frequency of 1 kHz. The solution was then stirred again at 1500 RPM for 24 hours. To deposit the electrolyte, 0.5 ml of solution was pipetted across the top of the PEDOT:PSS layer on either AgNWs or ITO, again making sure not to make contact with the silver conductive paste. Then, an RDS #95 Mayer Rod was used to achieve a 20 μm thick layer. Two samples of PET/electrode/PEDOT:PSS/electrolyte were then folded together and dried overnight in order to create a

total electrolyte thickness of 40 µm as shown in Figure 3.1(a). To characterize the electrochromic properties of the devices, the working electrode of the potentiostat was connected to either the AgNW or ITO electrode on one side of the device, and the reference and counter electrodes were connected together to the second electrode on the other side of the device. A schematic of this was shown in Figure 1.11(b).

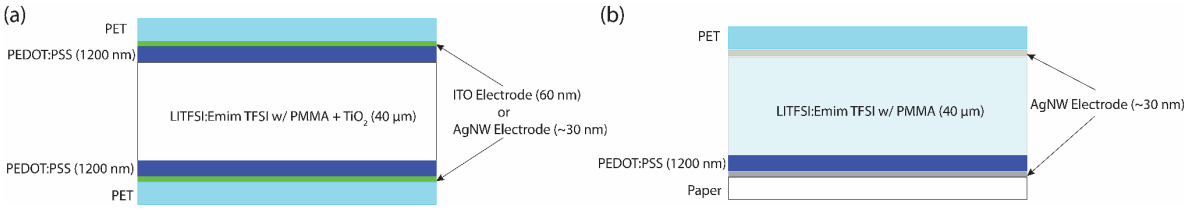

Figure 3.1: **(a) Schematic of the flexible electrochromic display on PET. (b) Schematic of the flexible electrochromic display on paper.**

To fabricate AgNW electrodes on paper, paper from POWERCOAT (PC Powercoat Xd 200) was first cut into 2.5 cm x 2.5 cm pieces. The AgNWs were coated in the same manner as on the PET, then pressed with the rolling press one time at room temperature. The subsequent hot rolling step was skipped as this step made the sheet resistance of the nanowire film worse due to nanowires peeling off and sticking to the warm steel rollers. The sheet resistance of these films was measured using a four point probe (Osilla, T2001A3) and found to be 4 Ω/sq. A strip of silver paste was painted along one side of the AgNW electrode on paper. On paper, the transmittance was not measured as it is irrelevant (the paper is not transparent). To make electrochromic films, a 1200 nm layer of PEDOT:PSS was rod-coated in the same manner above, then annealed at 120 °C for 10 minutes. For an electrochromic device, the electrolyte cannot contain TiO_2 nanoparticles as this would cause the device to be completely opaque and one would see no colour change from the PEDOT:PSS on paper, regardless of the applied electric potential. The electrolyte used was instead LITFSI:Emim TFSI with 40 wt% PMMA and was rod-coated overtop the PEDOT:PSS/AgNW/paper sample in the same manner outlined above for the device electrolyte. Because paper is not visibly transparent, a different substrate, in this case PET, was used on top. PET with a AgNW electrode was then placed on top of the electrochromic paper with liquid electrolyte film and left to dry overnight. A schematic of this device is shown in Figure 3.1(b). The electrochromic film on paper and the device were characterized using the three electrode and two electrode configurations in the same manner as for the films and devices on PET.

3.3 PEDOT:PSS Films: Results & Discussion

The purpose of characterizing electrochromic films only instead of just devices is to determine the ideal electrochromic properties in an ideal three-electrode setup for the specific electrochromic layer plus electrode on substrate. In a device, the setup is non ideal as the reference electrode is connected directly to the counter electrode instead of being on its own, as in the three-electrode setup. We first test the electrochromic properties of a PEDOT: PSS film on an ITO electrode using a voltage range from – 1.5V to +0.7 V. Photos of the film in the electrolyte in the on and off states are shown in Figure 3.2(a). The ΔE is 23.9. Figure 3.2(b) shows the CV of the film over five cycles. The stability of the ITO slightly decreases between -1.0 and -1.5 V as the current decreases with subsequent cycles. This can be attributed to slight erosion of the ITO at higher voltages. With repeated oxidation and reduction of ITO, a thin layer of indium can form from over-reduction of the ITO in the redox process [1]. This increases resistance and decreases transparency. Additionally, ITO can also degrade when in contact with acidic films and PEDOT:PSS is known to be acidic [1]. The CA plot over the first cycles in shown in Figure 3.2(c). The current is higher in the on or reduction state due to the higher voltage applied (-1.5 V). The current shows little variation across subsequent cycles. The on and off times are calculated to be 6.8 seconds and 15.1 seconds. These are not as quick as they need to be in an ideal display due to the lower conductivity of the ITO on PET compared to AgNW films on PET of the same transparency. At a wavelength of 550 nm, when the on and off voltages are applied to the film, the transparency changes by 22%. This leads to a calculated colouration efficiency of 77.9 cm^2/C.

Photos of PEDOT: PSS film on a passivated AgNW electrolyte in the electrolyte in the on and off states are shown in Figure 3.3(a) at the same on and off voltages as used for the ITO-based samples: -1.5 V and +0.7 V. ΔE of the electrochromic film is similar to that on ITO at a value of 24.3 (Table 3.1). Figure 3.3(b) shows the CV of the passivated AgNW and PEDOT:PSS film. The current density is more stable than the film on ITO as it does not decrease as much after subsequent cycles. Additionally, the highest current density values reached for the PU-NW electrodes is -0.2 mA/cm^2 and +0.4 mA/cm^2 compared to -0.13 mA/cm^2 and +0.12 mA/cm^2 for ITO. The higher current in the PU-NW based devices is due to its higher conductivity compared to the ITO. In Figure 3.3(c), the CA for five cycles is shown. The switching on time is calculated to be 1.47 seconds, and the off time is 10.6 seconds. These times are both quicker than the same PEDOT:PSS film on ITO, again due to the higher conductivity of the silver nanowire electrode. As with the ITO device, the off time is much slower than the on time. This is because the switching voltage for the off state is lower than the on state. Additionally, with each applied electric

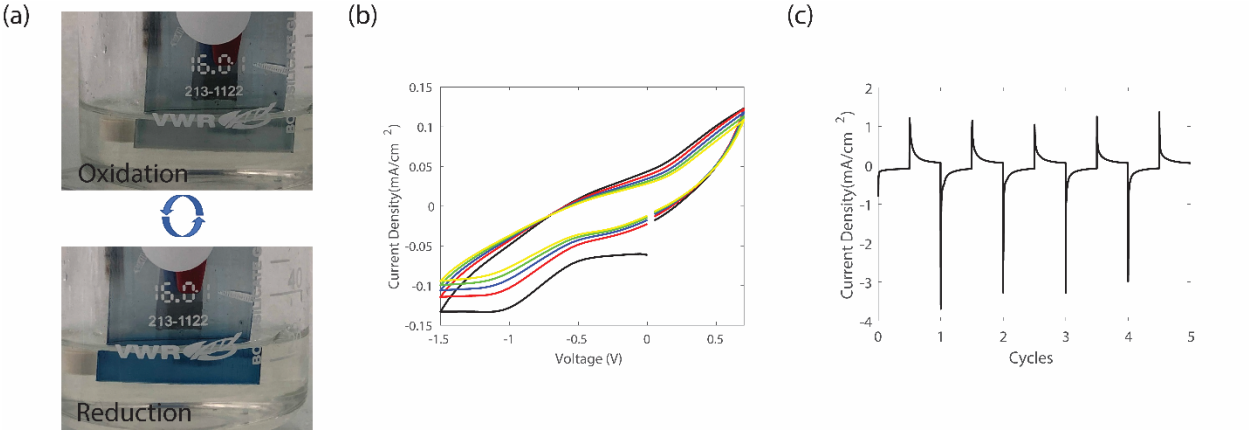

Figure 3.2: **Film of PEDOT:PSS on an ITO electrode on PET in the voltage range of -1.5 and +0.7 V. (a) Photos of the film in the oxidized (off) and reduction (on) state (observe the colour change of the film immersed in the liquid). (b) The CV profile for five cycles. (c) The CA profile.**

potential pulse to the film, there is incomplete insertion or extraction of the Li^+ ions after each cycle. The change in transmittance between the on and off states at a wavelength of 550 nm reaches a value of 22% which is almost identical to that on ITO (Table 3.1). The CE also ends up being close but a little lower than the film on ITO at a value of 74.2 cm^2/C. This is because even though the transmittance is the same, the charge transferred seems to be slightly lower. With the exception of the slightly lower CE, the films on AgNWs have the same performance (ΔE and ΔT) or better performance (switching time, stability) than films on ITO in an ideal three electrode cell setup. However, practically, these passivated NW films will be used in devices and not ideal three electrode setups. Therefore, next, we will integrate the passivated electrodes in electrochromic displays on PET.

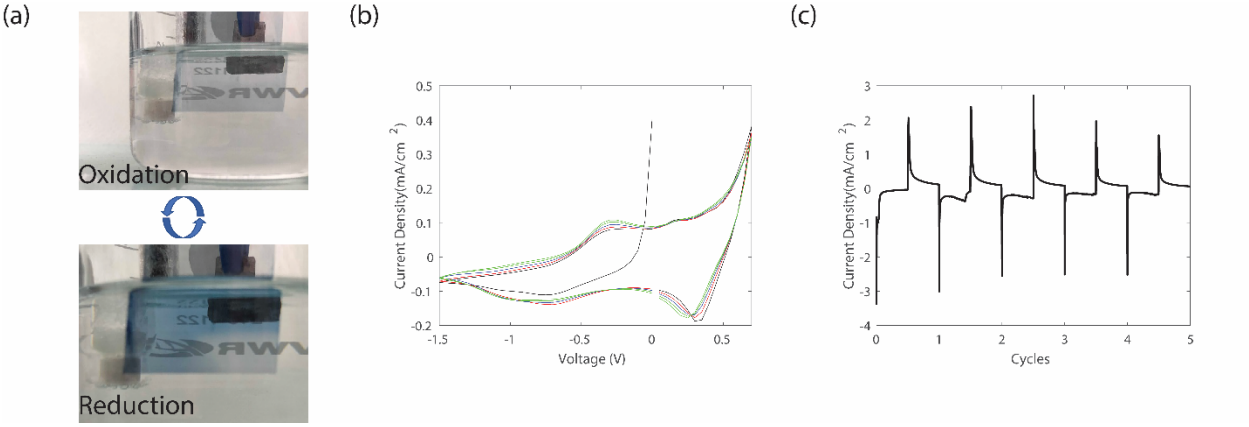

Figure 3.3: Film of PEDOT:PSS on AgNW electrodes on PET in the voltage range of -1.5 and +0.7 V. (a) Photos in in the oxidized (off) and reduction (on) state. (b) The CV profile for five cycles. (c) The CA profile.

Table 3.1: The colour change (ΔE), maximum change in transmittance (ΔT), colouration efficiency (CE) and switching times for PEDOT:PSS film on ITO and nanowire electrodes.

	ΔE	**Max ΔT (%)**	**CE (cm^2/C)**	**τ_{on} (sec)**	**τ_{off} (sec)**
PEDOT:PSS w/ ITO	23.9	21.9	77.9	6.8	15.1
PEDOT:PSS w/PU NWs	24.3	22.0	74.2	1.5	10.6

3.4 PEDOT:PSS Devices: Results and Discussion

3.4.1 Electrochromic Properties

Photos of the ITO and AgNW based device are shown in Figure 3.4 in the off and on states at voltages of ±1.0 V. To the eye, the switching looks uniform across both of the devices. For ITO, the ΔE is 11.8 compared to 14.8 for the passivated AgNWs (Table 3.2) which makes sense as Figure 3.4(d) appears to be slightly more blue than Figure 3.4(b), indicating a deeper colour change. At an operating voltage of +/-1.5 V, there is a larger difference. For ITO, the ΔE is 14.8, and for the PU-NWs the ΔE is 21.2. The passivated NWs are more conductive than the ITO and the PU increases their stability. This will lead to a higher

colour change value, along with the antireflection effect from the PU coating on the NWs discussed in Chapter 2.

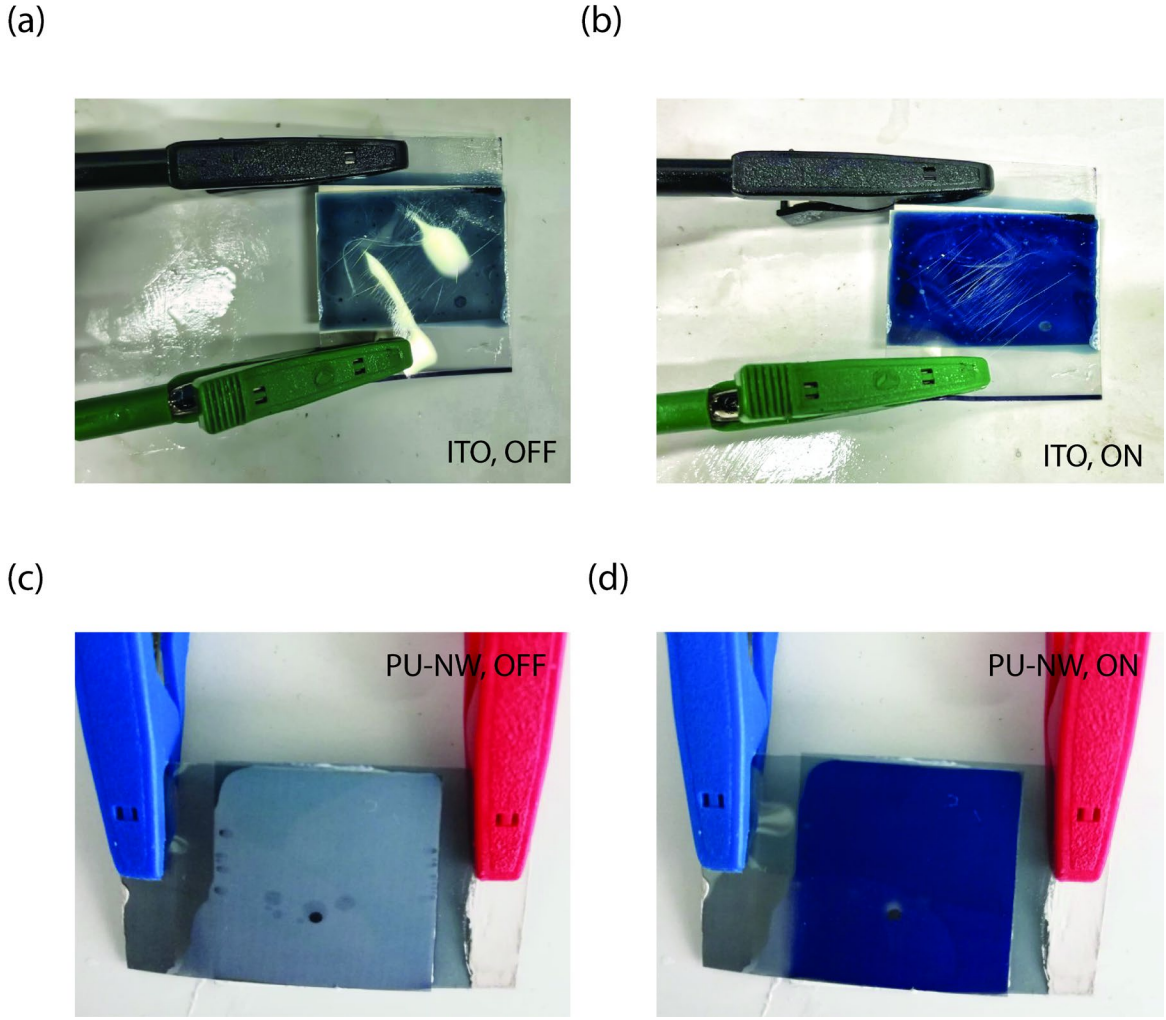

Figure 3.4: An ITO/PEDOT:PSS device in the off state (a) and on state (b). A passivated nanowire PEDOT:PSS device in the off state (c) and on state (d).

Table 3.2: The colour change (ΔE) for devices with ITO and passivated AgNW electrodes at operating voltages of +/-1.0 V and +/-1.5 V.

	ITO Electrodes (ΔE)	**Ag NW Electrodes w/ PU (ΔE)**
[- 1.0 +1.0] V Before 1000 Cycles	11.8	14.8
[- 1.5 +1.5] V Before 1000 Cycles	14.8	21.2

The same ITO and PU-NW devices had their reflectance measured from 400 – 900 nm using a Perkin Elmer Lambda 35 Spectrophotometer in reflectance mode. An Emstat 3+ potentiostat was attached to each device during measurement. The lid was closed and a black fleece blanket was placed over top to prevent stray room light from affecting the reflectance. Figure 3.5 compares the reflectance spectra of the ITO (black) and PU-NW (blue) at an operating voltage of +/- 1.5 V. The off state for both electrodes has the higher reflectance with ITO showing a higher value. However, in the on state, the PU-NWs have a lower reflectance. The overall change in reflectance is nearly identical. For the ITO electrodes, it is 9.41% and for the PU-NW electrodes, it is 9.47%.

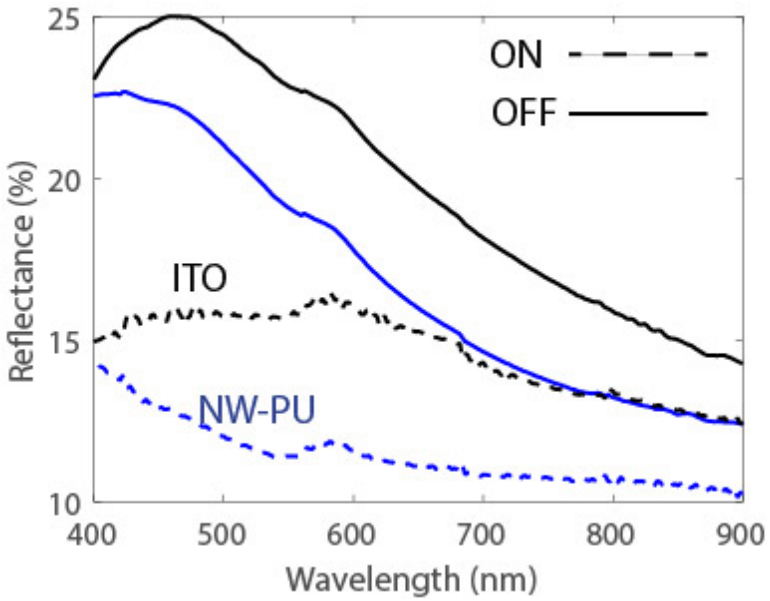

Figure 3.5: Reflectance of the PEDOT:PSS device with ITO and AgNW electrodes in the off and on state at +/-1.5 V.

Table 3.3: The colouration efficiencies of the ITO and passivated devices at operating voltages of +/-1.0 V and +/-1.5 V.

	ITO (cm^2/C)	Passivated NW (cm^2/C)
+/-1.0 V	13.52	94.95
+/-1.5 V	37.73	37.81

The third figure of merit to examine and compare between the two devices is the colouration efficiency. The calculation is described in detail in Section 1.6. The calculated efficiencies are shown above in Table 3.3 at operating voltages of +/-1.0 V and +/-1.5 V. At turn on voltages of +/-1.5 V, the efficiencies are nearly identical. However, at the lower turn-on voltages, there is a huge difference. The PU-NWs have a higher efficiency at 94.95 cm^2/C compared to only 13.52 cm^2/C for ITO. The colouration efficiencies were averaged from several cycles and different devices. At the +/-1.0 V operating voltage, the change in reflectance is the same. Examining Equation 1.5, this means the difference comes from the charge transferred, Q. Because of the longer switching time for the ITO displays and the current density in the CA not going all the way to zero, the charge transferred for the same change in reflectance is higher for an ITO device. This leads to the drastically different results. Hence, 1.0 V will be the ideal operating voltage for flexible displays with the PU-AgNW electrodes.

To compare the long-term stability of the devices, they were turned on and off for 1000 times. The devices in the off and on state for ITO electrode devices are shown in Figure 3.6(a) and (b) while the off and on state for PU-NW devices are shown in Figures 3.6(c) and (d). After 1000 cycles we can see a slight browning around the edges of the ITO. The ΔE after 1000 cycles is shown below in Table 3.4. There is minimum to no change in the ΔE value as for +/-1.0 V, it slightly increases from 11.8 (Table 3.2) to 12.0 and for +/-1.5 V it decreases from 14.8 to 13.6. For the PU-NW electrodes, there is also only minimal browning in the devices after 1000 cycles and the ΔE shows a slight increase from 14.8 to 16.6 at the lower operating voltage. At the higher operating voltage, there is a slight increase as well as the ΔE goes from 21.2 to 22.42. This shows that both devices are stable in their colour change when operated for long periods of time.

Table 3.4: The colour change (ΔE) for devices with ITO and passivated AgNW electrodes at operating voltages of +/-1.0 V and +/-1.5 V after 1000 on/off cycles.

	ITO Electrodes (ΔE)	**Ag NW Electrodes w/ PU (ΔE)**
[- 1.0 +1.0] V After 1000 Cycles	12.0	16.6
[- 1.5 +1.5] V After 1000 Cycles	13.6	22.4

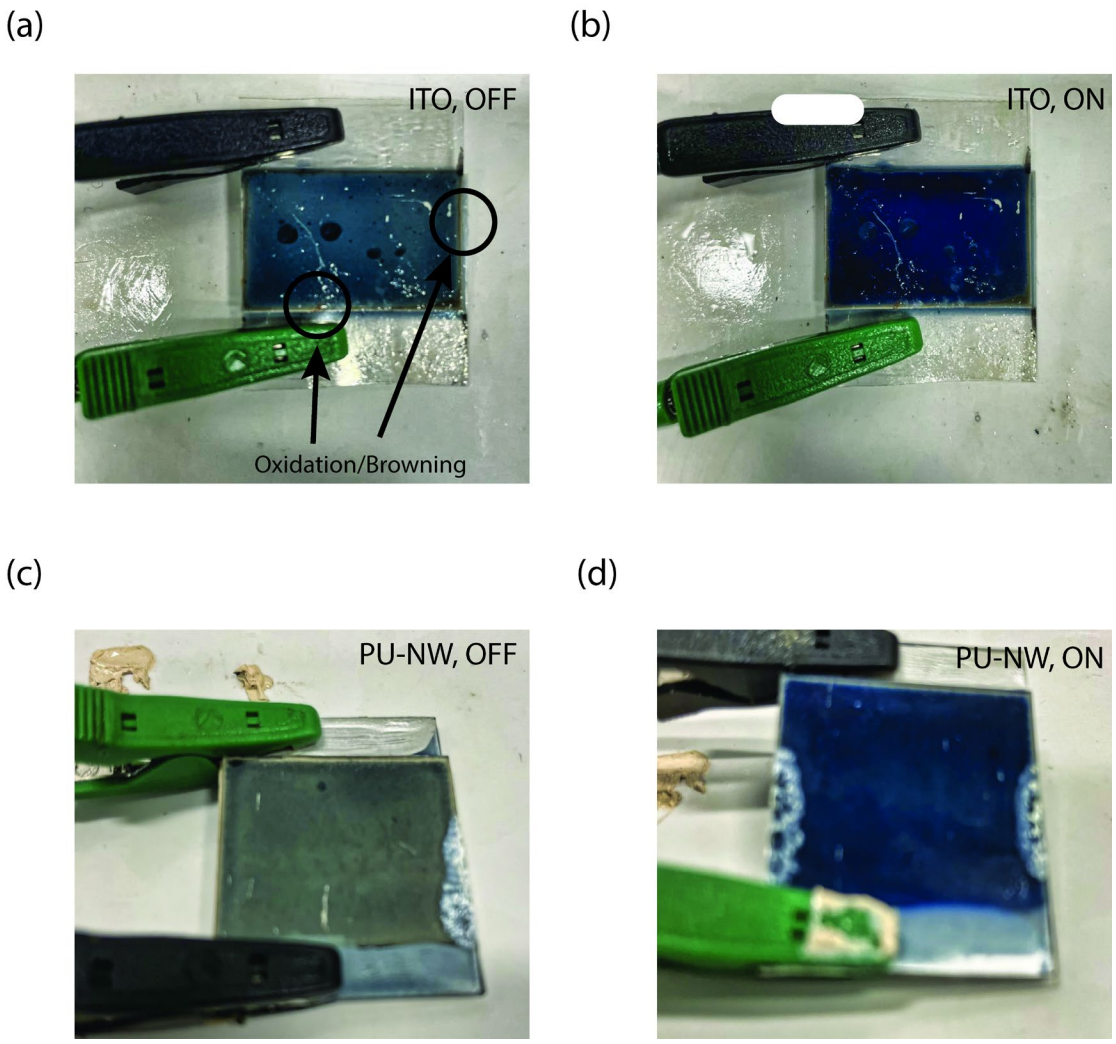

Figure 3.6: Photos of PEDOT:PSS devices after 1000 cycles of on/off switching at +/-1.5 V with ITO ((a) on and (b) off) and passivated Ag NW electrodes ((c) on and (d) off).

The CA plots, which show the current density of the electrochromic device after a potential difference is applied across the device, of the ITO and passivated devices throughout the 1000 cycles are shown in Figure 3.7. The main thing to note here is the stability of the CA plots. At +/- 1.0 V it can be seen that there is no fluctuation in the current density level in the ITO electrode device (Figure 3.7(a)) which shows device stability. The device with the passivated NW electrodes is just as stable (Figure 3.7(b)). At +/- 1.5 V, the current density of the ITO device continuously decreases over all cycles to finish at a value below 1 mA/cm^2 (Figure 3.7(c)). The current density of the passivated device does not level off nearly as severely and stays above 1 mA/cm^2 (Figure 3.7(d)). One reason for this is that the sheet resistance of the ITO increases after cycling: the sheet resistance of the ITO in a device after 1000 cycles was measured and found to increase

to 63 Ω/sq from 30 Ω/sq. As previously discussed, a thin film of indium can form on the surface of the ITO over several redox cycles, which increases sheet resistance [1]. Repeatability and stability are very important for device longevity. The ITO devices show slightly less stability at higher voltages than the passivated NWs. However, at a lower operating voltage, they are nearly identical.

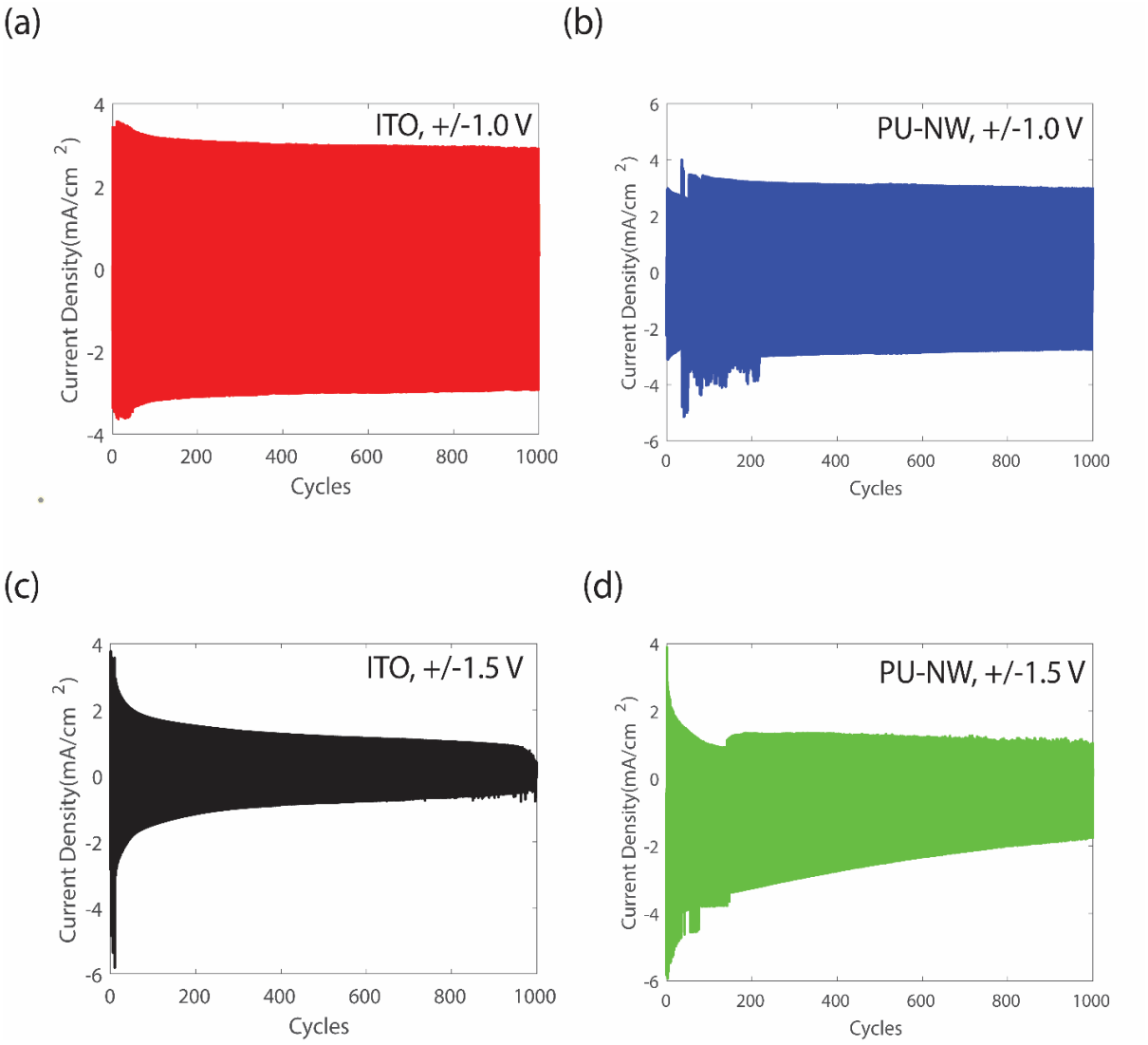

Figure 3.7: CA curves during 1000 cycles of devices with ITO electrodes ((a) and (c)) and passivated Ag NW electrodes ((b) and (d)) at operating voltages of +/- 1.0 V ((a) and (b)) and +/- 1.5 V ((c) and (d)).

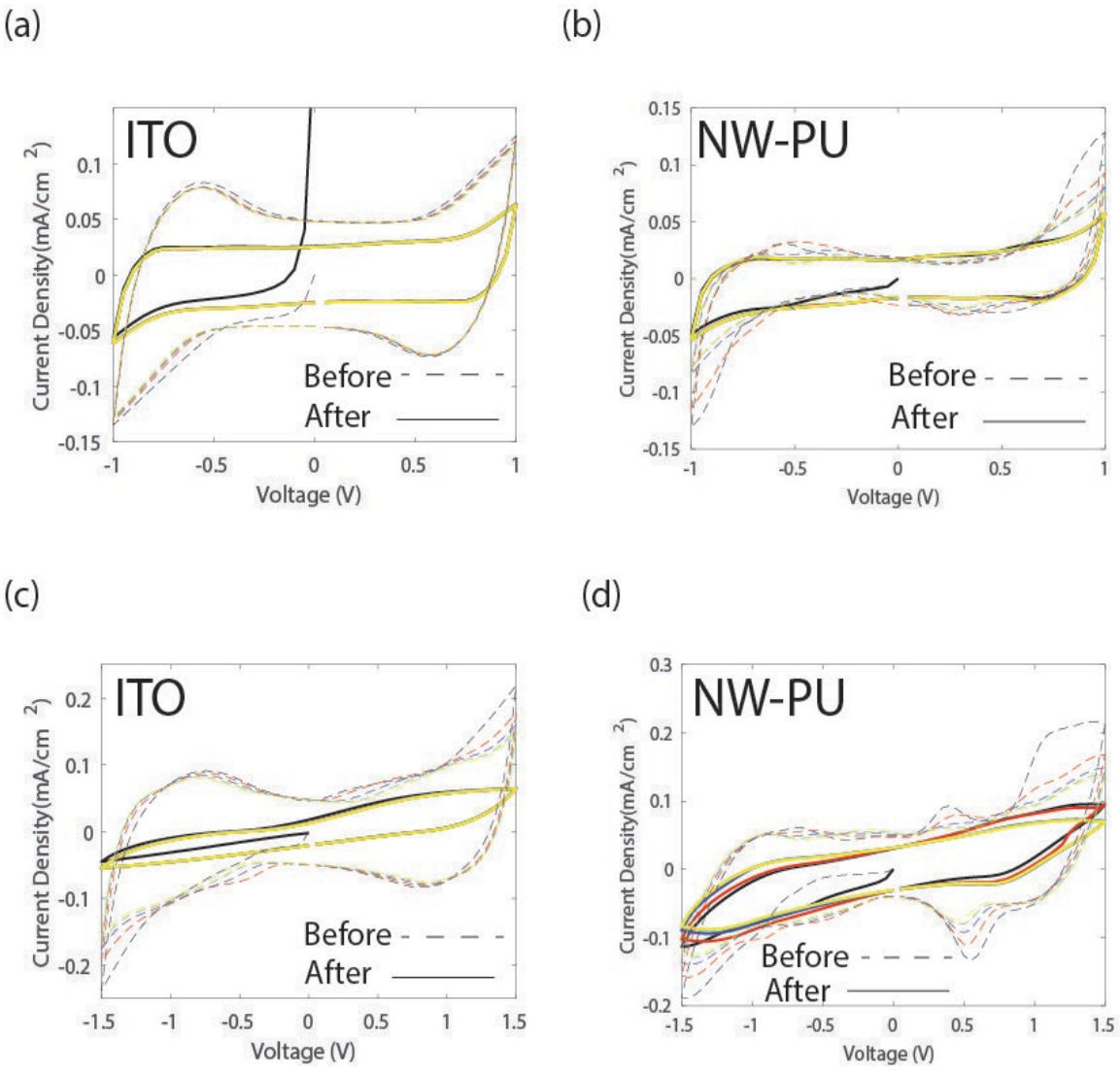

Figure 3.8: CV curves before and after 1000 on/off cycles of PEDOT:PSS devices with ITO ((a) and (c)) and passivated AgNW electrodes ((b) and (d)) at operating voltage of +/- 1.5 V ((a) and (b)) and +/- 1.0 V ((c) and (d)).

The CV curves of the first 5 and the last 5 of 1000 cycles of the two devices at both voltage ranges are displayed in Figure 3.8. The starting current is slightly higher in the ITO devices, since the PU of the NW electrode is insulating and lowers the out-of-plane conductivity. Thus, less current flows between the PEDOT:PSS and the NW electrode. However, as we have and will see, the important specifications of an electrochromic display such as ΔE, ΔR, colouration efficiency and lifetime are similar or better with the existence of the PU-NWs. At the smaller voltage window (Figure 3.8(a) and (b)), the NW devices are more stable, with the curves matching those before cycling except at the end voltage values. The current of the ITO devices drops at all voltages after cycling. At the larger voltage range, as expected, the stability in

both devices are worse. Before cycling, the AgNW curves have extraneous small peaks from the redox reaction of the AgNWs, which as noted before occur at +0.3 and +0.5 V. The peaks go away after 1000 cycles and the stability and performance of the device remains intact, because of the passivation. The average current density levels drop by about 0.05 mA/cm^2. In the ITO devices, the current drops by 0.08 mA/cm^2 on average. Thus, the passivated nanowire devices show more stability after 1000 cycles. The ITO is less stable due to the acidity of the PEDOT:PSS layer touching the ITO, and at higher voltages, the indium from the ITO undergoing reduction, which results in a decrease in conductivity after many cycles [1].

Table 3.5: The on and off switching times before and after 1000 on/off cycles.

	ITO Electrodes, t_{on}(sec)	**ITO Electrodes, t_{off} (sec)**	**Ag NW Electrodes w/ PU, t_{on} (sec)**	**Ag NW Electrodes w/ PU, t_{off} (sec)**
[- 1.0 +1.0] V Before 1000 Cycles	1.8	2.0	3.6	3.8
[- 1.0 +1.0] V After 1000 Cycles	4.0	2.0	1.4	1.2
[- 1.5 +1.5] V Before 1000 Cycles	1.7	6.2	1.7	4.5
[- 1.5 +1.5] V After 1000 Cycles	20	17.5	4	6.2

.

Another important parameter in electrochromic displays is switching time. The quickness of the switching time as well as repeatability over long periods are both important. The switching times for passivated and ITO devices, before and after 1000 cycles, at +/-1.0 V and +/-1.5 V, are tabulated in Table 3.5. These are collected from the CA plots and are defined as the times it takes for the current to drop or rise to 95% of its final value during the time of the applied on or off potential. At +/- 1.0 V, the initial switching times of the ITO devices are faster than those of the AgNW devices, due to the slightly higher initial current in the ITO devices. However, after cycling the switching time of the NW electrodes are faster, reducing to nearly 1 second. At +/-1.5 V, the switching times of both types of devices are initially very similar, but they

deteriorate much more in the ITO devices with cycling. Therefore, the AgNW devices have more stable switching times at both higher and lower operating voltages over long operating periods.

3.4.2 Device Mechanical Properties

In order to test device flexibility, passivated AgNW and ITO symmetrical PEDOT:PSS devices had their electrochromic properties measured before and after undergoing 50 bending cycles. Figures 3.9 (a) and (b) show the electrochromic device in the unstressed position and the bent or flexed position respectively. The bending angle was 80°. The same linear stage (Zaber Technologies, X-LHM150A) was used as the tests in section 2.5. For the ITO device, 5 cycles of the CV and CA measurements were collected before and after the 50 bends with the results shown in Figures 3.10. After the 50 bending cycles, both the CV and the CA undergo a major change. The area of the CV decreases significantly, due to a drastic increase in sheet resistance of the brittle ITO electrode with repeated bending. Examining films of ITO on PET, before and after 50 cycles at the same bending angle as the devices, it was observed that the sheet resistance increased from 30 Ω/sq to 23 000 Ω/sq. With the CV curve changing to a linear line, this indicates that the device no longer behaves like a capacitive electrochromic device. A straight line on a CV curve indicates just a resistor. The CA shows a big change as well as the curves in Figure 3.10(b) before (solid) and after (dashed) 50 bends are significantly different. The current does not decrease to almost zero after bending as it does at the beginning, indicating an incomplete switch of the colour has occurred. In Table 3.6, the ΔE is shown for the ITO devices before bending, after 50 bending cycles, and after 250 bending cycles. The ΔE drops significantly after 50 bending cycles going from 16.18 to 6.70. However, after 250 bending cycles the colour change no longer occurs and the ΔE is 0.45, which the human eye is not capable of seeing.

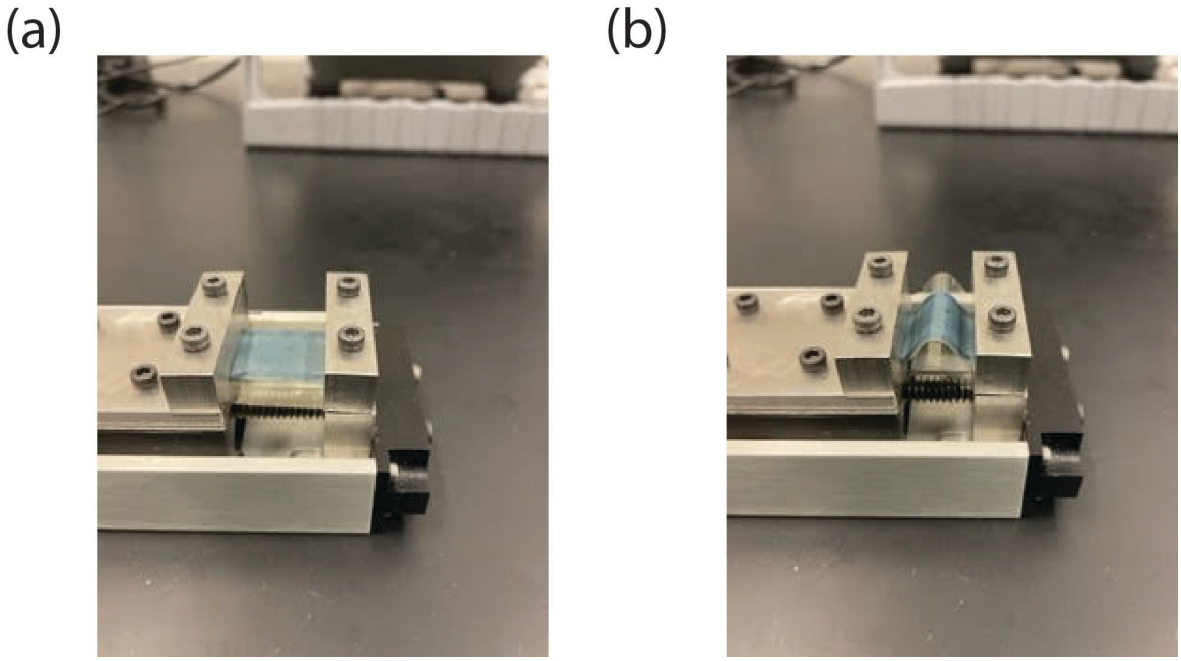

Figure 3.9: Photos of a PEDOT:PSS device in a linear stage in the unstrained (a) and bent (b) positions to test the flexibility performance of the devices.

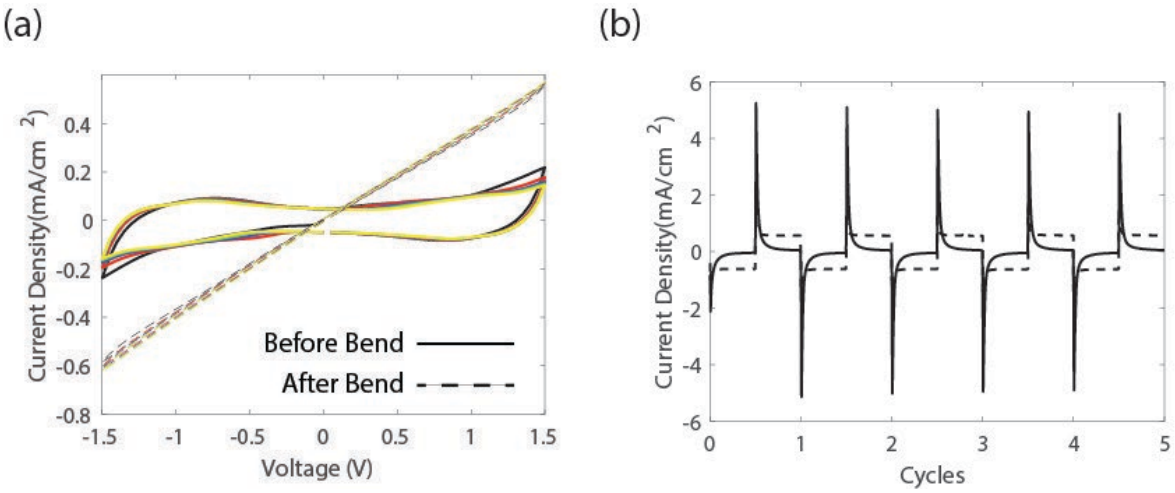

Figure 3.10: CV (a) and CA (b) of a PEDOT:PSS device with ITO electrodes before (solid line) and after (dashed line) 50 bending cycles.

The PEDOT:PSS AgNW electrode device also had its CV and CA values measured before and after 50 bending cycles. The resulting plots are shown in Figure 3.11(a) and (b), respectively. The CV only has a small decrease in area, which is likely related to the small increase in NW electrode sheet resistance with bending as determined in section 2.5. Similarly, the CA almost overlaps before and after the 50 bending

cycles. The ΔE of the passivated devices is almost similar to before bending as it only changes from 21.24 to 20.73. After 250 bending cycles, the passivation layer helps extensively by keeping the ΔE at 9.89 which is approximately 10. This is the lowest allowable value of the ΔE needed to see a visible change in an electrochromic display, compared to no noticeable difference in ΔE after 250 bending cycles for the ITO device. The mechanical performance of the devices made with NW electrodes strongly outperform those with ITO electrodes.

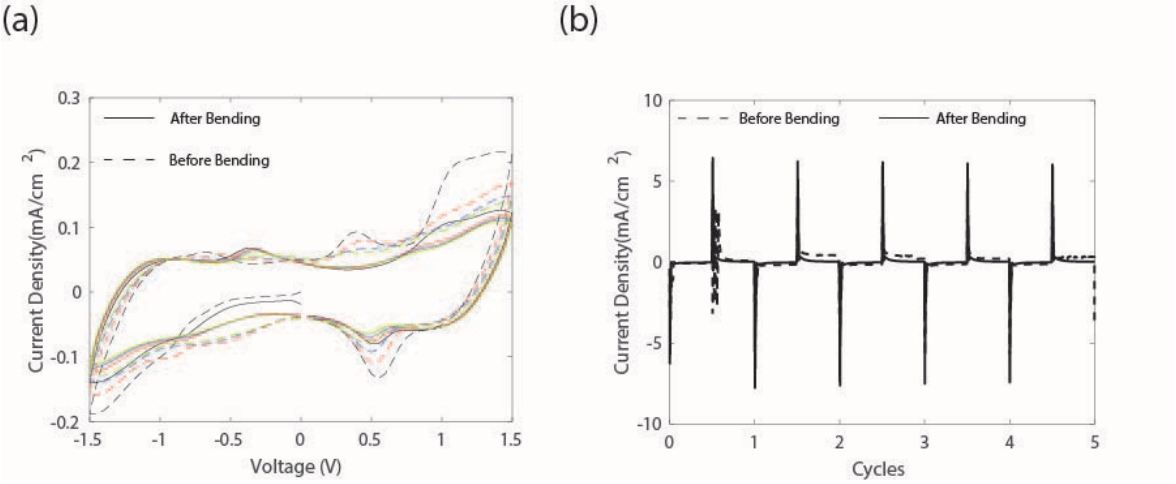

Figure 3.11: CV (a) and CA (b) of a PEDOT:PSS device with passivated AgNW electrodes before (solid line) and after (dashed line) 50 bending cycles.

Table 3.6: The colour change (ΔE) of PEDOT:PSS devices with ITO and NW electrodes before and after 50 bending cycles using on/off voltages of +/-1.5 V.

	ΔE ITO Electrodes	**ΔE AgNW w/ PU Electrodes**
Before Bending	16.18	21.24
After 50 Bending Cycles	6.70	20.73
After 250 Bending Cycles	0.45	9.89

3.5 PEDOT:PSS Films & Devices on Paper

Plastic substrates are made from petroleum products which are harmful to the environment. In order to create cheaper and more sustainable devices that can easily be recycled or disposed of and biodegrade, paper is an alternative. Electronic paper devices have become a hot topic over the last couple of years as they are low cost, biodegradeable, compostable, and flexible. They have several potential applications in the health care industry including wearable sensors, RFID, and paper displays [89]. More specifically, electrochromic paper is also being considered as a replacement for glass and plastic. PEDOT:PSS has been used as the electrode material in order to create electrochromic paper with three different colours [90]. ITO has been recently fabricated on paper substrates using low frequency pulsed laser deposition where the sheet resistance measured was 40 Ω/sq and transparency of 86.6% [91]. The optical and electrical properties are good, but the deposition requires high vacuum. Another problem is though that no electrical measurements were performed after putting the ITO on paper under mechanical strain. Considering that ITO on PET has a short lifetime when bent, the lifetime of ITO on paper would be similarly short. After a thorough search of literature, it is observed that there is no literature on using silver nanowire networks on paper as transparent electrodes for electrochromic paper. AgNW networks would be good for use on paper as they can be deposited using cheap, scalable deposition methods that do not require vacuum or high temperature annealing. This is important for paper which has a very low thermal budget. And since paper is flexible, the excellent mechanical flexibility of AgNW networks is highly valuable. Thirdly, silver nanowires can be recycled using laser ablation or sonication while recycling ITO is a much more complicated process [92], [93]. In this section, AgNW electrodes will be used in both electrochromic paper, and an electrochromic device that replaces one of the PET substrates with more environmentally friendly paper.

As described in the experimental Section 2.2, the paper used was Powercoat because it has a relatively low surface roughness for paper (average surface roughness is 2000 nm), has a high thermal budget (3% shrinkage when heated to 200°C for 5 min), and a low moisture content. Figure 3.12(a) shows photos of the electrochromic paper (i.e. a 3 layer stack consisting of paper with a AgNW electrode and PEDOT:PSS on top) in the LITFSI:Emim TFSI in the oxidation (off) and reduction (on) state. There is a clear colour switch between the on and off state. The ΔE was measured to be 15.67, well above the limit to see a switch by the human eye. Figure 3.12(b) displays the CV taken with a voltage interval from -0.8 V to +0.3 V for five cycles. The stability is quite good as the current density for all five cycles overlaps at nearly the same level. Additionally, the magnitude of the current density, 0.2 mA/cm^2 and -0.4 mA/cm^2, is similar to films

on PET. The CA is shown in Figure 3.12(c). Both the on and off current density profiles remain stable over the five cycles, outside of the first switch. This is normal as electrochromic films require a cycle or two to level out after initial fabrication [1]. The switching times of the electrochromic paper were found to be 2.18 seconds for the on time and 7.2 seconds. This is acceptable and comparable to the switching times on PET measured previously in Section 3.3 and Chapter 2.

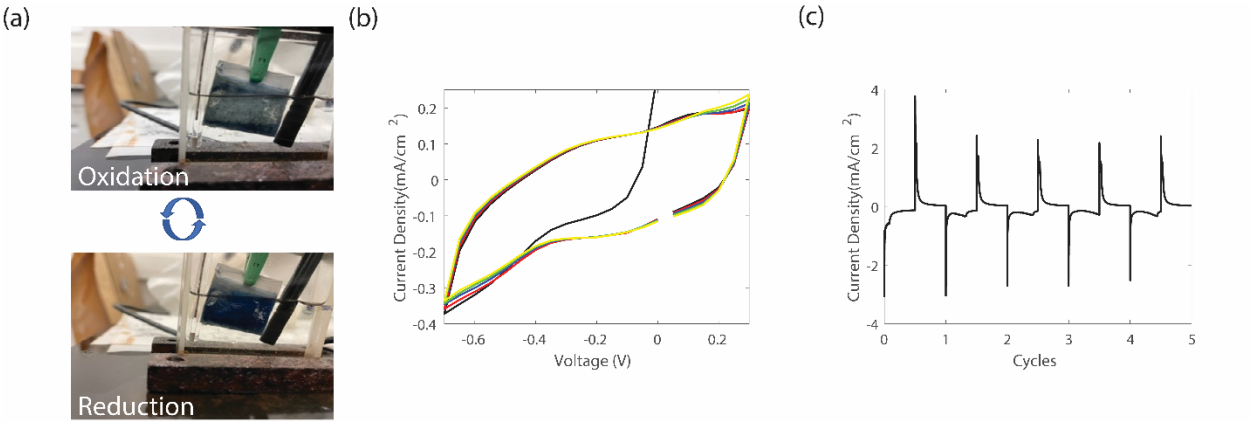

Figure 3.12: PEDOT:PSS films on a passivated AgNW electrode using a voltage range of -0.8 and +0.3 V: (a) photos in the oxidized (off) and reduction (on) state, (b) the CV profile for five cycles; (c) the CA profile.

The paper-based device in the off and on state is shown in Figure 3.13(a). The ΔE of this device was measured to be 9.27. This is close enough to the acceptable limit to notice a colour change detectable by the human eye. Figure 3.13(b) shows the CV between -1.0 and +1.0 V. Here, there is clear stability of the current density, even though the current density is slightly lower than the devices on PET. This agrees with the colour change being lower than the PET devices. This could be from more light scattering as the paper has a higher surface roughness than PET. The CA of the paper device is in Figure 3.13(c). The peak current density levels stay at the same level over five cycles. However, the current density does not go all the way to zero indicating non-ideal operation of the paper device. More research will have to be done to fully and further optimize the device. The switching times were calculated to be 20.9 seconds for the on time and the off times is 1.48 seconds. The ΔE is much lower than that reported in Lang et al. where values as high as ΔE = 56 were reported [90]. However, using PEDOT:PSS as the electrode is a disadvantage as the sheet resistance was 460 Ω/sq. Using a AgNW electrode with a sheet resistance of 10 Ω/sq should greatly improve the kinetics of the electrochromic paper compared to PEDOT:PSS. There is significant improvement to be done with these switching times and colour change measurements with future work.

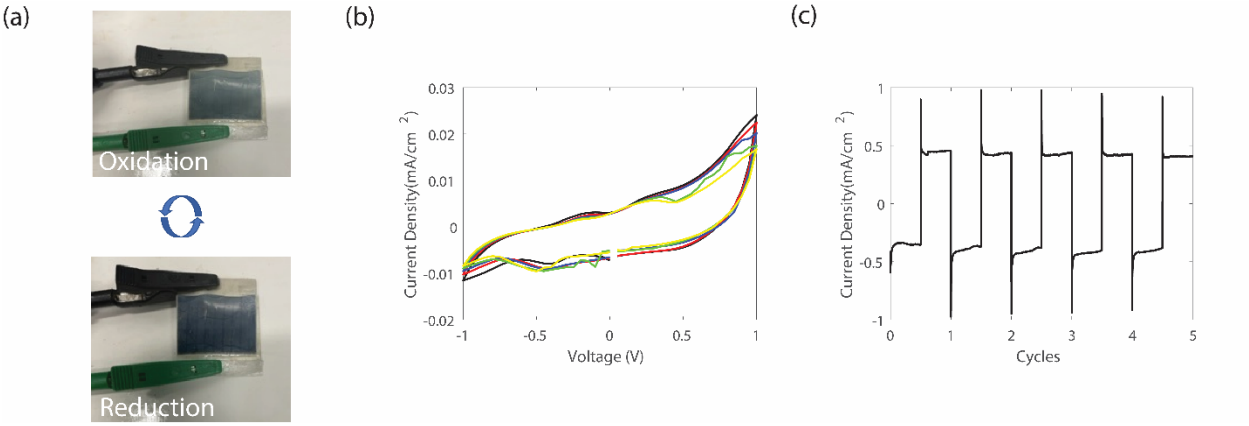

Figure 3.13: A PEDOT:PSS device using AgNW electrodes on paper, topped with PET, using the voltage range -1.0 to +1.0 V: (a) photos in the oxidized (off) and reduction (on) state; the (b) CV and (c) CA profiles for five cycles.

3.6 Conclusion

In this chapter the operation of flexible electrochromic devices with ITO electrodes and PU-NW electrodes on PET plastic was thoroughly studied. The electrochromic properties were comparable between the two different devices. However, over long periods of time, the PU-NW based devices showed to be more stable with lower switching times and better ΔE compared to the ITO devices. After 1000 cycles, there is a little browning from oxidation in the ITO devices, however there is no browning in the passivated nanowire devices. The current density drop is also slightly less in the PU-NW devices over 1000 cycles. The biggest strength of the NW-based devices is their mechanical properties, which far outperform the ITO devices. After 50 full bending cycles at a bending angle of 80°, the ITO devices no longer work as the CV is no longer a closed loop but a straight line and the ΔE decreases to 6.70. However, for the PU-NW devices, there is hardly any change in the CV and CA after 50 bending cycles and the ΔE only decreases from 21.24 to 20.73. Therefore, PU-NWs are a viable candidate as a replacement for ITO in PEDOT:PSS electrochromic devices, especially flexible ones.

Electrochromic paper and electrochromic paper devices were fabricated using the PU-NW electrodes and shown to have good initial stability and a good enough colour change to be seen by the human eye. Although the electrochromic parameters of the electrochromic paper and device were not as high as reported elsewhere, the sheet resistance achieved is much lower than that used in other sources. Therefore, AgNW

electrodes show promise for use on paper for disposable and foldable displays and require further research and development.

Chapter 4
Composite Silver Nanowire/PEDOT:PSS Electrochromic Layers

In this chapter, silver nanowires are mixed in with the PEDOT:PSS electrochromic layer itself rather than existing in a separate electrode. The optimal nanowire diameter, length, and concentration of AgNWs is determined to use in these mixed electrochromic films and passivate the nanowires with small molecules to minimize their corrosion. The properties of these films and devices will be compared to those with pure PEDOT:PSS. Finally, there is comparison of the turn-on voltage, switching time, reflectance, stability, and lifetime of these new devices compared to devices where the PEDOT:PSS electrochromic material and nanowire electrode are kept in separate layers.

4.1 Introduction

As discussed in Chapter 2 and 3, PEDOT:PSS has been extensively studied as the electrochromic layer in flexible electrochromic devices. However, because of its low conductivity it can have slow switching kinetics and require a large voltage window in order to get good colour contrast. The conductivity of PEDOT:PSS can be improved by mixing in conductive particles. Higher conductivity will lower the voltage required to change the colour of the PEDOT:PSS. And higher conductivity allows for a higher current at a given voltage, which will increase the speed at which charge is transferred from the electrolyte to the PEDOT:PSS resulting in the colour changing at a quicker rate.

Many studies have successfully mixed conductive particles into PEDOT:PSS to improve its conductivity for its use as a transparent electrode [54], [94]–[97]. The higher conductivity arises from the double electron transport channels that are created when you have two paths for electrons to travel through corresponding to the PEDOT:PSS and the added conductive particles [98]. But very few studies have mixed conductive particles into PEDOT:PSS for use as an electrochromic layer. As discussed in Section 1.6.1, Gomes et al. completed a study measuring the sheet resistance and electrochromic properties of PEDOT:PSS films mixed with a variety of conductive materials [54]. The materials included graphene, graphite, AZO, and AgNWs. They found that the average sheet resistance improved the best, from 600 to 275 Ω/sq, when graphite was added to PEDOT:PSS, and the transition time was reduced to <5 seconds [54]. However, the

transmittance in the off state was <70% in the visible region. The sheet resistance was almost as low when AgNWs instead were mixed with PEDOT:PSS, 290 Ω/sq, with a switching time of ~ 8 seconds, and the transmittance was better: >85% across the visible [54]. Importantly, the AgNW/PEDOT:PSS mix showed a higher current density and change in absorbance compared to the graphite composite and all the other mixed films.

Peng et al. also mixed AgNWs with PEDOT:PSS for use as electrochromic films [98]. Graphene electrodes on flexible substrates were used instead of ITO or no electrodes. They found the addition of the AgNWs increased the current density and change in transmittance beyond pure PEDOT:PSS. This therefore increased the colouration efficiency from 138 to 182 cm^2/C. Additionally, the sheet resistance was reduced, and ionic conductivity improved [98].

These early studies show the potential of mixing AgNWs with PEDOT:PSS to improve the electrochromic properties. However, particularly in the Gomes study, the sheet resistances of the mixed films are still quite high. Neither study explored how nanowire diameter, length, and concentration could be used to improve the film properties. And a full characterization of hybrid electrochromic PEDOT:PSS/AgNW films and devices was not done. Therefore, a more complete study of a mixed PEDOT/AgNW device needs to be completed. Secondly, the Peng et al. study still uses a graphene electrode. Ideally, the PEDOT:PSS/AgNW electrochromic film would not require an electrode at all as it could be conductive enough on its own. Not requiring an electrode is preferable as it reduces the cost and complexity of the device. Lastly, the silver nanowires are not passivated in either study which is an issue as they corrode when they are in direct contact with PEDOT as discussed in Chapter 2.

In this chapter, an optimization of the AgNW diameter, length, and concentration through characterization of the electrochromic properties is completed. These optimized films will be compared to pure PEDOT:PSS films. Next, a device will be made with the optimized film and the electrochromic parameters will be fully characterized. It will be shown that a 3 layer rather than 5 layer electrochromic device without ITO or any other electrode is possible to fabricate and operate. Because of lifetime issues of the nanowires, the passivation of the nanowires with two different passivation candidates and mixed them with PEDOT:PSS is studied. Lastly, the electrochromic properties of hybrid AgNW/PEDOT:PSS films will be compared and devices versus the case where AgNWs and PEDOT:PSS exist in separate layers will be fabricated and characterized.

4.2 Experimental

Glass substrates (Ted Pella, 26005) and ITO on glass substrates (SPI, ZO6401, 30-60 Ω/sq) were cut into 2.5 x 2.5 cm square pieces, cleaned in subsequent ultrasonication baths with acetone, IPA, and DI water for 60 seconds each, then dried with a nitrogen gun.

PEDOT:PSS (EL-P3165, AGFA) was mixed overnight with ethanol at a stirring rate of 1500 rpm with a magnetic stirrer at a proportion of 70 wt% (PEDOT:PSS) : 30 wt% (ethanol). The solution was then ultrasonicated with a probe sonicator continuously for 15 min at a frequency of 1 kHz. Silver nanowires dispersed in ethanol with nominal diameters of 30, 70, and 100 nm that were purchased from Novarials Corporation (A30UL, A70UL, and A100UL, Woburn, MA). Each of these solutions had very similar average nanowire lengths of 88 $\pm$ 19 µm as measured with SEM and using ImageJ as described in Section 2.2. These nanowires types will be referred to as 30UL, 70UL, and 100UL. Silver nanowires dispersed in ethanol with the same nominal diameter of 30 nm, but averaged measured lengths of 2.5, 21, and 88 µm, were also purchased from Novarials Corporation (A30SL, A30L, and A30UL). These samples will be referred to as 30SL, 30L, and 30UL (SL= short length, L = medium length, UL = ultralong). The distribution of the lengths of these nanowires are shown below in Figure 4.1. The average length and deviation is also shown below in Table 4.1. The as-received concentration of all nanowire types was 10 mg/ml and were diluted with ethanol to achieve the desired concentration.

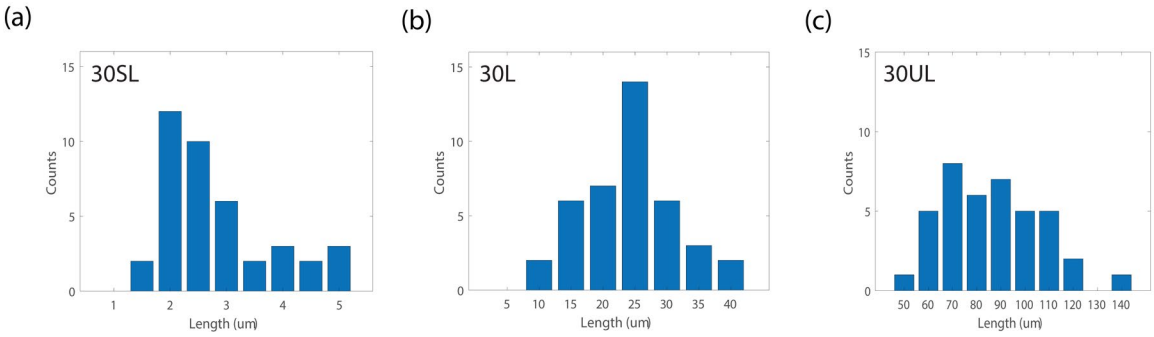

Figure 4.1: The nanowire diameter distribution calculated from ImageJ for 30SL (a), 30L (b), and 30UL (c) nanowires in ethanol purchased from Novarial.

Table 4.1: The nanowire average measured diameter and length with standard deviation calculated from ImageJ for 30SL, 30L, and 30UL nanowires in ethanol purchased from Novarial.

	Length (µm)
30SL	2.5 ± 1
30L	21 ± 7
30UL	88 ± 19

To optimize the nanowire diameter and length, 2 ml of the PEDOT:PSS/ethanol mix was mixed with 0.5 ml of the various AgNW samples at a concentration of 3 mg/ml (Figure 4.2(a)). The resulting solution was stirred at 1500 rpm for 2 hours with a magnetic stir bar. For a comparison sample without AgNWs, 0.5 ml of ethanol was added to 2 ml of PEDOT:PSS/ethanol and stirred.

0.5 ml of the NW/PEDOT:PSS composite or pure PEDOT:PSS was pipetted across the plain glass or ITO on glass substrate and then a Mayer Rod (RDS #60) was used to drag the solution across the glass substrate to form a thin film. The samples were annealed on a hot plate at a temperature of 120°C for 30 minutes to remove the PVP layer from the AgNWs, weld any AgNW junctions, and evaporate the ethanol from both the PEDOT:PSS and the AgNWs. An optical microscope image of the final hybrid films is shown in Figure 4.2(b) (SEM imaging would not be able to distinguish nanowires underneath the surface).

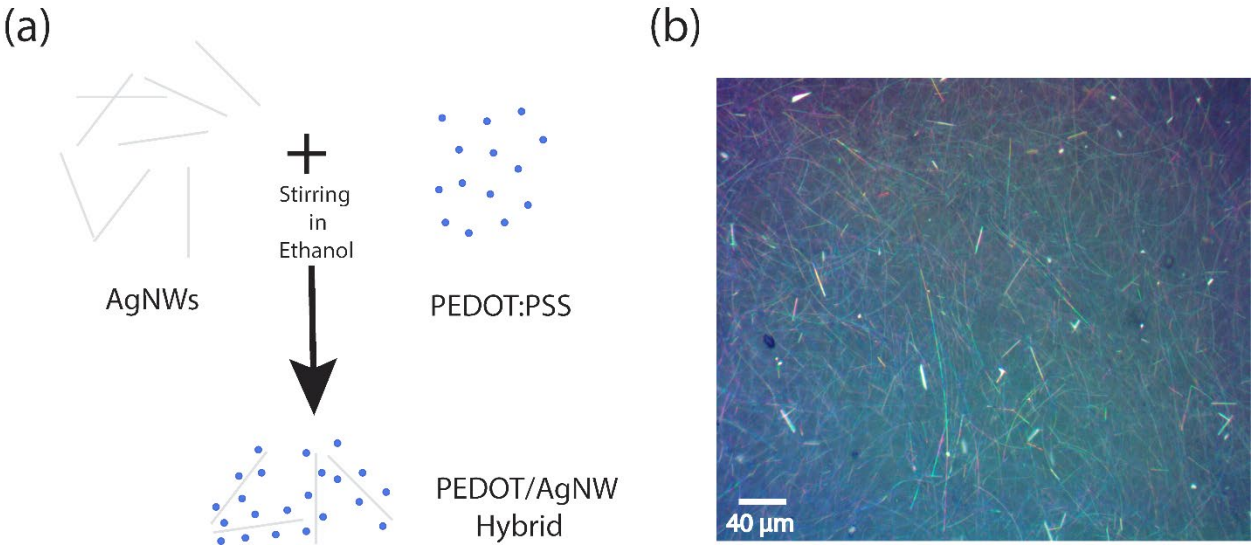

Figure 4.2: (a) Schematic of the fabrication of mixed PEDOT/NW films. (b) Optical microscope image of a hybrid PEDOT/AgNW film.

4.3 Optimization of Nanowire Parameters

4.3.1 Nanowire Diameter

The first parameter of the PEDOT:PSS/AgNW hybrid films to be optimized is the nanowire diameter. PEDOT:PSS was mixed with samples 30UL, 70UL, and 100UL to form three different types of hybrid films according to the process outlined in Section 4.2 on both glass and ITO on glass substrates. The CV curves of these three composite films are shown in Figure 4.3(a). The 100UL sample has the lowest turn-on voltage, peaking at -0.9 V and +0.7 V. 70UL and 30UL films both peak at +0.7 V but their turn-on voltages are -1.2 and -1.1 V, respectively. In Figure 4.3(b) we see the CA for these three films. The CA was measured by switching the films on in the reduced state for 30 seconds and then off to the oxidized state for 30 seconds. The film with 70UL nanowires had the fastest switching times because it has the lowest sheet resistance of the three diameters as shown in Table 4.2. However, the ΔT and ΔE the highest for the 30UL hybrid films (Table 4.2). This is because the smaller diameter of the 30UL does not block or scatter as much light like the larger diameter AgNWs do [99]. The colouration efficiency is highest for the 70UL film, but that of the 30UL film is a very close second. There are advantages and disadvantages of the 30UL versus 70UL, though due to its far better colour and transparency change, the 30 nm diameter AgNWs are determined to be the best diameter going forward.

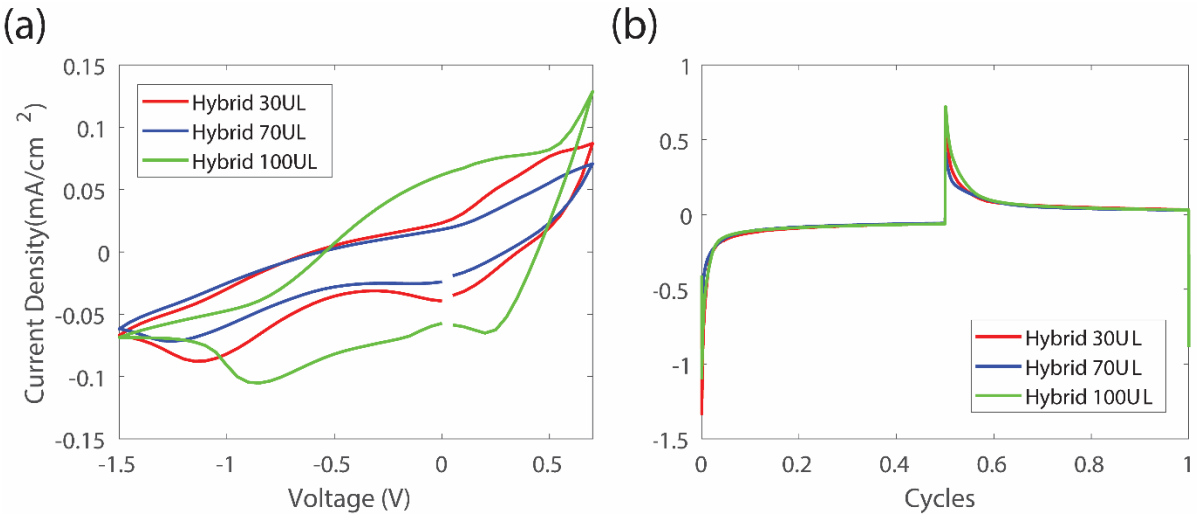

Figure 4.3: (a) CV and (b) CA curves of PEDOT:PSS/AgNW composites with nanowire diameters of 30, 70, and 100 nm.

Table 4.2: Sheet Resistance (R_s), ΔE, ΔT, switching times, colouration efficiency (CE) and turn-on voltage for different nanowire diameters.

	R_s (Ω/sq)	ΔE	ΔT	τ_{on} (s)	τ_{off} (s)	CE (cm^2/C)	V_{on} (V)
30UL	34	26	37	6.4	6.4	67.7	-1.1
70UL	14	17	13	2.7	4.3	68.1	-1.2
100UL	28	19	19	4.7	4.3	61.7	-0.9

4.3.2 Nanowire Length

The second parameter to optimize will be the length of the AgNWs. Figure 4.4(a) shows the CV of PEDOT:PSS/AgNW hybrid films with a nanowire diameter of 30 nm and average lengths of 2.5 μm, 21 μm, and 88 μm. They will be referred to as 30SL, 30L, and 30UL, respectively. The 30UL AgNWs have the lowest turn on voltage with the current density peaking at -1.2 V. Both 30L and 30SL peak at -1.3 V. All three films have the same turn off voltage of +0.7 V. In Figure 4.4(b) the CA is shown for these films. The 30UL film has the fastest switch-on time, second fastest switch-off time, and has the lowest sheet resistance. This is because with longer AgNWs the electrons can travel further before having to re-enter the PEDOT:PSS or encounter a resistive NW-NW junction, which have a higher resistance compared to the AgNW itself [100]. Examining the rest of Table 4.3, we can see that the longest AgNWs have the best ΔT as the trend increases from 14% to 37% as the length is increased from 3 μm to 88 μm. The ΔE also increases with AgNW length going from 12 to 26. Longer AgNWs are known to have a higher transmittance compared to shorter AgNW lengths. This will be explained further in Chapter 5. Lastly, the colouration efficiency is the second highest for the 30UL films. Overall, the 88 μm length AgNWs are the winner as they have superior optical properties along with the lowest sheet resistance, lowest turn on voltage, and good switching times.

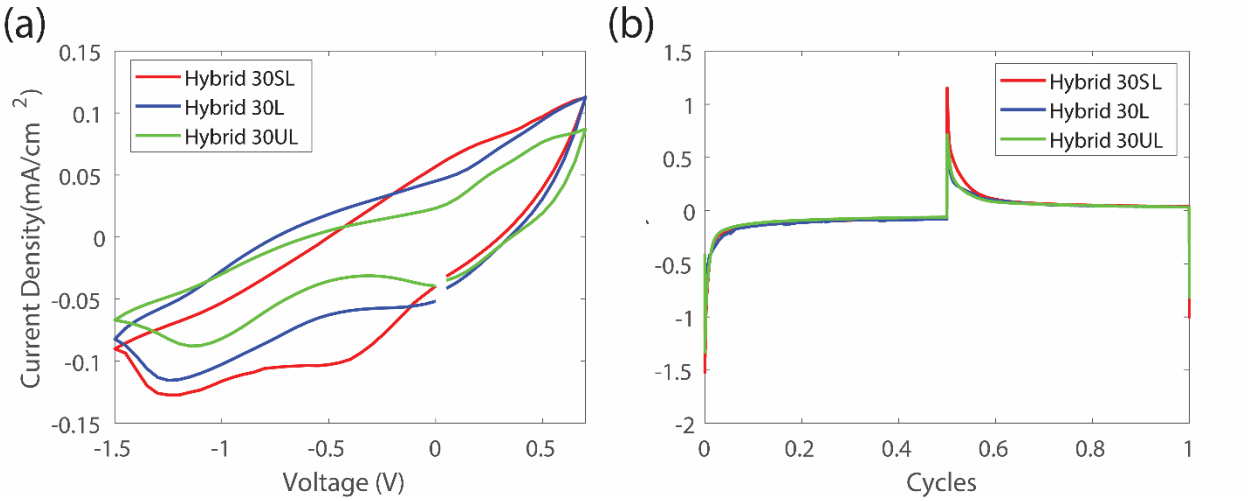

Figure 4.4: (a) CV and (b) CA curves of PEDOT:PSS/AgNW composites with nanowire lengths of 3 µm (30SL), 28 µm (30L), and 88 µm (30UL).

Table 4.3: Sheet Resistance (R_s), ΔE, ΔT, switching times, colouration efficiency (CE) and turn-on voltage for different nanowire lengths.

	R_s (Ω/sq)	ΔE	ΔT	τ_{on} (s)	τ_{off} (s)	CE (cm^2/C)	V_{on} (V)
30SL	57	12	14	4.4	8.1	50.9	-1.3
30L	40	14	26	8.3	10.9	76.1	-1.3
30UL	34	26	37	3.6	9.1	67.7	-1.2

4.3.3 Nanowire Concentration

In the previous two sections it was found that the longest, thinnest NWs are optimal. Therefore the 30 nm diameter and 88 µm length nanowires were used to optimize concentration. AgNW concentrations ranging from 1.0 to 10.0 mg/ml were mixed with PEDOT:PSS as described in Section 4.2. The CVs of these hybrid films at different concentrations are shown below in Figure 4.5(a). The current densities of the concentrations ranging from 4.0 to 10.0 mg/ml are very small, and are only appreciable for concentrations of 1.0, 2.0, and 3.0 mg/ml. In Figures 4.5(b) and (c) the quickest change in current density once the device is switched is seen for a concentration of 3.0 mg/ml. This concentration also has a low turn on voltage of -1.1 V.

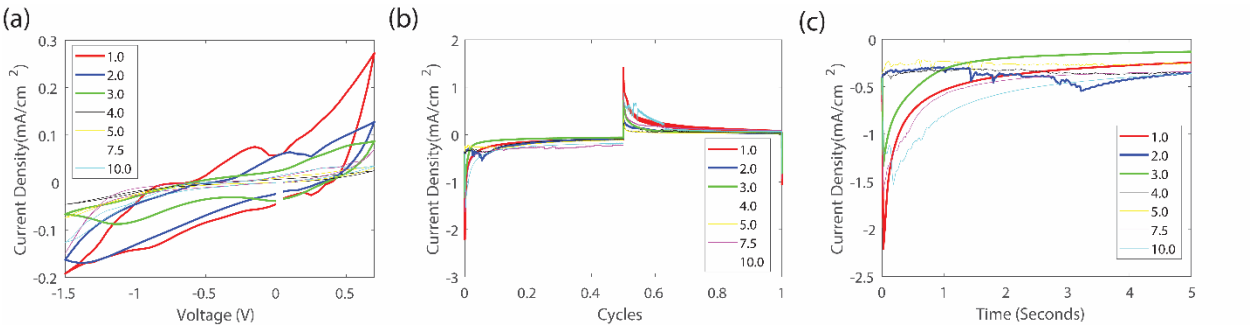

Figure 4.5: (a) CV and (b) CA curves of PEDOT:PSS/AgNW composites at nanowire concentrations ranging from 1.0 – 10.0 mg/ml. (c) Magnification of the first on-cycle of (b).

Table 4.4: Sheet Resistance (R_s), ΔE, ΔT, switching times, colouration efficiency (CE) and turn-on voltage of 30 nm diameter, 88 µm long nanowires at different concentrations.

NW concentration (mg/ml)	R_s (Ω/sq)	ΔE	ΔT	τ_{on} (s)	τ_{off} (s)	CE (cm^2/C)	V_{on} (V)
1.0	90	44	44	3.4	9.8	38	-1.3
2.0	66	36	27	15	9.2	40	-1.0
3.0	34	26	37	3.6	9.1	68	-1.1
4.0	43	23	21	1.7	9.6	44	-1.0
5.0	18	23	20	3	7.5	51	-1.0
7.5	5.5	22	21	2.2	11	38	-1.3
10.0	4.3	25	7.9	3.1	8	28	-0.9

The sheet resistance as expected improves as the AgNW concentration is increased from 1.0 to 10.0 mg/ml (Table 4.4). However, ΔE and ΔT are the highest as a pure PEDOT:PSS film is approached with no nanowires (concentration of 1.0 mg/ml). 3.0 mg/ml is the best compromise with the highest colouration efficiency of 68 cm^2/C, and good switching times and turn-on voltage.

4.4 Optimized Mixed Layers vs. PEDOT:PSS

4.4.1 Hybrid Films vs. PEDOT:PSS

In this section the optimized composite films (30 nm diameter, 88 µm length, 3.0 mg/ml) are compared to pure PEDOT:PSS films both with and without an ITO electrode. The latter will help determine if the ITO electrode is required and how much difference it makes to the optical and electrical properties. Figure 4.6(a) and (b) show PEDOT:PSS and hybrid films, respectively in the on and off states on an ITO-coated glass substrate. The on voltage used here is -1.5 V and the off voltage is set as +0.7 V. Figure 4.6(c) and (d) show the PEDOT:PSS and hybrid films again in the on and off states but this time on plain glass. There is a clear uniform switch in all 4 cases in the on and off state. This leads to the consideration of the electrochromic behaviour of each film in order to better tell the differences between each case.

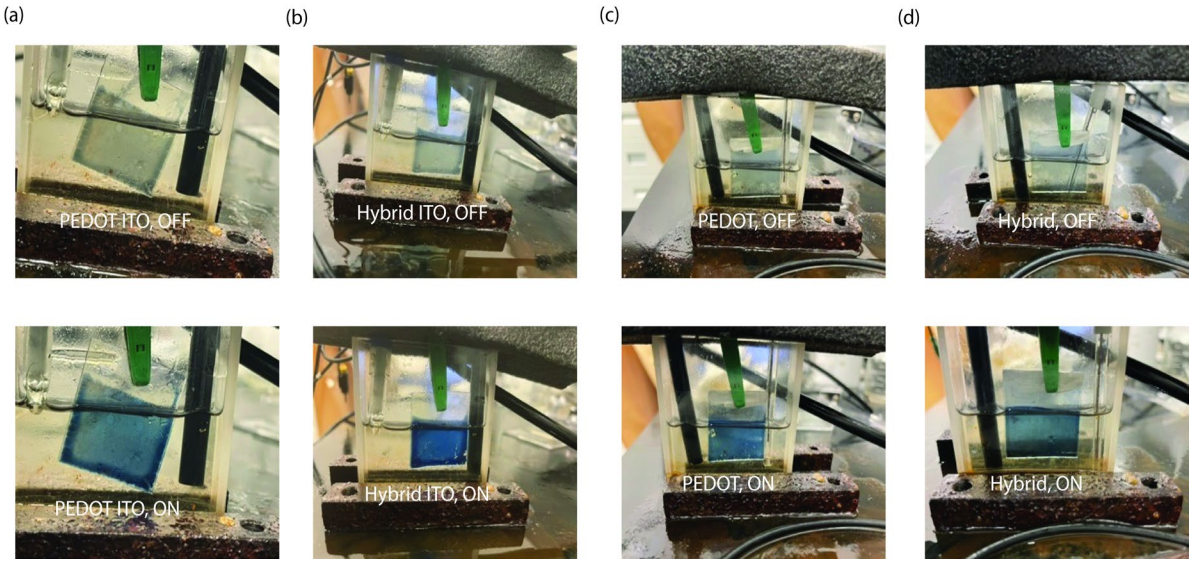

Figure 4.6: Pictures of pure PEDOT:PSS and PEDOT:PSS/AgNW hybrid films in the on and off states on (a),(b) ITO/glass and (c),(d) plain glass substrates.

CV curves (Figure 4.7) demonstrate that the performance of the hybrid film is superior to pure PEDOT:PSS both with and without ITO. Figure 4.7(a) compares the CV curves of hybrid films to pure PEDOT:PSS on ITO-coated glass. Because of the higher conductivity of the AgNW/PEDOT:PSS film, not as much potential is required to turn on the film; the current peaks for the redox reaction of the hybrid film are at -0.9 V compared to -1.5 V for the pure PEDOT:PSS. The magnitude of the current density at the on and off

voltages is also higher. When the ITO is taken away (Figure 4.7(b)), the peaks in the pure PEDOT:PSS film get broader to the point where the peak is not well defined. This is due to the low conductivity without the ITO. The broader the peak is, the slower the electrochemical reaction occurs. The peaks in the hybrid film can still clearly be seen, indicating a faster electrochemical reaction and switching time. The hybrid film has a sheet resistance of 34 Ω/sq (compared to 280 Ω/sq for the pure PEDOT:PSS), which is similar to the sheet resistance of the ITO. There is though, as expected, some decrease of performance of the hybrid film when ITO is not used. The turn on voltage increases from -0.9 to -1.1 V and the current density decreases.

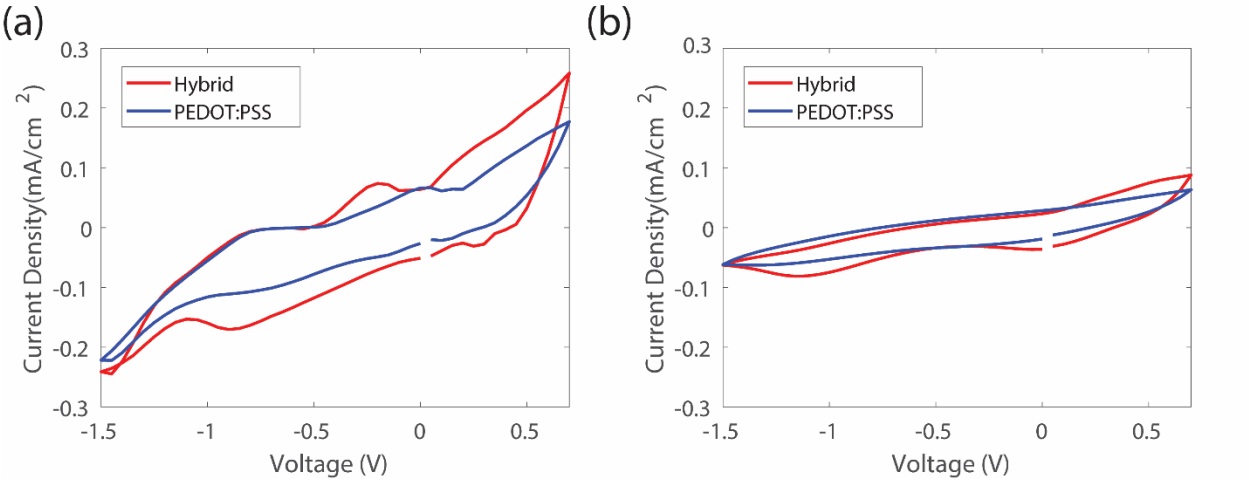

Figure 4.7: CV curves of mixed PEDOT/NW films ("Hybrid") and pure PEDOT:PSS films on (a) ITO glass and (b) plain glass.

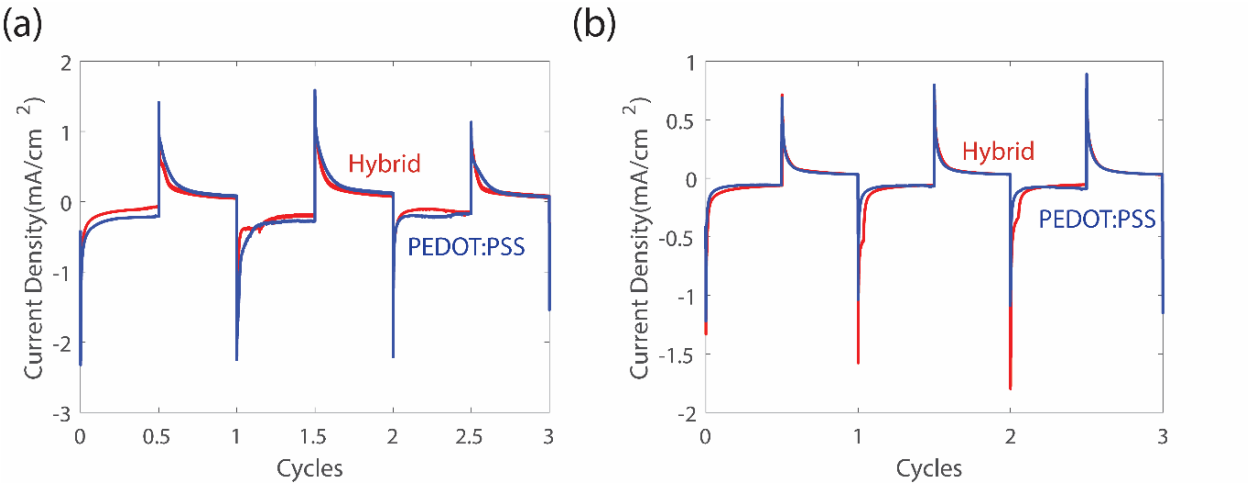

Figure 4.8: CA curves of mixed PEDOT/NW films compared to pure PEDOT films on (a) ITO/glass and (b) plain glass.

The CA curves for the first few cycles of PEDOT:PSS vs hybrid films on ITO glass are shown in Figure 4.8(a). The current density of the hybrid film on ITO drops off slightly faster compared to pure PEDOT:PSS on ITO because of its higher conductivity, indicating a faster switching time. Table 4.5 shows this and the other electrochromic properties of the pure PEDOT:PSS films vs hybrid films with the ITO electrode. The electrode sheet resistance is not stated in this case as the ITO electrode sheet resistance is the same for both hybrid and pure PEDOT:PSS films.. The ΔE on ITO is slightly better for the hybrid films, as expected from the higher current density seen in the CV and CA curves. However, because of the AgNWs, the change in transmittance, ΔT, is lower because the included nanowires decrease transmittance plus do change transparency upon switching. The hybrid film switch-on time is decreased by a factor of a half and the switch off time is also decreased by more than 2 seconds. Additionally, the switch-on voltage decreases from -1.5 V to -0.9 V and the colouration efficiency more than doubles, indicating superior performance to pure PEDOT:PSS films in almost all characterization parameters.

Table 4.5: Sheet Resistance (R_s), ΔE, ΔT, switching times, colouration efficiency (CE) and turn-on voltage of mixed PEDOT/NW films vs pure PEDOT films on ITO glass.

	R_s (Ω/sq)	ΔE	ΔT	τ_{on} (s)	τ_{off} (s)	CE (cm^2/C)	V_{on} (V)
PEDOT:PSS	-	25	46	7	11.7	29	-1.5
Hybrid	-	26	37	3.6	9.1	68	-0.9

In Figure 4.8(b), when the ITO electrode is removed, the current levels in the CA curves of the hybrid films are higher (more negative), indicating faster kinetics with the addition of the AgNWs. Table 4.6 below compares the electrochromic properties of the hybrid films vs pure PEDOT on plain glass. The sheet resistance is drastically reduced from 280 to 34 Ω/sq with the addition of the AgNWs. Additionally, the ΔE and ΔT improve due to the higher current density in the hybrid films transferring more charge to and away from the films when switched between the on and off state. The time it takes for the films to switch is also drastically reduced by 9.6 seconds and 12.6 seconds in the on and off state, respectively. The colouration efficiencies between the two different films are almost identical and lastly, the turn on voltage is again reduced by 0.4 V due to the improved conductivity of the hybrid films.

Table 4.6: Sheet Resistance (R_s), ΔE, ΔT, switching times, colouration efficiency (CE) and turn-on voltage of mixed PEDOT/NW films vs pure PEDOT films on plain glass.

	R_s (Ω/sq)	ΔE	ΔT	τ_{on} (s)	τ_{off} (s)	CE (cm^2/C)	V_{on} (V)
PEDOT:PSS	280	20	22	14.6	18.6	106	-1.5
Hybrid	34	24	26	5.0	6.0	101	-1.1

When examining the films with and without an ITO electrode, it becomes clear that an ITO electrode is not necessary when a hybrid film is used and thus the complexity of the fabrication and material cost can be reduced. The hybrid film with ITO has an almost identical ΔE to that without ITO. The transmittance changes between the on and off states is lower, but the colouration efficiencies without ITO are drastically improved. The switch off time is 3 seconds faster without ITO, but the switch on time is 1.4 seconds slower. The turn on voltage also increases by 0.2 V when the ITO is removed. Overall, because of the material cost savings, the high colouration efficiency and similar ΔE without the use of ITO, in spite of the slightly worse switching times and ΔT, the devices in the next section are fabricated without ITO electrodes.

4.4.2 Devices with Hybrid Electrochromic Films

Next, the AgNW/PEDOT:PSS hybrid films are integrated into full electrochromic displays and compared to displays with pure PEDOT:PSS electrochromic layers. Plain glass was used as the substrate. As described above, the lower material cost, superior colouration efficiency, and similar colour change justify not using ITO. The fabrication was the same process as described in Section 3.2; electrochromic displays were made from two electrochromic films with LITFSI:Emim TFSI in PMMA mixed with 5 wt% of titanium dioxide nanoparticles as the gel electrolyte. These devices in the on and off states are shown in Figure 4.9. Both devices show a clear and uniform switch between the on and the off state. The brown colouration of the hybrid device in the off state is due to corrosion of the silver nanowires, as will be discussed later. The colour in the on state of the hybrid device is slightly darker from the silver of the NWs.

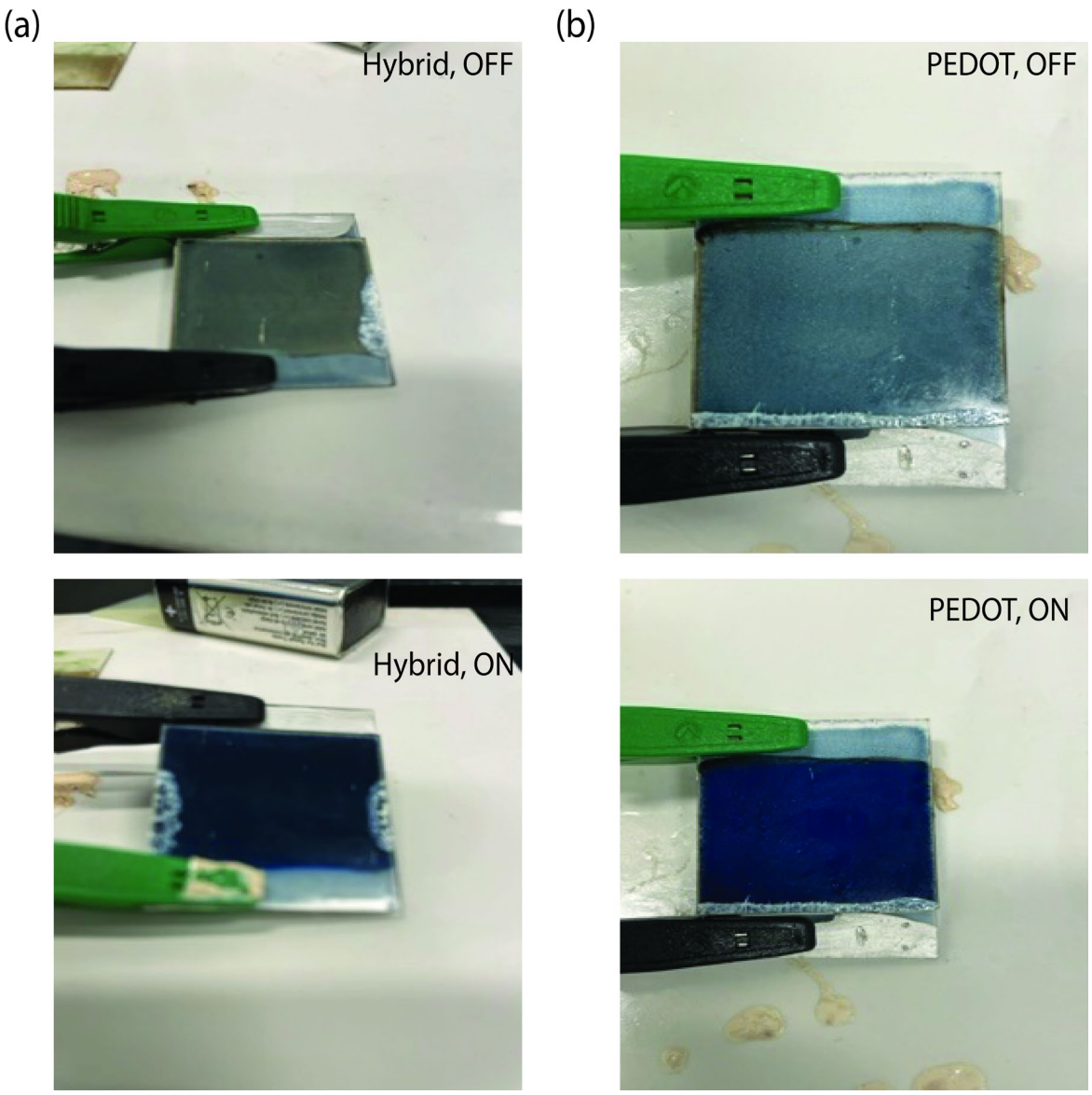

Figure 4.9: Pictures of devices fabricated with (a) AgNW/PEDOT:PSS electrochromic layers and (b) pure PEDOT:PSS layers in the off and on states.

Lifetime measurements were completed for both types of devices. Figure 4.10 compares the CA curves during 1000 cycles of a hybrid and pure PEDOT:PSS device. As expected, the current density in the pure PEDOT:PSS device is lower due to its lower conductivity: -3 and +2 mA/cm^2 compared to -6 and +4 mA/cm^2 for the hybrid device (values are the average over the 1000 cycles). Less obvious, however, was that the hybrid device is more stable, with little change in the current across all 1000 switching cycles performed, compared to the drop in current density seen in the pure PEDOT:PSS device.

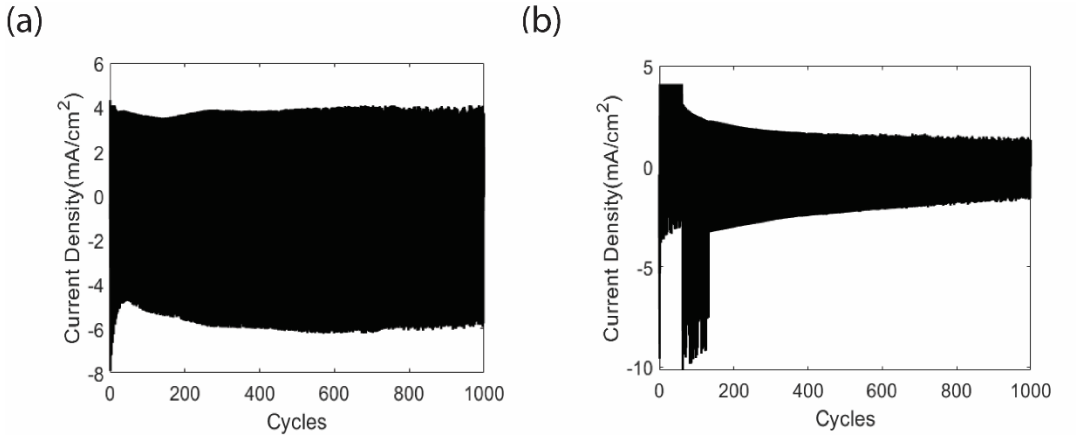

Figure 4.10: CA of a (a) mixed PEDOT:PSS/NW device and (b) pure PEDOT device on plain glass cycled for 1000 cycles.

Figure 4.11 shows the CV before and after the 1000 cycles for both devices. The peaks attributed to the colour switch are at potentials of +0.55 V and -0.55 V and are much better defined in the hybrid device in Figure 4.11(a) compared to the pure PEDOT:PSS device in Figure 4.11(b). The additional peaks in the hybrid device at +/-0.4 V are attributed to the redox reaction of AgNWs as described earlier in Chapters 2 and 3 and thus are only seen in the hybrid device. The area under the CV curve in the hybrid device is larger than that of the pure PEDOT:PSS device which indicates more charge is transferred as the device is cycled between +/-1.5 V and back. However, the areas under the curves and the current densities after cycling are very similar for both devices indicating that the AgNWs are not as effective after going through many cycles.

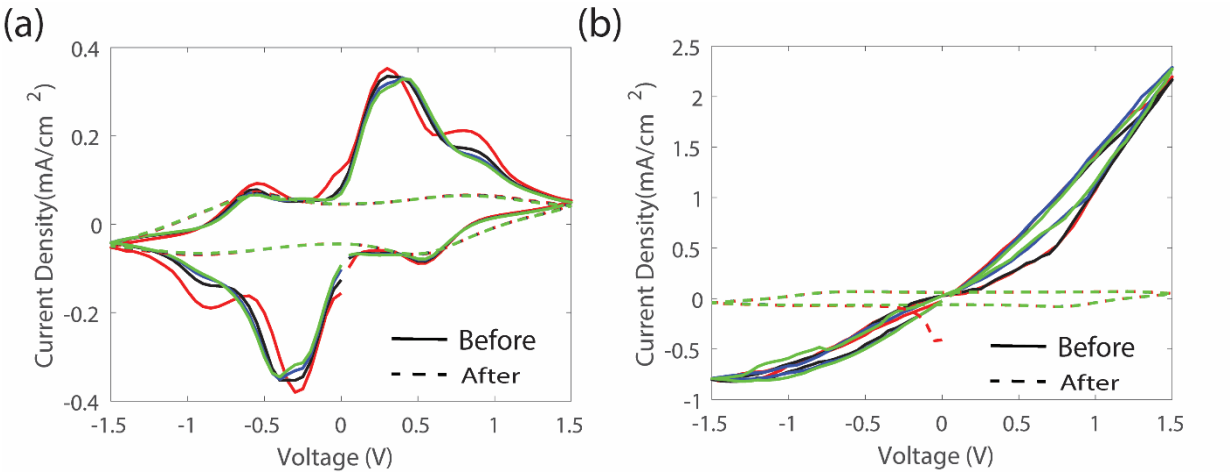

Figure 4.11: CV curves of a (a) mixed PEDOT:PSS/NW device and (b) pure PEDOT device on glass before and after 1000 cycles.

By examining the photos in Figure 4.12, we can see that there is clear browning of the hybrid device after being cycled 1000 times. This browning is not observed in the pure PEDOT:PSS device. The switching of the pure PEDOT:PSS device is still uniform in colour after 1000 cycles while the browning of the hybrid device after cycling leads to a reduced colour change.

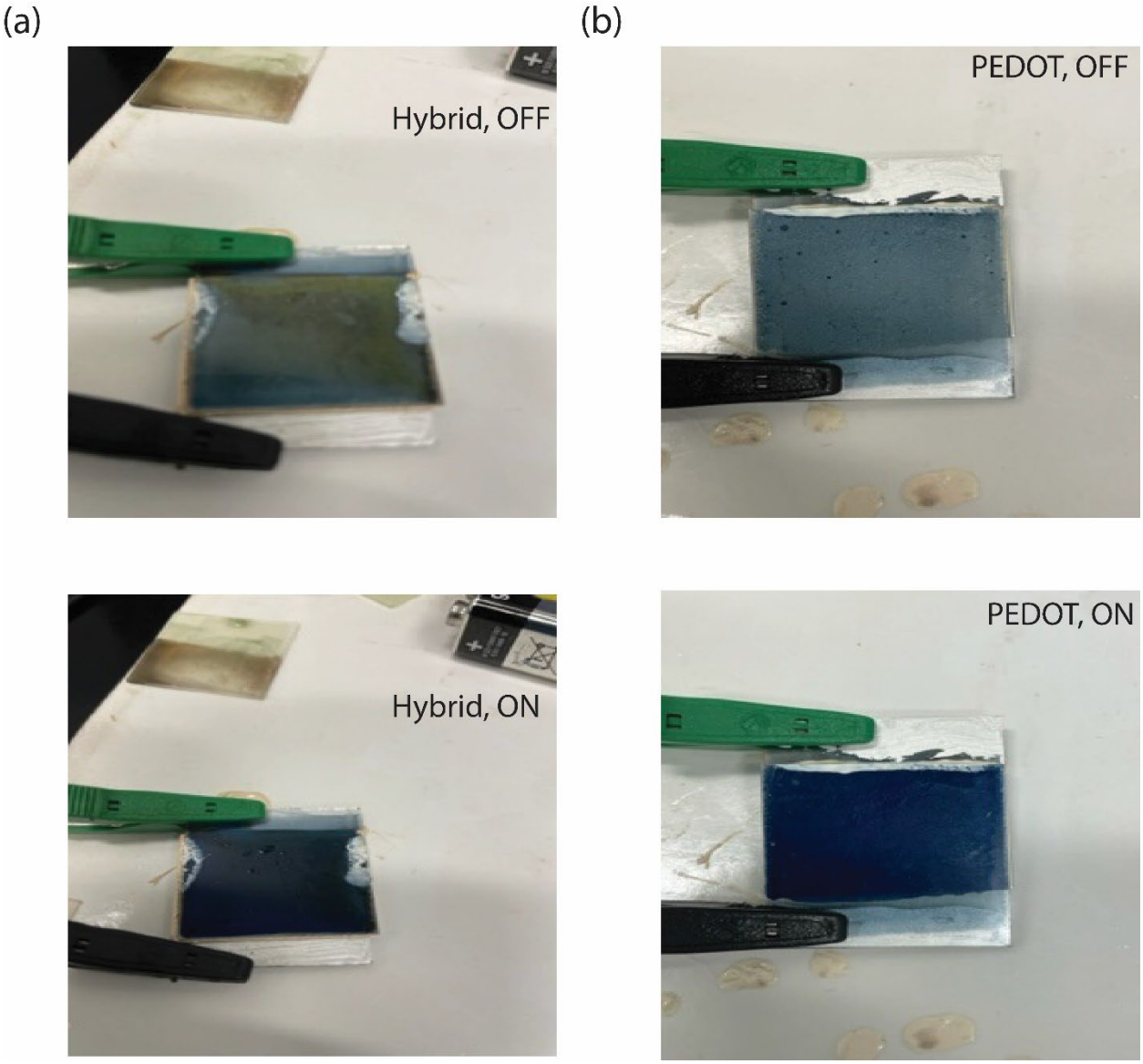

Figure 4.12: Photos of a (a) mixed PEDOT/NW device and (b) pure PEDOT device on glass in the off and on states after cycling.

Through further examination of the electrochromic properties of the devices in Table 4.7, the ΔE actually increases from before 1000 cycles to after 1000 cycles for both cases. However, because of the addition of the AgNWs, which do not have any electrochromic properties, the ΔE is lower than that of pure

PEDOT:PSS. The change in reflectance at a wavelength of 550 nm, ΔR, is higher at a value of 8.7% in the hybrid device compared to only 4.3% for a pure PEDOT:PSS device. More charge is transferred in the hybrid device as we saw in the CV and CA, leading to a higher change in reflectance. The colouration efficiency is also higher for the hybrid device due to the higher change in reflectance and better electrochromic properties that were seen in the CA and CV in Figures 4.10 and 4.11, above. The switching time for the pure PEDOT:PSS device increases after 1000 cycles from 2.6 to 6.6 seconds for the on time and 4.6 to 6.8 seconds for the off time. The hybrid device on time however actually gets quicker after 1000 cycles, reducing from 3.4 to 2.1 seconds, thereby becoming faster than the pure PEDOT:PSS device. Meanwhile, the off time worsens like the pure PEDOT:PSS device, going from 10.3 to 14 seconds. Overall, the switching off time is slower in the composite based device compared to the pure PEDOT:PSS based device, which is opposite to what was seen when comparing the films (Table 4.5). We emphasize that when comparing switching times of the composite versus pure PEDOT:PSS layer directly, however, the film half-cell measurements are more accurate [101]. In the film measurements there are fewer external factors such as the solid electrolyte composition and thickness, separation of the counter electrode, and accuracy of the voltage on the reference electrode. In the film three-electrode setup the reference and counter electrodes are not connected, allowing more accurate control of the applied potential from the potentiostat on the active electrochromic layer [102].

Table 4.7: ΔE, ΔR, switching times, and colouration efficiency (CE) mixed PEDOT:PSS/NW devices vs pure PEDOT:PSS devices on glass.

	ΔE (before cycling/after cycling)	**ΔR@550 nm (%)**	**τ_{on} (before cycling/after cycling)**	**τ_{off} (before cycling/after cycling)**	**CE (cm^2/C)**
PEDOT:PSS	14.51/21.74	4.3	2.6/6.6 sec	4.6/6.8 sec	19.7
Hybrid	13.91/18.67	8.7	3.4/2.1 sec	10.3/14 sec	31.6

Because of the visible browning of the hybrid device, which was also seen in Chapter 2 with AgNW electrodes in PEDOT:PSS displays, research of the passivation of the AgNWs in solution was done in order to improve device lifetime and further surpass the performance of the pure PEDOT:PSS devices for beyond 1000 cycles.

4.5 Passivation of Nanowires in Mixed Electrochromic Layers

4.5.1 The need for Passivation

It has been shown in the literature that AgNWs corrode when in contact with PEDOT:PSS [103][104]. This is due to the acidic nature of PEDOT:PSS (pH ~2.5) and possibly also because PEDOT:PSS has a tendency to absorb moisture which also accelerates silver corrosion [105]. Additionally, as mentioned in Section 2.3.1, the voltage cycling incurred in an electrochromic device also accelerates the oxidation of AgNWs. The previous passivation strategy used in Chapter 2 and 3, where a layer of PU is spin coated on top of a AgNW network will not suffice. In the current system, the AgNWs are mixed and in direct contact with PEDOT:PSS before a film is formed. Therefore, the individual AgNW surfaces must be passivated in solution, before mixing with the PEDOT:PSS and subsequent Mayer rod coating.

The approach taken here is to passivate the AgNW surfaces with organic short molecules. Unlike many other passivation strategies, small molecules can be applied on the NW surfaces while the NWs are still in solution. Such molecules can self assemble on the surface of AgNWs [74]. The molecular layers are not electrically conductive, but because they are only ~20 Angstroms in thickness, they should be short enough to allow some current to flow across it [75] so that the AgNWs and the PEDOT:PSS can be in electrical contact.

A variety of small molecules have been successfully used to passivate AgNWs for transparent electrode applications. Liu et al. deposited AgNW networks on glass substrates, then dip coated these networks in solutions of different small molecules [28]. Of the different molecules tested, it was found that the molecule MBI (2-mercaptobenizmidazole) was the best passivation candidate. The MBI-coated AgNW network showed no increase in sheet resistance when heated to 400°C [28]. When implemented in a transparent heater device, the AgNWs could also withstand a higher applied voltage of 12 V compared to just 6 V for the unpassivated NWs [28].

Similarly, Madeira et al. used the small molecule MuA (11-mercaptoundecanoic acid) mixed with ethanol to passivate AgNWs [75]. Like the previous study, AgNWs were rod-coated on glass substrates and then the AgNW networks were dipped in a solution of MuA in ethanol that was being constantly stirred in order to uniformly distribute the MuA over the surface of each AgNW. Madeira et al. reported no change in sheet resistance in the passivated AgNWs when stored in atmospheric conditions and exposed to daylight for 120 days [75].

An attempt will be made to passivate AgNWs in solution with MuA and MBI and then mix the passivated AgNWs with PEDOT:PSS. Then, electrochromic films and devices will be fabricated with the hybrid PEDOT:PSS/passivated AgNW inks.

4.5.2 Experimental

Separate solutions of 50 mM of MuA (Sigma Aldrich, 450561) and MBI (Sigma Aldrich, M3205) were prepared in ethanol. Each solution was stirred overnight to ensure adequate dispersion of the small molecules in ethanol. Next, 1.5 ml of 3 mg/ml 30UL AgNW solution was centrifuged at 6000 rpm for 10 minutes in order to separate the AgNWs from the ethanol. The ethanol was carefully pipetted out and then 1.5 ml of the MuA or MBI solution was added to the AgNWs. The AgNWs were redispersed into the MuA or MBI solution by stirring overnight. The next day each mixture was centrifuged again at 6000 rpm for 10 minutes and the excess MuA and MBI solution was pipetted out. Then, the MuA-AgNWs and MBI-AgNWs were rinsed twice with ethanol before being redispersed in 1.5 ml of ethanol.

0.5 ml each of MuA-AgNWs and MBI-AgNWs were mixed in separate solutions with 2 ml of 70 wt% PEDOT:PSS/30 wt% ethanol as outlined in Section 4.2 for unpassivated AgNWs. A schematic showing the coating of the AgNWs, followed by mixing them with PEDOT:PSS is shown below in Figure 4.13. Hybrid films and devices were then fabricated the same way as outlined in Section 4.2.

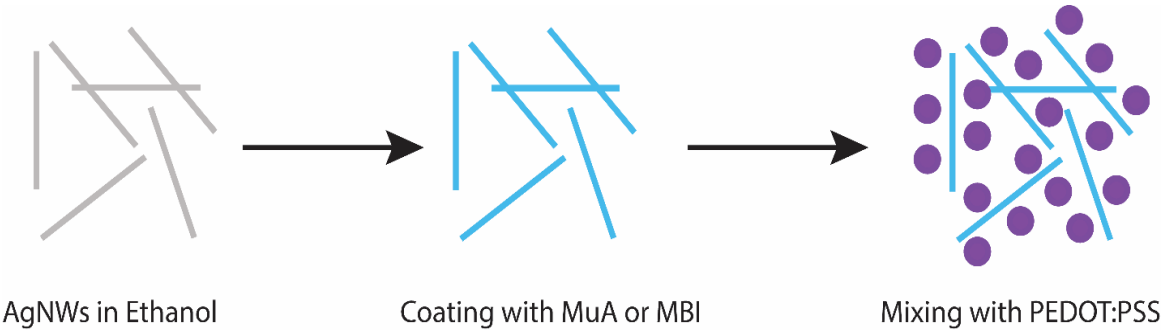

Figure 4.13 Schematic of the fabrication of MuA/MBI-passivated silver nanowire/PEDOT:PSS composites.

4.5.3 Passivation Results & Discussion

Hybrid films in the on and off state that are passivated with MuA (Figure 4.14(a)) and MBI (Figure 4.14(b)) show good uniform colour switching. However, to the naked eye, the MuA shows a slightly better switch in the on state as the blue in the centre of the film is darker compared to the MBI.

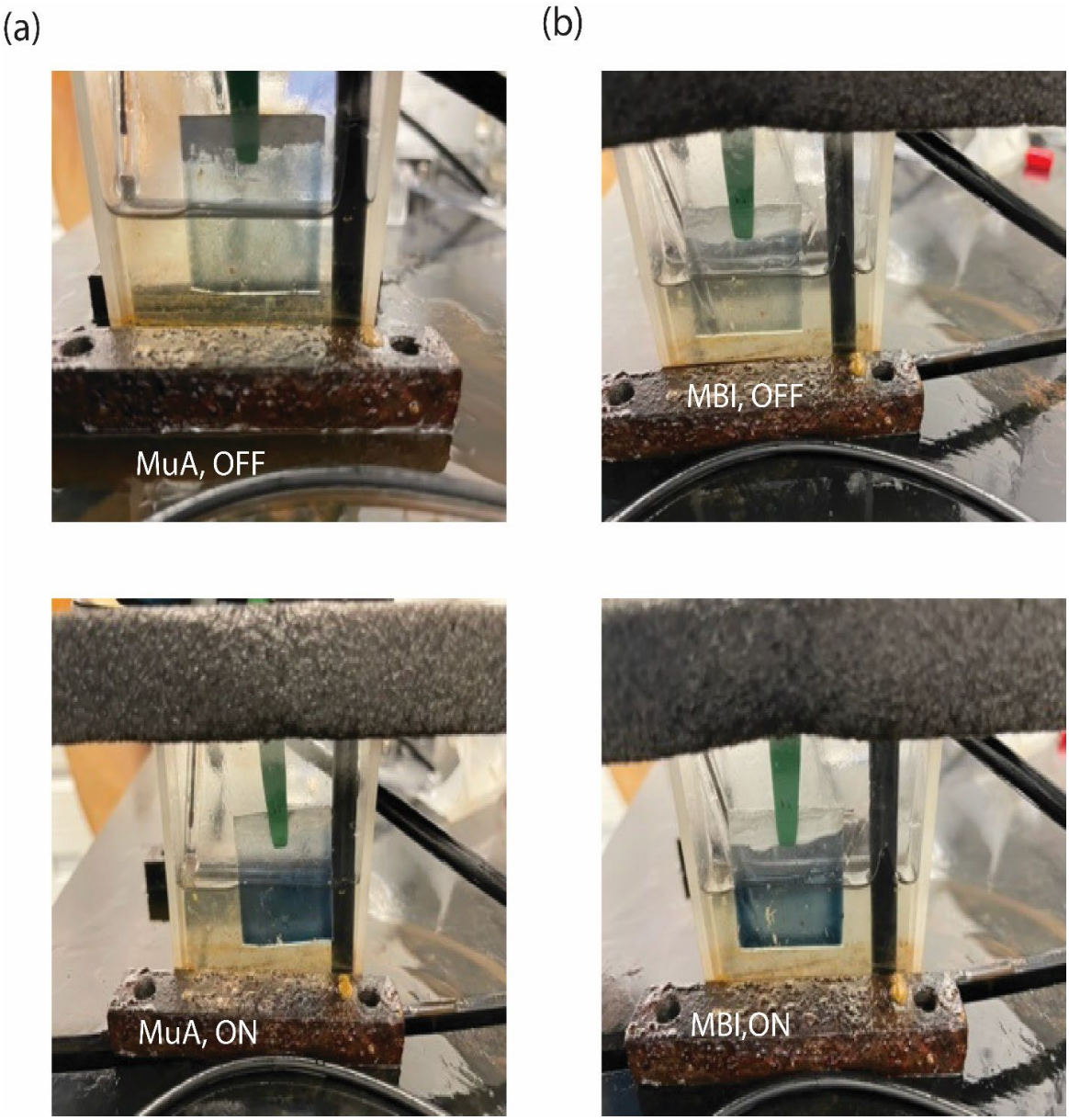

Figure 4.14: Photographs of AgNWs mixed with PEDOT on glass in the on and off states, where the NWs are passivated with (a) MuA and (b) MBI.

The CV curves for passivated hybrid films versus unpassivated hybrid films and pure PEDOT:PSS are shown below in Figure 4.15. The mixed films with either passivation show much lower turn on voltages compared to the unpassivated hybrid films and pure PEDOT:PSS, along with much higher current densities and hence better electrochromic behaviour. Based on the CV, there is little difference between the MBI and MuA passivation method to this point.

Table 4.8 shows the other electrical and electrochromic properties of the passivated films. The passivations increase the sheet resistance of the mixed films from 34 to 140 and 180 Ω/sq for MuA and MBI, respectively. The thin layers of MuA and MBI are insulating and thus reduce conduction between the NWs and the PEDOT:PSS. However, the sheet resistance of the passivated NW films are still lower than pure PEDOT:PSS. The ΔE and ΔT increase with the passivation of the AgNWs compared to PEDOT:PSS alone and unpassivated hybrid films.

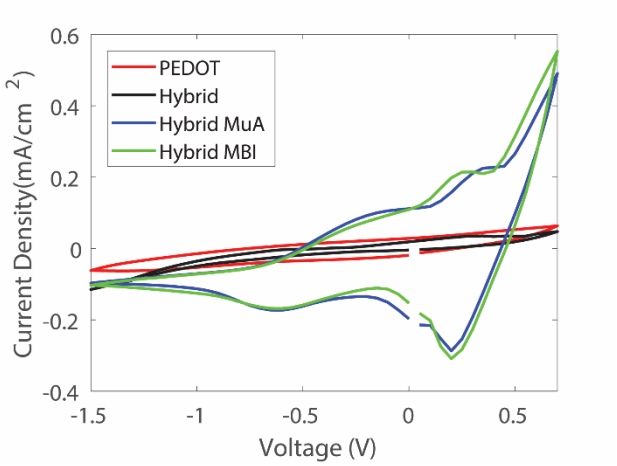

Figure 4.15: CV of MuA and MBI passivated AgNWs mixed with PEDOT:PSS on glass compared to unpassivated mixed films and pure PEDOT:PSS films on glass.

Table 4.8: ΔE, ΔT, switching times, colouration efficiency (CE) and turn-on voltage of films containing PEDOT:PSS mixed with passivated and unpassivated AgNW vs pure PEDOT:PSS.

	R_s (Ω/sq)	ΔE	ΔT	τ_{on} (s)	τ_{off} (s)	CE (cm^2/C)	V_{on} (V)
MuA	140	38	42	10.2	9.7	58	-0.6
MBI	180	31	49	7.8	10.9	53	-0.6
No passivation	34	26	37	3.6	9.1	68	-1.1
PEDOT:PSS	280	25	46	7	12	28	-1.5

The CA curves of the passivated hybrid films vs unpassivated films and pure PEDOT:PSS are shown below in Figure 4.16(a) (MuA) and Figure 4.16(b) (MBI). As discussed previously in Section 4.4, the PEDOT:PSS and hybid devices have a similar drop off. However, the MuA and MBI drop offs from their peak current densities are much slower. This aligns with their slower switching times seen in Table 4.8 and is a disadvantage of the passivation. One positive though is that the peak current density for both the MuA and MBI passivated hybrid films is higher than the PEDOT:PSS and unpassivated hybrid films. This aligns with the higher optical contrast seen above in Table 4.7 for the passivated samples.

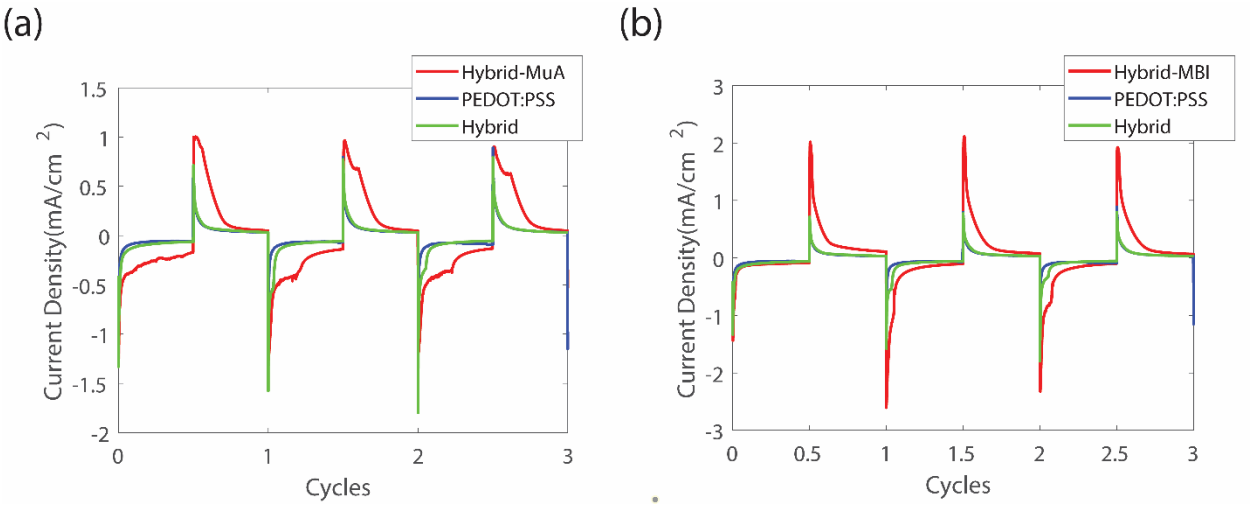

Figure 4.16: CA of (a) MuA and (b) MBI passivated AgNWs mixed with PEDOT compared to unpassivated hybrid films and pure PEDOT films on glass.

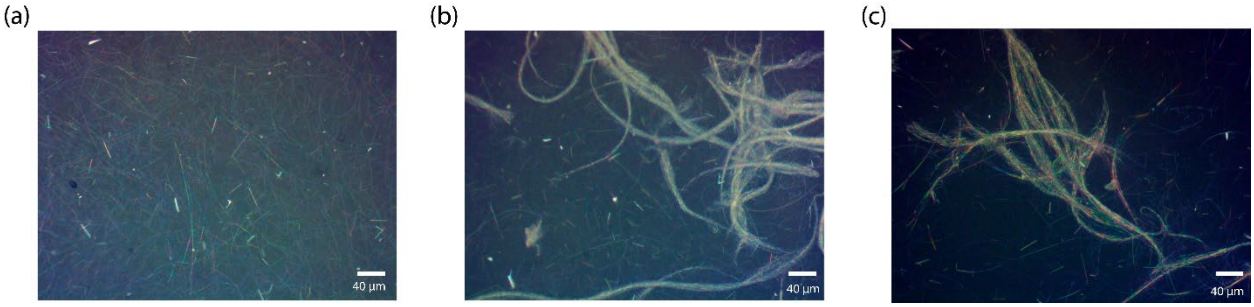

Figure 4.17: Optical microscope images of 30 nm diameter, 88 µm length, and 3.0 mg/ml AgNWs mixed with PEDOT:PSS for (a) unpassivated (b) MuA passivated AgNWs and (c) MBI passivated AgNWs.

To better understand the differences in electrochromic behaviour of the passivated hybrid films, optical microscope images of the unpassivated films were taken (Figure 4.17(a)) and compared to images of the MuA (Figure 4.17(b)) and MBI (Figure 4.17(c)) passivated AgNW mixed films. The unpassivated AgNWs in PEDOT:PSS are evenly distributed, whereas there is severe clumping in both types of passivated AgNWs. This can be explained through a phenomenon called the zeta potential. The zeta potential describes the electrical potential of a particle at the boundary between the particles and the solvent or fluid. If the zeta potential between two particles is large, positive or negative, they will repel each other. As discussed in Section 1.5.1, PVP (polyvinylpyrrolidone) is a polymer used in the polyol synthesis of AgNWs and it coats the AgNW surfaces in the as-received AgNWs. The surfaces of the unpassivated AgNWs are thus coated with PVP. The zeta potential of PVP in a solution of pH 7.33 is -47 mV [106]. However, for MuA and MBI, the zeta potential is approximately 0 mV and 5 mV, respectively [107], [108]. This means that there is little to no repulsion force between MBI and MuA molecules, leading to NW agglomeration.

In the work of Liu and Madeira where AgNWs were passivated with MBI and MuA, the AgNWs were passivated after the AgNWs were deposited as a network and the junctions welded [28], [75]. Thus the subsequent MBI and MuA passivation did not cause AgNW agglomeration as the NWs were already welded into a network to one another and as well as had some adhesion to an underlying substrate. This strategy unfortunately cannot be used here as the AgNWs need to be passivated before being mixed with PEDOT:PSS and deposited as a film.

With the bundled AgNWs in the NW/PEDOT:PSS composite, there are larger spacings between nanowires compared to unpassivated NW/PEDPOT:PSS composites, allowing for increased transmittance and a larger optical contrast. However, the sheet resistance and uniformity of this resistance is worse as the number of paths for the electrons to travel across decreases. This is not ideal.

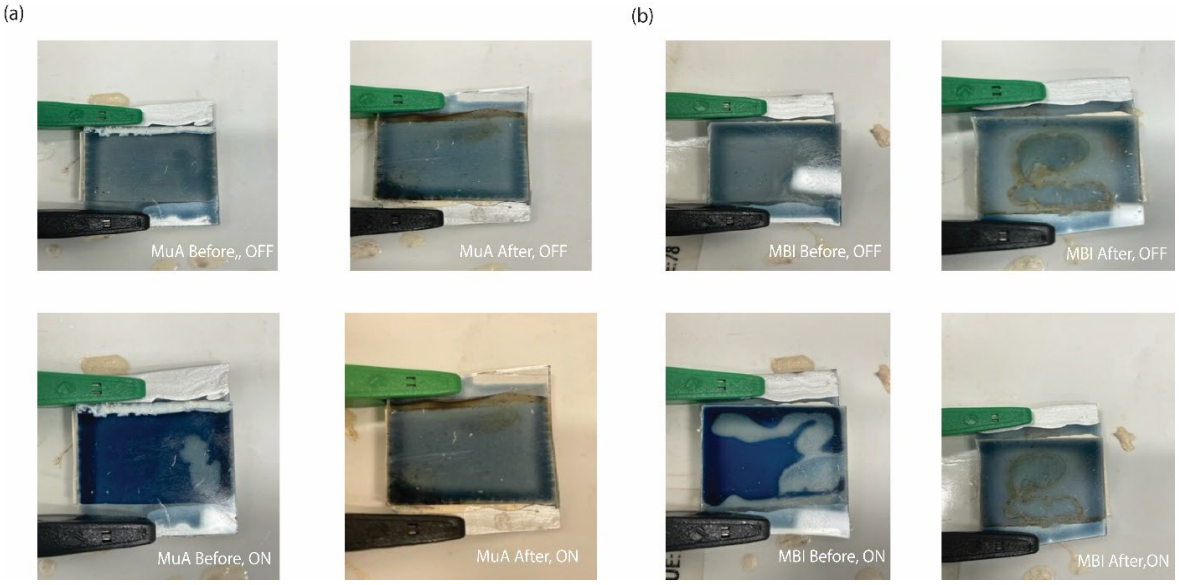

Figure 4.18: Photos of mixed (a) PEDOT:PSS/MuA-AgNW and (b) mixed PEDOT/MBI-AgNW devices on glass before and after cycling 1000 times.

The next step is to fabricate electrochromic displays with the passivated hybrid films and test the effectiveness of the passivations to improve lifetimes. Figure 4.18 shows photos of the passivated hybrid devices in the on and off state, before and after cycling 1000 times for MuA (Figure 4.18(a)) and MBI (Figure 4.18(b)). Note in both Figures 4.18(a) and (b), there is an artifact in the device that causes part of it not to switch. It is not a result of low device lifetime as it occurs both at the start and after cycling. It could be a result of the agglomeration of the passivated nanowires compared to the unpassivated nanowires. Both films show a clear uniform switch before cycling, but there is browning from corrosion of the AgNWs in the after-cycling photos. Additionally, there is no clear colour change seen to the naked eye after cycling the devices.

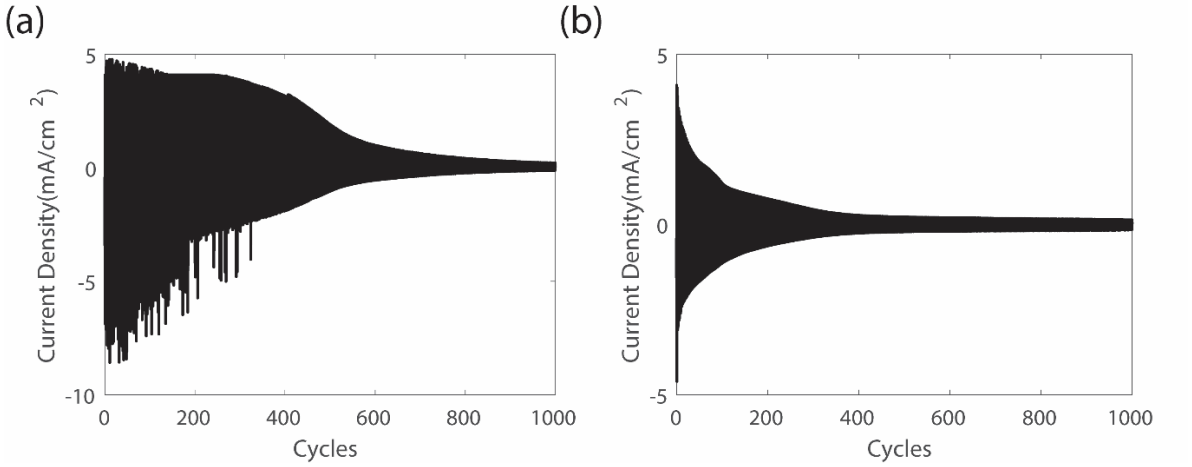

Figure 4.19: CA of mixed (a) PEDOT/MuA-AgNW and (b) mixed PEDOT/MBI-AgNW devices on glass cycled 1000 times.

Figure 4.19(a) and Figure 4.19(b) correspond to the CA plots during 1000 cycles of MuA-passivated and MBI-passivated hybrid devices, respectively. The magnitude of the current density falls off to almost 0 mA/cm^2 after the 1000 cycles. The MuA-passivated device shows better performance overall as the current density doesn't start falling off significantly until 500 cycles, while the MBI device starts falling off significantly around 150 cycles. However, compared to the unpassivated devices, both of the passivation materials have inferior performance. The current density remains constant across the 1000 cycles in the unpassivated devices (Figure 4.10), and the device still shows a clear colour change after 1000 cycles whereas both the passivated devices fail.

Examining the CV before and after cycling for each device (Figure 4.20), we see that there is a bit more of a difference between the two passivation types. The MuA and MBI device have the same colour switching peak of the PEDOT:PSS at -1.25 V. However, the MuA device in Figure 4.20(a) shows an additional redox peak at -0.3 V which is not present in the MBI passivated curve. Based upon previous results, this redox peak is from the oxidation/sulfidation of the silver [54]. This indicates that the MBI device has a slightly better performance in passivating the AgNWs.

The current density of the CV for the unpassivated devices after cycling is very similar in shape to both passivated devices. The main difference is magnitude. The highest and lowest current in the unpassivated devices is +/- 0.15 mA/cm^2 (Figure 4.11(a)), but for the passivated devices, the peaks are at +/- 0.1 mA/cm^2 and +/- 0.05 mA/cm^2 for MuA and MBI, respectively. This aligns with the photos of after cycling as the passivated devices no longer have a visible change in colour while the unpassivated devices have a clear change.

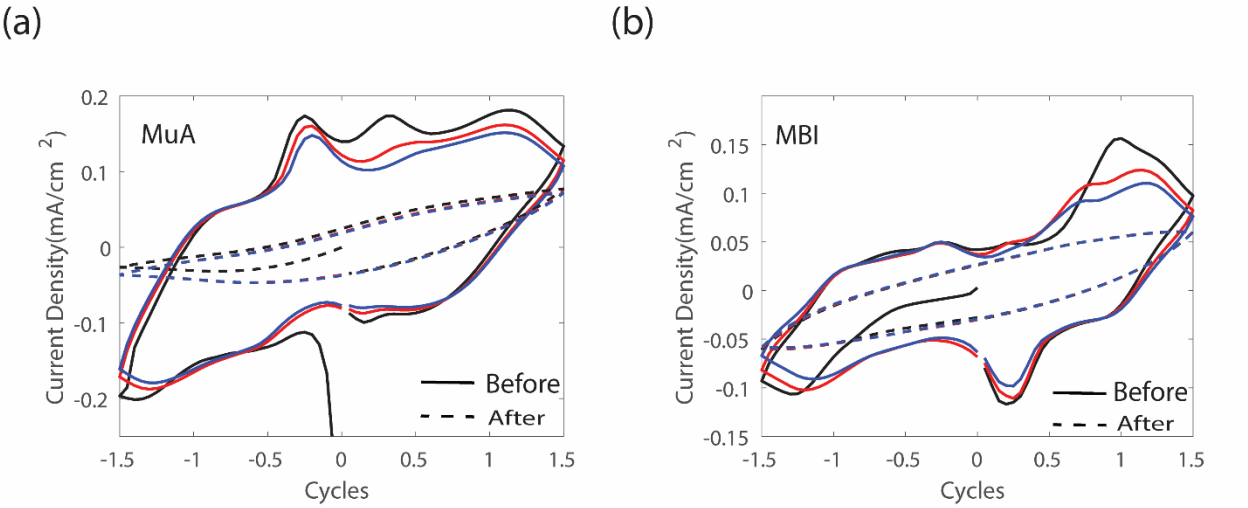

Figure 4.20: CV of mixed (a) PEDOT:PSS/MuA-AgNW and (b) PEDOT:PSS/MBI-AgNW devices on glass before and after cycling 1000 times.

Table 4.9: ΔE, ΔR, switching times, and colouration efficiency (CE) of PEDOT:PSS mixed with passivated AgNWs devices vs unpassivated AgNW/PEDOT:PSS and pure PEDOT:PSS devices.

	ΔE (before cycling/after cycling)	**ΔR@ 550 nm (%)**	**τ_{on} (before cycling/after cycling)**	**τ_{off} (before cycling/after cycling)**	**CE (cm^2/C)**
MuA	18/4.5	3.8	3.1/24.7 sec	6.3/27 sec	18.2
MBI	19/6.3	3.5	3.1/25 sec	6.2/27 sec	17
No Passivation	14/19	8.7	3.4/2.1 sec	10.3/14 sec	31.6
Pure PEDOT:PSS	15/22	4.3	2.6/6.6 sec	4.6/6.8 sec	19.7

Table 4.9 shows the electrochromic properties for the MuA passivated, MBI passivated, unpassivated and pure PEDOT:PSS devices. The ΔE decreases significantly and a colour change is no longer seen after 1000 cycles in each passivated case. The more uniformly distributed nanowires in the unpassivated device show an improvement in ΔE after cycling. The other specification in the table that is shown before and after cycling is the switching times. The passivation increases both the switching on and off times after cycling significantly. The switching times of the pure PEDOT:PSS device also increase. In the unpassivated device,

the switch-on time actually decreases while there is only a modest increase in the switch-off time after cycling. Unfortunately, the colouration efficiency of the passivated devices is less than the unpassivated ones and is similar to that of the pure PEDOT:PSS device. This is because the MBI and MuA molecules worsen the sheet resistance and resistance uniformity of the NW/PEDOT:PSS composite. The measured change in reflectance between the on and off state at a wavelength of 500 nm is almost half for the passivated devices compared to the unpassivated and is similar to pure PEDOT:PSS. This could be explained by the lower current density of the passivated devices compared to the unpassivated one as seen in their respective CV and CA curves. A lower current density leads to a lower change in reflectance.

Overall, there is little difference in the effectiveness of the passivation between MuA and MBI coated AgNWs. They both show significant agglomeration of the wires after coating and lead to poor device performance after 1000 cycles. The passivation of the AgNWs in PEDOT:PSS does not increase lifetime of the devices. Instead after cycling, ΔE decreases to the point that there is no discernable switching to the eye and the switching on and off times significantly increase. There are minor differences in the electrochromic properties of MuA and MBI, but the edge goes to MuA as it has a slightly better ΔE both before and after cycling. Every other electrochromic property shows no significant difference between the two molecules. The passivation worsens the sheet resistance of the NW/PEDOT:PSS composite because it is insulating and results in severe clumping of the AgNWs in the PEDOT:PSS. Further investigation must be completed in order to find a better passivation material that can coat AgNWs surfaces in solution. Ideally the passivation molecule or material should be conductive and have a large zeta potential to prevent clumping, yet still increase the lifetime of the hybrid films by preventing nanowire corrosion.

4.6 Nanowires as the Electrode versus Hyrid Silver Nanowire/PEDOT:PSS Films

In this subchapter, mixed AgNW/PEDOT:PSS films fabricated in this chapter are compared to a system where the AgNWs are separated from the PEDOT:PSS into its own electrode layer, like in the previous chapter. These two systems are illustrated in Figure 4.21. Here, no passivation is used in either case. The hybrid film reduces the number of layers and the number of nanowires used in the fabrication of the device, and as we will see, improves some of the electrochromic properties.

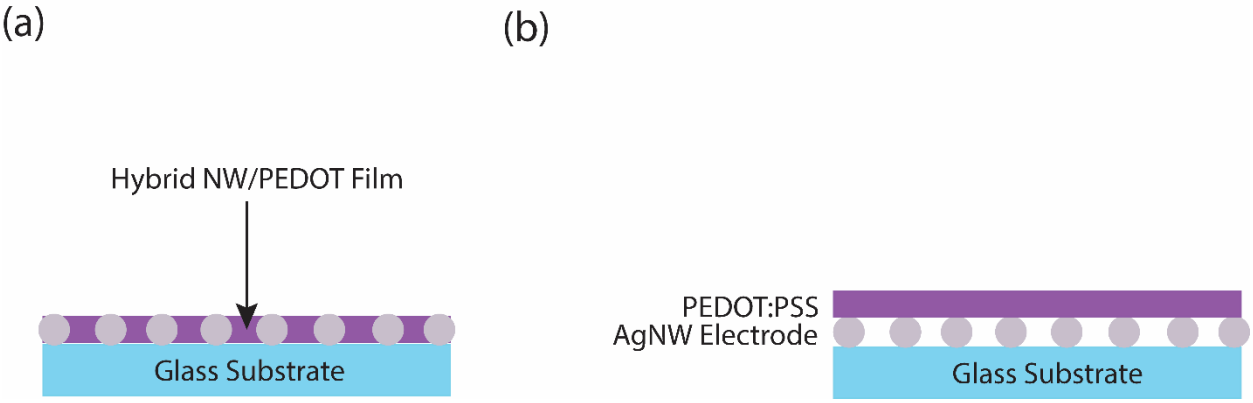

Figure 4.21: Schematic of (a) single mixed PEDOT:PSS/NW layer vs (b) pure PEDOT:PSS film with a AgNW transparent electrode.

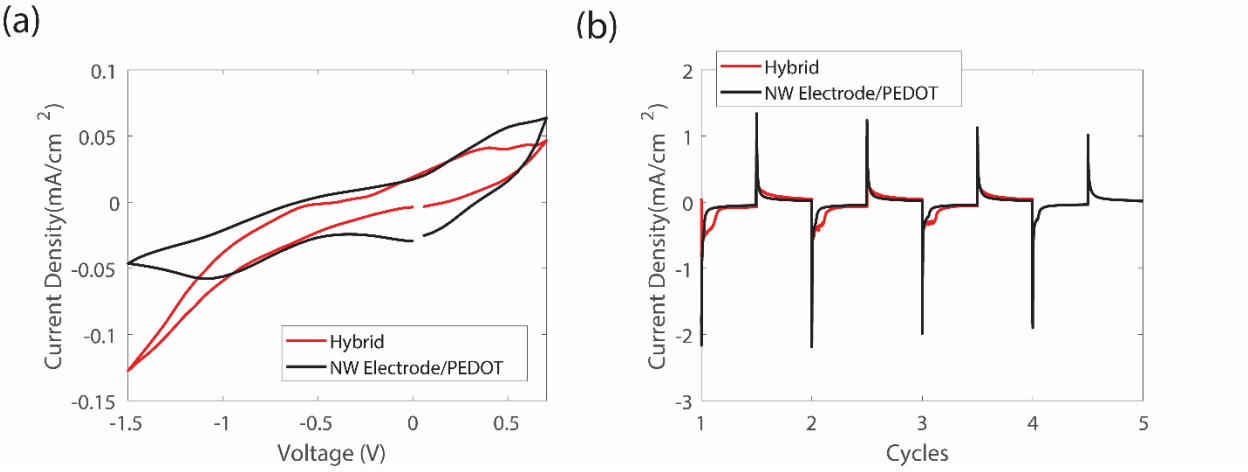

Figure 4.22: Comparison between single layer and two layer electrochromic films: (a) CV and (b) CA.

Figure 4.22(a) compares the CV of a hybrid film to a two layer AgNW/PEDOT:PSS setup. The peak current at the on state at -1.5 V is higher for the hybrid film. The current peaks at a lower voltage in the two-layer setup, meaning that the turn on-on voltage is smaller. This is because of the high conductivity of the AgNW electrode in which, unlike the hybrid films, the nanowires are connected in an overlapping network (in the AgNW/PEDOT:PSS composite, the AgNWs are mostly separated and not electrically connected to one another) allowing for a greater amount of electrons to flow in and out of the PEDOT:PSS layer. Examining the CA in Figure 4.22(b), we can see that the two-layer setup has a quicker drop off from the peak current value. The switching times themselves in each case are shown in Table 4.10. The hybrid device has a shorter off time while the on time for the two-layer setup is less than half the value of the on time for the hybrid device. The hybrid film has superior ΔT and ΔE values, arising from the dual electron

transport system and higher conductivity of the electrochromic layer. The colouration efficiency is higher for the two-layer setup as expected as the turn-on voltage is lower and higher colouration efficiency is traditionally associated with a higher optical contrast at a lower voltage.

Table 4.10: Comparison of ΔE, ΔT, switching times, colouration efficiency (CE) and turn-on voltage of single layer ("Hybrid") vs two layer electrochromic films ("AgNW Electrode").

	ΔE	ΔT	τ_{on} (s)	τ_{off} (s)	CE (cm^2/C)	V_{on} (V)
Hybrid	26	37	3.6	9.1	67.7	-1.2
AgNW Electrode	24	22	1.5	10.6	74.2	-0.7

The two-layer setup and the hybrid films were next implemented into devices. The CV curves in Figure 4.23(a) show that the hybrid device has much lower voltage redox peaks at -0.3 and +0.3 V. The current density peaks are also higher, attributed to the higher conductivity of the hybrid film compared to the PEDOT:PSS film alone with the AgNW electrode. The CA in Figure 4.23(b) shows similar peak current levels, with the hybrid film device being slightly higher, again from the higher conductivity with the addition of the AgNWs into the PEDOT:PSS. The other electrochromic properties (Table 4.11) show that the hybrid film device has a higher change in reflectance between the on and off state at an on/off voltage of +/-1.5 V. This is direct result of the higher conductivity leading to a higher optical contrast. This is backed up by the ΔE increasing from 15 to 19 when using the hybrid film in a device. The two-layer setup in a device has a colouration efficiency almost double that of the hybrid device. This could be a result of the lower turn-on voltage for the half cell redox reaction, as seen in Figure 4.23(a).

In summary, the reduction of the number of layers from five to three in an electrochromic display by using hybrid films shows a better optical contrast compared to a full five-layer device, as seen through ΔE and ΔR. However, the coloration efficiency is not as high. The switching on-time is faster in the five-layer device, but the switching-off time is slower. Depending on the application, it is viable to using three-layer hybrid devices without a separate electrode. However, the best performing is predicted to be one that uses both NWs mixed into the electrode chromic layer, and AgNWs in a separate electrode.

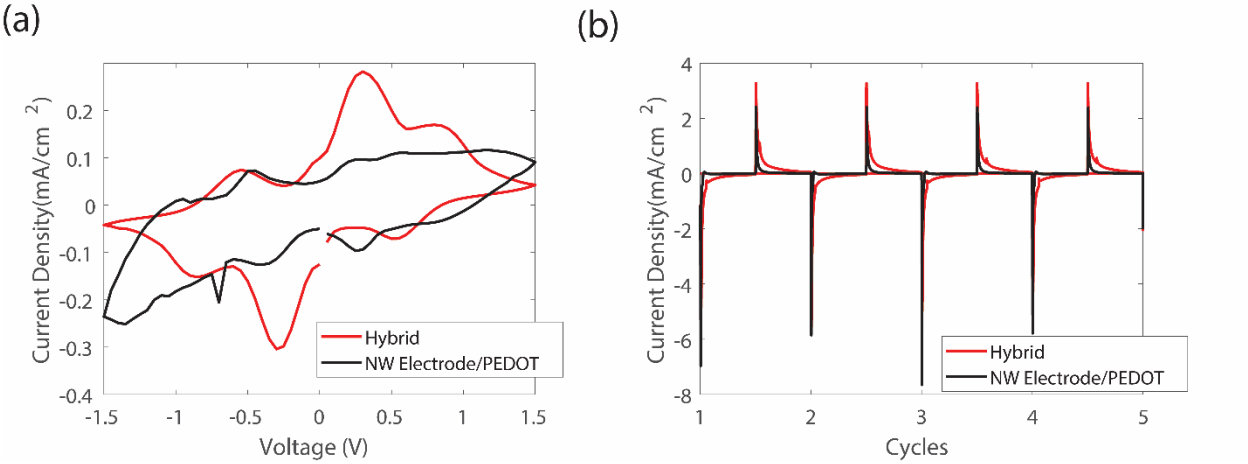

Figure 4.23: Comparison of single layer and two-layer electrochromic devices: (a) CV and (b) CA.

Table 4.11: Comparison of ΔE, ΔT, switching times, colouration efficiency (CE) of single layer vs two-layer electrochromic devices.

	ΔE	ΔR@550 nm (%)	τ_{on} (s)	τ_{off} (s)	CE (cm^2/C)
Hybrid	19	8.7	2.1	14	31.6
AgNW Electrode	15	6.5	3.5	2.0	56.6

4.7 Conclusion

The optimized AgNW/PEDOT:PSS composite film contained the longest (88 µm) and thinnest (30 nm diameter) nanowires at a concentration of 3.0 mg/ml. The AgNWs significantly improve the conductivity of PEDOT:PSS, which in turn improves switching times, lowers the turn-on voltage and increases the change in reflectance between the on and off states. The colouration efficiency of the devices based on the composite electrochromic layers is also higher, but ΔE is lower since the NWs do not have electrochromic properties themselves.

Hybrid devices showed browning after undergoing 1000 on/off cycles from corrosion of the AgNWs in the PEDOT:PSS. MuA and MBI were used to passivate AgNWs in solution before they were mixed with PEDOT:PSS. Both passivation molecules lead to increased switching times and fail to show a colour

change to the naked eye after cycling 1000 times between -1.5 and +1.5 V. Due to AgNW clumping and the non-conductive nature of the passivation molecular layer, the conductivity of the passivated AgNW/PEDOT:PSS films was significantly lower than unpassivated mixed films, resulting in some worse electrochromic properties.

Overall, mixing nanowires into the PEDOT:PSS electrochromic layer results in several advantages though there is a trade-off as they have a lower ΔE. NW corrosion also remains a problem. In Chapter 7, suggestions for better passivation strategies, such as using a small molecule with a larger zeta potential, will be given as future work.

Chapter 5
Near Infrared Properties of Silver Nanowire Networks

The optical properties of silver nanowire networks in the visible portion of the electromagnetic spectrum have been extensively studied, however, there has been little attention to their properties in the near-infrared portion of the spectrum. In this chapter, the optical properties of silver nanowire networks in the NIR and the dependence upon nanowire concentration, diameter, and length are determined and discussed. A portion of this chapter was published as: J. Atkinson, I. Goldthorpe, *Nanotechnology*, 31, 365201 (2020) [106].

5.1 Introduction

Many optoelectronic devices including liquid crystal displays [45], organic light emitting diodes [107], touch screens [108], thin-film solar cells [109], organic solar cells [24] and smart windows [22], [110] require one or two optically transparent, electrically conductive layers. Metal oxides such as indium tin oxide (ITO) and fluorine-doped tin oxide (FTO) are the predominant materials used as transparent electrodes, but they are expensive, have limited mechanical flexibility and require high temperatures and vacuum for deposition [6]. Another disadvantage of metal oxides for some applications is their low transparency in the near-infrared (NIR) region of the electromagnetic spectrum (wavelengths ranging from 700 - 3000 nm). This is due to a surface plasmon resonance at 1300 nm and 1050 nm in ITO and FTO, respectively [16], [19]. As will be shown in this chapter, ITO that is 96% transparent at visible wavelengths, for example, is only 35% transparent at longer wavelengths (2500 nm).

As discussed in Chapter 1, several alternative materials to replace metal oxides for transparent electrodes are being studied, and films of silver nanowire networks are a promising candidate [17]. Silver nanowire networks have transparency and conductivity values as high as ITO [44] while being mechanically flexible [107], less expensive [111], and can be fabricated using high-throughput roll-to-roll manufacturing methods [66]. Furthermore, unlike metal oxides, they can be nearly as transparent to NIR wavelengths as they are in the visible range. This is because their surface plasmon resonance is instead in the ultraviolet region of the electromagnetic spectrum, at approximately 375 nm [63] compared to 1300 nm for ITO [19]. Almost 52% of solar energy occurs at NIR wavelengths and transparency to these wavelengths, while still

being highly transparent in the visible, could be highly beneficial for switchable windows to allow more solar heat to enter a building in the winter. And since 2020, when a portion of the study below was published, several papers have cited this work and exploited the NIR transparency of silver nanowire networks in other applications. For example, silver nanowire networks have been used in low emissivity (low-e) window coatings in which, like switchable window technologies, lead to greater energy efficiencies in colder climates if they can permit the passage of solar NIR wavelengths [112]. Organic and multi-junction solar cells also benefit from transparent electrodes that are highly transparent to NIR wavelengths as this enables the device to more efficiently harvest the NIR range of the solar spectrum. NIR-transparent electrodes are needed in some switchable electrochromic devices including those used for camouflaging and optical communications [113]. Most recently, this work has been cited to exploit the NIR transparency of silver nanowire electrodes in photodetectors used in biosensing, since the skin and underlying layers are transparent in the NIR region [114].

The optical properties of silver nanowire films in the visible have been extensively studied [44], and some papers on their transparency at IR wavelengths > 5 μm exist due to the relevance of this part of the spectrum for heat radiation [57]. However, little attention so far has been paid to the transparency of silver nanowire films in the NIR region. Current literature shows the transmittance of randomly oriented silver nanowire networks in the NIR region [115], [116], but there is no experimental data and little discussion of how nanowire network parameters affect this NIR transmittance despite its importance for numerous applications. In this chapter, it is determined how and why nanowire diameter and its density affect the transparency of silver nanowire electrodes in the NIR region to provide understanding and guidance for improved device design. Additionally, there is a focus on how to select parameters to minimize the drop in transparency between the visible and the NIR, as high transparency in both regions is desired for many applications.

5.2 Experimental

5.2.1: Sample Preparation

All samples in this work were fabricated on 2.5 x 2.5 cm BK7 glass substrates of 1 mm thickness. Silver nanowires with diameters of 30, 70 nm, and 100 nm were purchased from Novarials Coporation (Woburn, MA) while silver nanowires with diameters 120 nm were purchased from ACS Materials (Pasadena, CA).

All nanowires were dispersed in ethanol with various concentrations depending on the desired film density. The silver nanowires were fabricated into electrodes using commonly used techniques: 40 μL of nanowire solution was pipetted at one end of the glass substrate, which was then drawn across the substrate with a Mayer rod (RDS 10). 4 coats were applied, with the substrate being rotated 90° between each coat to increase nanowire spatial uniformity across the substrate. Samples were then annealed for 30 minutes in a low vacuum oven in N_2 atmosphere. This welds the nanowire junctions and thereby reduces sheet resistance. The annealing temperature that led to the lowest sheet resistance depended on diameter: 150 °C (30 nm), 160 °C (70 nm), 170 °C (100 nm), and 180 °C (120 nm). The different temperatures required for different NW diameters can be explained through the Gibbs-Thomson effect. Smaller diameter nanowires have a higher surface area to volume ratio. Since surface atoms are more weakly bonded than the non-surface bulk atoms, less energy, i.e. a lower temperature, is required to melt the nanowire [117].

5.2.2: Optical and Electrical Characterization

For electrical measurements, conductive copper tape along with silver paste (Ted Pella Inc, Redding, CA,) was placed at either end of the film. Resistance was measured with a multimeter and converted into a sheet resistance. The transmittances of the films were characterized using a UV/VIS/NIR Cary 5000 spectrophotometer with an integrating sphere.

5.3: Results and Discussion

5.3.1 Optical Characterization

First, nanowire films that have high transparency are focused on as this is what is desired for smart window applications where high NIR is highly advantageous (required sheet resistance is $\leq \sim 400\ \Omega$/sq [118]). To obtain an electrode with 96% transparency in the middle of the visible spectrum (550 nm), the concentration of the nanowire solution required is similar for all diameters as shown in Table 5.1, with only the thickest nanowires permitting a slightly higher concentration (transparency and resistance data at other concentrations are listed in Table 5.2). The latter is because for larger diameters, more mass is contained out-of-plane leading to lower areal coverage (surface fill-fraction). Thicker nanowires scatter more as their scattering cross section is larger from their larger diameter [118], [119], but since an integrating sphere was

used this scattered light is included in the transparency measurement. Regarding sheet resistance, for this case of high transparency it is generally higher for thicker nanowires (Table 5.1, 5.2), which is consistent with earlier studies [120]. For a given concentration, there are a smaller number of total nanowires for the thicker diameters and at these sparse densities, a larger proportion of the nanowire lengths are not connected into the network and thus do not contribute to conduction. At higher nanowire densities, such as those needed for the low sheet resistances required for other applications such as solar cells, this trend is reversed: networks of thicker nanowires have lower sheet resistances at a given transparency than those made of thinner ones [120].

Table 5.1. The solution concentration of silver used and sheet resistance of nanowire networks at 96% transparency @ 550 nm.

Diameter (nm)	Average Length (µm)	Concentration (mg/ml)	Transparency @ 550 nm (%)	R_s (Ω/sq)
30	12	0.8	96	31
70	29	0.8	96	110
100	45	0.8	96	113
120	39	0.9	96	364

Table 5.2. The sheet resistances and transparencies (in brackets) of all nanowire diameters used at various densities.

Diameter (nm)	R_s@ 0.5 mg/ml (Ω/sq)	R_s@ 0.8 mg/ml (Ω/sq)	R_s@ 1.0 mg/ml (Ω/sq)	R_s@ 1.5 mg/ml (Ω/sq)
30	54 (95%)	31 (96%)	14 (93%)	11 (91%)
70	36000 (96%)	196 (96%)	131 (96%)	91 (93%)
100	169 (98%)	113 (96%)	24 (97%)	16 (94%)
120	194000 (98%)	164 (96%)	100 (97%)	34 (95%)

Figure 5.1(a) shows how the experimentally measured transmittance of the same four samples as shown in table 5.1 depends on wavelengths between 250 – 2500 nm. On the same plot, the transmittance of a film of ITO on glass (purchased from Sigma Aldrich), which is also 96% transparent at 550 nm, is shown. The

transmittance of the ITO falls dramatically in the NIR region to a transparency of 35% at 2500 nm. In contrast, the transparencies of the nanowire films drop by no more than 4 percentage points between the visible and 2500 nm in the NIR region. Secondly, the transparency of networks with thinner nanowires drops more in the NIR compared to thicker nanowires: four percentage points for the 30 nm diameter nanowires versus two percentage points for 120 nm nanowires. The nanowires in the four samples not only have different diameters, but also have different lengths and aspect ratios. For example, 30 nm nanowires are 12 um long while 120 nm are 39 um long. It will be shown in Section 5.3.6 that although nanowire length can significantly affect the network's sheet resistance, length has minimal impact on the total transparency of the network at the densities and lengths used here. This has also been shown to be the case elsewhere across wavelengths in the ultraviolet, visible, and into the near infrared region [120]–[122]. Therefore, the difference in transparency difference among these experimental networks is primarily attributed to diameter and not length differences [121].

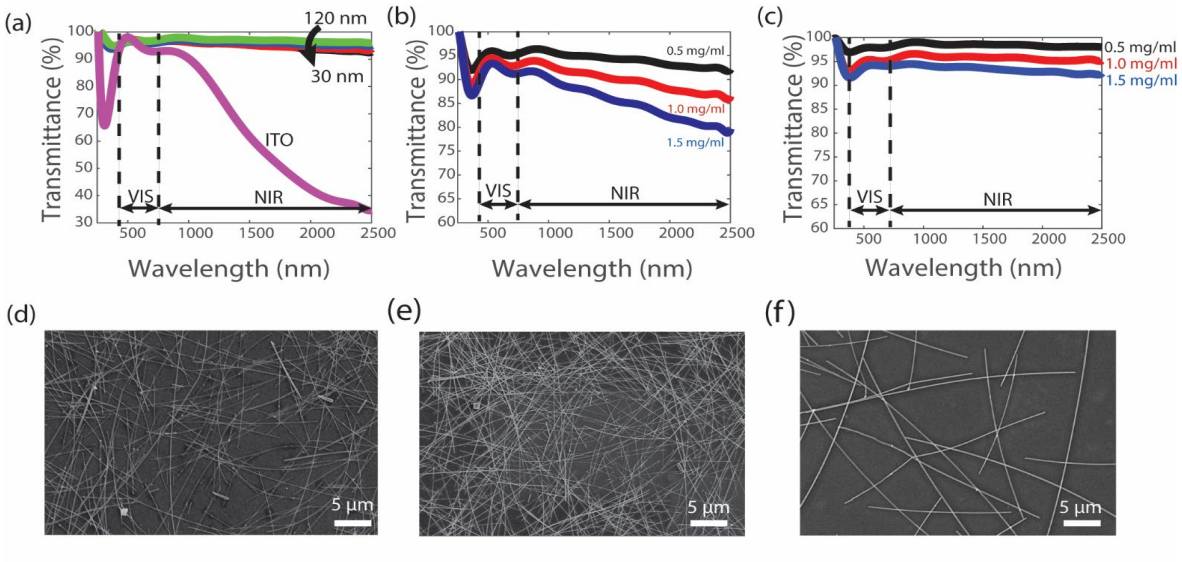

Figure 5.1: (a) Transmittance vs wavelength for silver nanowire networks at nanowire diameters of 30, 70, 100, and 120 nm. The transmittance of silver nanowire networks is much greater in the near-infrared region than commonly used indium tin oxide. The transmittance of (b) 30 nm and (c) 120 nm diameter nanowire networks made from solution concentrations of 0.5, 1.0 and 1.5 mg/ml. The transmittance drops more significantly over the NIR region for thinner and denser networks. SEM images of 30 nm diameter nanowires made with a silver solution concentration of (d) 0.8 mg/ml and (e) 1.5 mg/ml, and (f) 120 nm nanowires at a concentration of 0.9 mg/ml, which has the same transparency at 550 nm as the sample shown in (d).

Figures 5.1(b) and 5.1(c) show the dependency of transparency on nanowire concentration for 30 nm and 120 nm diameter nanowire networks, respectively. As expected, the transmittance across all wavelengths decreases with density due to there being an increased fraction of silver covering the surface of the glass which leads to an increase in absorbed and reflected light. Less obvious, however, is that the drop in transparency from visible to NIR increases with increased density. For example, for films made with a 30 nm diameter nanowire solution concentration of 0.5 mg/ml, the transparency drops four percentage points between 550 nm and 2500 nm (Figure 5.1(b)). With a solution concentration of 1.5 mg/ml, the transparency drops twelve percentage points over that same range. This effect is less pronounced for the thickest nanowires (as observed in Figure 5.1(c)). Figure 5.2 shows the transmittance vs. wavelength of the 70 nm and 100 nm nanowire networks at various densities, where these same trends are exhibited.

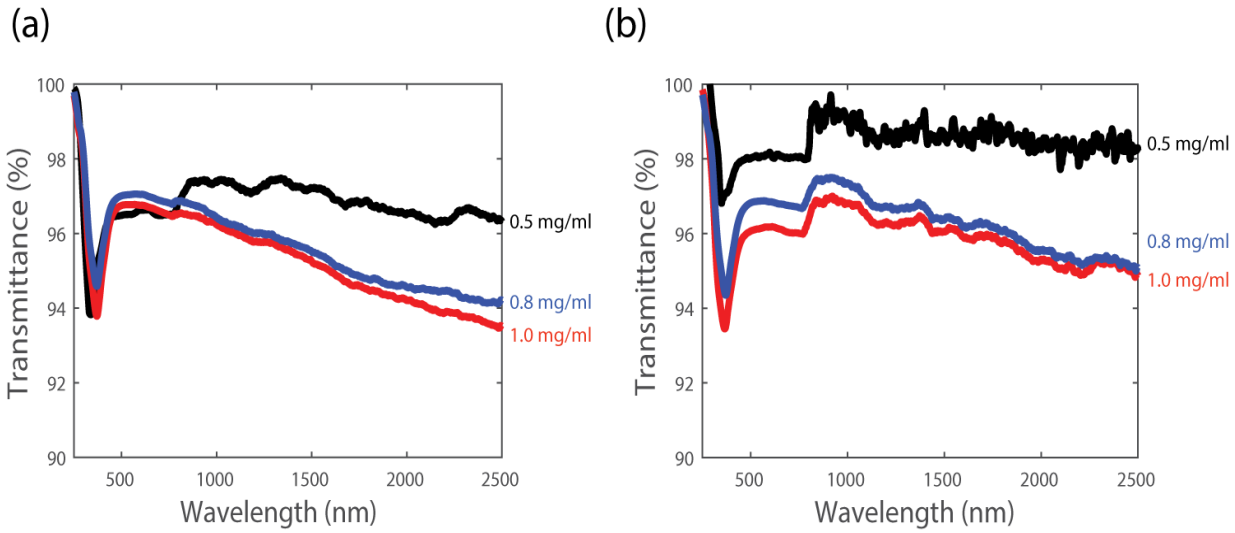

Figure 5.2: The transmittance of (a) 70 nm and (b) 100 nm diameter nanowire networks made from solution concentrations of 0.5, 0.8 and 1.0 mg/ml. Consistent with the observations in Figure 5.1, the transmittance drops more significantly over the NIR region for thinner and denser networks.

5.3.2 Transmittance Modelling

To further investigate the dependence of AgNW film transparency on diameter and density, systematic modelling is conducted. The nanowire networks are modeled using MATLAB software as a mesh wire grid with nanowire diameter, d, and nanowire spacing, *a*, as shown in Figure 5.3(a). I_o is the intensity of the transverse magnetic (TM) and transverse electric (TE) plane waves at normal incidence incident on the silver nanowire network and T is the transmitted intensity. The sheet impedance of the silver nanowire

mesh can be modeled by relating the averaged electric field, $\widehat{E_s}$, across the film to the surface current density, $\widehat{J_s}$, through Equation (5.1):

$$\widehat{E_s} = \overline{\overline{Z}}_s \cdot \widehat{J_s} \tag{5.1}$$

where $\overline{\overline{Z}}_s$ is a 2x2 matrix which has eigenvalue solutions $Z_{,TE}$ and $Z_{s,TM}$ to represent the equivalent sheet impedance for TE and TM polarized waves . These values are given by

$$Z_{s,TE} = Z_w a + j\omega L_s \tag{5.2}$$

$$Z_{s,TM} = Z_{s,TE} - \frac{j\omega L_s}{2} sin^2(\theta) \tag{5.3}$$

where θ is the incident angle of light hitting the nanowire film, ω is the angular frequency of the light, *a* is the wire to wire spacing, $Z_w = (\pi r^2 \sigma)^{-1}$ is the DC impedance for silver, and L_s is the sheet inductance parameter [123], [124]. This shows that at normal incidence, which is what is modelled here, the interaction of light with the nanowire film is entirely TE and thus we will only focus on TE in this study.

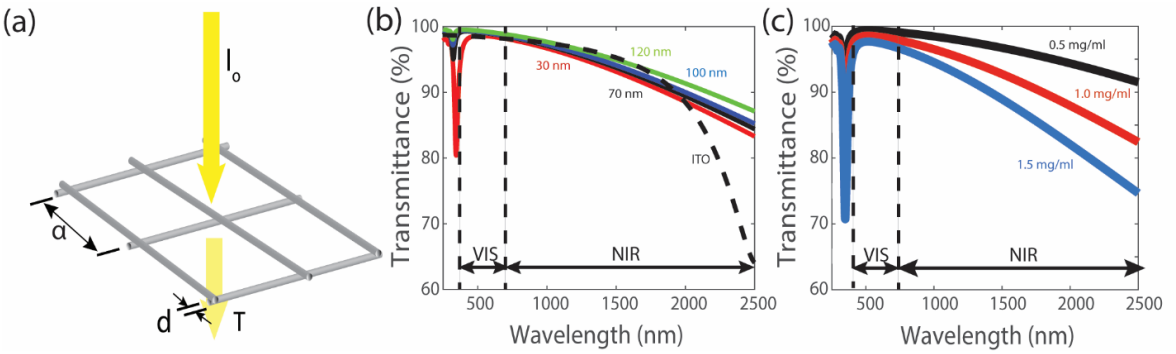

Figure 5.3: (a) Schematic of the modelled silver nanowire grid with nanowire spacing, *a*, and nanowire diameter, d. Light is incident from the top. (b) Simulated transmittance of indium tin oxide vs silver nanowire networks with diameters of 30, 70, 100, and 120 nm. (c) Simulated transmittance of a 30 nm diameter nanowire network at concentrations of 0.5, 1.0, and 1.5 mg/ml.

The sheet inductance parameter from Equations (5.2) and (5.3), related to the imaginary portion of the impedance in Equation (5.1), is given by

$$L_s = \frac{\mu_o a}{2\pi} ln\left(1 - e^{\frac{-2\pi r}{a}}\right)^{-1} \tag{5.4}$$

where r is the radius of the nanowire [123], [124]. To calculate the transmittance for TE polarized light, one can analyze the electromagnetic boundary conditions and using geometry we find

$$t_{TE} = \frac{2(\frac{Z_{s,TE}}{Z_o})\cos\theta}{1+2(\frac{Z_{s,TE}}{Z_o})cos\theta} \tag{5.5}$$

where Z_o is the impedance of free space [121], [122]. Figure 5.3(b) displays the modelled transmittance in the visible and near-infrared regions for d = 30 nm, 70 nm, 100 nm, and 120 nm. The transparency of ITO was modelled as a film with 40 nm thickness using a Drude model as demonstrated by others [9]. In addition, Figure 5.3(c) models the dependence of transparency on wavelength for d = 30 nm at densities corresponding to the same densities in Figure 5.1(b). Both Figures 5.3(b) and 5.3(c) yield similar results to the experimentally measured values in Figures 5.1(a) and 5.1(b), indicating that the model matches with experimental measurements. Additional plots showing the simulated transmittance of networks with nanowire diameters of 70 nm, 100 nm, and 120 nm at various densities are shown Figure 5.4, which confirms that this model matches experiment well for multiple nanowire diameters and densities.

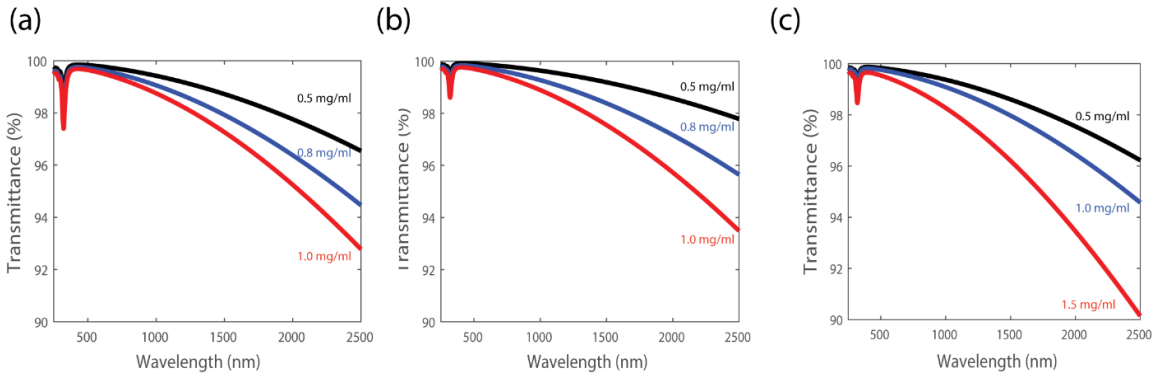

Figure 5.4: Simulated transmittance of nanowire networks at concentrations of 0.5, 1.0, and 1.5 mg/ml with diameters of 70 nm (a), 100 nm (b), and 120 nm (c).

5.3.3 The nanowire size effect

The real part of silver's dielectric permittivity (the polarizability of a material to an electric field), ε_1, is plotted in Figure 5.5(a) and is the same for both bulk silver and silver nanowires (and is not diameter dependent). It becomes more negative as the wavelength increases (frequency decreases) since the electrons can respond faster to the changing electromagnetic field and reflect longer wavelength radiation. This results in the transparency of all silver nanowire networks dropping at least slightly across the visible

and NIR regions. As for the reason for the decreased transparency at larger wavelengths for thinner nanowire networks (of a given concentration) and denser networks, Lee et al. attributes this to the smaller spacings between nanowires in such films [125]. Another significant additional factor is observed: the imaginary part of the permittivity, ε_2, in the NIR region is larger for thinner nanowires, resulting in a higher damping factor and hence larger absorption. This in turn results in a decrease in NIR transmittance. The permittivity of a silver nanowire can be modeled using one Drude oscillator along with five Lorentz oscillators for more accuracy [32], as shown in Equation 5.6:

$$\varepsilon_{Ag} = \varepsilon_\infty - \frac{\omega_p^2}{\omega^2 + i\gamma_p\omega} + \sum_{m=1}^{5} \frac{f_m\omega_m^2}{\omega_m^2 - \omega^2 - i\gamma_m\omega} = \varepsilon_1 + i\varepsilon_2 \tag{5.6}$$

where ω_p is the plasma frequency of silver, ω_m is the resonance frequency for each oscillator, f_m is the magnitude of the Lorentz oscillator, γ_m is the damping rate of each oscillator, γ_p is the damping rate of the Drude oscillator, and ε_∞ is the DC permittivity of silver [126]. This was already implemented into this model by converting the permittivity to conductivity and then substituting the altered conductivity into the equation for sheet impedance (equation (5.2)). When the nanowires are very thin, more electrons are in close proximity to the surface and thus scatter more as the mean free path between collisions of electrons is larger than the diameter of the nanowire itself. This causes the imaginary component of the permittivity, ε_2 in equation (5.6), to be larger since γ_p is larger as shown in Equation (5.7):

$$\gamma_p = \gamma_b + A_o \frac{v_F}{d} \tag{5.7}$$

where γ_b is the damping rate for bulk silver, v_F is the Fermi velocity of silver, d is the diameter of the nanowire, and A_o is a constant that depends on the details of the scattering process in the nanowire [126]. The imaginary part of the dielectric permittivity, ε_2, is shown in Figure 5.5(b). When ε_2 increases, the light absorption or loss increases due to electron scattering at the nanowire surface when the nanowire diameter is smaller than the electron mean free path. It can be seen that as the diameter gets smaller, the loss gets higher, and the difference between diameters increases as the wavelength increases. Figure 5.5(c) shows the simulated transparency of silver nanowire networks with diameters of 30 nm and 120 nm using the damping rate of bulk silver vs the damping rate of a silver nanowire. It can be seen that taking into account the dependence of the damping rate on diameter affects the transmittance curves of the thinner nanowires more significantly than the thicker nanowires (the results for 70 and 100 nm diameters shown in Figure 5.6 confirm the same). Thus, the size effect of the imaginary part of the permittivity (ε_2) contributes to the larger transparency drop of thinner nanowires in the NIR region. The curve for the 30 nm nanowires with

the damping effect considered is lower at 550 nm as the plasmon resonance at 375 nm is neglected in the non-damping effect model.

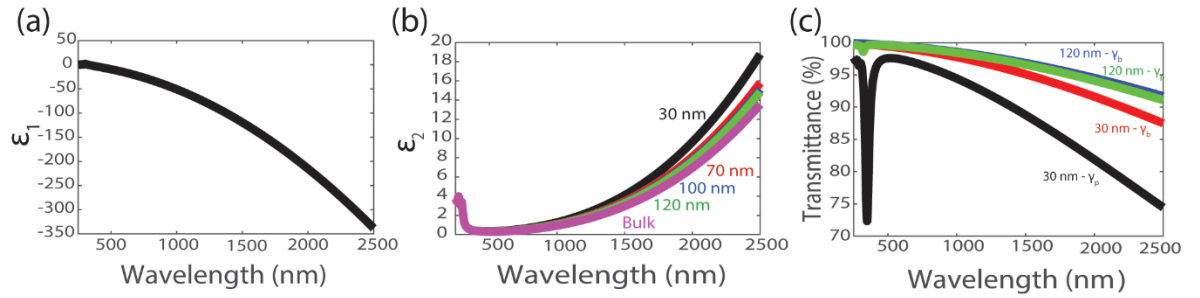

Figure 5.5: (a) The real part of the dielectric permittivity, ε_1, is the same for bulk silver and silver nanowires. (b) The imaginary part of the dielectric permittivity, ε_2, of nanowires with diameters ranging from 30 nm to 120 nm as well as that of bulk. (c) Transmittance vs wavelength of 30 nm and 120 nm nanowires with (γ_p) and without (γ_b) the diameter-dependence of ε_2 considered in the transmittance model. *5.3.4*

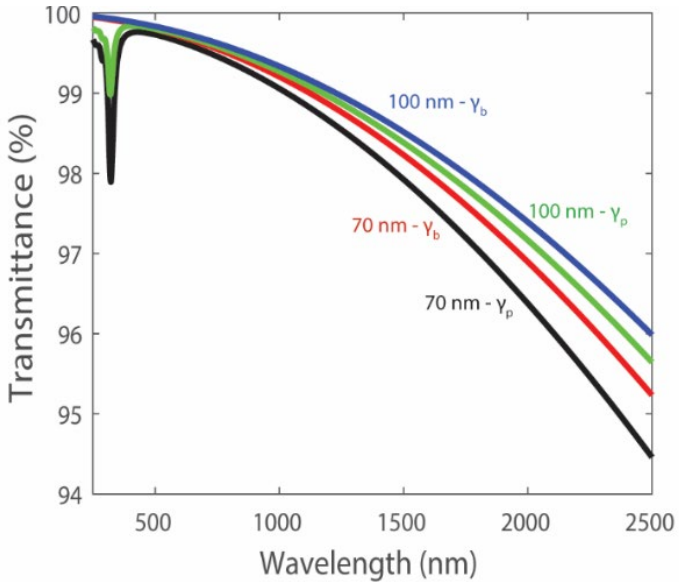

Figure 5.6: Transmittance vs. wavelength of 70 nm and 100 nm nanowires with (γ_p) and without (γ_b) the diameter-dependence of ε_2 taken into account in the transmittance model.

5.3.4 Nanowire Spacing

Another important factor that impacts optical properties over the NIR region for AgNW films is the nanowire spacing. In Figures 5.5(c) and 5.6 it is shown that when the size effect of the permittivity is not considered (curves labelled with γ_b), the network consisting of thinner nanowires still drops more over the

NIR region than the thicker nanowires. And the size effect also does not explain why the transparency of denser films drops more over the NIR region compared to sparser films of the same diameter. These effects can be explained by the smaller spacing between nanowires in films consisting of thinner or denser nanowires, which on average is smaller than NIR wavelengths [127].

Figures 5.1(d) and 5.1(e) show SEM images of 30 nm diameter nanowire networks made using a silver solution concentration of 0.8 mg/ml and 1.5 mg/ml, respectively. It is observed that at high concentrations, the average spacing between nanowires is smaller, and when the spacing of structures in a film is smaller than the wavelength of light, the power of light transmitted through a metal grid is equal to:

$$P_t = \frac{64}{54\pi} k^4 a^6 c \varepsilon_o E_i^2 \tag{5.8}$$

where E_i is the incident electric field, c is the velocity of light, k is the wave vector (inversely proportional to wavelength), a is the nanowire spacing and ε_o is the permittivity of free space [128].

At a given density, the transmittance drops over the NIR region since k decreases with increasing wavelength as explained by their inversely proportional relationship. However, as the density increases, the drop is more pronounced since the spacing between adjacent nanowires, a also decreases. Regarding diameter, Figure 5.1(f) shows a 120 nm diameter nanowire network that has the same transparency in the visible as Figure 5.1(d). It is clear that the average spacing is much larger than for the 30 nm diameter network and thus, according to Equation (5.8), the transmitted light in the NIR is greater because longer wavelengths can transmit more easily when there are larger gaps between nanowires [129].

To further elucidate these points, Figure 5.7 displays simulation results of how the ratio of Transmittance@2500 nm compared to Transmittance@550 nm depends on the nanowire diameter (Figure 5.7(a)) and density (Figure 5.7(b)), where the effect of nanowire size on permittivity is neglected. In Fgure 5.7(a), the networks have the same areal mass density (*amd*), or mass of nanowires per area, of 100 mg/m^2, which corresponds to the density of 30 nm diameter networks that have 96% transparency at 550 nm. The following equation is used to convert *amd* into spacing)[130], [131] if the nanowires are arranged in a grid:

$$amd = 4\pi d_{Ag} \left(\frac{r^2}{a}\right) \tag{5.9}$$

where d_{Ag} is the density of silver, r is the radius of the nanowires and a is the spacing of the nanowires [126], [128]. Figure 5.7(a) shows that networks of a given density made from thinner nanowires have a

smaller spacing which in turn, have a lower transparency at 2500 nm compared to the visible. Figure 5.7(b) indicates how the ratio of T@2500 nm to T@550 changes with nanowire *amd*. As the *amd* increases, the nanowire spacing decreases for all diameters, leading to a larger fall off in transparency in the near-infrared region compared to the visible region. As consistent with Equation (5.9), the 30 nm diameter samples will have the largest drop because they have the smallest nanowire spacing at the same *amd* compared to the 120 nm nanowire samples.

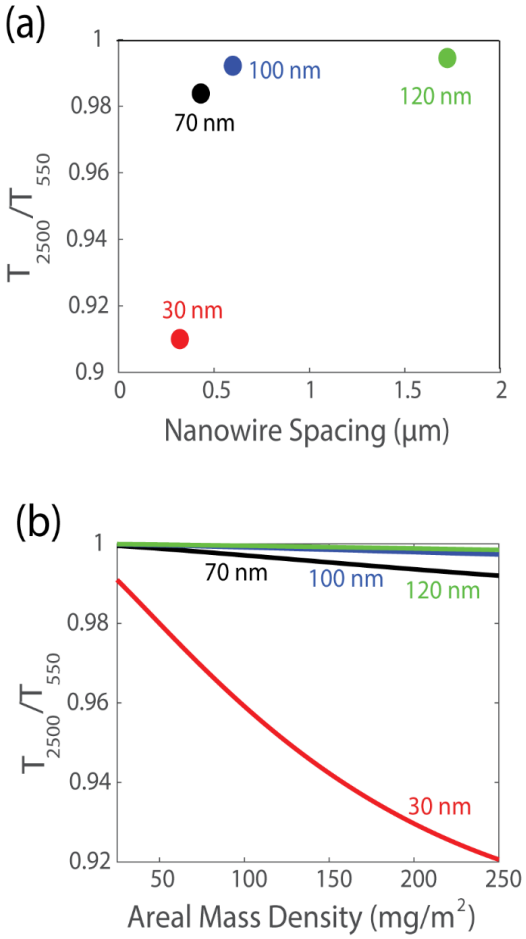

Figure 5.7. (a) The simulated ratio of transmittance in the NIR to transmittance in the VIS for nanowire networks of the same density with diameters of 30 nm, 70 nm, 100 nm, and 120 nm. The transparency of the 120 nm nanowires drops the least between the visible and near-infrared due to its larger spacing at a given visible transparency. (b) The simulated ratio of the transmittance at 2500 nm to 550 nm vs areal mass density. The ratio of NIR to VIS transmittance falls off faster for smaller diameter nanowires compared to larger ones.

To provide guidance on what AgNW spacing and hence concentration is required to achieve a certain transparency in the visible in NIR, modelling was done to show the dependence of transparency on spacing. Figure 5.8(a) shows the transmittance of silver nanowire networks with diameters of 30 nm, 70 nm, 100

nm, and 120 nm at a wavelength of 550 nm in the visible region, and how it depends on nanowire spacing. The transmittance increases drastically from 0% at zero spacing to greater than 80% once the nanowire spacing, or nanowire concentration, reaches a certain value. The 30 nm nanowires require the smallest spacing in order to reach a transparency of more than 80%, since for a given spacing thinner networks have a lower *amd* (because of this they would also, however, have a worse sheet resistance than the thicker nanowire grids at the same spacing). We show a similar plot in Figure 5.8(b) except in the near infrared region at a wavelength of 2500 nm. As shown above in Section 5.3, the transparency decreases in the NIR region for all nanowire diameters compared to their transparency in the visible because the power transmitted through an aperture increases with the wave vector k, at a rate of k^6 [128].

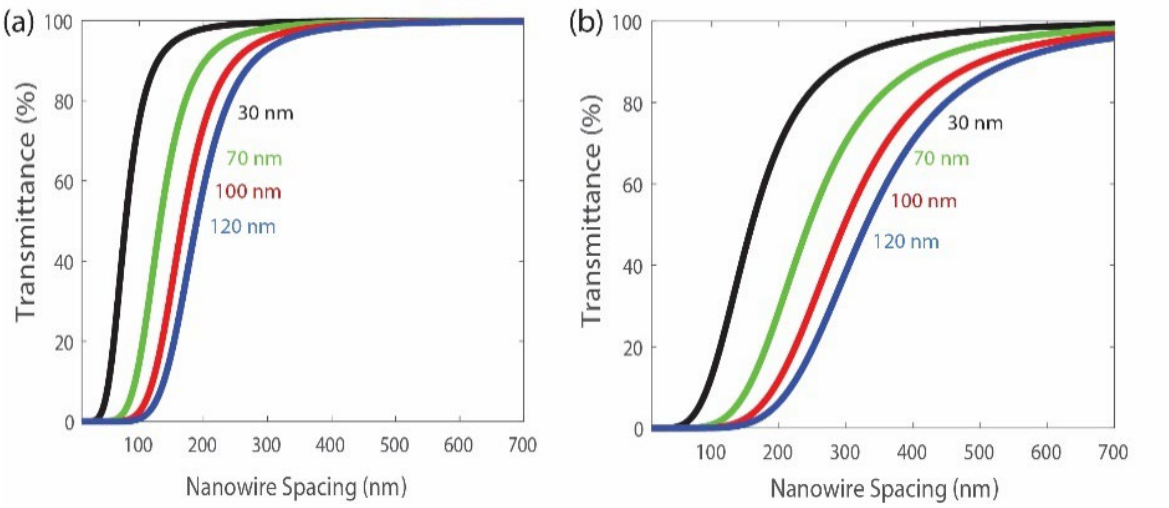

Figure 5.8: The transmittance vs nanowire spacing of silver nanowire networks for varying nanowire diameters at a wavelength of 550 nm (a) and 2500 nm (b).

5.4: Further Results and Discussion

After the publication of the above work in *Nanotechnology*, further modelling and experiments were performed for a more comprehensive understanding of the optical properties of these nanowire networks.

5.4.1 Reflectance and Absorption

The above work focused on transparency of nanowire networks only. However, whether transmittance loss is due to reflection or absorption is of interest. The reflectance and absorption can be related directly to the transmittance through the equation:

$$T+A+R = 100\% \tag{5.10}$$

where T is the transmittance, R is the reflectance, and A is the absorption (Fox, n.d.)[132].

Figure 5.9 shows the reflectance vs wavelength (Figure 5.9(a)) and absorption vs wavelength (Figure 5.9(b)) simulations for nanowire diameters of 30 nm and 120 nm with the same *amd* where the damping effect is included. Above, 500 nm, it is mostly reflectance rather than absorption that reduces the transparency of silver nanowire networks. The reflectance is larger for smaller diameter nanowires (30 nm) compared to larger ones (120 nm) at longer wavelengths because of two reasons: (1) the imaginary part of the permittivity being larger for thinner AgNWs as wavelength increases and (2) the NW spacing being smaller for thinner AgNWs at a given *amd*. This is demonstrated in the well-known relation for the reflectance of a thin film at normal incidence from air given by:

$$R = \frac{(n-1)^2+k^2}{(n+1)^2+k^2} \tag{5.11}$$

where n is the refractive index of the thin film, and k is the extinction coefficient of the thin film [132]. As k increases, which is related to the imaginary part of the permittivity through $\varepsilon_2 = 2nk$, the reflectance will increase as well [132]. n and k are also highly sensitive to changes in AgNW spacing and will both increase with decreasing spacing. Figure 5.9(b) shows that the absorption of the nanowire networks is quite low, with the exception of a strong peak at 375 nm corresponding to the plasmon resonance of silver. The slight red -shift of the surface plasmon resonance for thinner AgNWs is due to the geometrical dependence of the surface plasmon resonance [133]. For a material consisting of nanostructures with critical dimensions much smaller than the wavelength of light, it is well known that the effective permittivity of the homogenized material can be calculated using Maxwell-Garnett Effective Medium theory. The calculation includes a geometrical factor that will change the effective permittivity of the film, and hence the location of the absorption peak [133]. This resonance is stronger for smaller diameter nanowires as the nanowires are spaced closer together and consequently there is more overlap of the evanescent near field generated by the plasmon absorbance peak [37][37]. It is also important to note that the absorbance increases for longer

wavelengths for smaller nanowire diameters when the damping effect is accounted for. This is expected as the imaginary part of dielectric permittivity is directly correlated to absorption [63].

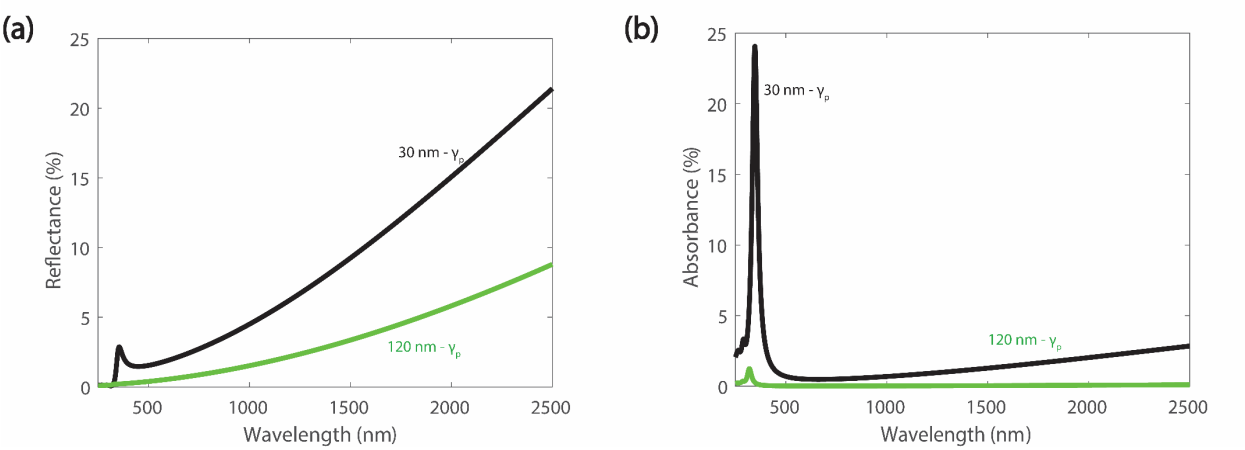

Figure 5.9: (a) The reflectance and (b) absorbance vs. wavelength of silver nanowire networks for 30 and 120 nm nanowire diameters with the damping effect included.

5.4.2 Nanowire Length

In this section the effect of nanowire length on transmittance is studied both experimentally and through modelling. Silver nanowires with a diameter of 30 nm with three different lengths were purchased from Novarials Coporation (Woburn, MA). Nanowire networks were coated on BK7 glass using the Mayer Rod coating method as explained previously in Section 5.2. In order to ensure the same mass of nanowires was used in each sample (thus leading to the same areal mass density, *amd*, in the network), 1 ml of each solution was centrifuged at 10,000 RPM and the ethanol solvent was removed. Then the exact same mass of nanowires was weighed, made equivalent, and 1 ml of ethanol was used to redisperse the nanowires into a solution for all samples. SEM images of the three networks are shown in Figure 5.10. The average length of the nanowires in the three samples were measured at 3 µm (a), 28 µm (b), and 88 µm (c).

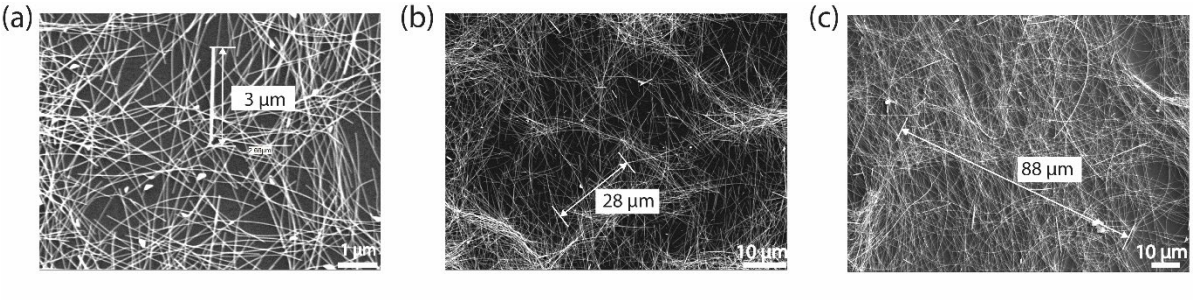

Figure 5.10: SEM images of silver nanowire networks with 30 nm diameters and average lengths of 3 µm (a), 28 µm (b), and 88 µm (c), all at the same areal mass density.

The sheet resistance of each silver nanowire network was measured using a digital multimeter. The AgNW films with nanowire lengths of 3 µm, 28 µm, and 88 µm had sheet resistances of 113 kΩ/sq, 142 Ω/sq, and 4.5 Ω/sq, respectively. The longest nanowires have the lowest sheet resistance as there are a fewer number of nanowire junctions [120]–[122]. Nanowire junctions can have a high contact resistance while the resistance along a nanowire itself is much lower [97].

The transmittance curves at normal incidence were obtained for all samples using a Perkin Elmer 1050 UV/VIS/NIR Spectrophotometer as shown below in Figure 5.11. Silver nanowire networks made with the nanowire lengths of 28 µm and 88 µm have very similar transmittance values throughout the visible and NIR regions. They only differ by 3 percentage points at a wavelength of 2500 nm. The length difference between these sets of nanowires is 3X, the same as the length difference between the thinnest (30 nm, 12 µm long) and thickest (120 nm, 39 µm long) nanowires measured experimentally in Section 2.3. This supports the reasoning that the differences in transparency among the samples experimentally characterized in Section 5.3.1 is primarily due to diameter differences rather than length.

As for the very short 3 µm-long nanowires characterized in Figure 5.11, they have similar transmittance to the longer nanowires in the visible, but the transmittance difference increases with increasing wavelength. At 2500 nm, the transparency of the short nanowires are 20 and 23 percentage points lower than the 28 and 88 µm long nanowire networks, respectively. Therefore, the difference in transmittance can be explained by considering the length of propagation of the surface plasmon polaritons (SPPs) along the surface in the longitudinal direction of the NW. For shorter AgNWs, the SPP will scatter at the end boundaries of the AgNW, resulting in more energy being absorbed compared to longer AgNWs where the SPP has a longer propagation length [134]. Additionally, the gaps between wires in the shorter AgNW networks are smaller (and more numerous) compared to the longer AgNWs. The electric field will be higher in these smaller

gaps, especially at wavelengths in the NIR, resulting in more absorption of incident light, and lowering transmittance [122].

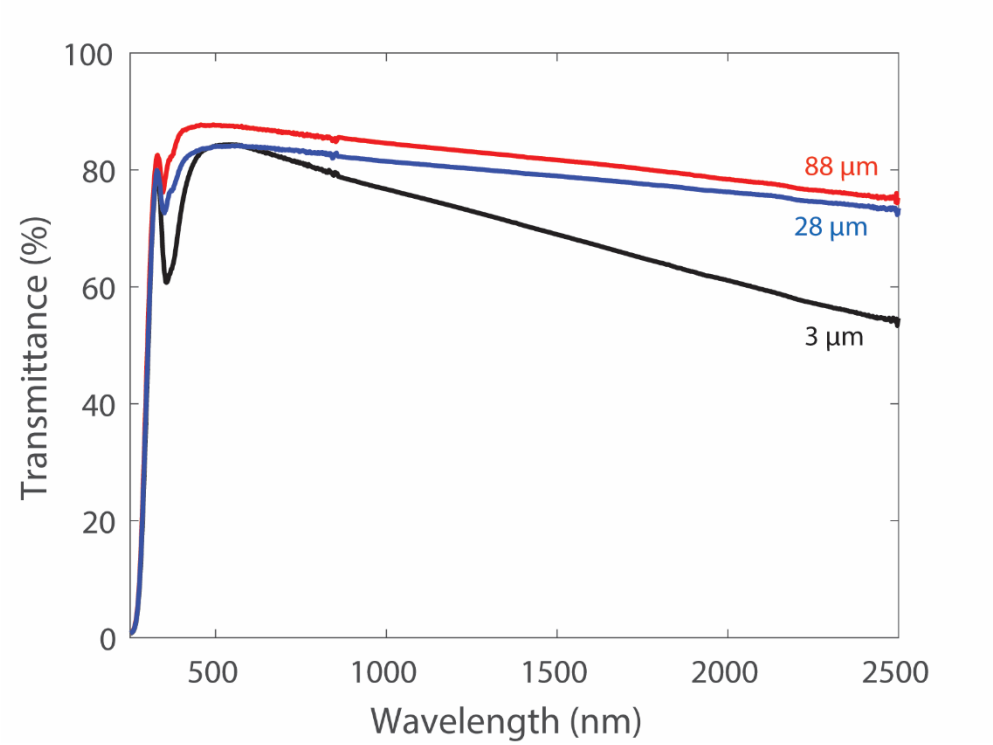

Figure 5.11: Transmittance of silver nanowire networks at three different lengths while the nanowire diameter and concentration are kept the same between all samples.

Simulations were performed to confirm and further understand the experimental results of the dependence of the silver nanowire length on their optical properties using Lumerical FDTD Software. A 15 µm x 15 µm square area was set up with a random distribution of nanowires with lengths of 3 µm and 12 µm. The total length of nanowires used in each case was 444 µm. This equated to using 37 randomly distributed 12 µm nanowires and 148 nanowires for the 3 µm nanowire network. The diameter of all nanowires was 30 nm, and the total transmittance was extracted for each nanowire network.

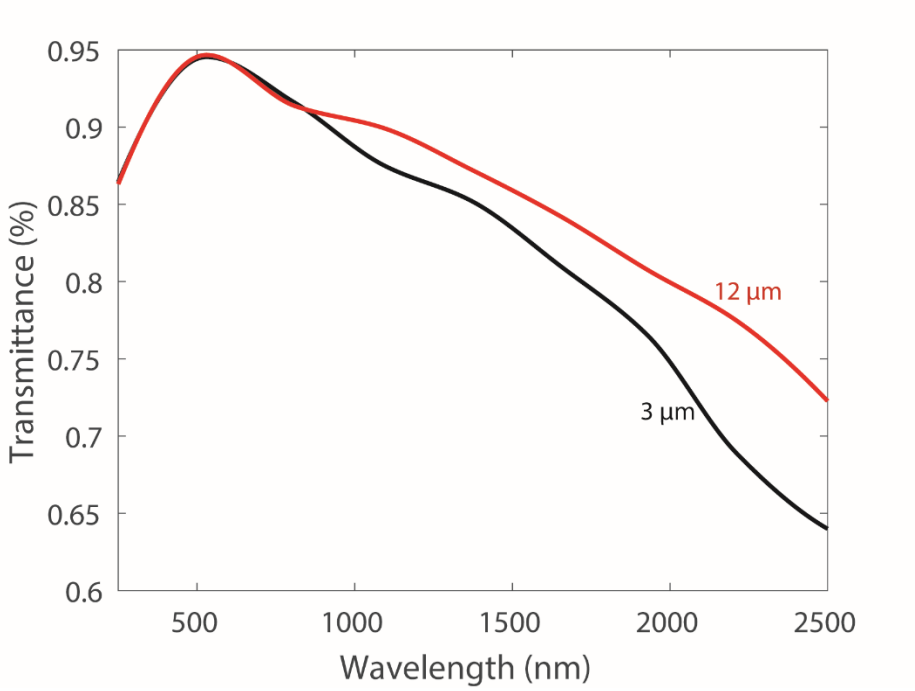

Figure 5.12: Simulated transmittance of silver nanowire networks using Lumerical FDTD at two different lengths while the nanowire diameter and total length of nanowires (concentration) are kept the same between all samples.

The results are shown in Figure 5.12. The trend matches with the measured experimental results in Figure 5.11, i.e. shorter nanowires show a larger drop off in their transmittance in the NIR region compared to the visible one. This, as mentioned above, can be explained through the shorter propagation length of the SPPs and the larger absorption of the smaller, more numerous gaps between NWs.

5.4.3 Nanowire Haze

For some applications including electrochromic displays and smart windows, electrode haze is important as it effects the quality of the image or the amount of distortion seen when looking through the device. The nanowire haze is defined mathematically as

$$Haze = \frac{T_t - T_s}{T_t} = \frac{T_d}{T_t} \tag{5.11}$$

where T_d is diffuse transmittance, T_s is the specular transmittance and T_t is the total transmittance measured through the sample [135], [136]. The total transmittance of a sample consists of the two parts, specular and diffusive transmittance. Specular transmittance accounts for light transmitted through the sample that

travels in the same direction as the incident light while diffuse transmittance represents forward scattered light that is scattered at a different angle to the incident light. In order to measure this experimentally, an integrating sphere must be used in order to calculate all light that is scattered at non-normal incidence angles as it travels through the nanowire network. A schematic of the experimental setup is shown in Figure 5.13(a). An acceptable value for the haze measurement of a window is < 10% of the total transmittance [135], [136]. It is only in the visible region where haze is important. Figure 5.13(b), (c), (d), and (e) show the dependency of haze on concentration for various NW diameters. As the concentration of nanowires increases, the haze increases as there are more nanowires on the substrate to scatter light. A concentration of 0.5 mg/ml is too low for the nanowire electrodes to be conductive enough for electrochromic applications while 1.5 mg/ml is getting towards the upper limit of what we want the measured haze to be. Therefore, there is a focus on a concentration of 1.0 mg/ml in the next chapter for making smart windows, which will align with the sheet resistance and transmittance measurements discussed earlier in Section 5.3.

Figure 5.13(f) compares the haze value from nanowire diameters of 30 nm, 70 nm, 100 nm, and 120 nm at a concentration of 1.0 mg/ml. AgNW films with a diameter of 70 nm have the highest haze values between 6 and 8%, while 100 nm nanowire networks have values ranging between 2.5 and 4% across the same spectrum. It is already known in the field that thinner nanowires scatter less light than thicker nanowire networks at the same concentration [137]; smaller diameter nanowires have a smaller cross-sectional area seen by light, and as a result a smaller amount of light is scattered off normal incidence. However, smaller diameter nanowires have smaller nanowire spacings at the same time so this can lead to higher haze as light is more likely to scatter when there are more nanowires. Therefore, to minimize haze, it is preferable to use a balance between thicker and thinner nanowires in the electrodes. 30 nm nanowires will be used as the haze values between 5.5 and 7% are good enough to not make objects blurry to the human eye.

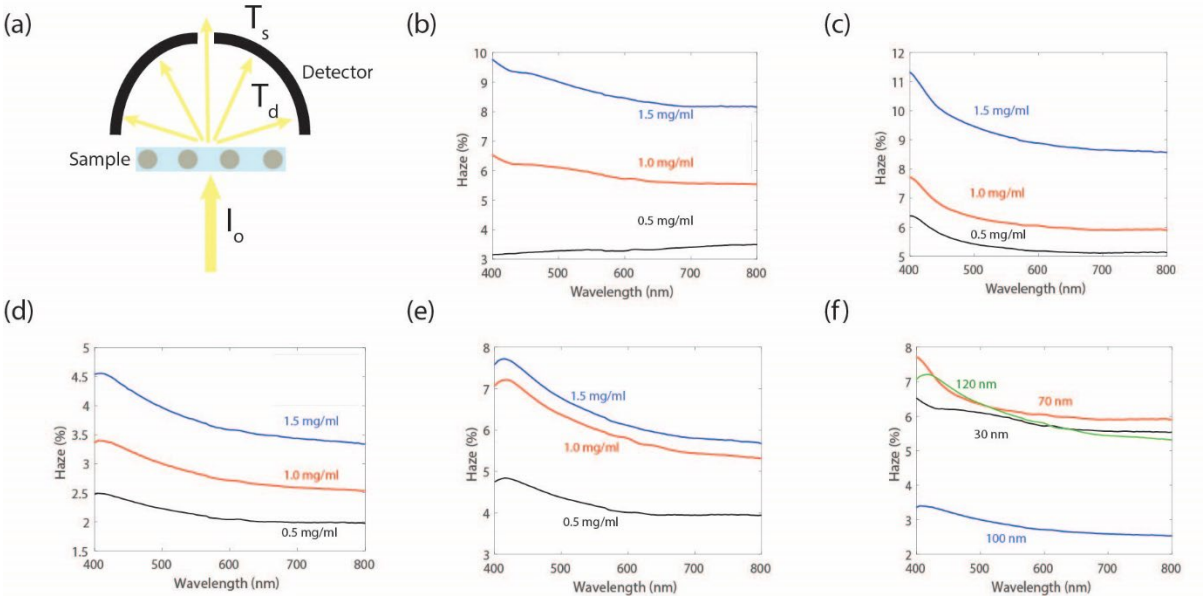

Figure 5.13: (a) Schematic illustrating how specular and diffuse transmittance measured using an integrating sphere. The haze at concentrations of 0.5, 1.0, and 1.5 mg/ml for nanowire networks with diameters of 30 nm (b), 70 nm (c), 100 nm (d), and 120 nm (e). (f) A comparison of the measured haze for nanowire diameters of 30, 70, 100, and 120 nm at a concentration of 1.0 mg/ml.

5.5 Conclusion

In conclusion, it was shown experimentally and theoretically that silver nanowire transparent electrodes can have far higher transparency in the NIR region compared to the current state-of-the-art technology, ITO. The transparency of nanowire networks drops across the visible and NIR wavelength ranges due to the wavelength dependency of the real and imaginary permittivity of the nanowires themselves and due to the larger relative size of the wavelengths to the average spacing between nanowires. Because sparser and larger diameter nanowire networks have larger average spacing, and the imaginary part of the nanowire permittivity is lower than for smaller diameters due to less surface scattering, such networks minimize the drop in transparency between visible and the NIR. The transmittance of 120 nm diameter nanowire networks with a transparency of 96% in the visible, for example, still maintains a high NIR transmittance of 94% which is advantageous for some applications such as smart windows. It was found that reflectance rather than absorption was primarily responsible for transparency loss in nanowire networks. It was also found that the length of the nanowires plays a role in network transparency, with very short nanowires (3 μm) in particular having an appreciably lower transmittance than nanowire lengths of 28 μm or more in the NIR. Because short nanowires also lead to higher sheet resistances, it is preferable to use long nanowires in transparent electrodes.

It is important to note that when designing an electrode for a particular application, there are many other properties that vary with nanowire diameter and density that must be considered in tandem with their effect on NIR transparency. It was shown that networks made from larger diameter nanowires have higher haze. Other potentially relevant properties include surface roughness, electric field uniformity (for capacitive switching applications such as smart windows), and charge collection efficiency (in solar cells).

The impact of the high NIR transparency of silver nanowire transparent electrodes on the performance of window coatings compared to metal oxide electrodes will be investigated in Chapter 6.

Chapter 6
The Higher NIR Transparency of Electrochromic Smart Windows with Silver Nanowire Electrodes

In this chapter indium tin oxide (ITO) is replaced with silver nanowire electrodes in electrochromic smart windows, placing particular focus on their ability to allow more NIR transmission in the winter. First, modelling is used to calculate the performance metrics of these windows, including the solar heat gain coefficient and U-factor. Then tungsten oxide/nickel oxide electrochromic thin films and completed smart windows on both ITO and AgNW electrodes are fabricated, characterized and compared in their performance.

6.1 Introduction

A major application of electrochromic devices is smart windows [1]. Smart windows are used in buildings, cars, planes, and even eyewear [1]. They have both economic and environmental impact with their potential for energy savings and reduction in carbon dioxide emissions. As discussed in Chapter 1, electrochromic smart windows are the best performing smart windows in terms of haze, on/off voltage, and transmittance on/off ratio [1]. Smart windows predominantly use two layers of metal oxides such as ITO, FTO or AZO as transparent electrodes, but as discussed thoroughly in this thesis so far, these metal oxides have a low NIR transparency which limits the amount of solar heat that can enter a building in the winter. These metal oxides are also costly and lack mechanical flexibility [40]. As reviewed in Section 1.6.2, AgNW electrodes have been integrated into a few electrochromic windows in the literature. Not only are AgNW electrodes lower in cost, more convenient to deposit and have better mechanical flexibility than metal oxides, the windows also can have better performance. In this chapter electrochromic films and devices using AgNW electrodes are fabricated and tested, with particular focus on the ability of these electrodes to permit more NIR radiation across the window in the off state. And for the first time, the solar heat gain coefficient (SHGC) of smart windows using AgNW electrodes is calculated and compared to devices using ITO.

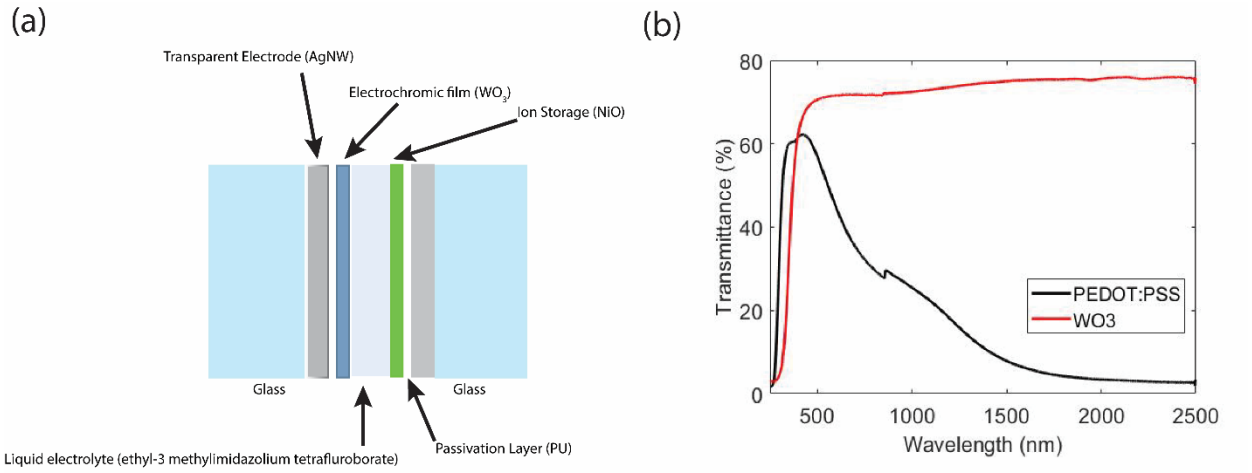

Figure 6.1: (a) Schematic of the smart window device. (b) Transmittance in the visible and near infrared of PEDOT:PSS and tungsten oxide.

In this chapter, smart windows are implemented using WO_3 and NiO, the most commonly used primary electrochromic material and ion storage (or secondary electrochromic) material, respectively. Unlike PEDOT:PSS used in Chapters 2 – 4, WO_3 is transparent to the NIR when in the off state (Figure 6.1(b)), and thus can allow solar heat to traverse the window if the electrodes are also transparent in the NIR. Regarding NiO, devices have been shown to be more stable when an ion storage layer is used. An ion storage layer acts in opposition to the primary electrochrome in terms of the polarity of the applied voltage causing it to be bleached or coloured [1]. When the primary electrochrome is bleached, the secondary electrochrome is also bleached even though it sees the opposite voltage polarity. This is also true when the window is switched on and both layers will become coloured. This increases the on/off ratio of the transmittance further. Together, WO_3 and NiO have a big transparency change between the on and off states, a good response time, and have good colouration efficiencies (WO_3 = 70 ξ/cm^2C^{-1} and NiO = -30 ξ/cm^2C^{-1}) [1]. The final designed device structure is shown in Figure 6.1(a). The electrolyte used will be lithium perchlorate salt dissolved in propylene carbonate. It was found that the LITFSI Emim TFSI with PMMA electrolyte used in previous chapters does not work in this case as the PMMA dries out the tungsten oxide and results in no colour change occurring, even when a current is measured in the CV or CA.

6.2 Window Performance Metrics

Figure 6.2 shows the general structure of a window. It usually consists of two panes of glass with a small gap (usually filled with an inert gas such as argon) in between and they are placed in a frame for structural support. There are three main places in the window setup where heat loss comes from: centre-of-glass, edge-of-glass, and the frame.

The U-factor of the window describes the rate of heat loss of a window. The lower the U-factor is, the more resistance the window is to heat flow. The overall U-factor of a window is given by

$$U = \frac{A_{cg}U_{cg} + A_{eg}U_{eg} + A_{fr}U_{fr}}{A_{cg} + A_{eg} + A_{fr}} \tag{6.1}$$

where A_i is the area for i = centre-of-glass, edge-of-glass, and the frame, while U_i is the U-factor of each component that contributes to energy loss in the window [141]. The U-factor (in units of W/m^2*K) for each component of the window can be described as

$$U_i = \frac{q_i}{A_i \Delta T} \tag{6.2}$$

where q_i is the heat transferred at the indoor surface of the window given in units of W, ΔT is the temperature difference between the building and the outside, and A_i is the area of the component [141].

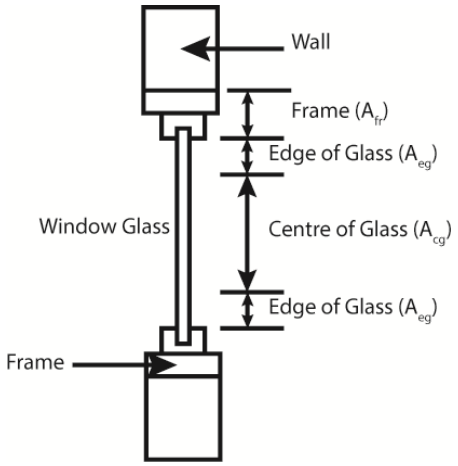

Figure 6.2 Schematic of a window when it is installed in a building, The areas of the frame, edge of glass, and center of glass are indicated for calculations of the U-factor and solar heat gain coefficient [141]**.**

A second figure of merit is called the Solar Heat Gain Coefficient (SHGC) which describes the fraction of solar radiation that enters a building. The SHGC can carry a value between 0 and 1 [141]. When the SHGC is 0, electromagnetic radiation emitted by the sun is completely blocked from entering the building. The SHGC is defined as

$$SHGC_{i=} = \tau_{sol} + \sum_{i=2}^{n-1} A_i N_i \tag{6.3}$$

where

$$N_i = \sum_{j=i}^{n-1} \frac{R_j}{R_{tot}} \tag{6.4}$$

where R_j is the reciprocal of the U-factor for each component, i, of the window [141]. In other words, it is the resistance to heat loss for each interface in the window. τ_{sol} is the solar transmittance of the window to sunlight, A_i is the absorbed portion of incident solar radiation and N_i is the inward flow fraction of the absorbed solar radiation [141]. The overall SHGC of the window can be found similar to the overall U-factor under the common assumption that $SHGC_{fr} = 0$ and $SHGC_{cg} = SHGC_{eg}$. The subscripts "fr", "cg", and "eg" represent the areas of the window referred to the frame, centre of glass, and edge of glass, respectively. The expression for the overall SHGC is

$$SHGC = \frac{(A_{cg} + A_{eg})SHGC_{cg}}{A_{cg} + A_{eg} + A_{fr}} \quad (6.5)$$

In order to achieve a SHGC that is higher in the winter and lower in the summer, a material or coating that can change its properties depending on the season or outside temperature has to be added to the glass.

The emissivity, ε, can be related to the absorption of a material at a certain temperature through Kirchoff's Law:

$$\varepsilon(\lambda, \theta, T) = \alpha(\lambda, \theta, T) \quad (6.6)$$

where α is the absorption which is dependent on incident angle of light, θ, wavelength, λ, and temperature T [142]. In other words, all radiation that is absorbed at a certain wavelength, angle, and temperature has to be re-emitted at the same wavelength, angle, and temperature. This allows us to model and measure emissivity quite easily. For a smart window, the goal is for the emissivity or absorption to be as low as possible at longer IR wavelengths in order to prevent radiation from being absorbed and re-emitted into the other side of the window, resulting in an indoor temperature decrease in winter and increase in summer.

6.3 Modelling and Simulations

The software WINDOW is used to determine the SHGC and U-factor of the window systems designed in this work. This is the industry standard as experimentally measuring the U-factor and SHGC is very costly and difficult to do. MATLAB will be used to calculate the transmittance, reflectance, and emissivity across the UV, visible and NIR to be used in the WINDOW simulations.

Silver nanowire electrodes consist of two different types of constituent structures in the overall layer: the silver nanowires and the air in the gaps between each wire. Effective medium theory (EMT) is used to homogenize the silver nanowire electrode so it can be treated as one uniform film by knowing the geometry and permittivity of the individual parts making it up. For a random network of silver nanowires, the Maxwell Garnett effective medium approximation is given by

$$(1-\rho)\frac{(\varepsilon-\varepsilon_{air})}{(\varepsilon_{silver}-\varepsilon)}=\frac{\rho}{3}\sum_{i=1}^{3}\frac{\varepsilon_{air}}{(\varepsilon_{air}+L_i(\varepsilon_{silver}-\varepsilon_{air}))} \tag{6.7}$$

where ε is the permittivity of the composite silver nanowire layer, ε_{silver} is the permittivity of a silver nanowire, ε_{air} is the permittivity of air, ρ is the fill fraction of silver nanowires covering the surface varying between 0 and 1, and L_i are the depolarization factors, accounting for the orientation of the nanowires in a random network [143]. For a random network, $L_1 = 0$, $L_2 = 0.5$, and $L_3 = 0.5$ [143]. The adjusted permittivity for silver nanowires was calculated for 30 nm nanowires and taken from my modelling in Section 5.4. The permittivity of WO_3 in the on and off state was taken from Rottkay et al. [144], [145]. In this case, an anisotropic model was used where the permittivity parallel to the NiO film is $\varepsilon_x = \varepsilon_y$ and the permittivity perpendicular is ε_z. The permittivity of NiO in the clear state was modelled using Valyukah et al. [145] and the permittivity in the coloured state was fit to Granqvist et al. [10]. The permittivity of ITO is taken from Askari et al. [10].

In order to simulate the reflectance, absorbance, and transmittance of the multilayer stack, the transfer matrix method is used. In this method 2x2 matrices are multiplied together with the interface between two layers and the propagation within each layer represented by each matrix [146]. The 2x2 matrices that represent each interface are different for p or TM polarized light and s or TE polarized light. For TM waves, it is defined as:

$$D_p=\begin{bmatrix}\cos\theta_i & cos\theta_i\\ n_{iz} & -n_{iz}\end{bmatrix} \tag{6.8}$$

and for TE waves:

$$D_s=\begin{bmatrix}1 & 1\\ n_{ix}cos\theta_i & -n_{ix}cos\theta_i\end{bmatrix} \tag{6.9}$$

where n_i is the complex refractive index for each layer, *i*, in the x and z direction, respectively. θ is the incident angle and in this case will always be taken as θ=0 for normal incidence. The propagation matrix for both TM and TE waves is given by

$$P_i=\begin{bmatrix}e^{i\varphi} & 0\\ 0 & e^{-i\varphi}\end{bmatrix} \tag{6.10}$$

where φ is the phase of the plane wave and is given by $\varphi = k_{ix}d_i$ where d_i is the thickness of the layer *i*, and k_{ix} is the x component of the wavenumber, given by $k = 2\pi/\lambda$, where λ is the wavelength of light. Then, the total matrix can be calculated as

$$\begin{bmatrix} M_{11} & M_{12} \\ M_{21} & M_{22} \end{bmatrix} = D_o^{-1}\left[\prod_{i=1}^{N} D_i P_i D_i^{-1}\right] D_N \tag{6.11}$$

where the -1 above the component in the multiplication of the matrices represents the inverse of the individual matrix and N is the final layer of the system. From the parameters M_{ij} in the final 2x2 matrix, we can calculate the reflectance and transmittance as follows:

$$R = \left|\frac{M_{21}}{M_{11}}\right|^2 \tag{6.12}$$

$$T = \frac{n_N cos\theta_N}{n_o cos\theta_o}\left|\frac{1}{M_{11}}\right|^2 \tag{6.13}$$

where n_N and n_o are the refractive index of the incident and transmitted medium (air) while θ_O and θ_N are the incident and transmitted angle of the electromagnetic radiation. For this modelling, both θ_O and θ_N were taken to be 0º or normal incidence. However, in reality, light comes from every angle of incident from 0º to 90º. From this, the absorbance can be calculated as A = 1 – (R+T). For the smart window system whose schematic was shown in Figure 6.1(a), the transmittance, T, reflectance, R, and absorbance, A are shown below in Figures 6.3(a), 6.3(b), and 6.3(c), respectively. We show the cases for silver nanowire electrodes and ITO electrodes when the smart window is in both the on and off state. The oscillations in the transmittance and reflectance plots are well known and come from Fabry-Perot resonances or thin film interference. These occur when standing waves are created when the wavelength of light matches the exact optical path length of a particular layer or system. In Figure 6.3(a), the transmittance of both devices is similar in the visible region, in both the on and off states. However, as expected, the device with the AgNW electrodes is more transparent in the NIR region. In the off or clear state, the AgNW based device has a transmittance above 80% at 3000 nm while that of the ITO based window drops to almost 40%. This is an advantage in winter or colder climates when more heat in the NIR can be transmitted through the window and assist in the heating of a building to reduce heating costs. In the coloured state, the transmittance at 3000 nm is near 30% for the device with AgNWs versus 21% for that with ITO. Overall, ΔT at 3000 nm for silver nanowire devices (~50%) is much greater than for ITO ones (~25%). The reflectance for the smart window in Figure 6.3(b) shows no appreciable differences between the devices with ITO and silver nanowire electrodes. For either device, when the window is turned on and off, there is a shift in the large peak in the NIR which is just due to the colour change of the window from light yellow to dark blue. Figure 6.3(c) shows the absorbance of the windows. Again, the silver nanowire-based windows perform similarly to the ITO based windows in the visible region. However, due to its plasmon resonance, ITO is more absorbing in the NIR. In the summer when you want to absorb or block NIR radiation, the device with

silver nanowire electrodes absorbs less than that with ITO electrodes (by 15 percentage points at 3000 nm), but the difference is smaller than in the off state (40 percentage points at 3000 nm).

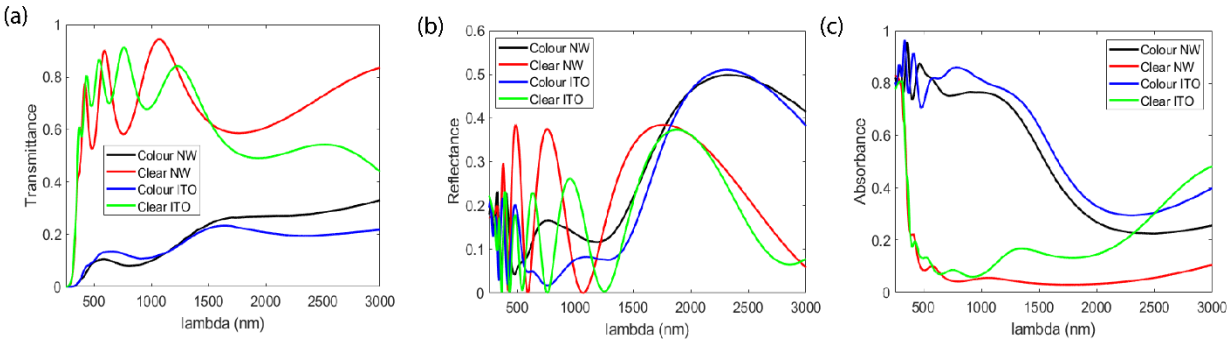

Figure 6.3: Modelled transmittance (a), reflectance (b) and absorption (c) of smart window devices in the clear and coloured state for ITO vs AgNW electrodes.

In order to better judge how well the silver nanowire and ITO based windows perform, it is important to examine the performance metrics of the window: the U-factor and the SHGC as discussed earlier in Section 6.2. Measuring these directly, however, is very expensive and difficult to do. It is more practical to measure or calculate the transmittance, reflectance, and emissivity of the window and then input it into the software called WINDOW 7.8 in order to calculate the U-factor and SHGC of the window. The transmittance and reflectance in the VIS and NIR along with the emissivity in the IR are all then used to calculate the U-factor and SHGC through Equations 6.1-6.4.

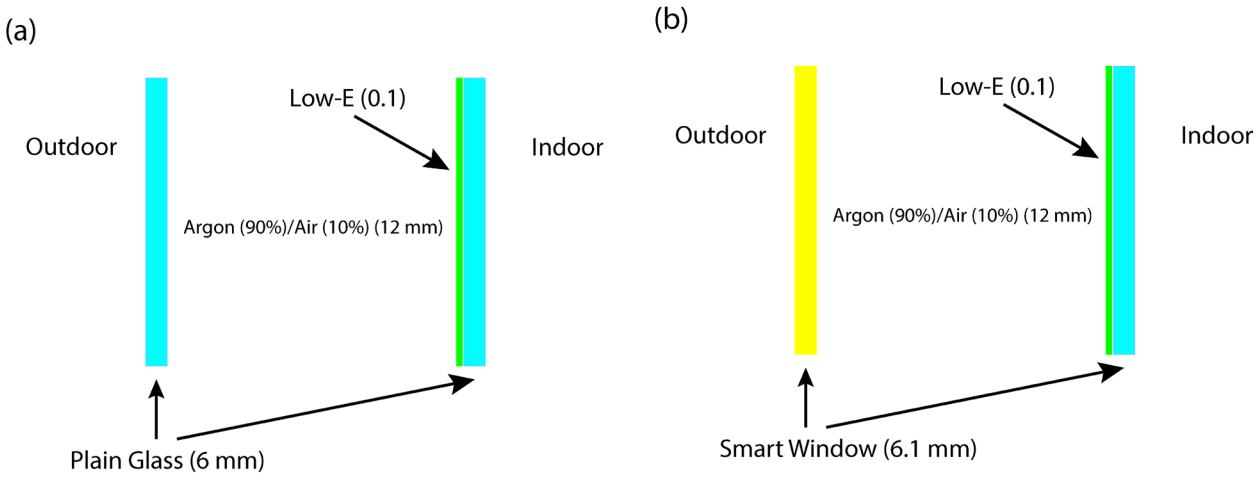

Figure 6.4: (a) Schematic of double glazing window system simulated in WINDOW with plain glass on the outdoor side. (b) Schematic of double glazing window system with a smart window replacing the glass on the outdoor side of the window.

Using Kirchoff's Law, the emissivity is calculated by averaging the emissivity at each wavelength in the mid and far infrared (5000 nm to 30,000 nm). Using the transfer matrix method in MATLAB described above with the same permittivities or refractive indexes for each layer in the on and off state, the transmittance, reflectance and emissivity were input into the WINDOW software. The window was modelled as a 2-pane window system with plain glass on one side, and a low-E coating ($\varepsilon = 0.1$) with a thickness of 6 mm on the indoor side. In between, the two panes, the gap was filled with a 90% argon and 10% air mixture in a gap thickness of 12 mm to help with insulation and prevent convection of heat across the window. A schematic of this setup is shown in Figure 6.4(a). The double pane setup is the most commonly used in buildings. The area of the window system was set to be 600 mm x 600 mm. The U-factor for this setup was calculated to be 1.455 W/m^2K and the SHGC was 0.602. The plain glass was then replaced with a 6.1 mm thick smart window device with the transmittance, reflectance, and absorption/emissivity properties calculated from MATLAB simulations. This setup is shown in Figure 6.4(b). These properties were calculated in the on and off state, both with PU-AgNWs and ITO as the transparent electrode.

Table 6.1: U-factor/SHGC simulations using WINDOW 7.8

	U-Factor (W/m^2*K)	SHGC
ITO Clear	1.449	0.510
AgNW Clear	1.367	0.534
ITO Colour	1.351	0.177
AgNW Colour	1.373	0.186

The calculated U-factors and SHGC for windows with ITO and AgNW electrodes in the coloured and clear states are shown above in Table 6.1. The U-factor, which relates more to heat convection and conduction across the window, is lower for AgNW devices in the clear state but higher in the on state. This can be explained by examining the emissivity of the windows for longer room temperature radiation between 5,000 and 30,000 nm. The emissivity is higher for ITO based windows in the winter but lower in the summer. This leads to a lower U-factor in the winter for PU-AgNWs but slightly higher value compared to ITO devices for summer months. The overall advantage therefore goes to the AgNW devices as the difference in U-factor is larger in the off state compared to ITO than the on state. The SHGC, which relates to radiation of solar heat through the window, is higher for the windows with AgNW electrodes due to their higher transparency in the NIR. This is desirable in the winter (clear state) as the solar heat can help heat a building thereby leading to energy savings. This is undesirable in the summer (coloured state), though the difference in the SHGC for the AgNW and ITO based devices is smaller in the coloured state, 0.009, compared to the difference in the clear state, 0.024. Thus overall, the devices with the AgNWs perform better in regards to these metrics, especially in climates like Ontario where there are many more months of cold weather than warm.

6.4 Device Fabrication

6.4.1 Electrochromic Materials Synthesis

WO_3 nanoparticles with an average diameter of 100 nm were used (Sigma Aldrich 550086). To make the WO_3 solution, 1.8 g of the WO_3 nanoparticles were placed in a glass vial. Then, 2.1 g of isopropyl alcohol and 2.1 g of DI water were mixed with the nanoparticles. The resulting solution was sonicated with a probe sonicator at a frequency of 19 kHz for 2 hours before being stirred at 500 RPM for 72 hours in order to ensure good dispersion of the nanoparticles.

To synthesize the NiO solution, 50 mg of NiO powder (Sigma Aldrich, 203882) was placed into a glass vial. Then, 3.65 ml of DI water and 6.65 mL of IPA were added to the solution. The resulting solution was sonicated with a probe sonicator at a frequency of 19 kHz for 2 hours before being stirred for 72 hours in order to ensure good dispersion of the nanoparticles.

For the electrolyte, 1.0 M of lithium perchlorate ($LiClO_4$, Aldrich, 431567) and 0.05 M of ferrocene (Aldrich, 98%, F408-5G) was combined with anhydrous propylene carbonate, (Aldrich, 99.9%, 310328). The resulting solution was covered, heated to 70°C, and stirred until the $LiClO_4$ and ferrocene were completely dissolved.

6.4.2 Device Fabrication

Ag NW electrodes were fabricated using nanowires with average diameters of 49 nm and length of 88 µm (Novarials Corporation, A30UL) as determined in Chapter 2. The concentration was 1.0 mg/ml. The NWs were deposited on 2.5 cm x 2.5 cm BK7 glass substrates using Mayer Rod coating with Bar #10 and 4 coats. The Ag NWs were then annealed in a vacuum oven for 30 minutes at 150 °C. Next, silver conductive paste (Ted Pella) was used to make one strip along one side of the AgNW coated substrate to create contacts for the final device. The electrodes were left to dry for 2 hours. Afterwards, the AgNWs were coated with PU using the synthesis method outlined in Chapter 3 at a spin speed of 3000 RPM for 60 seconds. PU passivated electrodes were cured using a UV oven (Norland, Traydex-18 UV/Visible Oven) for 180 seconds.

150 μL of WO_3 solution was dropped onto a PU-AgNW electrode in a spin coater. The dispensing of the solution was done statically. After the full 150 μL was dispensed, the spin speed was set to 3000 RPM for a time of 30 seconds. This was repeated once more. Then, the substrate was annealed on a hot plate at 150 °C for 15 minutes. 150 μL of NiO solution was deposited and annealed on a separate electrode in the same manner, except the coating was done 5 times. The film thicknesses were each measured using a Buker Dektak Profilometer. The thicknesses were found to be 100 nm for NiO and 975 nm for WO_3.

For devices with ITO electrodes (SPI, 06403-AF) instead of AgNW electrodes, the ITO had to be treated in order to make the surface hydrophilic. The natural hydrophobicity of the ITO surface does not allow for thin films to be easily spin coated onto them. Samples were placed in a Yield Engineering Systems CV200RFS Photoresist Strip & Descum system and etched in an O_2 plasma for 180 seconds at a power of 300W. This process made the samples hydrophilic. The plasma etch did not change the sheet resistance of the ITO. WO_3 and NiO films were then coated on separate ITO electrodes in the same manner as described above.

To complete device assembly, a 3 mm thick square gasket was cut out of Fel-Pro 3060 Gasket material. The gasket was 2.5 x 2.0 cm with a 1.75 x 1.75 cm window on the inside created for the electrolyte. Clear RTV silicone (JB Weld) was used to bond the gasket to one substrate. Then, 0.5 mL of $LiClO_4$-PC based electrolyte (synthesis details in Section 6.4.1) was placed into the gasket. The top side of the gasket was coated with RTV silicone, and the other substrate was placed on top of the gasket. The final devices were then left to dry in ambient conditions for two hours in order to ensure the electrolyte was fully dried before device characterization.

6.5 Thin Film Characterization

6.5.1 X-Ray Diffraction (XRD)

In order to determine and confirm the quality of the NiO and WO_3 nanoparticles, X-Ray diffraction (XRD) was performed. To do this, separate 2.5 cm x 2.5 cm x 1 mm glass substrates had 3 layers of NiO or WO_3 deposited on top of them using the same procedure as outlined in Section 6.5. The samples had their XRD spectrum measured over the full angular spectrum from 10° - 90° using a PANalytical X'pert Pro MRD HR-XRD. The results are shown below in Figure 6.5.

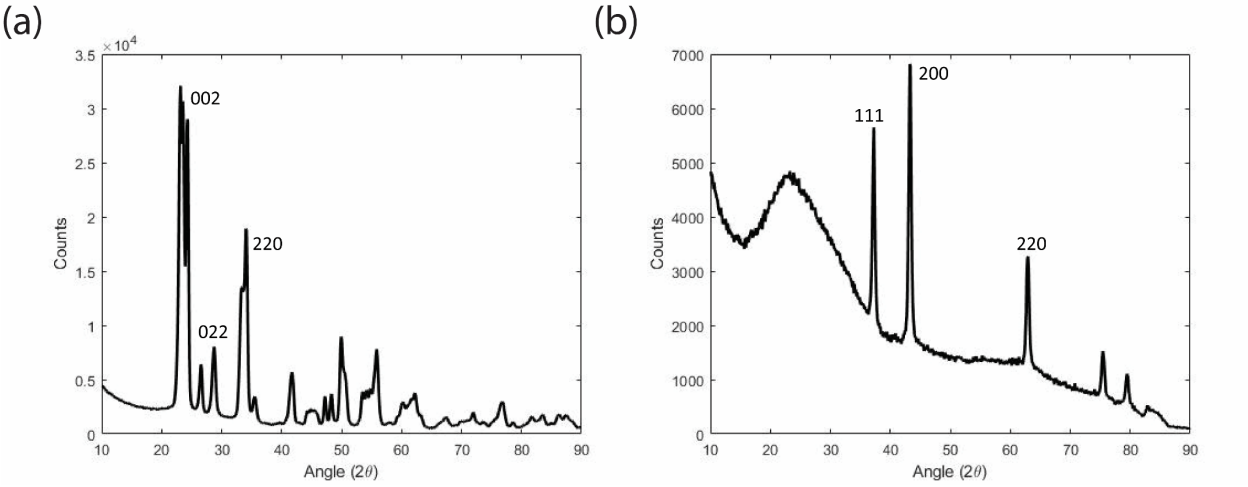

Figure 6.5: X-Ray diffraction spectra of WO_3 (a) and NiO (b) nanoparticle-based films used as the electrochromic and ion storage layers, respectively, in the smart window.

The tungsten oxide peaks of 002, 022, and 220 match best with orthorhombic tungsten oxide as shown in Kalhori et al. [147]. The nickel oxide peaks corresponding to 111, 200, and 220 best correspond to a fcc (face centre cubic) structure of NiO[148].

6.5.2 Transparent Electrode Transmittance and Sheet Resistance

In Chapter 5, it was found that 120 nm diameter silver nanowires had the highest transmittance in the NIR. However, the nanowire spacing for these wires were larger. In order to create a uniform switch, it is ideal for the gaps between nanowires to be minimized to obtain a more uniform E-field across the x-y plane. Also, the surface roughness of AgNW electrodes containing large diameter AgNWs, even when PU is used, is larger. This causes the thickness of layers spin-coated on top to be uneven, especially when these layers are very thin as is the case for the NiO film used here. Thirdly, as determined in Chapter 5, the sheet resistance of electrodes made using thinner AgNWs is lower. For these reasons, the nanowire diameter was chosen to be 30 nm. The longest average length available, 88 µm, was chosen as these lead to lower sheet resistance and higher NIR transparency.

For an accurate comparison between ITO and AgNW electrodes, the transmittance in the visible at a wavelength of 550 nm should be the same. Figure 6.6(a) shows the transmittance in the UV, VIS, and NIR measured on a Perkin Elmer Lambda 1050 of the ITO and AgNW electrodes at a concentration of 1.0 mg/ml. At 550 nm, the transmittance of the ITO and AgNWs overlaps at a value of 88%. At this transmittance, the sheet resistance of the ITO and AgNWs were found to be 41 Ω/sq and 7 Ω/sq, respectively. The most striking difference between the ITO and AgNW electrodes is the transmittance in the NIR. The AgNW transmittance stays above 80% but the transmittance of the ITO dips down to 20% at a wavelength of 2300 nm. For the AgNWs, the haze for a 30 nm nanowire film at a concentration of 1.0 mg/ml is below 7% across the visible region. This was shown in Figure 5.13. 7% is well below the acceptable limit of 10% for a film to show good enough clarity when looking through it.

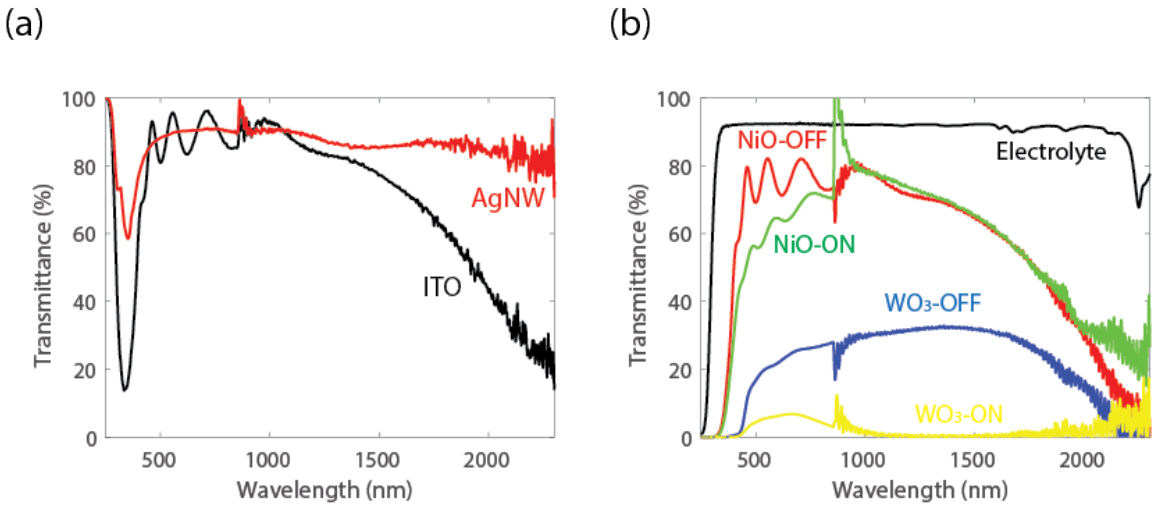

Figure 6.6: (a) Transmittance vs wavelength of AgNW and ITO electrodes which are 88% in the visible. (b) Transmittance vs wavelength of WO_3, NiO, and the $LiClO_4$ electrolyte.

Figure 6.6(b) shows the transmittance of the other components of the smart window system. The $LiClO_4$ - PC electrolyte has a transmittance of over 90% across the VIS and most of the NIR. At 2300 nm, there is a decrease in transmittance to 70% which starts to increase again as we measure deeper into the NIR. For NiO, a modest change in transmittance is seen between 500 nm and 800 nm, corresponding to the brown colour it turns when in the on state. The oscillations seen are from thin film interference or Fabry Perot modes. NiO also has a change in transmittance above 2000 nm. The WO_3 transmittance is much lower. In the off state is stays between 20 - 30% through most of the VIS and NIR but in the on-state dips to a peak of 8% at a wavelength of 650 nm. The thickness of the WO_3 being quite large is an explanation for this; it

is larger than what would be used in an ideal device. Lower wavelengths in the visible are strongly absorbed, leading to the dark blue colour that WO_3 shows when in the coloured or on state. The noise that is seen in the NIR for all films and comes from an artifact in the InGaAs (indium gallium arsenide) detector above 2200 nm.

6.5.3 Cyclic Voltammetry & Cyclic Amperometry of Films

Photos of WO_3 on ITO (Figure 6.7(a)) and AgNWs (Figure 6.7(b)) are shown in the on and off state. We can see a clear uniform switch and colour change from a pale yellow to a dark blue in both cases. In Figure 6.7(c), we see the on and off states for NiO on ITO. There is a clear colour switch from clear to brown for the device on ITO. However, in Figure 6.7(d), there is unfortunately no clear difference between the on and the off state when the NiO is deposited on AgNWs. The NiO layer is very thin, 100 nm. It was seen in Chapter 2 that even though the average surface roughness of the PU-passivated NW electrode is 16 nm, there are surface peaks on the electrode that are > 100 nm. Therefore, the thickness of the spin-coated NiO layer is likely non-uniform and possibly even non-continuous in some places. This would prevent the NiO from switching uniformly.

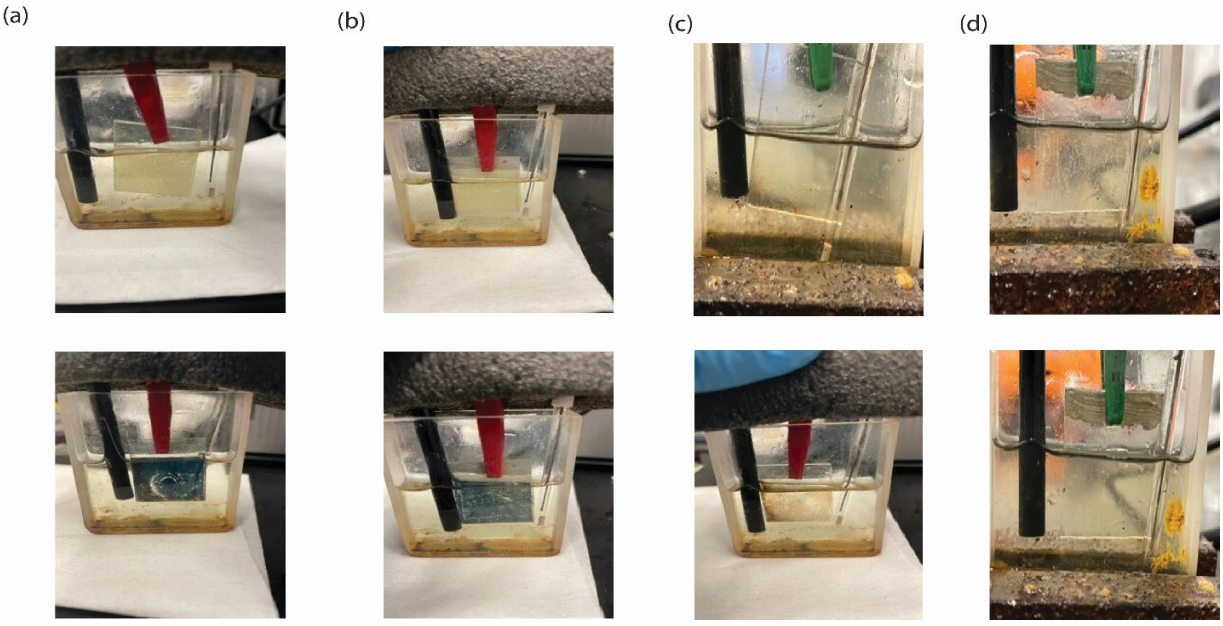

Figure 6.7: Photos of WO_3 in the on and off state on (a) ITO and (b) AgNW electrodes. Photos of NiO in the on and off state on (c) ITO and (d) AgNW electrodes.

The CV for WO_3 on ITO is shown in Figure 6.8(a). The reduction peak where the current is at its lowest occurs at -1.8 V. The oxidation peak then occurs back closer to -0.2 V where the colour changes back to pale yellow occurs. As multiple cycles are measured, the peak reduction current gets smaller and smaller. This is due to the WO_3 in the redox reaction not being completely reversible and some of the Li ions remaining with the WO_3, keeping it blue. This is also seen with the eye during CV measurements - the pale yellow colour seen at the start is not seen again once cycling starts and instead a light blue colour is seen. For the CV of WO_3 on AgNWs seen in Figure 6.8(b), we see a similar effect. The peak reduction current at -1.4 V gets smaller with each cycle due to non-reversible Li-WO_3 effects as with the ITO. The oxidation peak also shifts to larger and larger voltages with each subsequent cycle. This is due to the PU not completely passivating the AgNWs and the sheet resistance increasing due to the oxidation/sulfidation of AgNWs with an applied current.

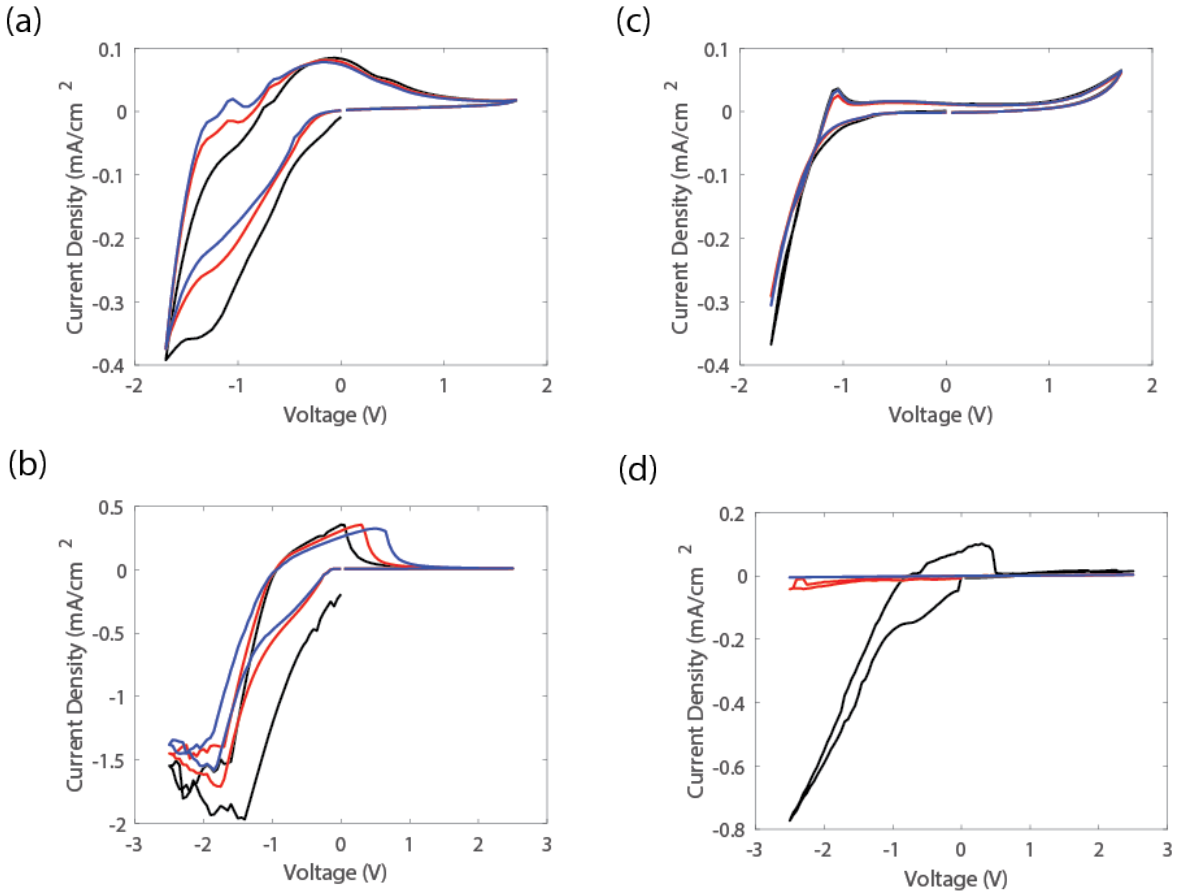

Figure 6.8: CV of WO_3 on ITO (a) and AgNWs (b) and CV of NiO on ITO (c) and AgNWs (d) over the first three cycles.

In Figure 6.8(c) the CV of NiO on ITO is shown. The overall curves are consistent with each subsequent cycle. This shows more stability and reversibility of the redox reaction. The reduction peak occurs at -1.8 V and the oxidation peak occurs at +1.8 V. These voltages are much higher than those reported in literature where the redox reaction for NiO usually lies between +/- 0.5 V. This is due to the lower crystallinity of the NiO compared to that used in other works. The annealing temperature used in this work is lower (150 ºC) compared to others where greater than 400 ºC is used. Higher temperatures cannot be used as the nanowires would not withstand higher temperatures. The CV of the AgNWs with NiO is shown in Figure 6.8(d). The first cycle (black curve) shows a high magnitude peak reduction current than NiO on ITO, but all subsequent cycles show very poor repeatability and low current values. This helps explain the lack of colour change of the NiO on AgNWs. There are no clear redox peaks seen and the area under the CV curve is small. A larger area would correspond to more charge transferred during the cycle.

The kinetics of the WO_3 and NiO on the electrodes are shown in Figures 6.8(a) and Figure 6.8(b), respectively. In Figure 6.9(a) the current on either electrode reduces with subsequent cycles because of the non-reversibility of the WO_3. The film on AgNWs (red curve) shows a quicker fall-off to a stable approximately zero current level which indicates a faster switching time. In Figure 6.9(b), the current through the NiO is higher for the ITO electrode. This is expected as there is a clear colour change on ITO but not for the AgNWs.

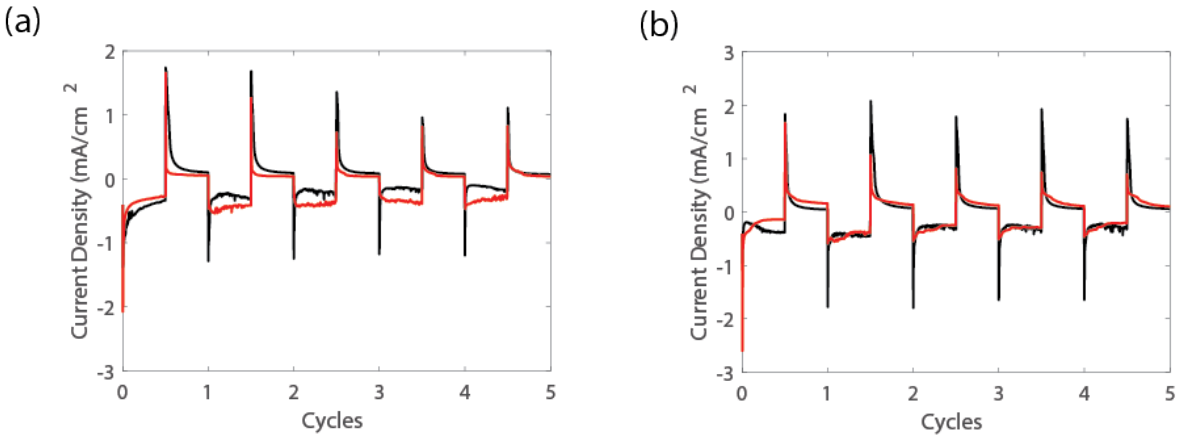

Figure 6.9: (a) CA of WO_3 on ITO (black curve) and AgNW (red curve). (b) CA of NiO on ITO (black curve) and AgNWs (red curve).

Table 6.2 shows the electrochromic properties of the WO_3 and NiO films on PU-AgNWs and ITO. For WO_3, the change in transmittance is slightly higher when AgNW electrodes are used and the change in colour is very similar for both electrodes. However, because of the higher current density seen in the CV for PU-AgNWs, the coloration efficiency is much lower as to get the same colour change, more charge is transferred compared to ITO. An advantage of the PU-AgNWs is the lower sheet resistance lowers the switching time dramatically compared to the WO_3 films on ITO. Additionally, the turn on voltage is lowered by 0.4 V. For NiO there is no visible observed colour change or change in transmittance with the AgNW electrodes. However, the ITO shows a good change in transmittance, an observable colour change, and decent switching times. Additionally, the redox peak occurs at the same voltage as WO_3. This is good for implementation into a device which is the next step in the fabrication of the smart window.

Table 6.2: ΔT, ΔE, CE, τ_{on}, τ_{off}, and V_{on} for WO_3 and NiO films on ITO and AgNW Electrodes.

	ΔT(%)	**ΔE**	**CE (cm^2/C)**	**τ_{on}**	**τ_{off}**	**V_{on} (V)**
WO_3 - ITO	23	49	47.6	41	19	-1.8
WO_3 - AgNW	27	45	7.4	18	2	-1.4
NiO - ITO	22	12	7.0	5	14	-1.8
NiO - AgNW	-	7	-	14	20	-

6.6 Device Characterization

Figures 6.10(a) and 6.10(b) shows the fabricated WO_3/NiO smart windows in the on and the off state on ITO and PU-AgNWs, respectively. We can see a clear colour change between the on and the off state from

a pale yellow to the dark blue in both cases. Figure 6.11 shows the transmittance of these smart windows in the on and the off state. Starting with the VIS region, the ITO window in the on and the off state has a lower and higher transmittance than the AgNW window, respectively. Part of the reason for the lower transmittance change in the visible for the device with AgNWs is that the NiO doesn't switch at all. However, even in Zhou et al. where only WO_3 was used, the transmittance of ITO based devices also had higher ΔT in the visible compared to AgNW based devices. Reasons for this could include higher haze values from the surface roughness of the AgNW electrodes.

In the NIR region and we can see that the device with NW electrodes are indeed more transparent than the ITO device in the off state. The transmittance is above 20% in the NIR for the PU-AgNW device whereas the transparency of the ITO based window dips down to below 5% by a wavelength of 2000 nm. Therefore, the window with AgNW electrodes would allow more solar heat in during the winter and then block a similar amount of solar heat as the ITO window in the warmer summer months.

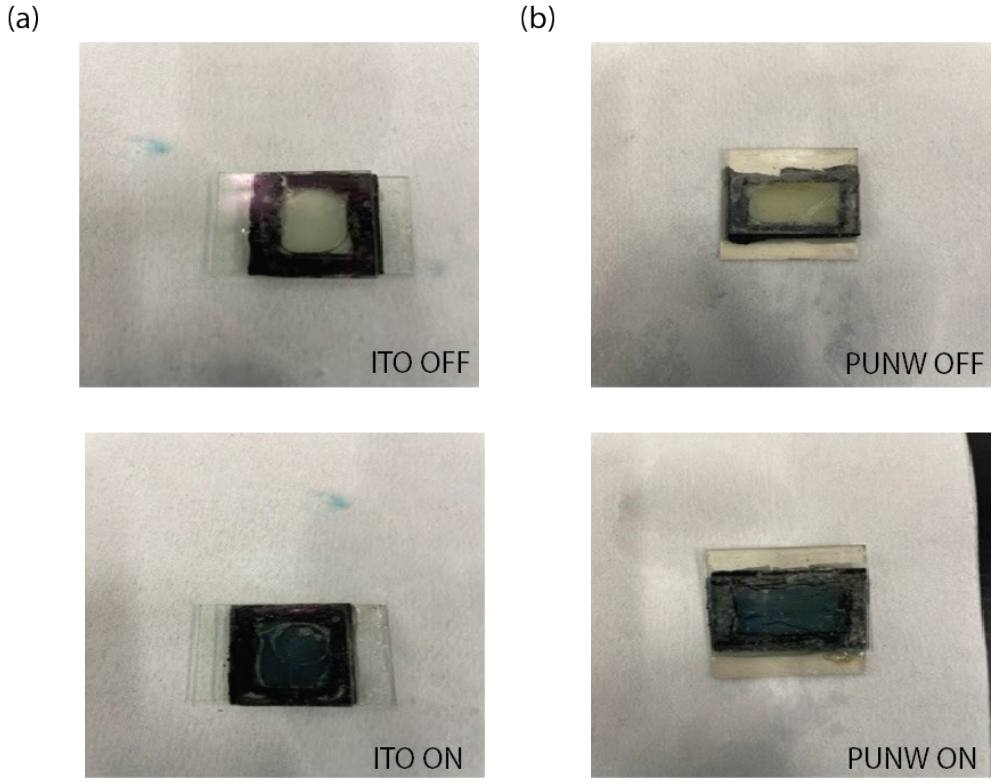

Figure 6.10: Fabricated smart window devices using WO_3 and NiO films on ITO (a) and PU-AgNW Electrodes (b).

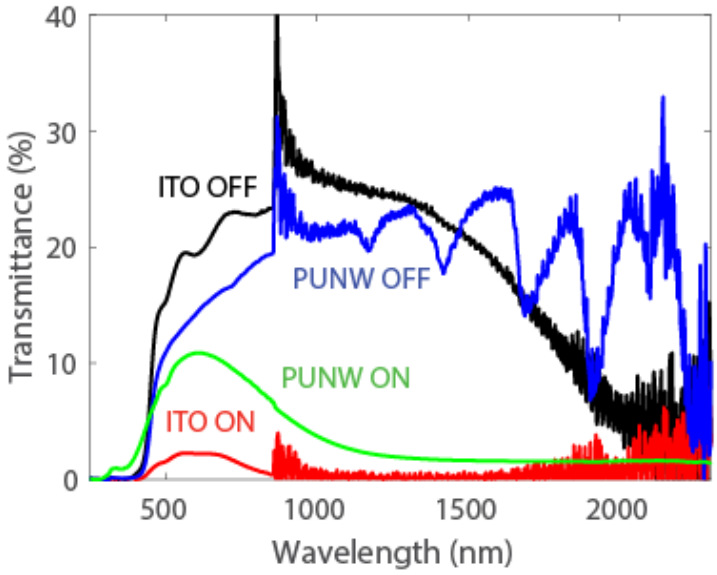

Figure 6.11: Transmittance of fabricated smart window devices using WO_3 and NiO films on ITO and PU-AgNW electrodes in the on and the off state.

Figure 6.12(a) and figure 6.12(b) shows the CV of the ITO smart window and PU-AgNW smart window, respectively. There are clear reduction and oxidation peaks at -4.0 V and +1.0 V for the ITO window. There is also good repeatability for the current level and location of the oxidation peak. However, due to the non-reversibility of the WO_3 reaction, the reduction peak decreases after each cycle. In Figure 6.12(b) the peaks are not so clear. There is an oxidation peak in the first cycle in the same location as ITO, attributing to the off state of the PU-AgNW device. However, after the first cycle, the device no longer switches; there is no defined peak as seen in the red and blue curves. This means the PU is not having as good of a passivation effect as anticipated and the sheet resistance of the AgNWs is therefore increasing. The applied voltage is higher than that used in Chapters 2-4 where PEDOT:PSS was the electrochromic material used. In fact, a full colour switch was not seen in either the ITO and AgNW based windows until a DC power supply was used to apply +/-4.5 V. At these voltages, there is much higher current levels that can lead to the oxidation/sulfidation of the AgNWs. In previous work, the WO_3 and NiO was deposited using high vacuum and then annealed at high temperatures. The applied voltages in the CV were lower as a result due to the higher crystallinity and quality of the films in these cases. Future work needs to be done in order to lower the operating voltage of the smart windows to prevent AgNW oxidation.

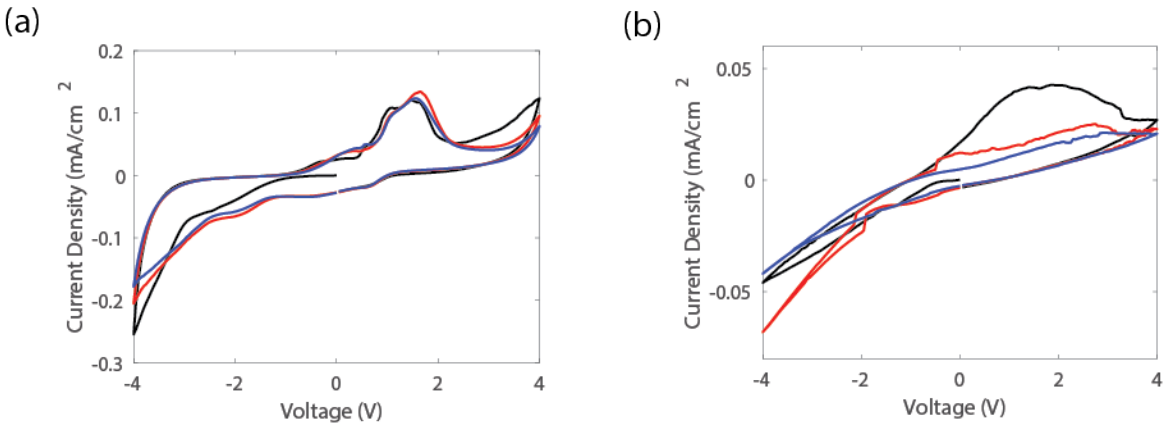

Figure 6.12: CV of fabricated smart window devices using WO_3 and NiO films on ITO (a) and PU-AgNW electrodes (b).

The CA plots of the ITO and PU-AgNW based windows are shown in Figure 6.13(a) and Figure 6.13(b). There is good stability over 5 cycles for the ITO based window with the current levels remaining constant. However, the current density in Figure 6.13(b) is -6 mA/cm^2 at the first cycle and then has a very low current density for every subsequent cycle. At such a large current density, the AgNWs are very susceptible to oxidation/sulfidation. The sheet resistance would increase and then may not be low enough to switch the window.

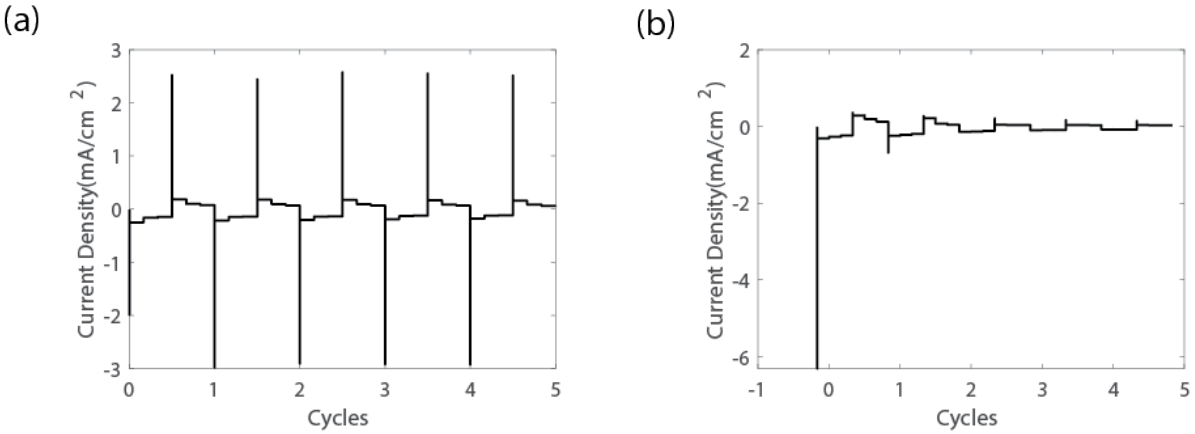

Figure 6.13: CA of fabricated smart window devices using WO_3 and NiO films on ITO (a) and PU-AgNW electrodes (b).

The electrochromic performance parameters of the two windows are shown below in Table 6.3. The change in transmittance is 9 percentage points higher for the ITO window partially due to the NiO not switching with the AgNW electrodes. The colour change is however very similar for both devices. The colouration efficiency is much improved for the ITO based device because of its lower peak current density. One advantage of the AgNW is their higher conductivity for a given transparency (during the first switching cycle) which leads to a strong improvement of switching on-time. Others have found AgNW based smart windows to show superior electrochromic performance to those made with ITO electrodes which leads us to believe that with further work, the PU-AgNWs will show more stability and hence superior electrochromic performance [20], [149].

Table 6.3: ΔT, ΔE, CE, τ_{on}, τ_{off}, and V_{on} for smart windows with ITO and PU-AgNW electrodes.

	ΔT(%)	**ΔE**	**CE (cm^2/C)**	**τ_{on}**	**τ_{off}**	**$V_{applied}$ (V)**
ITO	39	17	30.5	9.1	14.2	+/-4.5
PU-AgNW	28	15	7.8	1.6	19.8	+/-4.5

In highly variable climates such as in Canada, the performance of the windows when the outside temperature is very warm in the summer or bitterly cold in the winter are very important. In order to test the versatility of the windows with temperature, the windows were heated up to 50 ºC for 2 hours and another set of windows were left in a freezer at a temperature of -18 ºC for 48 hours. The resulting CV's are shown below in Figure 6.13 after the windows return to room temperature. In Figure 6.14(a) we see that the ITO based device has little change before and after heating. There is even a slight decrease in the oxidation peak to a lower voltage from +1.0 V to +0.8 V. It is possible the heating improved the quality of the films slightly. For the PU-AgNW device, the CV curve changes with each cycle and thus it is very difficult to assess the impact of the heating. However, compared to the freezing experiment, the CV curve does look worse with heating so it is possible AgNW electrodes would have difficulty performing well in

hot weather. AgNWs are indeed known to degrade faster at elevated temperatures so attention to preventing this may be needed for real-world smart windows.

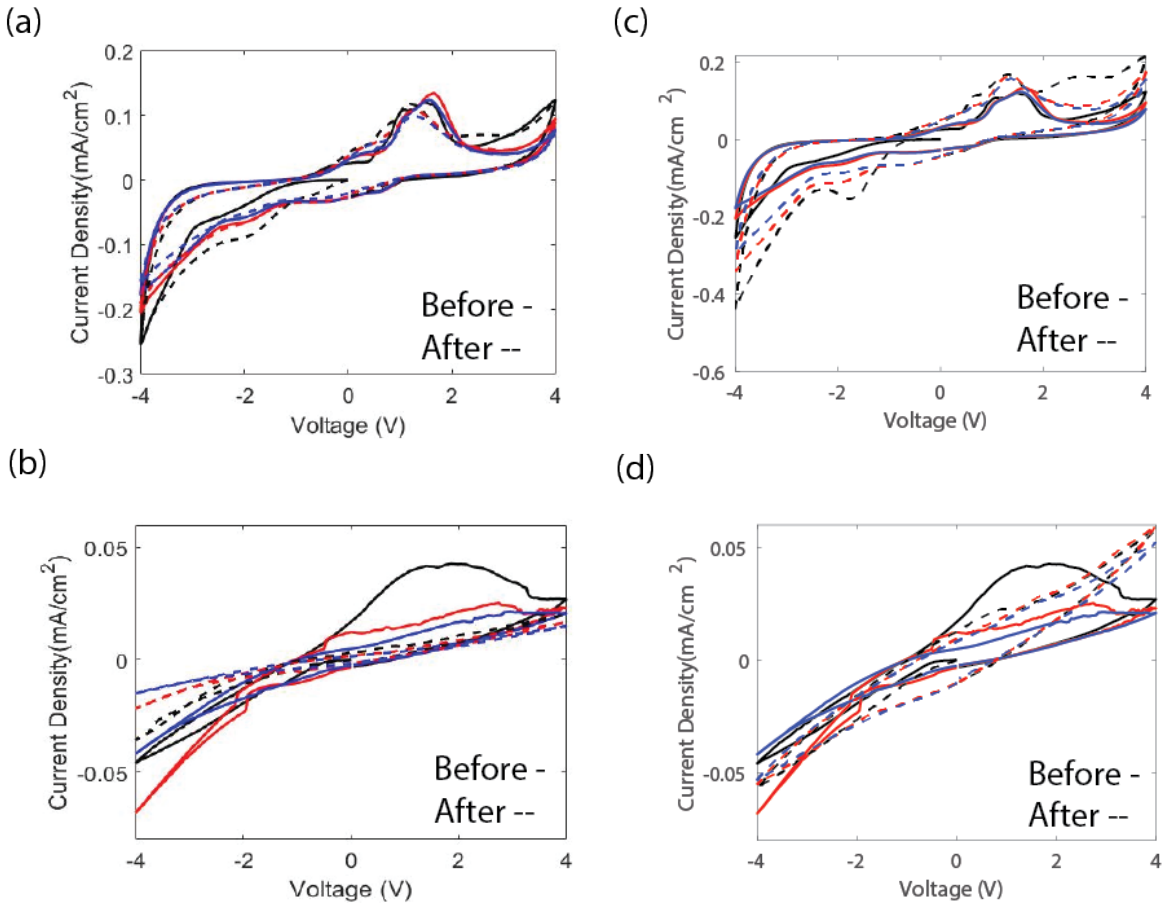

Figure 6.14: CV plots of an ITO (a) and PU-NW (b) smart window after being heated to 50 º C for 2 hours. CV plots of an ITO (c) and PU-NW (d) smart window after being frozen for 48 hours at -18 ºC.

After freezing, the reduction peak for the ITO device shown in Figure 6.13(c) gets slightly larger but then decreases again from the non-reversibility of the WO_3. However, it still shows a clear colour change, showing it can work in cold climates. For the PU-AgNW device, it is again difficult to assess, but it tentatively appears that the freezing did not worsen the performance of the device. These preliminary results show that the devices are stable enough to be used on the outdoor glass side of a two pane glazing system. However, further work is required requiring long term high and low temperature study as well as measuring the temperature of the devices in a solar simulator.

6.7 Conclusion

It was shown through both modelling and experiments that replacing ITO with AgNW transparent electrodes in smart windows leads to a higher transparency in the NIR. This was shown to lead to a higher solar heat gain coefficient and lower U-factor which is an advantage in the winter. Although the AgNW electrodes have a slightly higher solar heat gain and U-factor in the summer as well, the SHGC and U-factor difference between AgNW and ITO electrodes is lower in the summer compared to the winter. Fabrication issues in part lead to the AgNW based devices having some worse electrochromic properties than windows with ITO. However, due to their lower sheet resistance at the same visible transparency as ITO, windows that used AgNW electrodes had faster switching on times. Measurements with WO_3 films also indicate that AgNW electrodes can lower the turn-on voltage of smart windows. The repeatability of the windows with AgNW electrodes was poor, due to the high voltages required for operation. Better quality, more crystalline WO_3 and NiO films would help lower the operating voltage and mitigate AgNW degradation. Using a thicker NiO layer or avoiding large roughness peaks in the NW electrode through better dispersion or more uniform deposition is also needed.

Future work would also include improving the sealing of the electrolyte in the window.

Chapter 7
Conclusion and Future Work

7.1 Summary

This research focuses on the passivation, NIR properties and integration of silver nanowires into flexible displays and smart window devices, both in the electrode and the electrochromic layer itself. Silver nanowire electrodes were fabricated and shown to have superior optical and electrical properties at a lower cost with higher mechanical flexibility than current state of the art ITO on glass, PET, and paper substrates. Chapter 2 focused on testing several transparent polymeric layers to prevent nanowire electrode corrosion with polyurethane becoming the clear winner as it showed the lowest drop in conductivity of the AgNWs over a period of 180 days while allowing for minimal loss in transmittance. The passivation and hot rolling on flexible substrates reduce surface roughness and improves the elasticity of the electrodes as they are bent and strained over several cycles. This is critical for making long lasting flexible devices. Even though the nanowire electrode is not a continuous film like ITO, and the polyurethane passivation layer is not conductive, simulation and EFM measurements showed that the magnitude of the electric field drops by only 0.5 of the peak value 150 nm above the surface of the AgNW. Electrochromic displays made with the polyurethane-passivated NW electrodes had a uniform switch to the eye across its area.

Chapter 3 compared ITO vs PU-passivated AgNW electrodes when integrated into flexible electrochromic displays. PEDOT:PSS based electrochromic displays with PU-AgNW electrodes had a longer lifetime, lower operating voltage, higher mechanical flexibility, and improved reflectance and colour changing properties than those with ITO. These benefits, along with the low cost of AgNWs, make AgNWs a great candidate to replace ITO in devices that require transparent electrodes. Additionally, it was shown that the capabilities of making these displays not only flexible, but recyclable as well by printing them on biodegradable paper.

One issue with PEDOT:PSS is its low conductivity which reduces switching speeds and increases the operating voltage of PEDOT:PSS based devices. In chapter 4, AgNWs were mixed with PEDOT:PSS in solution, and showed that the conductivity can be increased. The optimal nanowire diameter, length and

concentration to mix with PEDOT:PSS were found to be 30 nm, 80 μm, and 3.0 mg/ml. By mixing the silver nanowires in solution with PEDOT:PSS and forming films, a transparent electrode such as ITO is no longer required to switch the electrochromic PEDOT:PSS. The hybrid PEDOT:PSS/silver nanowire films have a lower turn on voltage, similar coloration efficiency and half the switch on time compared to PEDOT:PSS film alone while keeping the electrochromic performance of the PEDOT:PSS. Passivating the silver nanowires in solution before mixing in PEDOT:PSS was attempted using two different polymer materials, MuA and MBI. However, these were not effective as the silver nanowires clumped, and shortened the lifetime of hybrid PEDOT:PSS/silver nanowire displays.

Chapter 5 showed that the near infrared properties of silver nanowire electrodes are far superior to those of ITO. The near infrared transmittance for ITO and silver nanowires was measured experimentally and then compared to a transmission line model for silver nanowire networks to determine the main mechanisms that control the near infrared optical properties of the silver nanowires. They were determined to be: (1) the nanowire spacing, where smaller nanowire spacings cause a faster fall off of transmittance in the NIR and (2) smaller diameter nanowires have higher loss in the NIR and causing a faster fall off of the transmittance compared to larger diameters. Later on in Chapter 5, longer nanowires are shown to have a higher transmittance in the near infrared and the haze of all nanowire diameters is below the acceptable value of 10% in the visible region.

In Chapter 6, PU-passivated nanowire networks were implemented as the transparent electrode in tungsten oxide/nickel oxide based smart windows and compared to the same windows with ITO electrodes. Modelling and experiments confirmed that the nanowire based windows are more transparent to the NIR, and as such the calculated solar heat gain coefficient was higher and the U-factore was lower in the winter than for a window using ITO. In the summer, the SHGC and U-factor of the PU-AgNWs windows were slightly higher compared to those with ITO, which is a disadvantage. The higher conductivity of the NW electrodes also lead to a shorter switch-on time and a lower turn-on voltage. Better fabrication processes are needed to improve other performance factors and the lifetime of the nanowire based windows.

7.2 Future Work

7.2.1 Alternative Passivation Methods for AgNWs in Solution

Mixing AgNWs into PEDOT:PSS electrochromic layers is a promising strategy to improve device switching times and operating voltages, but AgNW corrosion remains a problem. Coating the NW surfaces with a small molecule polymer before they are mixed with PEDOT:PSS could still be a reasonable approach, but molecules with a large positive or negative zeta potential should be explored. This will promote repulsion forces between molecules so that the AgNWs will not clump. Since zeta potential is highly dependent on pH, it is also important for the small molecule polymer to have the high zeta potential >40 mV at a pH of 4.0 or lower if mixed with PEDOT:PSS. Small molecules such as polyethylene glycol-polyethylene imine (PEG-PEI) and partially protonated polydimethylaminoethylmethacrylate (PDMAEMA) have large positive or negative potentials greater than +/-40 mV [138], [139]. An alternative approach would be to coat silver nanowires with graphene [140] or gold [141] in solution using the conformal deposition method with an acid and ligand molecule to coat each nanowire. Or possibly electroplate a more non-reactive metal than silver onto the nanowires such as nickel [142], [143] before the NWs are mixed with PEDOT.

7.2.2 Solid State Electrolytes for Flexible Smart Windows

One major issue with the fabrication of the smart windows in Chapter 6 is the use of lithium perchlorate in propylene carbonate liquid electrolyte. Over time, the liquid electrolyte leaked out of the gasket meant to contain it in the window. Several different methods were attempted to completely seal the device, but there was always an air bubble that appeared, indicating leaking. Additionally, when the fabrication of smart windows using PET substrates was attempted, the gasket and sealant performed even worse at sealing the device because of the flexibility of the PET. Other researchers in the literature have also noted leaking issues with liquid electrolytes [141].

In order to overcome these issues, it would be in the best interest to use a solid state electrolyte. PMMA, tantalum oxide (Ta_2O_5), gelatine, and nafion have been reported as the most viable candidates to make an all solid state electrochromic device [144]. Tantalum oxide as the electrolyte layer via sol gel deposition methods (spin coating) was attempted with little success. More complicated methods such as atomic layer deposition arc are needed in order to create a high quality film [145]. It has been reported that tantalum oxide in combination with a lithium based salt or pure lithium layer is necessary to conduct lithium ions in order to obtain a colour change in the device [144]. To use PMMA, it can be mixed into the lithium perchlorate and propylene carbonate in order to plasticize the electrolyte layer.

Because one advantage of silver nanowire electrodes is their mechanical flexibility, the fabrication and testing of flexible and even stretchable all-solid-state smart windows containing nanowire electrodes is suggested, as has been recently done [141].

7.2.3 Large Area Roll-to-Roll Smart Windows Integrated with Transparent Solar Cells

A necessary next step to realizing smart window devices with nanowire electrodes is to scale up the area. Producing ITO on a large scale is more difficult since it requires high temperatures, vacuum, and is costly. Because silver nanowire electrodes can be deposited using solution deposition methods in atmosphere and is compatible with roll-to-roll deposition methods if flexible substrates are used, they would make the scaling up process much less costly. In this work, WO_3, PU, and NiO were deposited using spin coating. This is a difficult process to scale up. Using rod coating instead could scale up the fabrication of smart window fabrication to larger areas, and is also roll-to-roll compatible.

Powering the smart window using a solar cell could further help in saving energy in buildings. This has been done before where a dye sensitized solar cell was able to produce 1.35 V of energy that was enough to power a tungsten oxide based smart window when connected in series [146]. Instead of using ITO as done in that work [146], silver nanowire electrodes could be used to allow more NIR radiation through. The NIR radiation could be absorbed by the solar cell to produce more power and/or allowed to enter the building in winter to assist in heating though solar heat gain.

7.2.4 Silver Nanowire Electrodes in Thermochromic Devices

Thermochromic materials undergo a change in optical properties upon heating. For example, vanadium oxide transitions between semiconducting and metallic like states when it changes temperature from 25°C to 68°C, causing a transmittance modulation in the NIR and IR where 40% of solar heat occurs [147]. This could be controlled with a silver nanowire network. With the application of a voltage, silver nanowire networks heat up through Joule heating [148]. Nanowire diameter, density and voltage levels need to be chosen accordingly to achieve the required temperature. The high NIR transparency of AgNW networks that was demonstrated in this research is desirable for thermochromic applications such as window glazings and optical switches.

It has previously been shown that the Joule heating of silver nanowire networks can be non-uniform and accelerates silver corrosion [18]. Coating the nanowire network with a layer of reduced graphene oxide has been shown to result in a uniform temperature distribution and additionally can assist in passivating the nanowire network [148].

7.2.5 Fully Recyclable Displays

In Chapter 3, recyclable, sustainable electrochromic displays were created. The paper substrate was disposable and biodegradable, and the silver nanowires can be recycled and reclaimed using either laser ablation or sonication [89], [90]. Devices were fabricated and characterized where one side was paper, but because the paper was not optically transparent, PET was used for the other side. Fully recyclable, transparent paper is available from multiple manufacturers such as Bee Paper, EcoEnclose, and Jam Paper. Transparent paper can be quite thin and brittle, however. Multiple layers or a biodegradable polymer would have to be used in order to strengthen the paper while maintaining its transparency. Additionally, a higher concentration of silver nanowires than either plastic or paper would be required to achieve a sheet resistance $< 50\ \Omega$/sq because of the larger surface roughness of the transparent paper. The transparent paper also has a low thermal budget. This is fine for the nanowire electrodes as they can be deposited at room temperature, and the junctions can properly be welded using hot rolling at 80°C or less as shown in this thesis. However,

the PEDOT:PSS would have to be annealed at a lower temperature than ideal. Achieving an electrochromic device on paper substrates would make flexible displays less harmful on the environment and have the ability to be recycled when they reach the end of their lifetime.

References

[1] P. M. S. Monk, R. J. Mortimer, and D. R. Rosseinsky, *Electrochromism and electrochromic devices*, vol. 9780521822695. 2007. doi: 10.1017/CBO9780511550959.

[2] C. G. Granqvist, "Electrochromics for smart windows: Oxide-based thin films and devices," *Thin Solid Films*, vol. 564, pp. 1–38, Aug. 2014, doi: 10.1016/j.tsf.2014.02.002.

[3] R. J. Mortimer, X. Li, K. Perera, J. He, A. Gumyusenge, and J. Mei, "Organic electrochromic materials," *J Mater Chem C Mater*, vol. 7, no. 18, pp. 2971–2981, 2019, doi: 10.1016/S0013-4686(99)00046-8.

[4] R. J. Mortimer, "Organic electrochromic materials," *Electrochim Acta*, vol. 44, no. 18, pp. 2971–2981, 1999, doi: 10.1016/S0013-4686(99)00046-8.

[5] R. J. Mortimer, D. R. Rosseinsky, and P. M. S. Monk, *Electrochromic Materials and Devices*. Weinheim, Germany: Wiley-VCH Verlag GmbH & Co. KGaA, 2015. doi: 10.1002/9783527679850.

[6] A. Kumar and C. Zhou, "The race to replace tin-doped indium oxide: Which material will win?," *ACS Nano*, vol. 4, no. 1. American Chemical Society, pp. 11–14, Jan. 26, 2010. doi: 10.1021/nn901903b.

[7] E. S. Lee, M. Yazdanian, and S. E. Selkowitz, "The Energy-Savings Potential of Electrochromic Windows in the US Commercial Buildings Sector," p. 54966, 2004.

[8] M. R. Donn, G. Thomas, E. Efficiency, and C. Authority, *Designing comfortable homes: Guidelines on the use of glass, mass and insulation for energy efficiency*. 2010.

[9] NRC, "Energy Efficiency Trends in Canada- 1990 to 2013," *Nrc*, no. March, pp. 1–51, 2016.

[10] "Smart Windows Market Opportunities and Analysis, 2021-2030." https://www.ntechresearch.com/market-reports/smart-windows-market-opportunities/ (accessed Jun. 10, 2022).

[11] "Smart Glass Market by Technology, Application, Control Mode and Geographic Analysis - Global Forecast to 2027." https://www.reportlinker.com/p05135706/Smart-Glass-Market-by-Technology-Application-And-Geography-Global-Forecast-to.html?utm_source=GNW (accessed Jun. 09, 2022).

[12] J. Al Dakheel and K. Tabet Aoul, "Building Applications, Opportunities and Challenges of Active Shading Systems: A State-of-the-Art Review," *Energies (Basel)*, vol. 10, no. 10, p. 1672, Oct. 2017, doi: 10.3390/en10101672.

[13] C. G. Granqvist, "Recent progress in thermochromics and electrochromics: A brief survey," *Thin Solid Films*, vol. 614, pp. 90–96, Sep. 2016, doi: 10.1016/J.TSF.2016.02.029.

[14] S. Papaefthimiou, E. Syrrakou, and P. Yianoulis, “Energy performance assessment of an electrochromic window,” *Thin Solid Films*, vol. 502, no. 1–2, pp. 257–264, Apr. 2006, doi: 10.1016/j.tsf.2005.07.294.

[15] R.-T. Wen, M. A. Arvizu, G. A. Niklasson, and C. G. Granqvist, “Electrochromics for energy efficient buildings: Towards long-term durability and materials rejuvenation,” *Surf Coat Technol*, vol. 278, pp. 121–125, Sep. 2015, doi: 10.1016/J.SURFCOAT.2015.06.047.

[16] B. Zhang, Y. Tian, J. X. Zhang, and W. Cai, “The characterization of fluorine doped tin oxide films by Fourier Transformation Infrared spectrum,” *Mater Lett*, vol. 64, no. 24, pp. 2707–2709, Dec. 2010, doi: 10.1016/j.matlet.2010.08.065.

[17] A. I. Hofmann, E. Cloutet, and G. Hadziioannou, “Materials for Transparent Electrodes: From Metal Oxides to Organic Alternatives,” *Adv Electron Mater*, vol. 4, no. 10, p. 1700412, Oct. 2018, doi: 10.1002/AELM.201700412.

[18] H. H. Khaligh *et al.*, “The Joule heating problem in silver nanowire transparent electrodes,” *Nanotechnology*, vol. 28, no. 42, 2017, doi: 10.1088/1361-6528/aa7f34.

[19] H. Askari, H. Fallah, M. Askari, and M. C. Mohmmadieyh, “Electrical and optical properties of ITO thin films prepared by DC magnetron sputtering for low-emitting coatings,” Sep. 2014, Accessed: Feb. 24, 2019. [Online]. Available: http://arxiv.org/abs/1409.5293

[20] K. Mallikarjuna and H. Kim, “Highly Transparent Conductive Reduced Graphene Oxide/Silver Nanowires/Silver Grid Electrodes for Low-Voltage Electrochromic Smart Windows,” 2018, doi: 10.1021/acsami.8b14086.

[21] A. R. Madaria, A. Kumar, and C. Zhou, “Large scale, highly conductive and patterned transparent films of silver nanowires on arbitrary substrates and their application in touch screens,” *Nanotechnology*, vol. 22, no. 24, Jun. 2011, doi: 10.1088/0957-4484/22/24/245201.

[22] H. Hosseinzadeh Khaligh, K. Liew, Y. Han, N. M. Abukhdeir, and I. A. Goldthorpe, “Silver nanowire transparent electrodes for liquid crystal-based smart windows,” *Solar Energy Materials and Solar Cells*, vol. 132, pp. 337–341, Jan. 2015, doi: 10.1016/j.solmat.2014.09.006.

[23] L. Li *et al.*, “Efficient white polymer light-emitting diodes employing a silver nanowire-polymer composite electrode,” *Physical Chemistry Chemical Physics*, vol. 14, no. 41, pp. 14249–14254, Nov. 2012, doi: 10.1039/c2cp41562c.

[24] L. Yang, T. Zhang, H. Zhou, S. C. Price, B. J. Wiley, and W. You, “Solution-processed flexible polymer solar cells with silver nanowire electrodes,” *ACS Appl Mater Interfaces*, vol. 3, no. 10, pp. 4075–4084, Oct. 2011, doi: 10.1021/am2009585.

[25] F. W. Campbell, “The Depth of Field of the Human Eye,” Scotland, 1959. [Online]. Available: http://myaccess.library.utoronto.ca/login?qurl=https%3A%2F%2Fwww.proquest.com%2Fdissert

ations-theses%2Fdepth-field-human-eye%2Fdocview%2F2188337205%2Fse-2%3Faccountid%3D14771

[26] N. E. C. Corporation, “1-Nm Diameter,” *Nature*, no. 3, pp. 603–605, 1993.

[27] B. Dan, G. C. Irvin, and M. Pasquali, “Continuous and scalable fabrication of transparent conducting carbon nanotube films,” *ACS Nano*, vol. 3, no. 4, pp. 835–843, Apr. 2009, doi: 10.1021/nn8008307.

[28] G.-S. Liu *et al.*, “Comprehensive Stability Improvement of Silver Nanowire Networks via Self-Assembled Mercapto Inhibitors,” *ACS Appl. Mater. Interfaces*, vol. 10, p. 50, 2018, doi: 10.1021/acsami.8b13329.

[29] L. Hu, D. S. Hecht, and G. Gr??ner, “Infrared transparent carbon nanotube thin films,” *Appl Phys Lett*, vol. 94, no. 8, p. 081103, Feb. 2009, doi: 10.1063/1.3075067.

[30] A. N. Obraztsov, “Making graphene on a large scale,” *Nat Nanotechnol*, vol. 4, no. 4, pp. 212–213, 2009, doi: 10.1038/nnano.2009.67.

[31] P. C. Wang *et al.*, “Transparent electrodes based on conducting polymers for display applications,” *Displays*, vol. 34, no. 4, pp. 301–314, 2013, doi: 10.1016/j.displa.2013.05.003.

[32] A. I. Hofmann, E. Cloutet, and G. Hadziioannou, “Materials for Transparent Electrodes: From Metal Oxides to Organic Alternatives,” *Adv Electron Mater*, vol. 4, no. 10, p. 1700412, Oct. 2018, doi: 10.1002/aelm.201700412.

[33] J. Van De Groep, P. Spinelli, and A. Polman, “Transparent conducting silver nanowire networks.”

[34] T. Sannicolo, M. Lagrange, A. Cabos, C. Celle, J.-P. Simonato, and D. Bellet, “Metallic Nanowire-Based Transparent Electrodes for Next Generation Flexible Devices: a Review,” 2016, doi: 10.1002/smll.201602581.

[35] Y. Sun, B. Mayers, T. Herricks, and Y. Xia, “Polyol Synthesis of Uniform Silver Nanowires: A Plausible Growth Mechanism and the Supporting Evidence,” *Nano Lett*, vol. 3, no. 7, pp. 955–960, Jul. 2003, doi: 10.1021/NL034312M.

[36] S. Coskun, B. Aksoy, and H. E. Unalan, “Polyol synthesis of silver nanowires: An extensive parametric study,” *Cryst Growth Des*, vol. 11, no. 11, pp. 4963–4969, Nov. 2011, doi: 10.1021/CG200874G/SUPPL_FILE/CG200874G_SI_001.PDF.

[37] A. R. Rathmell, S. M. Bergin, Y. L. Hua, Z. Y. Li, and B. J. Wiley, “The growth mechanism of copper nanowires and their properties in flexible, transparent conducting films,” *Advanced Materials*, vol. 22, no. 32, pp. 3558–3563, 2010, doi: 10.1002/adma.201000775.

[38] J. Kalowekamo and E. Baker, “Estimating the manufacturing cost of purely organic solar cells,” *Solar Energy*, vol. 83, no. 8, pp. 1224–1231, 2009, doi: 10.1016/j.solener.2009.02.003.

[39] H. Sohn, C. Park, J. M. Oh, S. W. Kang, and M. J. Kim, “Silver Nanowire Networks: Mechano-Electric Properties and Applications,” *Materials 2019, Vol. 12, Page 2526*, vol. 12, no. 16, p. 2526, Aug. 2019, doi: 10.3390/MA12162526.

[40] D. Langley, G. Giusti, C. Mayousse, C. Celle, D. Bellet, and J.-P. Simonato, “Flexible transparent conductive materials based on silver nanowire networks: a review,” *Nanotechnology*, vol. 24, no. 45, p. 452001, Nov. 2013, doi: 10.1088/0957-4484/24/45/452001.

[41] B. Hwang *et al.*, “Highly Flexible and Transparent Ag Nanowire Electrode Encapsulated with Ultra-Thin Al2O3: Thermal, Ambient, and Mechanical Stabilities.,” *Sci Rep*, vol. 7, p. 41336, 2017, doi: 10.1038/srep41336.

[42] Y. Seo, H. Ha, P. Matteini, and B. Hwang, “A review on the deformation behavior of silver nanowire networks under many bending cycles,” *Applied Sciences (Switzerland)*, vol. 11, no. 10, 2021, doi: 10.3390/app11104515.

[43] S. Pal, A. Verma, Y. K. Prajapati, and J. P. Saini, “Figure of Merit Enhancement of Surface Plasmon Resonance Biosensor Using Ga-Doped Zinc Oxide in Near Infrared Range,” *Photonic Sensors*, vol. 10, no. 4, pp. 340–352, 2020, doi: 10.1007/s13320-020-0583-4.

[44] F. Yu, W. Liu, S. W. Ke, M. Kurmoo, J. L. Zuo, and Q. Zhang, “Electrochromic two-dimensional covalent organic framework with a reversible dark-to-transparent switch,” *Nature Communications 2020 11:1*, vol. 11, no. 1, pp. 1–6, Nov. 2020, doi: 10.1038/s41467-020-19315-6.

[45] J. W. Cleary, E. M. Smith, K. D. Leedy, G. Grzybowski, and J. Guo, “Optical and electrical properties of ultra-thin indium tin oxide nanofilms on silicon for infrared photonics,” *Opt Mater Express*, vol. 8, no. 5, p. 1231, 2018, doi: 10.1364/ome.8.001231.

[46] H. G. Park, G. S. Heo, S. G. Park, H. C. Jeong, J. H. Lee, and D. S. Seo, “Silver nanowire networks as transparent conducting films for liquid crystal displays,” *ECS Solid State Letters*, vol. 4, no. 10, pp. R50–R52, Aug. 2015, doi: 10.1149/2.0031510ssl.

[47] T. Kim, Y. W. Kim, H. S. Lee, H. Kim, W. S. Yang, and K. S. Suh, “Uniformly interconnected silver-nanowire networks for transparent film heaters,” *Adv Funct Mater*, vol. 23, no. 10, pp. 1250–1255, 2013, doi: 10.1002/adfm.201202013.

[48] S. Ye *et al.*, “Metal Nanowire Networks: The Next Generation of Transparent Conductors,” *Advanced Materials*, vol. 26, no. 39, pp. 6670–6687, Oct. 2014, doi: 10.1002/ADMA.201402710.

[49] S. Lin *et al.*, “Roll-to-Roll Production of Transparent Silver-Nanofiber-Network Electrodes for Flexible Electrochromic Smart Windows,” *Advanced Materials*, 2017, doi: 10.1002/adma.201703238.

[50] G. Deignan and I. A. Goldthorpe, “The dependence of silver nanowire stability on network composition and processing parameters,” *RSC Adv.*, vol. 7, no. 57, pp. 35590–35597, Jul. 2017, doi: 10.1039/C7RA06524H.

[51] B. Deng *et al.*, “Roll-to-Roll Encapsulation of Metal Nanowires between Graphene and Plastic Substrate for High-Performance Flexible Transparent Electrodes,” *Nano Lett*, vol. 15, no. 6, pp. 4206–4213, Jun. 2015, doi: 10.1021/acs.nanolett.5b01531.

[52] S. Yu, X. Ma, X. Li, J. Li, B. Gong, and X. Wang, “Enhanced adhesion of Ag nanowire based transparent conducting electrodes for application in flexible electrochromic devices,” *Opt Mater (Amst)*, vol. 120, no. March, p. 111414, 2021, doi: 10.1016/j.optmat.2021.111414.

[53] P. S. Huang and T. Gao, “Current development of 1D and 2D metallic nanomaterials for the application of transparent conductors in solar cells: Fabrication and modeling,” *Nano-Structures and Nano-Objects*, Oct. 2017, doi: 10.1016/j.nanoso.2017.09.001.

[54] L. Gomes, A. Branco, T. Moreira, F. Feliciano, C. Pinheiro, and C. Costa, “Increasing the electrical conductivity of electrochromic PEDOT:PSS films - A comparative study,” *Solar Energy Materials and Solar Cells*, vol. 144, pp. 631–640, Jan. 2016, doi: 10.1016/j.solmat.2015.10.001.

[55] E. B. Franke, C. L. Trimble, J. S. Hale, M. Schubert, and J. A. Woollam, “Infrared switching electrochromic devices based on tungsten oxide,” *J Appl Phys*, vol. 88, no. 10, p. 5777, Nov. 2000, doi: 10.1063/1.1319325.

[56] K. L. Zhou *et al.*, “Electrochromic modulation of near-infrared light by WO3 films deposited on silver nanowire substrates,” *J Mater Sci*, vol. 52, no. 21, pp. 12783–12794, Nov. 2017, doi: 10.1007/s10853-017-1391-0.

[57] Y. T. Park, S. H. Lee, and K. T. Lee, “Electrochromic properties of silver nanowire-embedded tungsten trioxide thin films fabricated by electrodeposition,” *Ceram Int*, vol. 46, no. 18, pp. 29052–29059, 2020, doi: 10.1016/j.ceramint.2020.08.076.

[58] M. C. Larciprete *et al.*, “Infrared properties of randomly oriented silver nanowires,” *J Appl Phys*, vol. 112, no. 8, p. 083503, Oct. 2012, doi: 10.1063/1.4759374.

[59] E. Pantoja, R. Bhatt, A. Liu, and M. C. Gupta, “Low thermal emissivity surfaces using AgNW thin films,” *Nanotechnology*, vol. 28, no. 50, p. 505708, Nov. 2017, doi: 10.1088/1361-6528/aa96c2.

[60] N. N. Elgrishi, K. J. Rountree, B. D. Mccarthy, E. S. Rountree, T. T. Eisenhart, and J. L. Dempsey, “A Practical Beginner’s Guide to Cyclic Voltammetry,” 2017, doi: 10.1021/acs.jchemed.7b00361.

[61] D. Levasseur, I. Mjejri, T. Rolland, and A. Rougier, “Color tuning by oxide addition in PEDOT:PSS-based electrochromic devices,” *Polymers (Basel)*, vol. 11, no. 1, pp. 1–12, 2019, doi: 10.3390/polym11010179.

[62] P. W. Chen, C. Te Chang, T. F. Ko, S. C. Hsu, K. D. Li, and J. Y. Wu, “Fast response of complementary electrochromic device based on WO3/NiO electrodes,” *Scientific Reports 2020 10:1*, vol. 10, no. 1, pp. 1–12, May 2020, doi: 10.1038/s41598-020-65191-x.

[63] H. Hosseinzadeh Khaligh and I. A. Goldthorpe, “Hot-rolling nanowire transparent electrodes for surface roughness minimization,” *Nanoscale Res Lett*, vol. 9, no. 1, pp. 1–5, 2014, doi: 10.1186/1556-276X-9-310.

[64] S. Maier, *Plasmonics: Fundamentals and Applications*, 1st ed. New York, NY, USA: Springer Science & Business Media LLC, 2010.

[65] C. Pradére *et al.*, “The Joule heating problem in silver nanowire transparent electrodes,” *Nanotechnology*, vol. 28, no. 42, p. 425703, 2017, doi: 10.1088/1361-6528/aa7f34.

[66] C. Mayousse, C. Celle, A. Fraczkiewicz, and J. P. Simonato, “Stability of silver nanowire based electrodes under environmental and electrical stresses,” *Nanoscale*, vol. 7, no. 5, pp. 2107–2115, Feb. 2015, doi: 10.1039/c4nr06783e.

[67] D. Y. Choi, H. W. Kang, H. J. Sung, and S. S. Kim, “Annealing-free, flexible silver nanowire-polymer composite electrodes via a continuous two-step spray-coating method,” *Nanoscale*, vol. 5, no. 3, pp. 977–983, Feb. 2013, doi: 10.1039/c2nr32221h.

[68] K. Mallikarjuna, M. A. Shinde, and H. Kim, “Electrochromic smart windows using 2D-MoS2 nanostructures protected silver nanowire based flexible transparent electrodes,” *Mater Sci Semicond Process*, vol. 117, no. April, p. 105176, 2020, doi: 10.1016/j.mssp.2020.105176.

[69] J. Jensen, M. Hösel, I. Kim, J.-S. Yu, J. Jo, and F. C. Krebs, “Fast Switching ITO Free Electrochromic Devices,” *Adv Funct Mater*, vol. 24, no. 9, pp. 1228–1233, Mar. 2014, doi: 10.1002/adfm.201302320.

[70] X. Shi *et al.*, “Improving the stability of silver nanowire/polyimide composite films for transparent film heaters,” *Journal of Materials Science: Materials in Electronics*, vol. 30, no. 3, pp. 2089–2095, Feb. 2019, doi: 10.1007/s10854-018-0480-4.

[71] B. Hwang, C. H. An, and S. Becker, “Highly robust Ag nanowire flexible transparent electrode with UV-curable polyurethane-based overcoating layer,” *Mater Des*, vol. 129, pp. 180–185, Sep. 2017, doi: 10.1016/j.matdes.2017.05.042.

[72] M. S. Miller, J. C. O’Kane, A. Niec, R. S. Carmichael, and T. B. Carmichael, “Silver Nanowire/Optical Adhesive Coatings as Transparent Electrodes for Flexible Electronics,” *ACS Appl Mater Interfaces*, vol. 5, no. 20, pp. 10165–10172, Oct. 2013, doi: 10.1021/am402847y.

[73] Z. Yu, L. Li, Q. Zhang, W. Hu, and Q. Pei, “Silver Nanowire-Polymer Composite Electrodes for Efficient Polymer Solar Cells,” *Advanced Materials*, vol. 23, no. 38, pp. 4453–4457, Oct. 2011, doi: 10.1002/adma.201101992.

[74] X. Y. Zeng, Q. K. Zhang, R. M. Yu, and C. Z. Lu, “A new transparent conductor: Silver nanowire film buried at the surface of a transparent polymer,” *Advanced Materials*, 2010, doi: 10.1002/adma.201001811.

[75] A. Madeira, M. Plissonneau, L. Servant, I. A. Goldthorpe, and M. Tréguer-Delapierre, “Increasing silver nanowire network stability through small molecule passivation,” *Nanomaterials*, vol. 9, no. 6, pp. 13–16, 2019, doi: 10.3390/nano9060899.

[76] B. Hwang *et al.*, “Highly Flexible and Transparent Ag Nanowire Electrode Encapsulated with Ultra-Thin Al2O3: Thermal, Ambient, and Mechanical Stabilities,” *Sci Rep*, vol. 7, p. 41336, Jan. 2017, doi: 10.1038/srep41336.

[77] R. Ramachandramoorthy, W. Gao, R. Bernal, and H. Espinosa, “High Strain Rate Tensile Testing of Silver Nanowires: Rate-Dependent Brittle-to-Ductile Transition,” *Nano Lett*, vol. 16, no. 1, pp. 255–263, Jan. 2016, doi: 10.1021/acs.nanolett.5b03630.

[78] T. A. Yemata *et al.*, “Modulation of the doping level of PEDOT:PSS film by treatment with hydrazine to improve the Seebeck coefficient,” *RSC Adv*, vol. 10, no. 3, pp. 1786–1792, Jan. 2020, doi: 10.1039/c9ra07648d.

[79] Y. Lin, Y. Zhao, Q. Xin, C. Jiang, and A. Song, “Electrical control of the optical dielectric properties of PEDOT:PSS thin films,” *Opt Mater (Amst)*, vol. 108, p. 110435, Oct. 2020, doi: 10.1016/J.OPTMAT.2020.110435.

[80] M. A. Garakani *et al.*, “Scalable spray-coated graphene-based electrodes for high-power electrochemical double-layer capacitors operating over a wide range of temperature,” *Energy Storage Mater*, vol. 34, no. November, pp. 1–11, 2021, doi: 10.1016/j.ensm.2020.08.036.

[81] “(PDF) Some optical properties of polyurethane.” https://www.researchgate.net/publication/305929150_Some_optical_properties_of_polyurethane (accessed May 16, 2021).

[82] K. Wang, J. Cheng, S. Yao, Y. Lu, L. Ji, and D. Xu, “Determination of electrostatic force and its characteristics based on phase difference by amplitude modulation atomic force microscopy,” *Nanoscale Res Lett*, vol. 11, no. 1, pp. 1–9, Dec. 2016, doi: 10.1186/S11671-016-1765-2/TABLES/2.

[83] “Sulfur Dioxide Basics | US EPA.” https://www.epa.gov/so2-pollution/sulfur-dioxide-basics (accessed May 02, 2023).

[84] “Global Flexible Display Market Size & Trends Report, 2019-2025.” https://www.grandviewresearch.com/industry-analysis/flexible-display-market (accessed Feb. 16, 2023).

[85] Y. Seekaew, S. Lokavee, D. Phokharatkul, A. Wisitsoraat, T. Kerdcharoen, and C. Wongchoosuk, “Low-cost and flexible printed graphene–PEDOT:PSS gas sensor for ammonia detection,” *Org Electron*, vol. 15, no. 11, pp. 2971–2981, Nov. 2014, doi: 10.1016/J.ORGEL.2014.08.044.

[86] H. S. Park, S. J. Ko, J. S. Park, J. Y. Kim, and H. K. Song, “Redox-active charge carriers of conducting polymers as a tuner of conductivity and its potential window,” *Scientific Reports 2013 3:1*, vol. 3, no. 1, pp. 1–6, Aug. 2013, doi: 10.1038/srep02454.

[87] D. Bellet *et al.*, “Transparent electrodes based on silver nanowire networks: From physical considerations towards device integration,” *Materials*, vol. 10, no. 6, p. 570, May 2017, doi: 10.3390/ma10060570.

[88] S. Nam *et al.*, “Ultrasmooth, extremely deformable and shape recoverable Ag nanowire embedded transparent electrode,” *Sci Rep*, vol. 4, no. 1, pp. 1–7, Apr. 2014, doi: 10.1038/srep04788.

[89] Y. Xu *et al.*, “Paper-based wearable electronics,” *iScience*, vol. 24, no. 7, p. 102736, Jul. 2021, doi: 10.1016/J.ISCI.2021.102736.

[90] A. W. Lang, A. M. Österholm, and J. R. Reynolds, “Paper-Based Electrochromic Devices Enabled by Nanocellulose-Coated Substrates,” *Adv Funct Mater*, vol. 29, no. 39, p. 1903487, Sep. 2019, doi: 10.1002/ADFM.201903487.

[91] H. T. Kim, S. K. Jung, and S. Y. Lee, “Properties of ITO films deposited on paper sheets using a low-frequency (60 Hz) DC-pulsed magnetron sputtering method,” *Vacuum*, vol. 187, p. 110056, May 2021, doi: 10.1016/J.VACUUM.2021.110056.

[92] B. Yoo, Y. Kim, C. J. Han, M. S. Oh, and J. W. Kim, “Recyclable patterning of silver nanowire percolated network for fabrication of flexible transparent electrode,” *Appl Surf Sci*, vol. 429, pp. 151–157, 2018, doi: 10.1016/j.apsusc.2017.07.285.

[93] J. S. Hwang *et al.*, “Recycling silver nanoparticle debris from laser ablation of silver nanowire in liquid media toward minimum material waste,” *Sci Rep*, vol. 11, no. 1, pp. 1–11, 2021, doi: 10.1038/s41598-021-81692-9.

[94] D. Choi *et al.*, “Fabrication of transparent conductive tri-composite film for electrochromic application,” *Appl Surf Sci*, vol. 425, pp. 1006–1013, Dec. 2017, doi: 10.1016/j.apsusc.2017.07.076.

[95] Q. Xu *et al.*, “Solution-Processed Highly Conductive PEDOT:PSS/AgNW/GO Transparent Film for Efficient Organic-Si Hybrid Solar Cells,” 2015, doi: 10.1021/am508006q.

[96] J. P. Thomas *et al.*, “Highly Conducting Hybrid Silver-Nanowire-Embedded Poly(3,4-ethylenedioxythiophene):Poly(styrenesulfo nate) for High-Efficiency Planar Silicon/ Organic Heterojunction Solar Cells,” 2018, doi: 10.1021/acsnano.8b04848.

[97] N. Duraisamy, S. J. Hong, and K. H. Choi, “Deposition and characterization of silver nanowires embedded PEDOT: PSS thin films via electrohydrodynamic atomization,” *Chemical Engineering Journal*, vol. 225, pp. 887–894, Jun. 2013, doi: 10.1016/j.cej.2013.04.007.

[98] F. Polymer and I. Technology, “High-performance and ultraflexible PEDOT / silver nanowires / graphene films for electrochromic applications,” vol. 45, no. 8, 2020.

[99] J. van de Groep, P. Spinelli, and A. Polman, “Transparent Conducting Silver Nanowire Networks,” *Nano Lett*, vol. 12, no. 6, pp. 3138–3144, Jun. 2012, doi: 10.1021/nl301045a.

[100] A. T. Bellew, H. G. Manning, C. Gomes da Rocha, M. S. Ferreira, and J. J. Boland, “Resistance of Single Ag Nanowire Junctions and Their Role in the Conductivity of Nanowire Networks,” *ACS Nano*, vol. 9, no. 11, pp. 11422–11429, 2015, doi: 10.1021/acsnano.5b05469.

[101] X. Li, K. Perera, J. He, A. Gumyusenge, and J. Mei, “Solution-processable electrochromic materials and devices: Roadblocks and strategies towards large-scale applications,” *J Mater Chem C Mater*, vol. 7, no. 41, pp. 12761–12789, 2019, doi: 10.1039/c9tc02861g.

[102] “Two,Three,Four Electrode System Gamry 4-Probe Potentiostats Gamry Instruments.” https://www.gamry.com/application-notes/instrumentation/two-three-four-electrode-experiments/ (accessed Nov. 27, 2022).

[103] D. Lee, H. Lee, Y. Ahn, Y. Jeong, D. Y. Lee, and Y. Lee, “Highly stable and flexible silver nanowire-graphene hybrid transparent conducting electrodes for emerging optoelectronic devices,” *Nanoscale*, vol. 5, no. 17, pp. 7750–7755, 2013, doi: 10.1039/c3nr02320f.

[104] Y. Ahn, Y. Jeong, and Y. Lee, “Improved thermal oxidation stability of solution-processable silver nanowire transparent electrode by reduced graphene oxide,” *ACS Appl Mater Interfaces*, vol. 4, no. 12, pp. 6410–6414, Dec. 2012, doi: 10.1021/AM301913W/SUPPL_FILE/AM301913W_SI_001.PDF.

[105] C. Mayousse, C. Celle, A. Fraczkiewicz, and J.-P. Simonato, “Stability of silver nanowire based electrodes under environmental and electrical stresses,” *Nanoscale*, vol. 7, no. 5, pp. 2107–2115, Jan. 2015, doi: 10.1039/C4NR06783E.

[106] “No Title.” https://nanocomposix.com/pages/polyvinylpyrrolidone-pvp-surface

[107] G. M. Dougherty *et al.*, “The zeta potential of surface-functionalized metallic nanorod particles in aqueous solution,” *Electrophoresis*, vol. 29, no. 5, pp. 1131–1139, Mar. 2008, doi: 10.1002/ELPS.200700448.

[108] M. Finšgar, “Surface analysis by gas cluster ion beam XPS and ToF-SIMS tandem MS of 2-mercaptobenzoxazole corrosion inhibitor for brass,” *Corros Sci*, vol. 182, no. November 2020, 2021, doi: 10.1016/j.corsci.2021.109269.

[109] J. Atkinson and I. A. Goldthorpe, “Near-infrared properties of silver nanowire networks,” *Nanotechnology*, vol. 31, no. 36, 2020, doi: 10.1088/1361-6528/ab94de.

[110] L. Zhou *et al.*, “High-performance flexible organic light-emitting diodes using embedded silver network transparent electrodes,” *ACS Nano*, vol. 8, no. 12, pp. 12796–12805, Dec. 2014, doi: 10.1021/nn506034g.

[111] A. R. Madaria, A. Kumar, and C. Zhou, “Large scale, highly conductive and patterned transparent films of silver nanowires on arbitrary substrates and their application in touch screens,” *Nanotechnology*, vol. 22, no. 24, p. 245201, Jun. 2011, doi: 10.1088/0957-4484/22/24/245201.

[112] J. Krantz, M. Richter, S. Spallek, E. Spiecker, and C. J. Brabec, “Solution-processed metallic nanowire electrodes as indium tin oxide replacement for thin-film solar cells,” *Adv Funct Mater*, vol. 21, no. 24, pp. 4784–4787, Dec. 2011, doi: 10.1002/adfm.201100457.

[113] A. Azens and C. G. Granqvist, “Electrochromic smart windows: energy efficiency and device aspects,” *Journal of Solid State Electrochemistry 2003 7:2*, vol. 7, no. 2, pp. 64–68, 2003, doi: 10.1007/S10008-002-0313-4.

[114] S. De *et al.*, “Silver nanowire networks as flexible, transparent, conducting films: Extremely high DC to optical conductivity ratios,” *ACS Nano*, vol. 3, no. 7, pp. 1767–1774, Jul. 2009, doi: 10.1021/nn900348c.

[115] S. Hanauer *et al.*, “Transparent and Mechanically Resistant Silver-Nanowire-Based Low-Emissivity Coatings,” *ACS Appl Mater Interfaces*, vol. 13, no. 18, pp. 21971–21978, May 2021, doi: 10.1021/ACSAMI.1C02689/SUPPL_FILE/AM1C02689_SI_001.PDF.

[116] E. Sefer, S. O. Hacioglu, M. Tonga, L. Toppare, A. Cirpan, and S. Koyuncu, “A Novel Near-IR Effective Pyrene-Based Donor-Acceptor Electrochrome,” *Macromol Chem Phys*, vol. 216, no. 8, pp. 829–836, Apr. 2015, doi: 10.1002/macp.201400584.

[117] N. Cui *et al.*, “Stretchable transparent electrodes for conformable wearable organic photovoltaic devices,” *npj Flexible Electronics 2021 5:1*, vol. 5, no. 1, pp. 1–8, Nov. 2021, doi: 10.1038/s41528-021-00127-7.

[118] K. H. Choi, J. Kim, Y. J. Noh, S. I. Na, and H. K. Kim, “Ag nanowire-embedded ITO films as a near-infrared transparent and flexible anode for flexible organic solar cells,” *Solar Energy Materials and Solar Cells*, vol. 110, pp. 147–153, Mar. 2013, doi: 10.1016/j.solmat.2012.12.022.

[119] L. Hu, H. S. Kim, J. Y. Lee, P. Peumans, and Y. Cui, “Scalable coating and properties of transparent, flexible, silver nanowire electrodes,” *ACS Nano*, vol. 4, no. 5, pp. 2955–2963, May 2010, doi: 10.1021/nn1005232.

[120] J. M. Back, S. W. McCue, and T. J. Moroney, “Including nonequilibrium interface kinetics in a continuum model for melting nanoscaled particles,” *Scientific Reports 2014 4:1*, vol. 4, no. 1, pp. 1–8, Nov. 2014, doi: 10.1038/srep07066.

[121] S. Bae, S. J. Kim, D. Shin, J. H. Ahn, and B. H. Hong, “Towards industrial applications of graphene electrodes,” *Phys Scr*, vol. 2012, no. T146, p. 014024, Jan. 2012, doi: 10.1088/0031-8949/2012/T146/014024.

[122] D. Bellet *et al.*, “materials Transparent Electrodes Based on Silver Nanowire Networks: From Physical Considerations towards Device Integration,” *Materials*, vol. 10, p. 570, 2017, doi: 10.3390/ma10060570.

[123] S. M. Bergin, Y.-H. Chen, A. R. Rathmell, P. Charbonneau, Z.-Y. Li, and B. J. Wiley, “The effect of nanowire length and diameter on the properties of transparent, conducting nanowire films,” *Nanoscale*, vol. 4, no. 6, p. 1996, Mar. 2012, doi: 10.1039/c2nr30126a.

[124] S. Sorel, P. E. Lyons, S. De, J. C. Dickerson, and J. N. Coleman, “The dependence of the optoelectrical properties of silver nanowire networks on nanowire length and diameter,” *Nanotechnology*, vol. 23, no. 18, p. 185201, May 2012, doi: 10.1088/0957-4484/23/18/185201.

[125] M. Marus *et al.*, “Effect of silver nanowire length in a broad range on optical and electrical properties as a transparent conductive film,” *Opt Mater Express*, vol. 7, no. 3, p. 1105, Mar. 2017, doi: 10.1364/ome.7.001105.

[126] P. C. Hsu *et al.*, “Personal thermal management by metallic nanowire-coated textile,” *Nano Lett*, vol. 15, no. 1, pp. 365–371, 2015, doi: 10.1021/nl5036572.

[127] K. F. Casey, “Electromagnetic Shielding Behavior of Wire-Mesh Screens,” *IEEE Trans Electromagn Compat*, vol. 30, no. 3, pp. 298–306, 1988, doi: 10.1109/15.3309.

[128] J. Y. Lee, S. T. Connor, Y. Cui, and P. Peumans, “Solution-processed metal nanowire mesh transparent electrodes,” *Nano Lett*, vol. 8, no. 2, pp. 689–692, 2008, doi: 10.1021/nl073296g.

[129] W. Chen, M. D. Thoreson, S. Ishii, A. V. Kildishev, and V. M. Shalaev, “Ultra-thin ultra-smooth and low-loss silver films on a germanium wetting layer,” *Opt Express*, vol. 18, no. 5, p. 5124, Mar. 2010, doi: 10.1364/oe.18.005124.

[130] J. Lee *et al.*, “Solution-Processed Metal Nanowire Mesh Transparent Electrodes,” vol. 8, no. 2, pp. 689–692, 2008, doi: 10.1021/nl073296g.

[131] J. Weiner, “The physics of light transmission through subwavelength apertures and aperture arrays,” *2009 Optical Data Storage Topical Meeting, ODS 2009*, pp. 13–15, 2009, doi: 10.1109/ODS.2009.5031731.

[132] J. Y. Lee, S. T. Connor, Y. Cui, and P. Peumans, “Solution-processed metal nanowire mesh transparent electrodes,” *Nano Lett*, vol. 8, no. 2, pp. 689–692, Feb. 2008, doi: 10.1021/nl073296g.

[133] T. Sannicolo and T. Sannicolo, “Transparent electrodes based on silver nanowire networks : electrical percolation , physical properties , and applications,” no. October 2017, 2018.

[134] M. Lagrange, D. P. Langley, G. Giusti, C. Jiménez, Y. Bréchet, and D. Bellet, “Optimization of silver nanowire-based transparent electrodes: Effects of density, size and thermal annealing,” *Nanoscale*, vol. 7, no. 41, pp. 17410–17423, 2015, doi: 10.1039/c5nr04084a.

[135] M. (Anthony M. Fox, “Optical properties of solids,” p. 396, Accessed: Feb. 19, 2023. [Online]. Available: https://global.oup.com/academic/product/optical-properties-of-solids-9780199573370

[136] R. Starko-Bowes *et al.*, “Optical characterization of epsilon-near-zero, epsilon-near-pole, and hyperbolic response in nanowire metamaterials,” *Journal of the Optical Society of America B*, vol. 32, no. 10, p. 2074, Oct. 2015, doi: 10.1364/josab.32.002074.

[137] P. Johns, G. Beane, K. Yu, and G. V Hartland, “Dynamics of Surface Plasmon Polaritons in Metal Nanowires,” 2017, doi: 10.1021/acs.jpcc.6b12748.

[138] F. Selzer *et al.*, “Electrical limit of silver nanowire electrodes: Direct measurement of the nanowire junction resistance,” *Appl Phys Lett*, vol. 108, no. 16, p. 163302, Apr. 2016, doi: 10.1063/1.4947285.

[139] C. Preston, Y. Xu, X. Han, J. N. Munday, L. Hu, and S.-V. Berlin, “Optical haze of transparent and conductive silver nanowire films”, doi: 10.1007/s12274-013-0323-9.

[140] C. Preston, Y. Xu, X. Han, J. N. Munday, and L. Hu, “Optical haze of transparent and conductive silver nanowire films,” *Nano Res*, vol. 6, no. 7, pp. 461–468, May 2013, doi: 10.1007/s12274-013-0323-9.

[141] M. Collins, “Passive Solar Windows,” 2015.

[142] J.-J. Greffet, P. Bouchon, G. Brucoli, E. Sakat, and F. Marquier, “Generalized Kirchhoff law,” pp. 1–6, 2016, doi: 10.1103/PhysRevX.8.021008.

[143] G. Khanarian *et al.*, “The optical and electrical properties of silver nanowire mesh films,” in *Journal of Applied Physics*, Jul. 2013. doi: 10.1063/1.4812390.

[144] K. Von Rottkay, M. Rubin, and S. J. Wen, “Optical indices of electrochromic tungsten oxide,” *Thin Solid Films*, vol. 306, no. 1, pp. 10–16, Aug. 1997, doi: 10.1016/S0040-6090(97)00254-X.

[145] I. Valyukh *et al.*, “Spectroscopic ellipsometry characterization of electrochromic tungsten oxide and nickel oxide thin films made by sputter deposition,” 2010, doi: 10.1016/j.solmat.2009.12.011.

[146] P. Yeh, “Matrix Formulation for Isotropic Layered Media,” *Optical Waves in Layered Media*, 2005, Accessed: Feb. 22, 2023. [Online]. Available: https://www.wiley.com/en-us/Optical+Waves+in+Layered+Media-p-9780471731924

[147] H. Kalhori, M. Ranjbar, H. Salamati, and J. M. D. Coey, “Flower-like nanostructures of WO3: Fabrication and characterization of their in-liquid gasochromic effect,” *Sens Actuators B Chem*, vol. 225, pp. 535–543, 2016, doi: 10.1016/j.snb.2015.11.044.

[148] H. Yan *et al.*, “Solution growth of NiO nanosheets supported on Ni foam as high-performance electrodes for supercapacitors,” *Nanoscale Res Lett*, vol. 9, no. 1, pp. 1–7, 2014, doi: 10.1186/1556-276X-9-424.

[149] K. L. Zhou *et al.*, “Electrochromic modulation of near-infrared light by WO3 films deposited on silver nanowire substrates,” *J Mater Sci*, vol. 52, no. 21, pp. 12783–12794, 2017, doi: 10.1007/s10853-017-1391-0.

[150] B. Tangeysh, M. Fryd, M. A. Ilies, and B. B. Wayland, “Palladium metal nanoparticle size control through ion paired structures of [PdCl4]2− with protonated PDMAEMA,” *Chemical Communications*, vol. 48, no. 71, pp. 8955–8957, 2012, doi: 10.1039/c2cc34401g.

[151] A. Sharma *et al.*, “Physical characterization and in vivo organ distribution of coated iron oxide nanoparticles,” *Sci Rep*, vol. 8, no. 1, pp. 1–12, 2018, doi: 10.1038/s41598-018-23317-2.

[152] H. Li, Y. Liu, A. Su, J. Wang, and Y. Duan, “Promising Hybrid Graphene-Silver Nanowire Composite Electrode for Flexible Organic Light-Emitting Diodes,” *Sci Rep*, vol. 9, no. 1, pp. 1–10, 2019, doi: 10.1038/s41598-019-54424-3.

[153] S. Huang *et al.*, “Highly Stable Ag–Au Core–Shell Nanowire Network for ITO-Free Flexible Organic Electrochromic Device,” *Adv Funct Mater*, vol. 31, no. 14, p. 2010022, Apr. 2021, doi: 10.1002/ADFM.202010022.

[154] S. Wang, Y. Tian, C. Hang, and C. Wang, “Cohesively enhanced electrical conductivity and thermal stability of silver nanowire networks by nickel ion bridge joining,” *Sci Rep*, vol. 8, no. 1, pp. 1–9, 2018, doi: 10.1038/s41598-018-21777-0.

[155] H. Kang *et al.*, “Electroplated Silver-Nickel Core-Shell Nanowire Network Electrodes for Highly Efficient Perovskite Nanoparticle Light-Emitting Diodes,” *ACS Appl Mater Interfaces*, vol. 12, no. 35, pp. 39479–39486, 2020, doi: 10.1021/acsami.0c10386.

[156] B. W. C. Au and K. Y. Chan, “Towards an All-Solid-State Electrochromic Device: A Review of Solid-State Electrolytes and the Way Forward,” *Polymers (Basel)*, vol. 14, no. 12, pp. 1–16, 2022, doi: 10.3390/polym14122458.

[157] J. H. Han *et al.*, “Atomic layer deposition of tantalum oxide and tantalum silicate from TaCl 5 , SiCl 4 , and O 3 : growth behaviour and film characteristics”, doi: 10.1039/c3tc31172d.

[158] K. S. Ahn, S. J. Yoo, M. S. Kang, J. W. Lee, and Y. E. Sung, “Tandem dye-sensitized solar cell-powered electrochromic devices for the photovoltaic-powered smart window,” *J Power Sources*, vol. 168, no. 2, pp. 533–536, 2007, doi: 10.1016/j.jpowsour.2006.12.114.

[159] G. A. Niklasson, S. Y. Li, and C. G. Granqvist, “Thermochromic vanadium oxide thin films: Electronic and optical properties,” *J Phys Conf Ser*, vol. 559, no. 1, 2014, doi: 10.1088/1742-6596/559/1/012001.

[160] H. H. Khaligh *et al.*, “The Joule heating problem in silver nanowire transparent electrodes,” 2017, doi: 10.1088/1361-6528/aa7f34.